New Insights into the Molecular Mechanisms of Islet Dysfunction in Human Diabetes

By

John T. Walker

Dissertation

Submitted to the Faculty of the

Graduate School of Vanderbilt University

in partial fulfillment of the requirements

for the degree of

DOCTOR OF PHILOSOPHY

in

Molecular Physiology and Biophysics

June 30, 2021

Nashville, Tennessee

Approved:

Richard O'Brien, Ph.D., Chair

Maureen Gannon, Ph.D.

Owen McGuinness, Ph.D.

Jeffrey Rathmell, Ph.D.

ACKNOWLEDGEMENTS

Vanderbilt Community

First, I want to thank the Vanderbilt Medical Scientist Training Program (MSTP). Their belief in me gave me an opportunity to pursue becoming a physician-scientist and the environment they have created has advanced my scientific and medical growth immensely. The MSTP has been led by two exceptional directors during my time, Dr. Terence Dermody and Dr. Chris Williams, who have been thoughtful leaders, dedicated scientists, and compassionate individuals and to whom I am incredibly thankful for helping me navigate numerous trying situations. The MSTP wouldn't be what it is without the dedicated work of the entire leadership team including Danny Winder, Sally York, Ambra Pozzi, Megan Williams, Lourdes Estrada, Bryn Sierra, and Julie Gannon. They have all have played important roles in my training and I am so thankful to be in an environment that makes students a priority. I want to extend a special thanks to Melissa Krasnove, a former assistant director, for constantly going above and beyond the expectations of her role and becoming a close friend.

I want to thank the Molecular Physiology and Biophysics department at Vanderbilt for providing an excellent home during my research training. I am grateful for the work from Drs. Roger Colbran as interim chair and for our new chair, Dr. Nancy Carrasco in orchestrating a departmental training environment with diverse scientific viewpoints. Thank you to Richard O'Brien as Director of Graduate Studies and to Karen Gieg and Kandi Granberry for all their work coordinating and organizing behind the scenes that allows us to focus on the science. I also want to thank the Vanderbilt Diabetes Research and Training Center (DRTC) and the Vanderbilt University Medical Center Division of Diabetes, Endocrinology, and Metabolism. Their leadership were instrumental in shaping the direction of our science and my training.

I would like to thank my thesis committee, Drs. Richard O'Brien, Maureen Gannon, Owen McGuinness, and Jeff Rathmell for the advice, feedback, and guidance on this Dissertation and in my career. They have helped direct my scientific training and have provided helpful feedback on our findings. I especially want to thank Maureen for her mentorship and inviting me to informal meetings with other leaders in the field at conferences, especially early in my career. These were particularly helpful to me to build confidence as I was learning the islet biology field. I would also like to thank additional scientific mentors at Vanderbilt, especially Dr. Roland Stein, who was always available for scientific discussions, constructive feedback, and encouragement. His calm approach often helped me see the big picture and helped me navigate numerous situations. I want to thank Dr. David Jacobson and his lab for helpful comments during several years of our joint lab meetings. Additionally, Dr. Daniel Moore has been a steadfast mentor who graciously welcomed me into his Pediatric Endocrinology Clinic, was always enthusiastic to hear about my latest science, and has been and continues to be a fantastic advocate for me as I pursue a career as a physician-scientist in pediatric endocrinology.

Powers and Brissova Lab

I have had the immense honor of working in the laboratory of Dr. Al Powers and Dr. Marcela Brissova. The resources and opportunities they have provided are the foundation on which my scientific training in islet biology was cultivated. The environment of our lab has thought me to be a critical scientist with a commitment to identifying the important questions that remain unanswered and identifying the best approach to address that question. Al has had a tireless dedication to my career, our lab, the Vanderbilt community, the international islet biology community, and to patients with diabetes. He exemplifies what it means to be a physician-scientist, a leader, and a mentor and I will forever be immensely grateful. If I ever make a mark on one of my trainees like he has made on me, I know I will have been exceptionally successful. Marcela has provided truly unwavering support. Countless late nights talking through a new experimental set up or thinking about how to interpret an odd set of results have shown me firsthand what it means to be a good scientist. Her commitment to trainees extends beyond the lab and I am so grateful to have her as a mentor.

All of this work is a reflection of the rich scientific environment of the Powers and Brissova lab and all the people in it. I would like to extend a special thank you to Chunhua Dai, whose dedication and vision for setting up and executing experiments taught me so much about how to be effective scientist. Chunhua and I worked closely with throughout my training, especially the studies described in Chapter III. Thank you to Diane Saunders who has been a close scientific partner with an uncanny ability to keep me organized and on task. We have accomplished a great deal together, especially in the last 18 months, and I look forward to continuing this partnership. Diane established multiplexed imaging in our lab and was critical to studies in Chapter V and Chapter VI.

I am grateful to have received advice and support from an exceptional group of post-graduate trainees during my time in the lab including Nathaniel Hart, Jordan Wright, Shristi Shrestha, Heather Nelson, Neil Phillips, Danielle Dean and Katie Coate. I am especially grateful to Jordan for the career mentorship he's provided on being a physician-scientist in residency, fellowship, and early career. Additionally, Shristi, a computational biologist, has greatly elevated my analytical training and was a leader in our single cell efforts described in Chapter VI. I am fortunate to have been part of a fantastic group of graduate students, including Rachana Haliyur, Tiffany Richardson, and Yasminye Pettway whose scientific creativity have helped work through many challenges in lab. I want to extend a special thanks to Rachana whose dedication laid the foundation for numerous projects that I took over in the lab, specifically projects described in Chapter IV and Chapter V.

I would like to acknowledge our incredible group of research specialists, Radhika Aramandla, Greg Poffenberger, Conrad Reihsmann, and Alexander Hopkirk. Their expertise and enthusiastic contributions have added important insight into our group, and they have assisted me or performed many experiments in this Dissertation (perifusions, assays, animal studies, etc.). Radhika has been one of my closest bench-side partners and made my time in lab a joy. Radhika's commitment to the lab and support of me throughout my training has been

instrumental in my progress. I want to highlight Regina Jenkins, Jill Lindner, Amber Bradley who have been instrumental in our work on human tissue samples. Finally, I want to thank our neighbors in the Islet Procurement and Analysis Core. Their expertise has been invaluable in pushing our research forward and they create such a thoughtful and joyful environment.

I would like to acknowledge the funding sources which enabled my training and the studies described in this Dissertation: the MSTP training grant (T32GM007347), a Ruth L. Kirschstein National Research Service Award (F30DK118830-01), and the support provided to Dr. Al Powers and Dr. Marcela Brissova through multiple grants from the NIH, Juvenile Diabetes Research Foundation (JDRF), and the U.S. Department of Veterans Affairs. This funding enabled us to pursue models and techniques on the cutting edge of science and also facilitated me gaining additional computational data analysis skills during my training. I am extremely grateful for all the behind the scenes work that goes on to make these funds available in the pursuit of science.

Finally, I would like to acknowledge the invaluable contribution made by organ donors and their families. My work was performed almost exclusively with human tissues and their amazing generosity has led to incredible advancements in our understanding of human islet biology and diabetes. I have had the honor to study tissue from nearly 150 different organ donors in this Dissertation. Their gift to science is critical to this work and to working towards a cure in diabetes and I thank them for entrusting us with the thoughtful and judicious use of the most precious resource.

Outside Collaborators and Mentors

I have had the privilege of participating in team science and collaborating with numerous outstanding scientists across the nation and world. From sharing of resources, to data discussions via conference call, and guidance about research direction, our collaborators have been wonderful partners in science. Our lab is fortunate to be part of the NIDDK-funded Human Islet Research Network (HIRN) and the Human Pancreas Analysis Program (HPAP), a consortium within HIRN that has emphasized the role of collaborative science. During my training, I got the opportunity to contribute to the successful application for a multi-principal investigator U01 for HPAP that involved working closely with Drs. Seung Kim and Anna Gloyn of Stanford, Dr. Patrick MacDonald of Alberta, Dr. Dirk Homann of Mount Sinai, Dr. Rita Bottino of Imagine Pharma, and Dr. Mark Atkinson of Florida. These experiences have embodied how team science is necessary to advance our knowledge of human diabetes and disease

I would like to thank Drs. Ashutosh Agarwal and Matthew Ishahak of the University of Miami for the opportunity to revisit my days as an engineer and think about fluid dynamics in our microfluidic device that is described in Chapter IV. Dr. Stephen Parker and Vivek Rai of the University of Michigan are wonderful collaborators who have been instrumental to studies described in Chapter V. They have taught me an immense amount about computational data analysis of large genomic datasets and brought new components to my training that will make me a better scientist. In particular, Steve’s enthusiasm for the intricacies of science and making

meaningful discoveries is truly infectious. Finally, I must extend a huge thanks to Rita Bottino and her team who processed a majority of the human pancreas/islet preparations in this Dissertation. None of this work would have been possible without their dedication, often working overnight to processes the organ in a timely fashion.

I am very grateful to my previous labs who helped build my scientific curiosity and set me on this path. Dr. Mark Fisher of Kansas University Medical Center (KUMC) enthusiastically welcomed me into science and his passion for molecular chaperones and the ways in which proteins assumed and moved between specific conformational states showed me what it meant to do what you love. Dr. Fisher is no longer with us, but I very much hope he knows he was the spark that lit my interest in scientific research. Dr. Jed Lampe of KUMC oversaw me in some of my earliest days in the lab when my ratio of questions to productivity was probably 100-to-1 which I'm certain was challenging as a new PI but I am thankful for his investment in me. Dr. Joshua Maurer of Washington University in St. Louis showed me how to be cutting edge in our application of novel chemical tools across disciplines to make biological discoveries. He trusted me a more independent scientist and gave me great opportunity to grow in ability to form hypotheses and venture into scientific writing.

Family and Friends

I would like to thank my friends both in Nashville and across the country who have supported me during my PhD. Spending this amount of time so singularly focused on a topic is not always the most relatable, but I greatly appreciate all those who have humored me with interest in what I do on a daily basis and provided much needed escapes from the lab. A special thank you to our dear friends in Nashville, Caleb, Elizabeth, Joe, Christelle, Cam, Liz, Ben and Virginia for being an exceptional crew to take on this unique path through all the twists and turns and ups and down with.

I am extremely thankful to my family whose unconditional support has undoubtedly gotten me to where I am today. My successes are a direct reflection of the values, work ethic, and perpetual curiosity that I get from all of them. My mom has shown me everyday what it means to be selfless and put the dreams of her children above herself—it does not go unnoticed. My dad has believed in me and provided the resources and environment for me chase my passions. And he continued to support me even after he figured out the numbers on the return on investment of pursuing additional training to become a researcher in addition to a clinician. My siblings, Elli, Dan, and Abby, are my rocks who I can always count on. They inspire me daily by demonstrating what can be achieved with hard work and bring immense joy to my life. My grandparents have been true role models and sources of constant support. My in-laws, Sara, Dean, Savannah, Rainey, Barbara, and Dean, welcomed me into their family, encouraged me unconditionally, and took a personal interest in the things I was studying. Gaining a second family has benefitted me in so many ways and their belief in me has helped me get to this point.

I cannot overstate how thankful I am for my wife, Brooke. She is my forever partner and should probably be getting an honorary doctorate. She has arranged her life in such a way that

supports my dreams no matter what it turns out that means. She changed jobs and moved to Nashville for our relationship. She has dealt with my bad moods after long days that didn’t turn out well and encourages me to keep at it. She shares in my excitement when we made breakthroughs and inspires me to always be pushing my boundaries. I am thankful for all the times she has let us schedule plans around an experiment or deadline and has made my training as much of a priority for her as it is for me. She has been with me through the trying times and built back our home together. She is my best friend, and I could not have tackled this without her. I would be remiss if I did not also thank my dogs, Ruby and Parker for bringing a great deal of joy and balance to my life; Parker gets the award of never going to bed without me which led to some late nights for him.

TABLE OF CONTENTS

LIST OF TABLES

LIST OF FIGURES

LIST OF ABBREVIATIONS

ADI	Alberta Diabetes Institute IsletCore
AHN	Allegheny Health Network
ANOVA	Analysis of variance
ARX	Aristaless-related homeobox
ATP	Adenosine triphosphate
AUC	Area under the curve
BMI	Body mass index
cAMP	Cyclic adenosine monophosphate
Cav1	Caveolin-1
CFRD	Cystic fibrosis related diabetes
CNS	Central nervous system
ColIV	Collagen IV
DAPA	Dapagliflozin, an SGLT2 inhibitor
DAPI	4’6-diamidino-2-phenylindole
DREADD	Designer receptor exclusively activated by designer drugs
ECM	Extracellular matrix
EC	Endothelial cell
ER	Endoplasmic reticulum
ESC	Embryonic stem cell
Ex-4	Exendin-4
FACS	Fluorescence-activated cell sorting
FBS	Fetal bovine serum
FGF	Fibroblast growth factor
FOXA2	Forkhead box A2
GABA	gamma-aminobutyric acid
GCK	Glucokinase
GDM	Gestational diabetes mellitus
GFP	Green fluorescent protein
GLP-1	Glucagon-like peptide 1
GLUT	Glucose transporter
GPCR	G-protein coupled receptor
GSIS	Glucose-stimulated insulin secretion
GTT	Glucose tolerance test
HbA1C	Glycated hemoglobin
HIRN	Human islet research network
HLA	Human leukocyte antigen
HNF1A	Hepatic nuclear factor 1 alpha
IAPP	Islet amyloid polypeptide
IEQ	Islet equivalent
IHC	Immunohistochemistry
IIAM	International Institute for the Advancement of Medicine
IIDP	Integrated Islet Distribution Program

iPSC	Induced pluripotent stem cells
ISD	Immunosuppressive drugs
MAFA	V-maf musculoaponeurotic fibrosarcoma oncogene homolog A
MAFB	V-maf musculoaponeurotic fibrosarcoma oncogene homolog B
MODY	Maturity-onset diabetes of the young
ND	Non-diabetic Donors
NDM	Neonatal diametes mellitus
NDRI	National Disease Research Interchange
NGN3	Neurogenin 3
NKX2.2	Nirenberg and Kim 2 homeobox 2
NKX6.1	Nirenberg and Kim 6 homeobox 1
nPOD	Network for Pancreatic Organ Donors with Diabetes
NSG	NOD-*scid*-*IL2rγ*^{null}
PAX6	Paired box 6
PDX1	Pancreatic and duodenal homeobox 1
PHHI	Persistent hyperinsulinemic hypoglycemia of infancy
PKA	Protein kinase A
PP	Pancreatic polypeptide
PTDM	Post transplantation diabetes mellitus
RFX6	Regulatory Factor X 6
RT-PCR	Quantitative reverse transcription polymerase chain reaction
scRNA-seq	Single cell RNA-sequencing
SGLT2	Sodium-glucose cotransporter 2
TCA	Tricyclic acid (citric acid)
TGF-β	Transforming growth factor β
T1D	Type 1 diabetes
T2D	Type 2 diabetes
VEGFR2	Vascular endothelial growth factor receptor 2
5-HT	Serotonin

CHAPTER I:
BACKGROUND AND SIGNIFICANCE

Some text and figures in this chapter have been published in Walker, Saunders et al. 2021[1].

The pancreatic islet

Anatomy and physiology

The pancreas, which is broadly divided into head, body, and tail regions, lies behind the stomach in back of the abdominal cavity, with the head positioned in the curve of the duodenum and the tail extending towards the spleen (**Figure 1**) and is a dual function organ responsible for controlling both food digestion and blood glucose homeostasis. The exocrine compartment, which makes up 98% of the pancreas mass, encompasses clusters of cells arranged in acini that secrete digestive enzymes including proteases, amylases, nucleases, and lipases into a branched ductal network that joins the common bile duct and releases into the small intestine to break down macromolecules in food[2,3]. The endocrine compartment is composed of pancreatic islets, vascularized and innervated mini-organs that are dispersed throughout the gland. Islets are composed primarily of endocrine cells: α cells, which secrete glucagon; β cells, which secrete insulin; δ cells, which secrete somatostatin; γ cells (formally called pancreatic polypeptide cells), which secrete pancreatic polypeptide (PP); and ε cells, which secrete ghrelin (**Figure 1**). The islet also contains capillaries (endothelial cells and pericytes), neuronal projections, resident immune cells, and fibroblasts. In contrast to exocrine cells, endocrine cells of the islet secrete their hormones directly into the blood stream though paracrine actions of these hormones within the islet are also important. Islet hormones from the pancreas are first delivered to the liver through the portal vein before reaching systemic circulation.

The primary function of the islet is to exert hormonal control on whole body glucose metabolism through the actions of the two primary hormones insulin and glucagon which are secreted in coordinated and pulsatile fashion[4–6]. Insulin lowers blood glucose by stimulating glucose uptake in peripheral tissues such as muscle and fat and promoting the liver to suppress glucose production and increase glycogen synthesis (**Figure 2**). In contrast, glucagon, a catabolic hormone, raises blood glucose by acting on the liver to stimulate the breakdown of glycogen and to activate gluconeogenesis (**Figure 2**). While the tight control of blood glucose through regulation of carbohydrate metabolism is the classical role of the islet, insulin and glucagon also have important roles in lipid and protein metabolism where insulin, an anabolic hormone, promotes uptake and storage of amino acids and fatty acids while inhibiting the breakdown of lipids and proteins[7–9], while glucagon, a catabolic hormone, promotes the breakdown of lipids and proteins, particularly for use in gluconeogenesis[10–12]. In particular, recent work have highlighted a liver-α cell signaling axis where α cell-derived glucagon signals in the liver to control levels of circulating amino acid levels[13–17].

Tools to study human pancreatic islet physiology and pathophysiology

Given this central role of the pancreatic islet in glucose homeostasis, there is great interest in investigating the mechanisms of islet function. The human pancreas is a difficult organ to study in part because of the risk of live-biopsy of the pancreas and challenges in viable post-mortem tissue processing due to from auto-digestion of exocrine tissue. As such, investigation of pancreatic islet biology has been greatly advanced by the use of numerous experimental animal model systems which have produced critical insight into islet physiology and pathophysiology. However, we continue to learn that in some circumstances, model systems may not translate into clinically relevant information[18–21]. Importantly, human islets show a number of key differences from rodent islets including their endocrine cell composition and arrangement, vascularization, gene expression, glucose set-point, both basal and stimulated insulin and glucagon secretion (key differences highlighted below)[22–26].

To overcome these differences, a great effort has been placed on increased availability of human islets and human pancreata for research in the past decade. Numerous groups have helped develop infrastructure to collect pancreatic tissue and islets from same donor along with the donor's de-identified medical record in order to place findings in the appropriate clinical context. Additionally, building off knowledge gained from rodents, numerous human-based model systems and approaches have been developed (**Figure 3**) to probe various components of the islet. These include intact tissue which can either be analyzed in a static manner in fixed/frozen sections or studied as live pancreas slices and isolated islets which can be studied in vitro or in vivo through transplantation into immune-deficient mice. Aggregated organoids known as pseudoislets can also be used in analogous studies. Further, single cell analyses can be performed on primary islet cells, immortalized cell lines, or on β-like cells resulting from induced differentiation of embryonic stem cells or induced-pluripotent stem cells. A summary of these approaches and their advantages and disadvantages is shown in **Table 1**. This Dissertation includes many of these approaches including integrated study of the entire pancreas, use of tissue sections processed in multiple complementary ways, studies on isolated islets both in vitro and in vivo, and analyses of dispersed single cells from the islet. Further, a portion of this Dissertation describes the development and implementation of a new pseudoislet approach.

Islet composition

In contrast to rodent islets, which contain a β cell-rich "core" and α and δ cells on the periphery, adult human islets display more variability in composition and exhibit more heterotypic contacts between α, β, δ, γ, and ε cells[27–29]. While rodent islets typically consist of 75-80% β cells and 15-20% α cells, human islets have proportionately fewer β cells (45-65%) and more α cells (30-50%)[27–32] (**Figure 4**). Much less abundant are δ and γ cells (representing less than 10% each), with ε cells being particularly rare (estimated <1% of all islet cells)[30]. Islets range considerably in size (from approximately 50-500 μm in diameter), with an average of 1,500 cells per islet. Variability in endocrine cell ratios between individuals is mirrored by significant variation in β cell mass[33,34], though differences in endocrine cell distribution between pancreatic regions are relatively minor[35]. The exception is that γ cells are strikingly abundant in a posterior lobe of the pancreatic head region, referred to as the "uncinate process"[36–39]. Quantification of endocrine

cell populations has come from both isolated islets and pancreatic sections[27,30,32,40] but contribution of other cell types such as endothelial cells, stromal cells, leukocytes, neuronal elements, and extracellular matrix to islet volume has not been systematically examined. Interestingly, studies suggest that most δ cells are located close to islet capillaries and have an elongated shape as well as filopodia-like processes that increase their potential influence on non-immediate neighboring cells[41,42]. There is a growing evidence of a critical role of somatostatin and δ cells in regulation of islet function in health and disease; somatostatin is a potent paracrine inhibitor of both insulin and glucagon secretion[43].

Non-endocrine cells and the extracellular matrix of the islet likely play important, yet incompletely defined, roles in islet homeostasis – either by delivering nutrients and soluble factors or by providing signals that influence islet cell health and function[44]. While rodent islets are highly vascularized, with thick and highly fenestrated capillaries[45–48], human islets have a much lower vascular density[49,50] (**Figure 5**). Due to experimental limitations, knowledge of *in vivo* human islet vascularity and blood flow remains elusive, though a recent report suggests that blood flow may not be uni-directional[51,52]. Islet capillary networks are lined with elongated endothelial cells[53–55] and though it is clear pericytes are present, our knowledge of their function in human islets is still evolving[44,56]. Since endothelial cells respond to diverse stimuli such as hypoxia, angiogenic factors, and cytokines, and secrete growth factors, signaling molecules, and basement membrane components, it is likely that such interactions with human islet cells influence their function[57–60].

Neuronal processes and immune cells are found with human pancreatic islets, suggesting that these provide signals influencing islet hormone secretion. For example, neuronal processes project into the human islet from extra-pancreatic nerves and may enable modulation of islet function by the central nervous system[61,62]. Autonomic axons are closely associated with capillaries[63–65], setting up the possibility that they coordinate with endothelial cells to influence hormone secretion from the islet. Resident immune cells in islets largely belong to T cell and macrophage lineages, with occasional B cells[66–69]. Interestingly, these cells tend to be more numerous in peri-islet regions (representing the interface between endocrine and exocrine tissue[66,68]. Since islet macrophages are known to play crucial roles in mouse pancreas and islet development, their role in human islet development and in Type 2 diabetes (T2D)-associated inflammation is of great interest[70–72].

The human islet extracellular matrix (ECM) is unique in that human endocrine cells produce a basement membrane that is distinct from the basement membrane of the endothelium and is composed of collagens, heparan sulfate proteoglycans, and laminin[73–76]. The islet interstitial matrix consists of collagen, elastin, fibronectin, and various polysaccharides, and together with the basement membrane provides cell support and anchorage[54,59,77–79]. In addition, it is becoming increasingly appreciated that ECM also influences cell phenotype and function, signaling primarily through integrins but also providing a “sink” for secreted growth factors that interact with unique receptors[59,77–80]. It has also been proposed that the islet ECM provides a polarized microdomain to promote endocrine granule fusion[81,82].

Endocrine cell structure and identity

At the ultrastructural level, the common function of all islet endocrine cells is readily apparent: these cells are protein-producing, -packaging, and -secreting factories, with distinctive secretory granules that also serve as the site of most prohormone processing. The β cell has been most extensively studied, catalyzed by the identification of insulin secretory granules in early electron microscopy studies and seminal studies of prohormone processing[83–87]. Glucagon-containing secretory granules are similar in size to those of β cells, but their electron-dense cores are distinct, surrounded by a tightly fitted membrane and chromogranins and synaptophysin variably distributed throughout the granule[83,85,88]. Delta cells contain larger (450-800 nm) secretory granules with lower electron density with synaptophysin and chromogranins present throughout the granule matrix[41,83,85,88]. Less abundant γ and ε cells tend to have small secretory granules that resemble α cells[85,89,90].

Insulin is synthesized and secreted only by the islet β cell. Expression of the insulin gene *INS* and the components necessary for the processing and regulated secretion of insulin are controlled by a network of enhancer elements, transcription factors, and their coregulators which are crucial for both establishing and maintaining β cell identity[91–93]. Insulin is translated as a preprohormone and is processed to proinsulin upon cleavage of the signal sequence in the endoplasmic reticulum (ER) (**Figure 6**). Within the ER, proinsulin is folded and undergoes formation of three disulfide bonds (two between the A and B domain and one within the A domain)[94]. This proinsulin is trafficked through the Golgi apparatus into immature secretory granules where it is processed by the prohormone convertases PC1/3 and PC2 to release C-peptide[95]. Further, carboxypeptidase E removes C-terminal basic amino acids and mediates targeting to the secretory pathway for the 51 amino acid fully processed insulin[96].

To achieve high concentrations of insulin within these granules, mature insulin complexes with Zn^{2+} ions that are transported into the granule by ZnT8/*SLC30A8*[97]. These hexameric crystals form the dense core of mature insulin granules which must traverse through a cortical actin network before docking at the plasma membrane as part of a primed “readily releasable pool”[94,98]. These processes ensure that only a small portion of the overall insulin content within a cell is released in response to an appropriate signal. While insulin makes up the majority of the protein content of the insulin granules, there are other components within the granules. In addition to the aforementioned C-peptide and Zn^{2+} ions, the peptide islet amyloid polypeptide (IAPP), members of the neuroendocrine chromogranin family, and neurotransmitters such as adenosine-triphosphate (ATP), and serotonin (5-HT), among others are co-secreted with insulin from β cells[97].

Like insulin, preproglucagon gene expression is controlled by a network of transcription factors and regulatory elements[99]. Preproglucagon is predominantly expressed in intestinal enteroendocrine L cells, the pancreatic islet α cells and various regions of the brain[12,100]; however, the 160 amino acid proglucagon is processed in a tissue specific manner depending on expression of prohormone convertase enzymes[101,102] (**Figure 7**). α cells predominantly express PC2, which generates the 29 amino acid glucagon peptide along with the major proglucagon fragment, glicentin-related polypeptide, and intervening-peptide-1 in equimolar

amounts[101,103,104]. In contrast, enteroendocrine cells predominantly express PC1 which generates a variety of peptides including glucagon-like peptide 1 (GLP-1)[105]. The similarity of these peptide products has led to numerous challenges with specificity and cross reactivity of assays measuring glucagon[106]. Similar to insulin, mature glucagon is packaged into secretory granules in preparation for an exocytotic stimulus although less is known about the composition of α cell granules in comparison to β cell granules[100]. Further, α cells have been reported to have granules of various sizes and other more minor α cell secretory products such as acetylcholine have been hypothesized to be stored and secreted in a different fashion than glucagon[107].

Beyond distinctive hormones, secretory granules, and subcellular machinery, islet endocrine cells are often defined by their signature of cell surface proteins (*e.g.*, receptors, ion channels) or by a network of signaling molecules and transcriptional regulators that define cell identity and function. For example, canonical transcription factors in β cells such as MAFA, NKX6.1, PDX1, PAX6, NKX2-2, ISL1, NEUROD1, FOXO1 and FOXA2 are crucial for both establishing and maintaining β cell identity as well as coordinating production and secretion of insulin[108–112]. All β cells are not the same, as heterogeneity and different β cell subsets have been defined by cell surface markers and cell function[113–115]. Similarly, α cells express factors regulating glucagon production and secretion, notably ARX, IRX1/2, MAFB, PAX6, NKX2-2, ISL1, NEUROD1, and FOXA2[108–110,116]. Less is known about regulatory networks in δ, γ, and ε cells, but HHEX is thought to direct δ cell differentiation[117,118], and γ and ε cells express subsets of transcription factors also found in α cells[108,119]. While there are clear similarities in cellular identity markers between human and non-human islets, there are some important differences, most highlighted by discrepancies in the phenotype of certain forms of monogenic diabetes in mice and man[116,120]. For example, while mice and humans heterozygous for PDX1 mutations are phenotypically similar[121–124], heterozygous mutations in HNF1α, HNF4α and other MODY transcription factors do not appear to result in similar islet dysfunction in mice compared to that seen in man[125–127]. Moreover, compensatory mechanisms likely differ; for example, while Ngn3-deficient mice do not develop endocrine cells at all, NGN3 loss-of-function mutations in humans produce variable (and less severe) phenotypes[116,128,129].

β cell function

Nutrient control

Glucose-stimulated insulin secretion (GSIS) involves the coordinated relay of metabolic, electrical, and chemical signals within the β cell[130–136]. A representative insulin secretory profile from islet perifusion and a schematic of β cell signaling with the components of the GSIS pathway highlighting the secretagogues within the perifusion is shown in **Figure 8A** and **8B**.

One unique aspect of GSIS in human β cells is that the facilitated diffusion of glucose occurs via transporter GLUT1, in contrast to GLUT2 in rodent β cells[137–139], while most subsequent steps in this glucose triggering pathway are thought to be similar in non-human and human β cells. After entry into the cell, glucose is phosphorylated by glucokinase (GCK) to generate glucose-6-phosphate (G6P)[24,140]. As GLUT1 is insulin-independent, glucose transport into the β cell is not

limiting. Instead, GCK's relatively low affinity for glucose allows it to act as the rate limiting step for glucose flux into glycolysis and exert significant control on whole-body glucose homeostasis. Glucose metabolism in the β cell through both glycolysis and the TCA cycle ultimately lead to the generation of ATP from ADP. This increase in ATP:ADP ratio closes ATP-sensitive K^+ (K_{ATP}) channels on the plasma membrane, depolarizing the membrane and converting the metabolic signal into an electrical signal. With sufficient membrane depolarization (~ -50 mV), voltage gated Ca^{2+} channels open leading to an influx of Ca^{2+} which then triggers exocytosis of insulin granules and insulin is secreted[141]. As the major stimulus for exocytosis, intracellular Ca^{2+} is tightly regulated, primarily by the ER[142]. Indeed, stimulated β cells undergo characteristic Ca^{2+} oscillations that reflect this tight regulation[143]. Ca^{2+} ions are transported into the ER by sarco-ER Ca^{2+}-ATPase (SERCA) pumps and are released in response to various signals including Ca^{2+}-induced Ca^{2+} release (CICR). Further, β cells within an islet synchronize their electrical and Ca^{2+} responses through gap junctional coupling. Importantly, this coupling is crucial to a robust insulin secretory response as individual β cells do not respond with the same magnitude or dynamics as an intact islet[144,145].

Glucose metabolism also has a potentiating effect on insulin secretion via the so-called amplifying pathway[146–149] that is downstream of intracellular Ca^{2+} increase and thought to be mediated by mitochondrial-derived metabolic coupling factors such as guanosine triphosphate, isocitrate, or NADPH[133,150–154]. Thus, mitochondrial metabolism is crucial for both the generation of ATP as well as the intersection of various metabolic pathways and the regulation of these coupling factors[155–158]. The triggering and amplifying pathways help to create the characteristic bi-phasic insulin secretory response seen *in vitro* with an abrupt increase in glucose (**Figure 8A**).

While glucose is the primary physiological regulator of insulin secretion, circulating amino acids such as arginine, leucine, alanine, glutamine, and glycine [159–162], metabolites such as glutamate[163], and lipids[164] can also influence insulin secretion. For amino acids, this effect may be mediated by transport and metabolism, through binding to extracellular receptors, or via direct depolarization of the plasma membrane[165]. Glutamate, an excitatory neurotransmitter, may signal through ionotropic or metabotropic glutamate receptors to influence insulin secretion, though the significance of these pathways in human β cells is not as well understood[166,167]. Importantly, amino acids may also influence insulin secretion indirectly, particularly through the α cell[168]. In addition to intracellular lipid metabolism providing a pool of lipid signaling molecules that contribute to the amplifying pathway, extracellular fatty acids can signal though G-protein-coupled-receptors (GPCR), the most well studied being GPR40 (FFAR1), a G_q-coupled GPCR activated by medium and long chain fatty acids[169–172].

Neurohormonal control

While nutrients are the primary driver of the insulin secretory response, other neurohormonal signals act to modulate and optimize insulin secretion (**Figure 9**). This is most clearly illustrated by the fact that oral glucose delivery results with a much greater increase in plasma insulin levels compared to the same amount of glucose given intravenously[173,174]. This phenomenon, known as the incretin effect, was discovered to be due to hormones secreted from

enteroendocrine cells of the intestine, most notably GLP-1 from L cells and glucose-dependent insulinotropic polypeptide (GIP; formally gastric-inhibitory polypeptide) from K cells, which act through GPCRs[175–181]. Receptors for GLP-1 and GIP are G_s-coupled GPCRs that primarily signal by activating adenylyl cyclase to increase cyclic adenosine monophosphate (cAMP) (**Figure 8B**)[182–186]. Signaling from GLP-1 and GIP alone is not sufficient to stimulate insulin secretion but acts synergistically to potentiate GSIS[179,187,188]. Epinephrine, a sympathetic hormone primarily from the adrenal glands acts to raise blood glucose and prevent hypoglycemia in part by inhibiting insulin secretion (**Figure 8A**). Epinephrine is a ligand for multiple receptors, but human β cells primarily express α_2-adrenergic receptors, G_i-coupled GPCRs that signal by inhibiting adenylyl cyclase to reduce cAMP and by activating G-protein-coupled inwardly rectifying potassium channels (**Figure 8B**)[189,190].

While systemic signals are crucial in the control of insulin secretion, the structure of the islet creates a unique microenvironment for local intra-islet signals[131,134,191]. There are many secreted factors from the various cells within the islet which can often act on numerous receptors and cell types, thus in this chapter we highlight a selection of the most well studied factors (**Figure 9**). These paracrine signals, which have been shown to be active in human islets but have been mechanistically studied primarily in non-human islets, allow for an additional layer of β cell control. Indeed, individual β cells do not display the same coordinated secretion pattern seen in intact islets; paracrine signals from α cells are crucial in establishing species-specific glycemic set points [26,135]. Recent work has demonstrated that within islets, β cells may take on different roles – some may be fine-tuned to be more sensitive to glucose and act as a pacemaker or "hub" β cell in the islet[192,193]. These studies, which were performed in mice, are supported by mathematical modeling of human islets[113,194], but require more work to clearly establish this concept in human islets. Further, the means by which these hubs cells may transmit signals remains debated[195–197].

Despite the opposing physiological actions of insulin and glucagon, glucagon can regulate and potentiate insulin secretion[198]. The glucagon receptor (GCGR) is expressed by β cells and is a G_s-coupled GPCR acting through cAMP[199]. The GCGR has a high degree of sequence homology with GLP-1R[175] and several groups have demonstrated that the ligands to these receptors, glucagon and GLP-1, respectively, are capable of activating either receptor[168,200,201]. Physiologically, this is thought to predominantly manifest as α cell-derived glucagon signaling through both GLP-1R and GCGR on the β cell; however, as GLP-1 is also derived from proglucagon, GLP-1 produced within the islet may contribute to islet signaling[202,203]. This foundational α-to-β cell communication within the islet also sets up scenarios where nutrient signaling to the β cell, such as from amino acids, can come indirectly through the α cell[168].

It is becoming clear that δ cells provide important local inhibition to β cells. The regulation of δ cells is not as well understood, but somatostatin secretion increases with glucose in a dose-dependent manner and involves calcium-induced calcium release[132,204,205]. Somatostatin secretion may also be stimulated by local signals, including the peptide urocortin3 released from β cells or by ghrelin from ε cells[206,207]. Somatostatin signals to the β cell through one of five SSTR isoforms, with SSTR2 thought to be the most prominent in humans[208,209]. All isoforms are

G_i-coupled GPCRs that signal similarly to the α_2-adrenergic receptor discussed above. Thus, under physiologic conditions, while somatostatin provides inhibitory feedback to modulate and possibly prevent the over secretion of insulin, it does not completely block insulin secretion[132,210].

Other signals derived in the islet that modulate hormone secretion include ghrelin, extracellular ATP, serotonin, γ-aminobutyric acid (GABA), and acetylcholine. Ghrelin is secreted primarily from cells of the gastric mucosa and would be delivered to islets in the circulation, but it can also be secreted locally in the islet by ε cells. It is most well-known for its role as an appetite stimulant but also acts to inhibit insulin secretion via the growth hormone secretatgogue receptor (GHS-R) which is G_i-coupled in β cells[211–215]. ATP is stored in insulin granules of the β cell and can be co-secreted with insulin or secreted by "kiss-and-run" exocytosis where dense insulin cores are retained within the granule [216,217]. Human β cells primarily express ionotropic purinergic (P2X) receptors, thus setting up an autocrine feedback network[218,219]. These receptors are permeable to Na^+, K^+, and Ca^{2+}, and thus when activated depolarize the cell and increase insulin secretion. In addition, ATP can be converted to ADP, AMP or adenosine via ectonucleotidases such as NTPDase3, a highly specific human β cell specific marker[220].

Serotonin, a monoamine neurotransmitter, is produced by the β cell and co-secreted from insulin granules[221]. Serotonin signaling is particularly important during pregnancy, when its increased production mediates islet adaptations to metabolic demands[222,223]. Serotonin can signal on numerous receptors on the β cell, including the G_q coupled 5-HT_{2B} receptor and the excitatory ionotropic 5-HT_3 depending on the context[224]. In addition, 5-HT intracellular has been shown to lead to serotonylation of small GTPases in a receptor independent fashion[225].

GABA, the major inhibitory neurotransmitter in the central nervous system (CNS), is derived from glutamate via glutamic acid decarboxylase (GAD) and is synthesized in β cells at some of the highest levels outside the CNS[226]. While small amounts of GABA may be released with insulin granules, most GABA is secreted independently of glucose from the cytosol of β cells via an alternative pulsatile secretory pathway[227]. Human β cells express the ionotropic $GABA_A$ receptors which are permeable to Cl^- when activated[228]. Acetylcholine is the major neurotransmitter of parasympathetic nerves; however, parasympathetic innervation is relatively sparse in the human islet and thus the major local source of acetylcholine is likely the α cell[64,229]. Acetylcholine signaling is complex, with multiple receptors at play, though the G_q-coupled M3 receptor is thought to be the primary cholinergic receptor in β cells[230]. Acetylcholine signaling generally has a stimulatory effect on β cells though this is dependent on the surrounding conditions[107,231,232].

α cell function

Nutrient control

In comparison to glucose-stimulated insulin secretion, the molecular mechanism by which glucose regulates glucagon secretion is far less clear, with multiple, often contradictory, hypotheses presented and no single model explaining all the dynamics of glucagon release [100,233–237]. Furthermore, even less is known about human α cells; thus, much of glucagon secretion modeling is based on studies of non-human islets or α cells. Since the cell

arrangement and islet composition differ considerably in human islets, one must be cautious in extrapolating studies in rodent islets to glucagon secretion by human α cells. A representative glucagon secretory profile from islet perifusion and a schematic of presumptive α cell signaling pathways related to Ca^{2+} and cAMP with components that relate to the perifusion highlighted is shown in **Figure 8C** and **8D**.

Human α cells express several of the same key components in the glucose sensing pathway as β cells, including GLUT1 and GCK, suggesting that they may have a similar mechanism to intrinsically sense and respond to glucose[238,239]. However, compared to β cells, α cells have different expression and localization of numerous ion channels including voltage-dependent Na^+ channels and T-, L-, and P/Q-type Ca^{2+} channels, leading to a substantially different electrophysiologic profile[233,235,240]. Like in the β cell, depolarization of the α cell induces a rapid influx of Ca^{2+} and secretion of glucagon; however, unlike the β cell, it is not well understood how changes in glucose concentration relate to membrane polarization[233,241].

Significant research has been devoted to understanding how the K_{ATP} channel may function in the α cell[242–245]. A K_{ATP}-centric model of α cell regulation postulates that under low glucose conditions, K_{ATP} channels are mostly closed and generate sufficient activity to open P/Q Ca^{2+} channels. With high glucose, metabolism leads to closure of the remaining K_{ATP} channels and inactivation of voltage dependent Na^+ channels, thereby preventing voltage-dependent Ca^{2+} channels from opening and inhibiting glucagon secretion. In contrast, the endoplasmic-reticulum dependent model proposes that a key role of glucose derived ATP is to activate SERCA pumps to drive Ca^{2+} into the ER[246–248]. In low glucose, low ATP leads to low SERCA activity and a net release of Ca^{2+} from the ER. This activates the depolarizing store-operated pathway, leading to activation of voltage-dependent Ca^{2+} channels and glucagon release. In high glucose, abundant ATP activates SERCA pumps and shut down the store-operated pathway, thus inhibiting glucagon release.

While these models place significant emphasis on Ca^{2+} in the control of glucagon secretion, there is abundant evidence that its role is more complex and nuanced[249]. In the α cell, Ca^{2+} changes are modest, and oscillations are not as synchronous as they are in β cell[233,249]. Further, while there is a positive correlation of Ca^{2+} signal and glucagon secretion at low glucose, the two are uncoupled at high glucose[250]. In fact, α cell Ca^{2+} activity appears to elevate with high glucose despite glucagon secretion decreasing[251]. This suggests, additional signals likely work in concert with Ca^{2+} to regulate glucagon secretion, a role that may be filled by the second messenger cAMP which can act in parallel to Ca^{2+} in the α cell[252]. cAMP acts primarily through cAMP-dependent PKA and exchange proteins activated by cAMP (EPACs) and may even be under direct control from glucose[253].

While the traditional role of the islet has centered on hormonal control of glucose levels, recent work has highlighted that glucagon, in particular, has a fundamental role in regulating protein metabolism and amino acid homeostasis. Interrupting glucagon signaling in the liver leads to elevations in circulating amino acids, which in turn can induce α cell proliferation[254–259]. In addition to regulating α cell mass, amino acids such as arginine, glutamine, and alanine have

long been recognized as a strong stimulatory signal for glucagon secretion, which physiologically protects against insulin-induced hypoglycemia after a protein-rich meal[260–262]. The cellular mechanisms behind amino acid-induced glucagon secretion are poorly defined but likely involve a combination of metabolic, electrical, and receptor-mediated processes depending on the individual amino acid[165,263–266]. The fact that amino acids can stimulate glucagon secretion independently of glucose has suggested the possibility that they play a primary role in glucagon secretion[168,200,267].

Lipids may also play a role in regulating glucagon secretion, though the precise effects and mechanisms in human islets have not been well studied[263]. In humans, lipid ingestion or IV injection has varied effects on glucagon secretion[268,269]. Fatty acid stimulation of glucagon secretion is concentration-dependent and varies with chain length. It is thought to be mediated by the G_q-coupled FFAR1 signaling through calcium[270,271].

Neurohormonal control

Circulating hormones can also modulate α cell function. Most notably, epinephrine, a strong stimulus for glucagon secretion as part of the counter-regulatory response to hypoglycemia, can signal through multiple receptors. In the α cell it is thought to primarily signal through the β_2-adrenergic receptor, a G_s-coupled GPCR, and the α_1-adrenergic receptor, a G_q-coupled GPCR[272]. Activation of both receptors may explain why epinephrine is such a potent stimulus, increasing both cAMP and Ca^{2+} within the α cell[273–275].

Paracrine signaling likely plays a fundamental role in the control of α cell secretion of glucagon[134,136,233,276] (**Figure 9**). Most notably, isolated α cells do not respond appropriately to stimuli (glucose in particular), which suggests that signals and interactions within the islet microenvironment are necessary for appropriate α cell function[277,278]. These paracrine actions are thought to be particularly important in high glucose environments when the β and δ cell derived products are highly secreted, but their relative contribution in low glucose environments is still an active area of research.

Given their abundance within the islet, β cells are likely a prime source for local regulation of glucagon secretion, with insulin being the prime source as the most abundant β cell secretory product[279]. α cells express the insulin receptor, a transmembrane receptor tyrosine kinase that autophosphorylates itself when activated with insulin and initiates a signaling transduction cascade. The precise downstream signaling induced in the α cell by insulin is not fully understood but may include activation of phosphodiesterases to breakdown cAMP or activation of K_{ATP} channels to hyperpolarize the α cell and close voltage-dependent Ca^{2+} channels and ultimately inhibiti insulin secretion[280,281]. Interestingly, insulin signaling can also cause translocation of $GABA_A$ receptors, allowing it to thus act in concert with another β cell secretory product, GABA[282]. When ionotropic $GABA_A$ receptors on the α cell are activated they become permeable to Cl^- and thus hyperpolarize the α cell[283,284].

Other β cell-derived molecules include serotonin, which can act on G_i-coupled 5-HT_{1F} GPCRs on α cells to lower cAMP and inhibit glucagon secretion[221], and ATP, which can signal through

G_q-coupled $P2Y_1$ receptors on α cells to increase intracellular Ca^{2+}. β cell-derived ATP may explain elevations in intracellular Ca^{2+} in α cells at high glucose despite reduced glucagon secretion[285,286], thus providing a signal to balance the other inhibitory signals from β cells. Further, juxtacrine signaling from nearby islet cells may also help regulate α cells. Recently, EphA forward signaling through the EphA4 receptor on α cells was shown to provide tonic inhibition of glucagon secretion through maintenance of F-actin density that was lost in isolated α cells[287].

Somatostatin secretion from δ cells provides important local inhibition to the α cell[132]. Like β cells, human α cells primarily express the SSTR2 receptor, a G_i-coupled GPCR shown to reduce cAMP in the α cell and robustly inhibit glucagon secretion[208,288,289]. The unique distribution of δ cells has also led to numerous models whereby other signals ultimately affect glucagon secretion through δ cells. For example, acetylcholine, which is secreted by human α cells, can stimulate δ cells and thus provide indirect negative feedback[135,230].

Finally, autocrine signaling by α cells may help regulate glucagon secretion. Glutamate, an abundant amino acid but also a major excitatory neurotransmitter, is packaged in α cell granules and co-secreted with glucagon[290]. Human α cells express ionotropic α-amino-3-hydroxy-5-methyl-4-isoxazolepropionic acid (AMPA) receptors capable of responding to glutamate by allowing Ca^{2+} and Na^{+} entry into the cell; thus, signaling through these receptors both depolarizes the cell and increases intracellular Ca^{2+} to act as a positive autocrine signal[291]. In addition, it has been suggested that α cells express G_s-coupled glucagon receptors that would signal by increasing cAMP as well [292]. Thus, there are numerous potential pathways for positive autocrine signaling in the α cell, which may explain how relatively minor changes in other stimuli (such as lowered glucose) can so effectively promote glucagon secretion[291].

Diabetes mellitus

Diabetes mellitus is a metabolic disease characterized by abnormally elevated blood glucose levels, or hyperglycemia. The 2020 National Diabetes Statistics Report (CDC) estimates that 34.2 million US individuals—10.5% of the total population—had diabetes in 2018, with another 88 million US adults having prediabetes[293]. The consequences of hyperglycemia include microvasculature complications including retinopathy, autonomic neuropathy, and nephropathy along with macrovasculature complications including cardiovascular disease and stroke. The social and economic burden of diabetes is substantial within the U.S. as direct and indirect estimated costs were $327 billion in 2017 and diabetes was the seventh leading cause of death[293].

The classification of diabetes is still quite rudimentary, with the categories of diabetes based on clinical criteria rather than molecular pathogenesis. The most common form of diabetes is type 2 diabetes (T2D) which accounts for ~90-95% of all cases and is characterized by a relative insulin deficiency. Type 1 diabetes (T1D) is characterized by a near complete insulin deficiency and accounts for ~5% of total cases. Less commonly, diabetes can result from genetic mutations, such as neonatal diabetes mellitus or maturity-onset diabetes of the young (MODY)

or even be secondary to other medical conditions such as post-transplantation diabetes mellitus. Major types of diabetes are summarized in **Table 2**. While nearly all forms of human diabetes are associated with impaired islet cell function and/or reduced β cell mass, the molecular events and mechanisms leading to dysfunction or reduced mass in different forms of human diabetes are either incompletely characterized or largely unknown[294,295].

Type 1 diabetes

T1D is characterized by a dysregulated autoimmune response of both the adaptive and innate immune system, ultimately resulting in destruction of β cells. Recent consensus divides the natural progression of T1D into three stages (**Figure 10A**). Stage 1 is characterized by the presence of 2 or more islet autoantibodies and is thought to mark the initiation of β cell loss despite maintenance of normoglycemia[296,297]. The autoimmune process is thought to be initiated or potentiated by a triggering event, such as early life exposure to food antigens or exposure to certain viral infections, although the triggering event is likely different in different individuals. Stage 2 is characterized by dysglycemia and dysfunctional insulin secretion in response to glucose challenge, while stage 3 is characterized by symptom onset and is thought to occur after loss of ~60-90% of an individual's β cell mass, though exact quantification is not currently feasible[298]. Despite this general model, there is poorly understood T1D heterogeneity in terms of age of onset, rate of disease progression, and residual C-peptide production[299,300]. For example, one report estimated that as many as 40% of T1D patients developed the disease after the age of 30[300], while T1D has also been reported to occur within the first six months of life[301]. Borrowing a paradigm from other diseases with clinical heterogeneity, the emerging concept is that there are "endotypes" of T1D based on incompletely defined genetics and pathologic processes[302,303].

Islet-immune interactions are crucial in T1D. Modest insulitis, or lymphocytic infiltration of the islet, is a hallmark pathologic feature of T1D – though there is significant variability in cellular composition and frequency of insulitis among donors[304,305]. Insulitis is often characterized by tight focal aggregation of immune cells at one islet pole and the immune cells are primarily CD8+ T cells, though B cells, CD4+ T cells, and macrophages may also be present[299,306–308]. Islet β cells in T1D show elevated expression of HLA class I and class II components, potentially facilitating autoimmune surveillance and destruction[309,310]. Furthermore, a majority of identified genetic loci associated with T1D are linked to immune-related genes with HLA loci accounting for more than 50% of the risk[297,299]. Understanding the role that β cells play in the autoimmune process is of great interest, with the growing sense that β cells or the β cell response contributes to β cell demise[311]. Recent multiplexed imaging studies have highlighted that prior to destruction, β cells lose markers of cell identity and show altered protein expression, though it is unclear if these changes are indicative of adaptations to avoid immune detection or pathologic changes that invite destructive, autoreactive T cells[40,312]. Interestingly, β cells that remain in T1D appear to have nearly normal insulin secretion profiles, highlighting that T1D defects are primarily related to changes in β cell mass rather than function[313].

While T1D pathophysiology is primarily focused on β cells, there is evidence for the involvement of other cell types in the pancreas. Individuals with T1D have an impaired counter regulatory

response that can lead to potentially dangerous hypoglycemia. This defect is multifactorial but appears to involve dysregulated glucagon secretion and compromised gene expression in α cells in T1D[313–316]; how the α cell responds to the immune and metabolic stresses of T1D, as well as to the loss of local paracrine signaling from β cells and disrupted islet architecture, will be important to define going forward. Further, there is emerging evidence for involvement of the entire pancreas in T1D pathogenesis, as individuals with T1D have significantly smaller pancreas size characterized by a loss of acinar cell number, highlighting an important, but understudied, interaction of islet pathology with exocrine tissue[317–320].

Type 2 diabetes

T2D is a very heterogenous disorder from a clinical standpoint, with likely multiple molecular pathways and time courses to reach hyperglycemia. T2D is characterized by islet dysfunction, defined by insufficient insulin secretion from β cells and inappropriate glucagon secretion, often on a background of peripheral insulin resistance that arises in states such as obesity or advancing age[321]. Insulin resistance in T2D tends to stay comparatively stable throughout disease while β cell functional mass declines, highlighting both initial and progressive β cell failure as a key determinant of T2D pathogenesis (**Figure 10B**)[322]. This decline in insulin production mirrors the clinical disease course where escalating treatment paradigms are needed to promote glucose homeostasis[323]. Rather than the development of insulin resistance being the primary event, an alternate hypothesis for the sequence of events leading to T2D is that insulin hypersecretion and subsequent hyperinsulinemia is the initial defect, with the hyperinsulinemia leading to insulin resistance and obesity that eventually results in β cell failure[324].

While there are ongoing arguments about whether T2D is accompanied by reduced β cell mass or reduced β cell function, most favor a combination of the two. For example, cross sectional post-mortem studies suggest a mild reduction in β cell mass in T2D, but there is significant overlap in β cell mass among T2D and normal individuals. Thus, it remains unclear whether this mild mass reduction is the result of disease-associated β cell loss or merely a different baseline in β cell mass that gives rise to differential susceptibility to T2D[325–330]. The central role of the β cell is further highlighted in GWAS studies, where the majority of the loci identified are related to β cell biology[331–335]. The identified GWAS variants (>500), which collectively explain only a small proportion of the overall genetic risk attributed to T2D, lie largely in non-coding regions that may allow them to have broad effects on β cell processes and function, but makes specific study of their effects challenging[336–338]. How most of the GWAS-defined loci contribute to T2D is still unclear, with many studies underway to examine the impact on islet function.

Mirroring the clinical heterogeneity in T2D, molecular studies suggest considerable variability and complexity in defects leading to inadequate insulin secretion. Indeed, there is increasing evidence that points to a complicated interplay of stress pathways and impaired β cell function as a major driver of decreases in β cell functional mass[339–341]. Components such as gluco- and lipotoxcity and chronic inflammation are proposed to cause activation of stress pathways in the islet, including ER stress, oxidative stress, cytokine stress, and hypoxic stress[342–346]. However, many of these processes have only been studied in human islets manipulated *in vitro* and thus,

the actual molecular events of human islets in vivo remain uncertain. In addition, a subset of T2D islets shows amyloid, an aggregation of fibrillary IAPP hormone which is normally co-secreted from β cells[328,347,348]. This striking pathologic hallmark has prompted significant investigation into the pathologic processing that underlies aggregation in T2D islets, as well as whether the intermediate oligomers formed during amyloid formation or the end deposits themselves cause further stress to the islet[349–354]. These processes remain incompletely understood but are the topic of many ongoing studies.

While the β cell may initially be able to compensate for elevated insulin demand, islet function eventually fails and results in processes that may include dysregulated secretion, autophagy, loss of cell identity, dedifferentiation, and/or apoptosis. Despite this general paradigm, it should be noted that there is likely great variability in the relative contribution, temporal sequence, and underlying etiologies of these components in different populations and individual patients, reflecting individual differences in genetics and environment[321,355]. For example, T2D in youth is associated with faster and more substantial β cell deterioration than T2D in adults, underscored by a different response to diabetes-directed therapies[356]. This complex heterogeneity highlights the difficulty in making precise mechanistic determinations about islet dysfunction in T2D. While the focus is primarily on β cells, islet dysfunction in T2D involves other cell types as well. Notably, dysregulated glucagon secretion from α cells, particularly apparent with the failure glucagon suppression after a meal, results in increased hepatic glucose output and can exacerbate insulin insufficiency[357,358]. More work is needed to identify whether this α cell dysfunction in T2D results from intrinsic α cell defects, from the loss of appropriate paracrine signals from β cells, or from the metabolic environment in T2D. Additionally, T2D is associated with disruptions to non-endocrine cells including macrophages, endothelial cells, and pericytes that aid in overall function[56,60,359,360]. In particular, amyloid deposits in the T2D have been proposed to activate intra-islet macrophages and have also shown to disrupt intraislet vasculature[49,361,362].

Other forms of diabetes

While T1D and T2D are most common, there are many other forms of diabetes (**Table 2**). Gestational diabetes mellitus (GDM) occurs in individuals who do not appropriately respond to the metabolic challenges and insulin resistance of pregnancy[363–366]. Studies in rodents suggest that normally pancreatic β cells and islets compensate through increased insulin production and hypertrophy/hyperplasia; however, our knowledge of specific structural and functional changes in the human islet during pregnancy or during gestational diabetes is quite limited. After resolution of pregnancy, most individuals with GDM return to normoglycemia, but they are at significant increase risk for the future development of T2D relative to women who do not develop GDM[367].

In addition to polygenic forms of diabetes, there are also numerous monogenic forms of diabetes – these have greatly advanced the understanding of human islet development and function by highlighting critical genes for β cell differentiation, maturation, and insulin secretion. MODY is classically defined as monogenic diabetes with (1) onset before 25 years of age, (2) autosomal dominance inheritance, and (3) absence of autoimmunity[368]. While mutations have

been identified in >15 different genes, some familial forms of monogenic diabetes have no mutation yet defined. Identified subtypes generally are defined by mutations to genes related to transcriptional regulation (MODY1: *HNF4A*, MODY3: *HNF1A*, MODY4: *PDX1*, MODY5: *HNF1B*, MODY6: *NEUROD1*, MODY7: *KLF11*, MODY9: *PAX4*, MODY11: *BLK*), enzyme disorders (MODY2: *GCK*), protein misfolding (MODY8: *CEL*, MODY10: *INS*), ion channels (MODY12: *ABCC8*, MODY13: *KCNJ11*), and signal transduction (MODY14: *APPL1*) with MODY2 and MODY3 being the most common[369–371]. MODY subtypes are unified by their cause of a β cell defect and disruption of insulin release but generally have their own unique clinical, functional, and structural characteristics which have provided important clues into the role of the underlying genes in human islet biology[368,372,373].

In contrast to MODY, neonatal diabetes describes a monogenic form of diabetes that presents within the first 6 months of life. Like MODY, these mutations can lead to diabetes in a variety of ways but are unified in having a substantial effect on islets and β cells[374,375]. Common causes of neonatal diabetes include activating mutations in K_{ATP} channel genes *KCNJ11* or *ABCC8*, which misregulate channel opening and prevent insulin secretion [376–378]. In contrast, inactivating mutations in *KCNJ11* or *ABCC8*, leads to inappropriate insulin secretion and hyperinsulinism[379–381]. Mutations in the insulin gene or islet-enriched transcription factors can also cause neonatal diabetes[374,375].

Pancreatogenic diabetes, meaning diabetes resulting from disease processes in the exocrine pancreas such as chronic pancreatitis or a mutation in carboxyl-ester lipase, highlight the connection between the endocrine and exocrine pancreas[382]. Cystic fibrosis-related diabetes (CFRD) has become more frequent with the improved clinical outcomes in cystic fibrosis. CFRD usually requires insulin treatment, with reduced insulin secretion likely caused by islet loss, dysmorphia, and dysfunction that results from pronounced exocrine destruction and infiltration of immune cells, especially T-cells[383,384]. This pathology is not a direct impact of *CFTR* (cystic fibrosis transmembrane conductance regulator) mutations in β cells but rather is a result of *CFTR* mutations in the exocrine pancreas[382–384].

Post-transplantation diabetes, which also shares numerous risk factors with T2D, is a common but significant complication after organ and cell transplantation that threatens the health of both the graft and the transplant recipient[385,386]. Post-transplantation diabetes is likely multifactorial but is strongly associated with certain immunosuppressive agents[387–389].

Emerging therapeutic approaches to diabetes

Given the pancreatic islet's central role in all forms of diabetes, it follows that many new or emerging therapeutic approaches focus on impacting islets – especially preserving, replacing or enhancing β cell mass. Most emerging strategies have not yet been tested in humans with diabetes but can be divided into two broad categories: 1) β cell replacement and 2) maintenance, expansion, or modulation of functional β cell mass (**Figure 11**).

β cell replacement

In T1D and in some individuals with T2D, it would be highly desirable to replace or supplement the inadequate β cell mass. Within the approach of β cell replacement or transplantation, there are two sources of insulin-producing cells, one of which is islet transplantation (which replaces more than just β cells) and one of which uses insulin-producing cells that are derived from other cells but are technically not β cells. Whole pancreas transplantation is sometimes an option when combined with renal transplantation[390].

Islet allotransplantation in combination with immunosuppression has been the focus of intense efforts by many groups since the improved results of Shapiro and colleagues in 2000[391]. In this procedure, normal human islets isolated from cadaveric donor(s) are infused into the portal vein (percutaneous transhepatic portal vein delivery) with subsequent engraftment in distal liver vasculature[390,392,393]. This approach, which benefits from use of mature, fully functioning islets with relatively intact microenvironment and cell composition, has been effective in ameliorating life-threatening, severe hypoglycemia[394]. Improved quality of life after islet-after-kidney transplantation have been recently reported[395], but this therapeutic approach faces a number of significant challenges, including islet loss in post-transplantation period, need for lifelong immune modulation to prevent ongoing allo- and autoimmunity, need for islets from more than one donor pancreas in some transplant recipients, and β cell toxicity from common immunosuppressive agents[386,387,392,394,396,397]. Even if such challenges are overcome, the very limited supply of human islets will not allow widespread adoption of islet transplantation for T1D[390].

To develop a new source of β cells for transplantation, intense and ongoing efforts are directed towards creation of human β-like cells using human ESCs or human iPSCs[390]. Using knowledge from developmental islet biology, investigators have developed protocols involving sequential stimulation and inhibition of specific developmental pathways with growth factors and small molecules to generate insulin-producing cells that are glucose responsive and can reverse diabetes in mice[398–401]. In contrast to most islet transplant procedures, iPSCs could use a patient's own cells and remove alloimmunity concerns[402] though there are also efforts to generate islet-like cells capable of evading immune detection[403]. Directed differentiation is a rapidly evolving area of research with many recent protocol modifications, such as endocrine cell clustering[404], circadian entrainment[405], estrogen-related receptor γ expression[406], and enhanced transforming growth factor β (TGF-β) signaling[407]. Current efforts are focused on speeding up and refining the maturation process, improving dynamic insulin secretion, generating mono-hormonal cells. While this is an exciting area of research, there are important questions, including the safety profile, before transplantation of insulin-producing cells can move into the clinical area. For example, safety concerns about undifferentiated cells becoming transformed after transplantation remain, especially if cells were allografts and immunosuppression was needed. Additional questions include: 1) how many insulin-producing cells are needed for diabetes reversal as insulin production in these cells is less than that of native human islets; 2) how long these cells survive and function after transplantation, and 3) if transplantation of insulin-producing cells alone will be sufficient to restore glucose homeostasis

or whether a more complete islet microenvironment involving glucagon-producing cells[408] or other components of the native islet will be required.

Maintenance, expansion, or modulation of functional β cell mass

In many forms of diabetes, β cells remain but are not capable of meeting insulin demands. Here, therapeutic approaches seek to restore or bolster β cell function and maintain or expand β cell mass. In the cases of expanding β cell mass, there is also a need to ensure that the newly generated β cells are fully functional and ultimately, there may be an opportunity to combine approaches that stimulate β cell proliferation with those that bolster β cell function.

While attractive, improving β cell function has been a difficult therapeutic path since our current understanding of the reason(s) for impaired β cell function, and thus the target of intervention, is quite limited. As discussed earlier for T2D, multiple abnormalities have been postulated, but it is not known if one abnormality is primary or if there are multiple pathways to β cell dysfunction. The progressive nature of T2D indicates that most current antihyperglycemic medications such as sulfonylureas, meglitinides, metformin, and glitazones do not prevent the progressive decline in insulin secretory capacity[409]. Medications that modulate the GLP-1 pathway (GLP-1 receptor agonists and DPP-4 inhibitors) or target the sodium glucose transporter-2 (SGLT2) improve glycemic control and have positive impact on cardiovascular or renal outcomes, but the influence on human islet health and mass are largely unknown. Dual GIP and GLP-1 receptor agonists are also under investigation and have shown encouraging effects of β cell function and weight loss[410,411].

Importantly, several studies have indicated an ability for β cell function to improve in certain circumstances. Bariatric surgery appears to lead to improved β cell function, prior to significant weight loss, through a mechanism that is not yet determined[412–416]. Additionally, intensive dietary interventions (very low calorie or carbohydrate diets), particularly early in the T2D course, can lead to diabetes remission, but only do so when β cell function is restored[417–421]. For T2D particularly, defining how such interventions improve β cell function will potentially reveal additional ways to target these pathways.

An attractive approach has been to protect β cells and promote β cell survival in the face of cytokine, ER, or metabolic stressors that lead to β cell death. There are currently no therapeutics which have been definitively shown to mitigate deleterious effects of these stress pathways, but numerous targets have shown promise in preclinical or early clinical trials. In T1D, immune modulation through targeting immune cells or signals has shown promise in protecting β cells and slowing β cell loss[422–424]. In particular, teplizumab, an anti-CD3 (T cell) antibody, and golimumab, an anti-TNFα antibody, have shown promising results in phase 2 trials at delaying onset of clinical T1D or boosting endogenous insulin production, respectively[425,426]. Alternatively, numerous other targets focus on the β cell and seek to modulate its response to such stressors. The calcium channel blocker, verapamil, has been shown to promote β cell survival in patients with recently diagnosed T1D by reducing thioredoxin-interacting protein (TXNIP), which normally promotes apoptosis in β cells[427,428]. Targeting of the vitamin D nuclear receptor appears to promote β cell survival by modulating its

response to inflammatory and metabolic signals[429]. Modulation of prostaglandin E_2 receptor signaling with EP3 blockade and EP4 activation may also promote β cell survival[430,431]. Histone deacetylase 3 (HDAC3) inhibition protects from cytokine-induced β cell death perhaps by preventing transactivation in response to inflammatory signals[432,433]. The anti-inflammatory lipid family palmitic acid esters of hydroxy stearic acids (PAHSAs) also appear to reduce cytokine-induced ER stress in mice and human islets *ex vivo*[434]. Finally, GLP-1R agonists, already used clinically to boost β cell function, have been proposed to also have a role in reducing β cell ER stress and promoting survival[435,436]. Translating these broad range of pathways to protect endogenous β cell mass to the clinic will be an exciting next avenue in the treatment of diabetes.

Currently, there are two general approaches to stimulate endogenous β cell growth in effort to increase β cell mass: 1) harnessing the mechanisms, growth factors, hormones, and signals involved in normal, physiologic islet growth; and 2) identifying small molecules and/or compounds that induce proliferative pathways. Compared to mouse β cells, human β cells are less likely to proliferate, which remains a challenge in the field. Nonetheless, intracellular signaling through phosphoinositide-3-kinase (PI3K), the calcineurin/nuclear factor of activated T cells (NFAT), and the mechanistic target of rapamycin (mTOR) pathways have been implicated in inducing human islet cell proliferation[437–442]. While the machinery for cell cycle progression is largely conserved between humans and rodents, the majority of cyclins and cyclin-dependent kinases (CDKs) in human β cells are sequestered in the cytoplasm rather than the nucleus, possibly explaining the resistance to proliferative signals[443–447]. Studies performing high-throughput small molecule screens have identified candidate molecules such as harmine and 5-iodotubercidin that target the dual-specificity tyrosine-regulated kinase 1a (DYRK1A) to induce β cell proliferation[448,449]. Recently, inhibition of DYRK1A combined with either stimulation of the GLP-1R or with inhibition of TGFβ were shown to be additive in promoting human β cell proliferation[450–452]. This is significant because it allows for use of both agents at lower doses that limit off-target effects, since these pathways are not β cell-specific and in the case of DYKR1A, both over and underproduction have been linked to CNS effects[453]. Alternatively, cell-specific targeting and active compound delivery, as discussed below, will be essential. Further, new developments with intact human pancreatic slices will aid in our understanding of how these compounds control long-term endocrine regeneration with intact cytoarchitecture[454]. Finally, work remains to establish that newly formed β cells via targeting of these pathways are appropriately functional.

Cellular reprogramming through induced differentiation (neogenesis) or transdifferentiation are exciting concepts to replenish β cell mass, though much work remains to establish this as a viable approach. While multipotent pancreatic progenitors have a clear role in development, there is not yet convincing evidence for a true pancreatic stem cell that could be targeted in the adult human islet or pancreas[455]. On the other hand, cellular plasticity of other terminally differentiated cell types has been demonstrated in several mouse models. Models of extreme β cell loss[456,457] and numerous genetic approaches[458–464] have led to increased β cell neogenesis or transdifferentiation of other cell types. While equivalent studies in human islet cells are quite limited, a recent study reported that human islet non-β (mainly α) cells can transdifferentiate into

insulin producing with exogenous expression of MAFA and PDX1[465]. There is a need for more work to characterize the phenotype of reprogrammed cells in order to understand how similar they are to native human β cells.

Importantly, many of the pathways in pancreatic islet biology targeted to improve β cell function, protect β cells, and manipulate β cell growth are also present in in other cells, making it unlikely there is β cell-specific process that can be therapeutically targeted. While certain pathways or targets may be enriched in islet cells and thus inherently targeted, it is more likely that safe and effective therapeutic manipulation of desired pathways will require delivery of the therapeutic compound to islet cells using an engineered carrier (e.g., an aptamer, an antibody, or a virus). Another challenge for delivery is that the unique macro- and microanatomy of the islet may make targeting and cargo delivery to the β cell difficult. To meet these challenges, numerous groups are working to identify and validate cell surface markers that are specific to or enriched in the β cell, such as NTPDase3 and GLP-1R, or in the α cells, such as HPa3, or in all islet endocrine cells, such as HPi1[466–468]. In this way, aptamer- or antibody-based systems may allow cell- or islet-specific delivery of a therapeutic agent that would otherwise have broad effects[469]. Additional targeting approaches include the use of viruses, primarily adeno-associated viruses (AAVs), to achieve cell specificity, either through pseudotyping to achieve the desired tropism[470] or through the identification of cell-specific promoters to regulate gene expression of the viral cargo[471–473]. Finally, chimeric antigen receptor T cells (CAR T cells), T cells with genetically engineered artificial T cell receptors, are being used in cancer biology to target specific cell populations and may represent an attractive approach to islet targeting[474,475]. Overall, it is clear that approaches to provide β cell or islet specificity are critical in the development of islet- or β cell-directed therapeutics.

Aims and Summary of Dissertation

Pancreatic islets are central in the control of blood glucose and their dysfunction is a hallmark of diabetes. Our understanding of islet biology has grown exponentially; however, significant barriers to translation remain. Among these are the difficulty in obtaining and mechanistically studying primary human islets which have known differences between commonly used animal model systems. As such**, the primary goal of the research included in this Dissertation is to advance our understanding of the molecular mechanisms of human islet function and dysfunction in diabetes.** These new molecular insights will impact both the diagnosis and treatment of diabetes.

We approached this through both the application of existing tools to new scientific questions and the development of new experimental tools and approaches to study primary human islets. Materials and methods for these studies are described in **Chapter II**.

In **Chapter III**, we describe the application of an in vivo transplantation model to study the effect of therapeutics on human islets and how they may contribute to diabetes. We show that the immunosuppressive agents tacrolimus and sirolimus contribute to the pathogenesis of post-transplantation diabetes mellitus after cell or solid organ transplantation by leading to β cell

dysfunction. We further show that these effects are reversible with withdrawal of the immunosuppressive agent and preventable with co-treatment with a GLP-1 receptor agonist, an existing clinically approved therapeutic in the treatment of type 2 diabetes. In another study, we investigate the effects of dapagliflozin, an SGLT2-inhibitor also used in the treatment of diabetes and conclude that effects on the islets by this therapeutic are indirect through changes in glucose.

In **Chapter IV**, we describe the development of a system where human islets are dispersed into single cells and then reaggregated into pseudoislets. We describe how the resulting pseudoislets are similar to native islets in morphology, function, composition, and cellular identity. This system is advantageous by allowing for both the genetic and cellular manipulation of primary human islet cells while studying them in an aggregated context similar to native islets. We investigate human islet cell GPCR physiology through the use of designer receptors exclusively activated by designer drugs (DREADDs) as well as genetically-encoded calcium biosensors in pseudoislets to reveal cell type differences in GPCR signaling. We additionally use FACS to manipulate the cell composition of pseudoislets and targeted fluorescent viral delivery to monitor cell specific biosensor response as well as real-time pseudoislet formation.

In **Chapter V**, we describe an integrative approach to robustly study the isolated islets and pancreas from 20 donors with short-duration T2D to reveal early, disease-driving mechanisms in T2D. Our approach assessed islet function both in in vitro and in vivo using transplantation, analyzed the islet transcriptome by bulk RNA-seq from whole islets, and from FACS-purified β cells and α cells, and explored pancreatic tissue via traditional and multiplexed imaging approaches for a deep understanding of the T2D islet microenvironment. Integration of these studies reveals that that human β cell dysfunction in short-duration type 2 diabetes is defined by RFX6-mediated transcriptional dysregulation and a disrupted islet microenvironment associated with amyloid deposition. Additionally, we used our integrative approach to investigate an atypical pathobiological finding of substantial insulin secretion in a donor with presumed T1D and describe how we integrated studies of islets, tissue, and genetics to investigate the donor and understand the etiology of their diabetes. This work expands the fields understanding of T1D heterogeneity and how different disease mechanisms can manifest as a common clinical phenotype.

In **Chapter VI**, we describe studies using multiple approaches to investigate the role of islet-enriched transcription factors in α and β cell identity and function. Changes in transcription factor expression and cell type specificity have been described in numerous important processes including the pathogenesis of diabetes and islet cell development. To define the consequences for these states, we utilized single cell RNA-seq to understand heterogeneity within α and β cell states based on combinatorial transcription factor expression and link these states to changes in genes involved in hormone secretion as well as changes in electrophysiological parameters for β cells. In addition, we investigate the role of the transcription factor RFX6 by using shRNA knock down in human pseudoislets. Together these studies reveal important cell-type specific roles for transcription factor expression and how these govern islet function and cellular states.

In sum, the studies in this Dissertation provide new insight into the development and progression of several types of human diabetes and highlight numerous cell-type specific molecular responses important for understanding how human islet cells sense and respond to signals and nutrients. The significance of these findings, as well as proposed future directions, is discussed in **Chapter VII**.

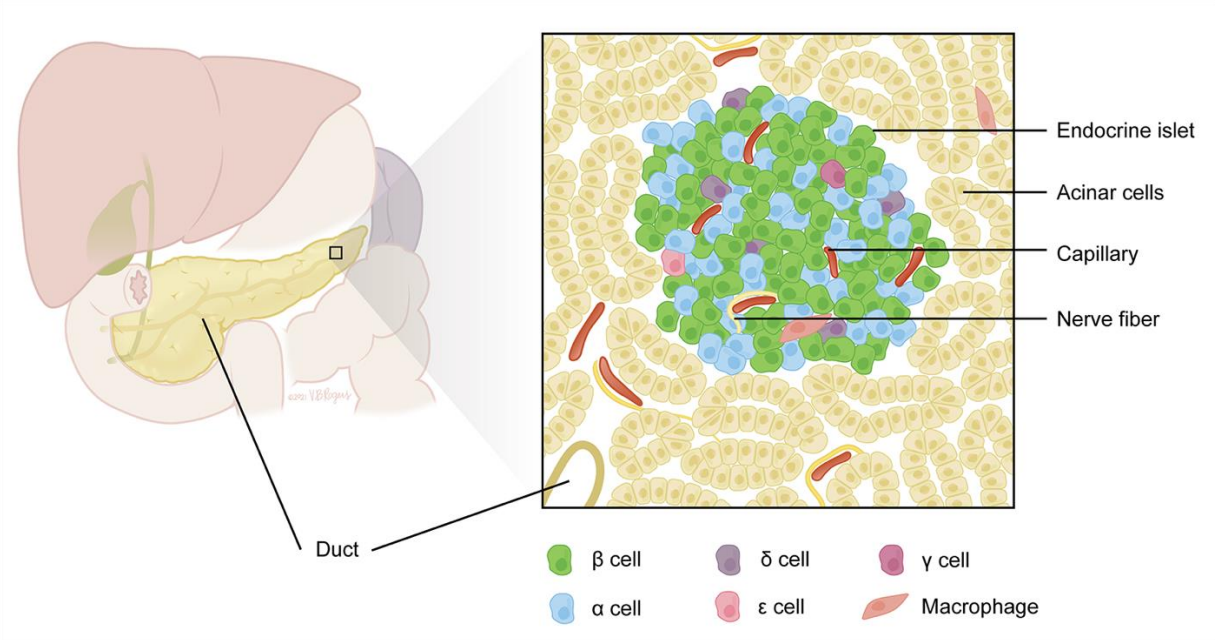

Figure 1. The pancreatic endocrine islet is a mini-organ that coordinates glucose homeostasis.

The pancreas, which is broadly divided into head, body, and tail regions, lies behind the stomach in back of the abdominal cavity, with the head positioned in the curve of the duodenum and the tail extending towards the spleen. Most of the pancreatic mass is exocrine tissue, encompassing clusters of digestive enzyme-secreting cells arranged in acini that feed into a branched ductal system joining the common bile duct for secretion into the small intestine. Note that variations in cystic duct anatomy exist but the most common anatomy is shown here. Blood flow from the pancreas feeds into the portal vein and flows directly to the liver. Endocrine islets are dispersed throughout the gland; they are composed of α, β, δ, γ, and ε cells and also contain capillaries, nerve fibers, and resident immune cells (shown here: macrophages). Text labels refer to examples of anatomic and cellular features; both pancreatic duct and capillary in inset are schematized to show lumen but are lined by ductal epithelium and vascular endothelium, respectively. Figure adapted from Walker, Saunders, et al., 2021[1].

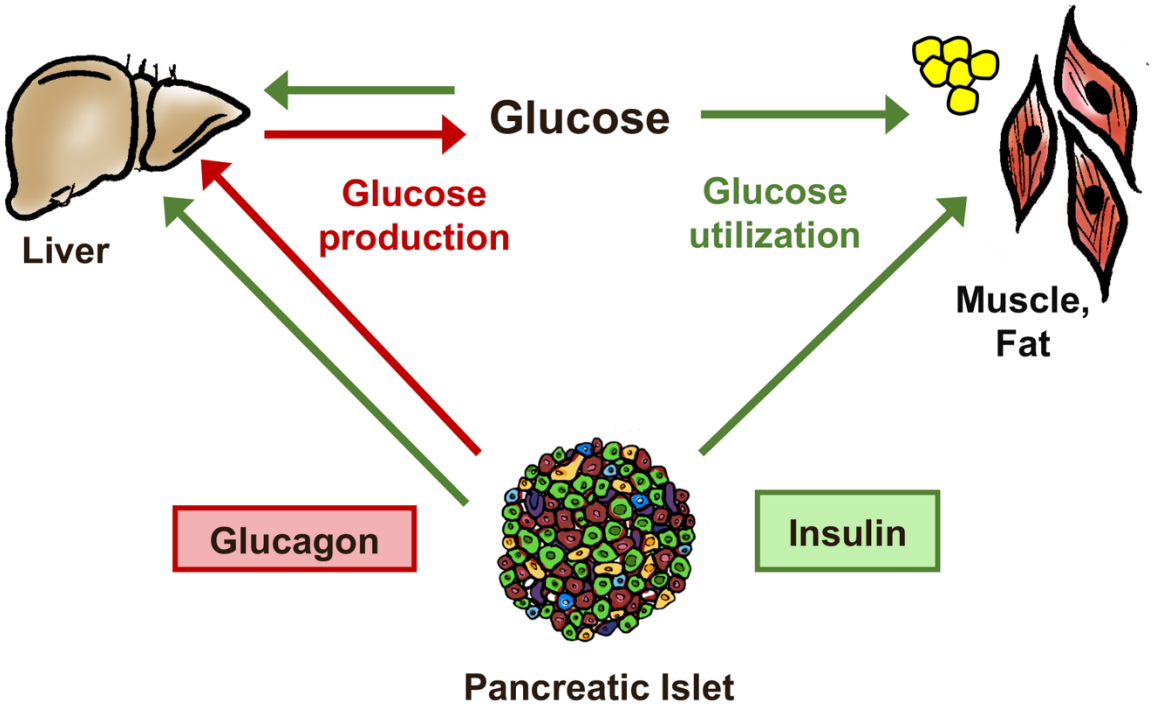

Figure 2. The pancreatic islet is central to glucose homeostasis.
Glucose homeostasis is regulated by coordinated effort between multiple organ systems in the body with the islet playing a central role. Insulin from β cells acts on the muscle/fat and liver to cause glucose uptake while glucagon from α cells acts on the liver to promote glucose production.

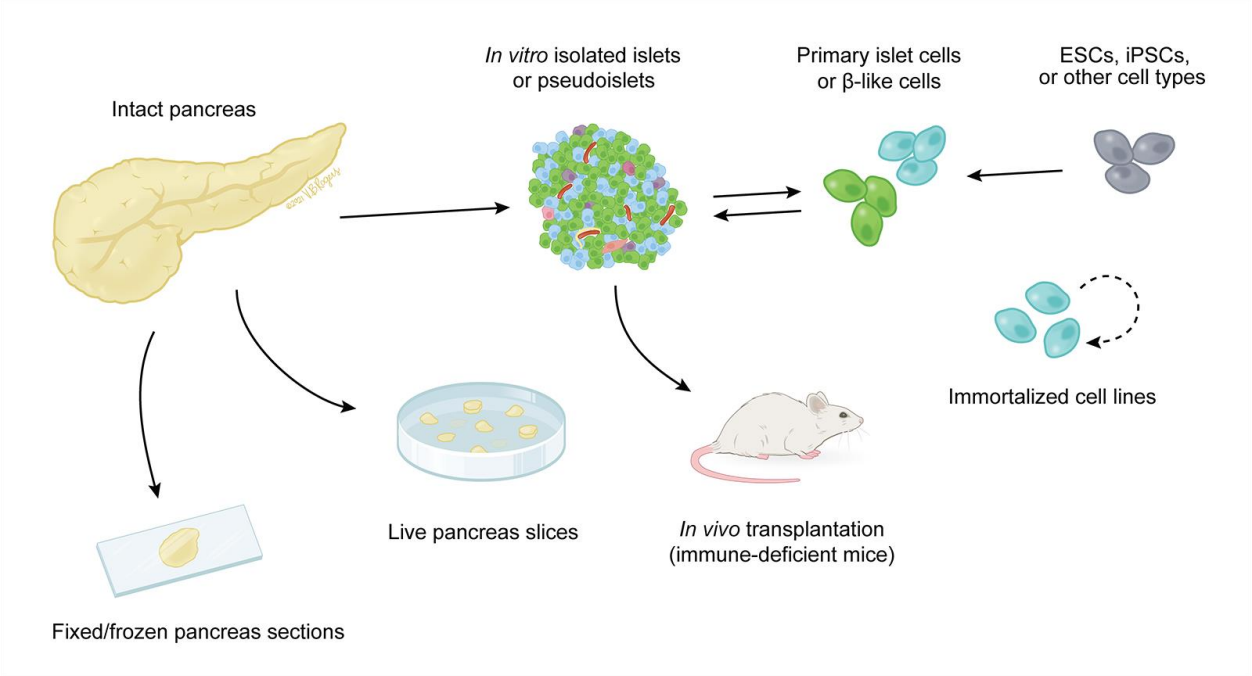

Figure 3. Models utilized to study the human pancreatic islet.
Using a cadaveric donor organ, islets can be isolated from surrounding exocrine tissue or can be dispersed further into single cells. Additionally, pancreatic sections can be fixed and/or frozen for histological analysis or processed into "slices" to perform experiments ex vivo. As an alternative to primary tissue, β-like cells can be generated from embryonic stem cells (ESCs), induced pluripotent stem cells (iPSCs), or other cell types, and immortalized β cell lines are also available. Cells from multiple sources can be (re)combined to form pseudoislets, and native islets or pseudoislets may also be transplanted into immune-deficient mice for in vivo physiological analysis. See Table 1 for detailed information about these model systems. Figure adapted from Walker, Saunders, et al., 2021[1].

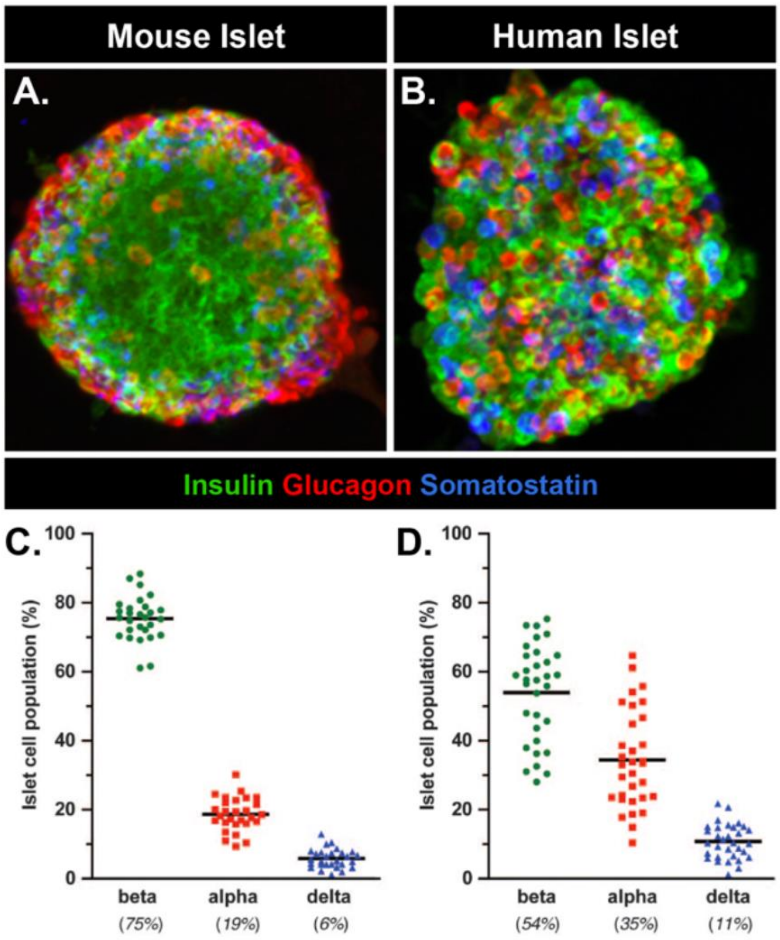

Figure 4. Islet composition and morphology varies between human and mouse.
(**A**) Mouse and (**B**) human islets labeled for insulin (green), glucagon (red), and somatostatin (blue). Endocrine composition of (**C**) mouse islets, n=28, and (**D**) human islets, n=32, determined by analysis of optical sections taken throughout entire islets. Human islet composition differed significantly ($p<0.0001$) across all endocrine cell populations examined. Horizontal bar represents the mean of each cell population. Figure adapted from Brissova et al., 2005[22].

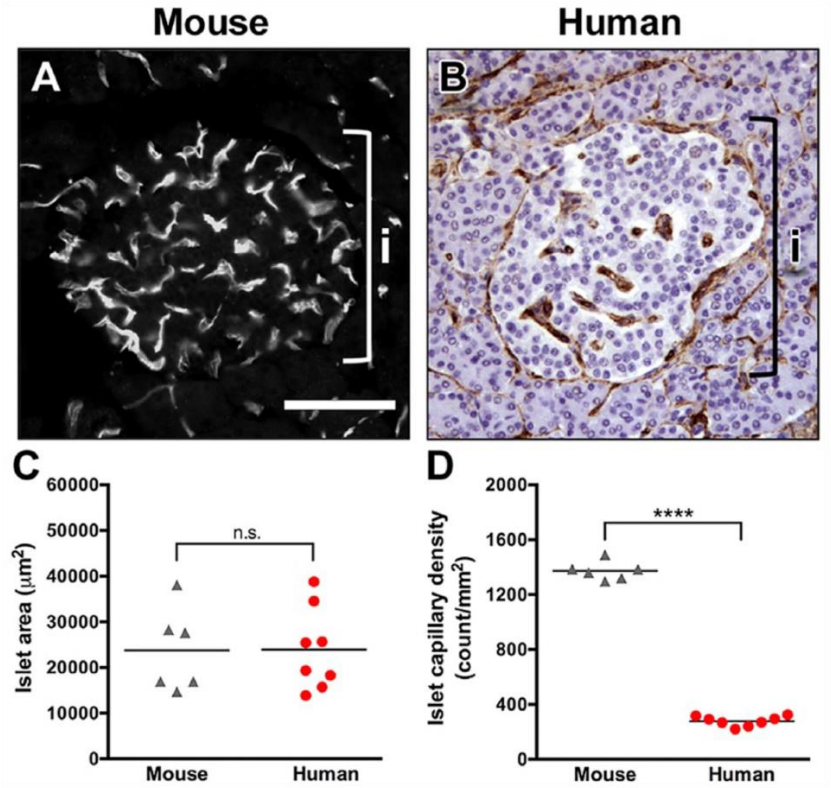

Figure 5. Human islets are less vascularized than mouse islets.
Islet vasculature visualized by endothelium-binding lectin-FITC (**A**, mouse) or endothelial cell marker CD34 (**B**, human). Brackets in A and B denote an islet (i). C) Area of individual islets was similar in the mouse (*n*=6) and human (*n*=8). *p*=0.97. (D) Human islets (*n*=8) had a lower capillary density as compared with that of the mouse (*n*=6). ****$p<0.0001$. Scale, 100 μm. Figure adapted from Brissova *et al*., 2015[23].

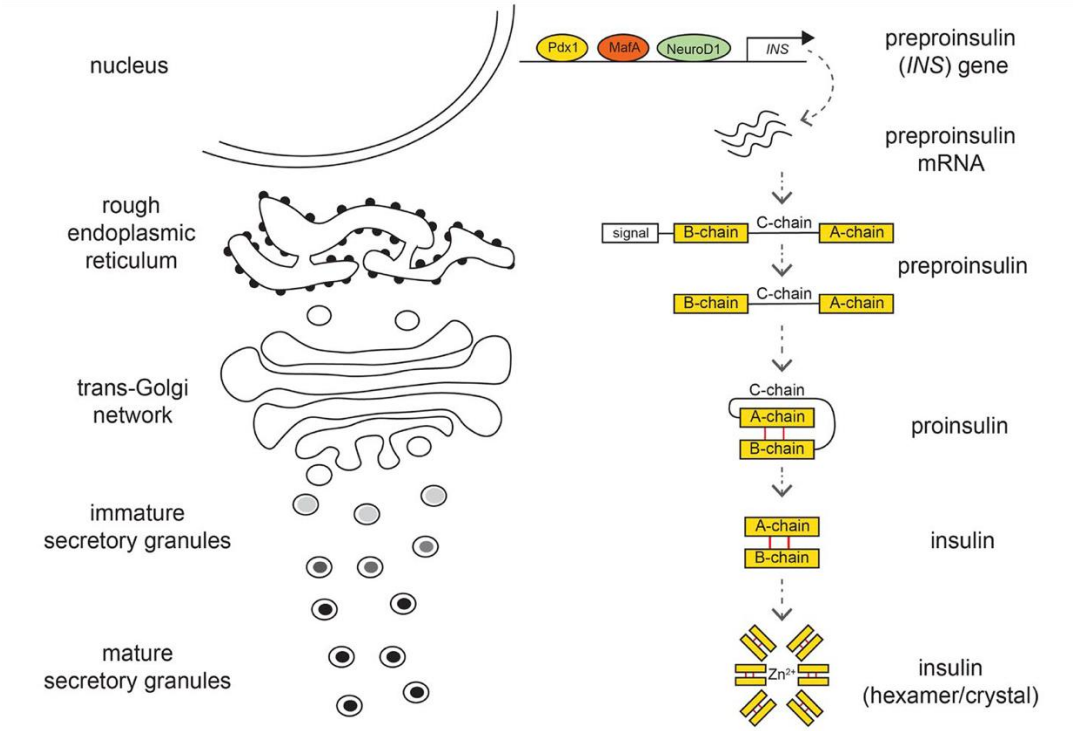

Figure 6. Insulin biosynthesis and secretion.
Insulin maturation along the granule secretory pathway. Preproinsulin mRNA is transcribed from the INS gene and translated to preproinsulin peptide. As this transits through the rough ER and trans-Golgi network, the prepropeptide is processed to its mature form and ultimately stored as hexameric insulin/Zn^{2+} crystals within mature secretory granules. Figure adapted from Tokarz et al., 2018[94].

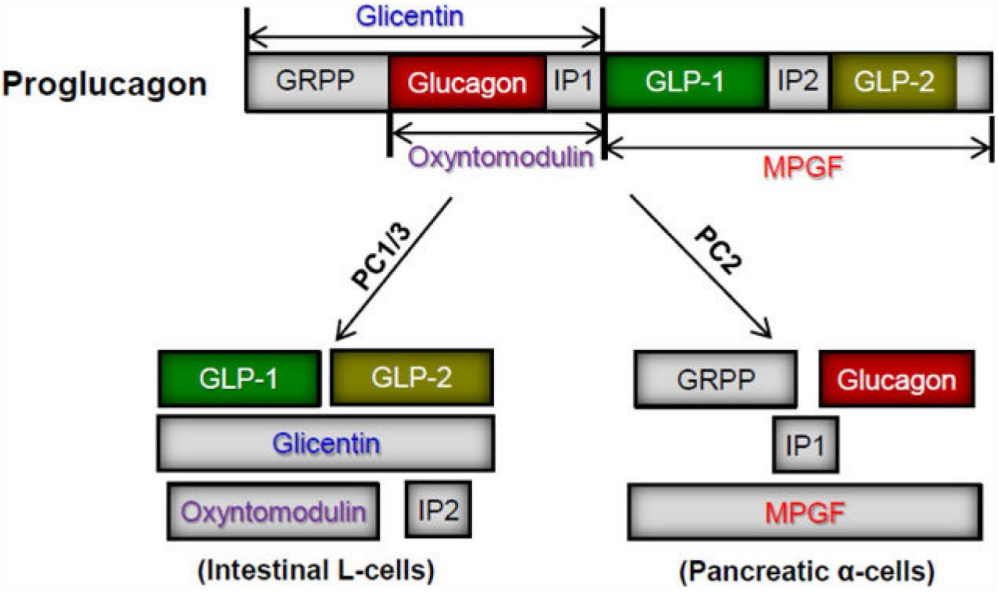

Figure 7. Cell-specific posttranslational processing of proglucagon.
Proglucagon is synthesized as a polypeptide that is cleaved into different fragments. In the intestinal L cell, PC1/3 is preferentially expressed, leading to GLP-1 and other products. In the pancreatic α cell, PC2 is preferentially expressed leading to glucagon and other products. GRPP: glicentin-related polypeptide; IP: intervening peptide; MPGF: major proglucagon fragment. Figure adapted from Fava et al., 2016[476].

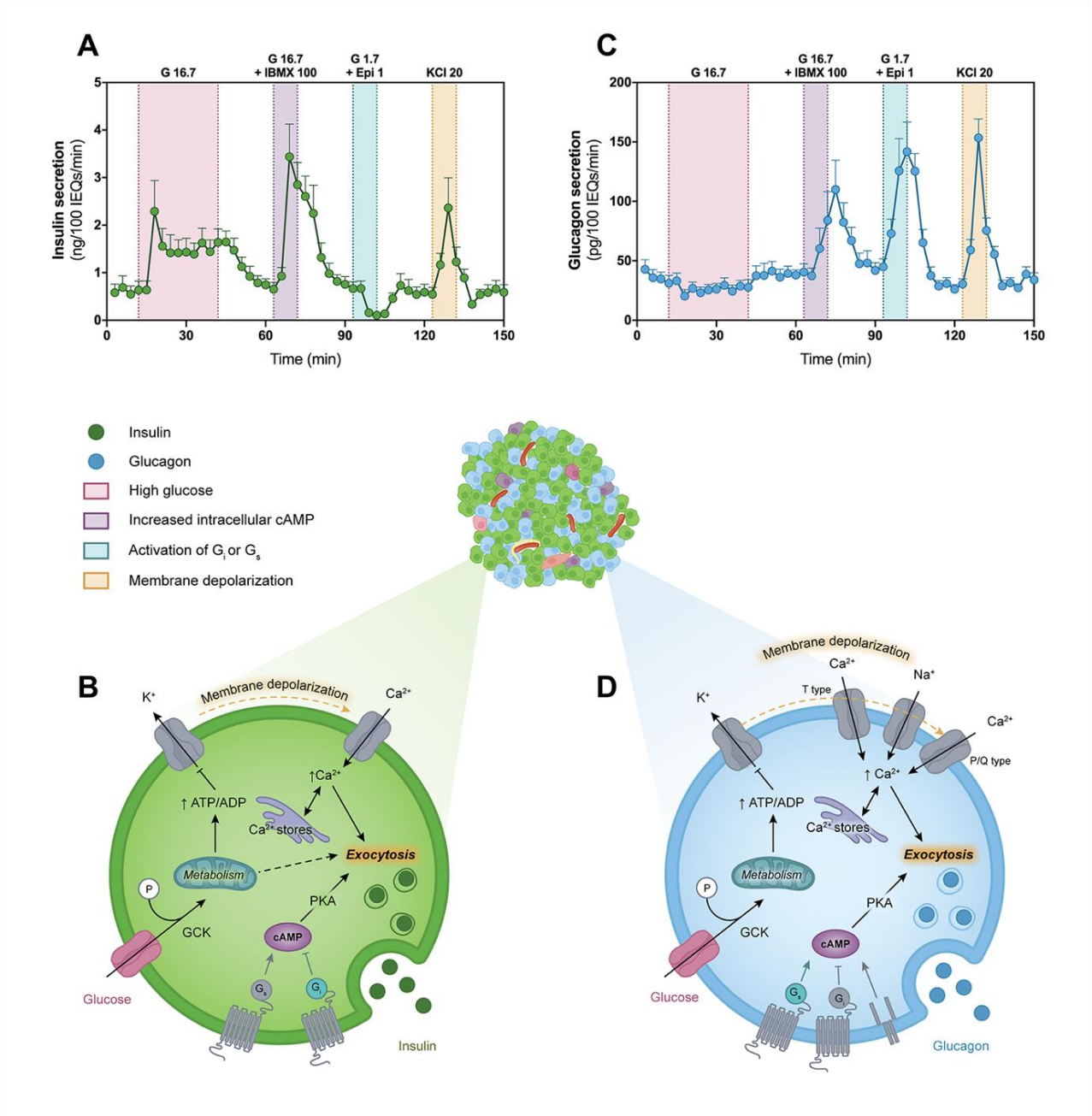

Figure 8. Intracellular mechanisms controlling insulin and glucagon secretion from β and α cells.

Perifusion traces depict endocrine cell function and associated schematics of insulin secretion from β cells **(A–B)** and glucagon secretion from α cells **(C–D).** Exposure to high glucose (pink), a cAMP-potentiator (IBMX; purple), low glucose and epinephrine (teal), and direct depolarization (KCl; orange) represent the standardized protocol used by the Human Pancreas Phenotyping Program (HIPP) to evaluate human islet preparations distributed through IIDP and the Alberta IsletCore; traces shown are from 7 non-diabetic donors, ages 17-49 years, analyzed through HPAP (hpap.pmacs.upenn.edu). Schematics of the β cell (**B**) and α cell (**D**) highlight major signaling pathways controlling hormone secretion; in the α cell these pathways are less well

defined and so the pathways shown are presumptive. Key components within the cell are color coordinated with the corresponding perifusion stimuli to conceptualize how the intracellular pathways result in the secretion dynamics shown in (**A**) and (**C**). Figure adapted from Walker, Saunders, et al., 2021[1].

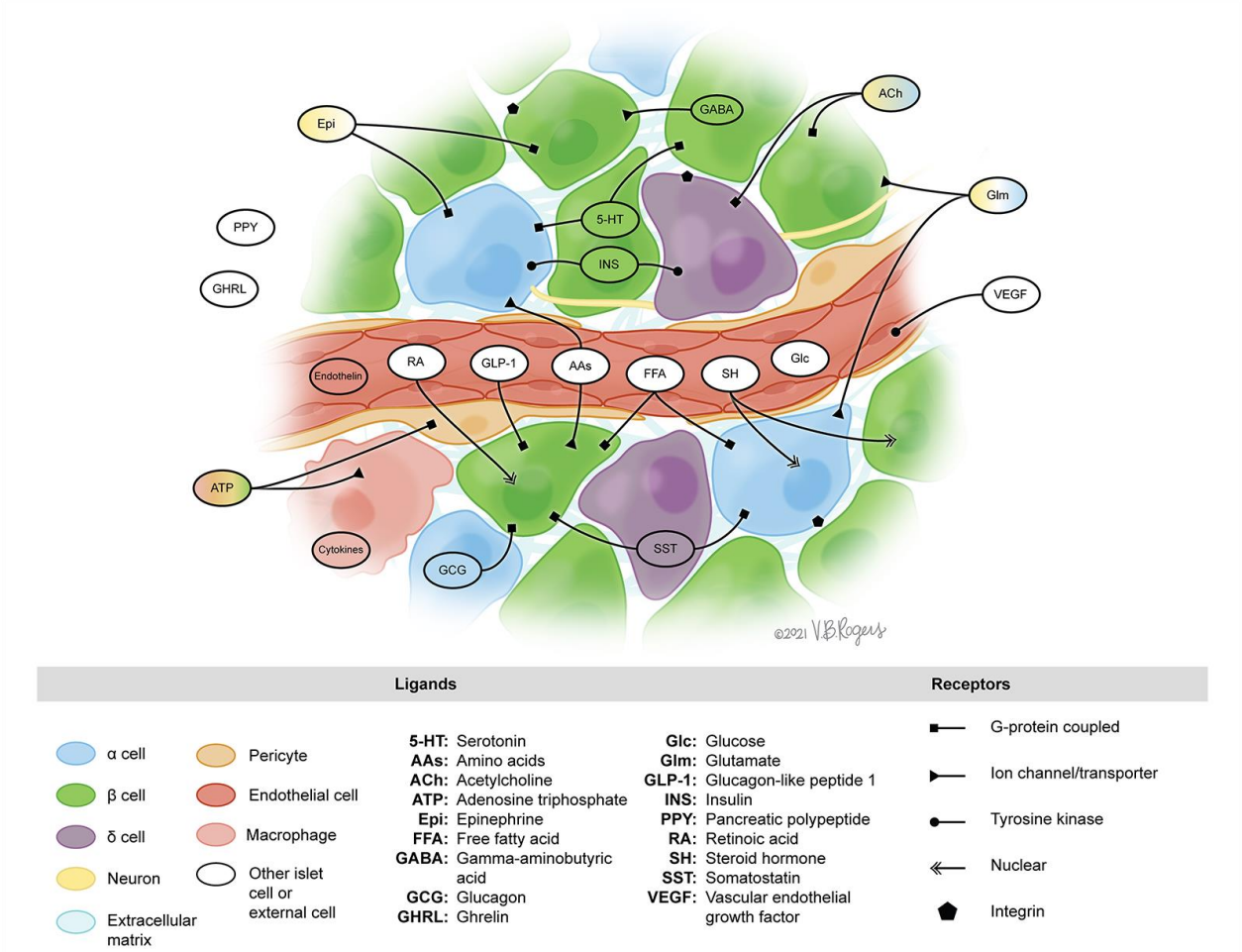

Figure 9. The human islet microenvironment contains a diversity of cells that are intricately connected.

Schematic depiction of endocrine cells (β, dark green; α, blue; δ, purple), islet vasculature (red), neuronal processes (yellow), macrophages (pink), and pericytes (pale green). Ligands are colored according to the predominant cell type(s) that produces them or to show they are primarily delivered to the islet via the systemic blood flow; in addition to acting as ligands, some nutrients can also be metabolized (glucose, AA, FFA). Lines depict local action on islet cells through major receptor categories. Key signaling molecules and receptors are shown; see text for discussion of several of these ligands and their effects on α and β cells. the complex nature of signaling within the islet microenvironment is emphasized but the reader should note that many pathways are necessarily excluded in this depiction due to space constraints. Figure adapted from Walker, Saunders, et al., 2021[1].

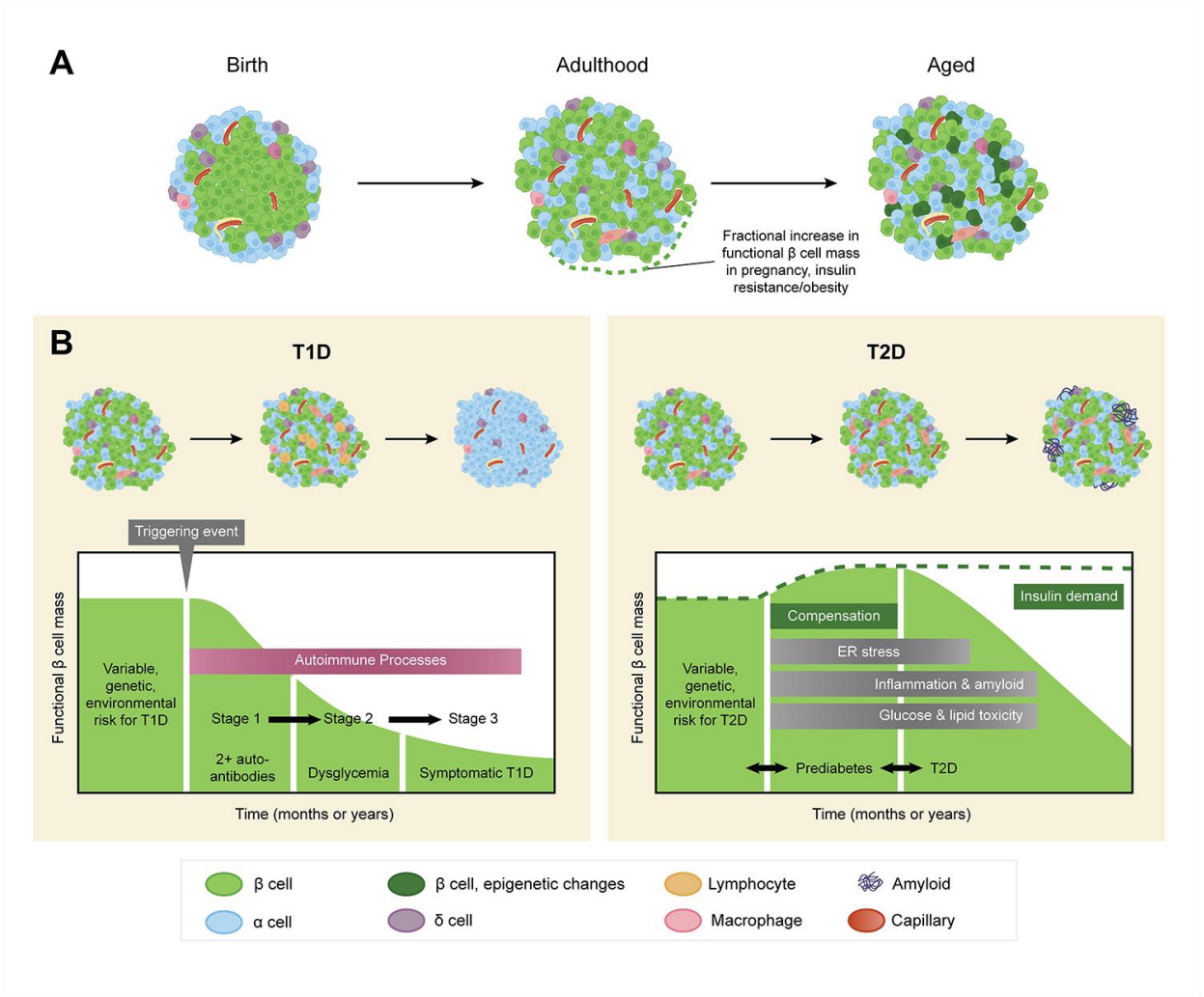

Figure 10. Diabetes-related changes to islet structure and function.
Schematics showing development of type 1 (A) and type 2 (B) diabetes. In the T1D model, a yet-to-be-defined “triggering event” or multiple events are thought to initiate an autoimmune process, development of islet autoantibodies, and progressive loss of β cell mass. While this schematic depicts an islet containing only α and δ cells, the degree of β cell loss varies in individuals and with disease progression and some β cells can still be detected in the pancreas of individuals with T1D. In the T2D model, progressively insufficient insulin secretion to meet (potentially elevated) insulin demand may be characterized by glucose and lipid toxicity and/or inflammation. In some cases, islet capillaries increase in size, macrophages infiltrate the islet, and/or amyloid deposits disrupt islet architecture. While curves showing changes in β cell mass are smooth, it is likely that the loss of functional β cell mass may stop and restart. Figure adapted from Walker, Saunders, et al., 2021[1].

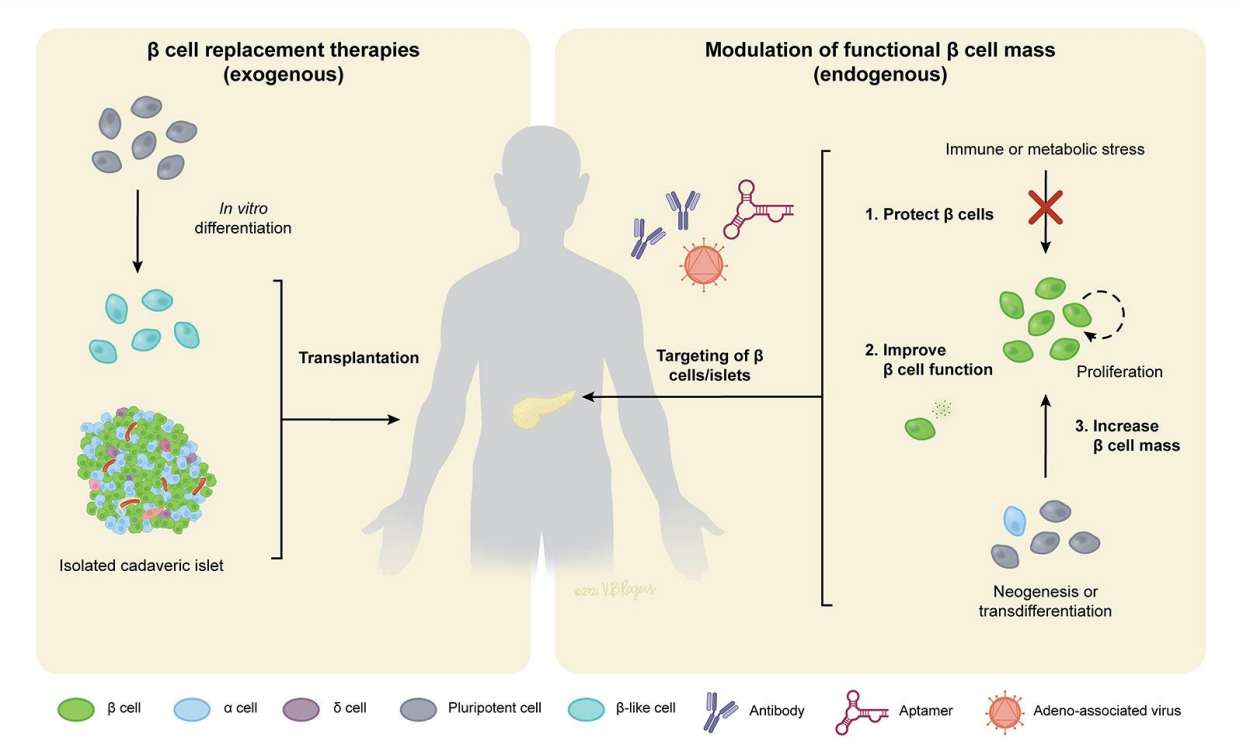

Figure 11. Clinical strategies to restore functional β cell mass.
Exogenous β cell replacement approaches (left panel) include transplantation of cadaveric islet (human or xenograft) or of stem cell-derived β-like cells. Endogenous approaches (right panel) can be categorized into those that 1) protect β cells from immune or metabolic stress, 2) increase β cell mass through proliferation, neogenesis, or transdifferentiation, and 3) improve β cell function. Modulation of these strategies may require use of β cell or islet-targeting approaches such as antibodies, aptamers or adeno-associated viruses. Figure adapted from Walker, Saunders, et al., 2021[1].

Table 1. Model systems for studying human islets

Model	Description	Applications & Advantages	Limitations	Key References
Histological sections	Pancreas processed and sections mounted onto slides for imaging	• Reflective of endogenous pancreas • Can be processed in multiple ways for several techniques	• Static snapshots • No ability to manipulate tissue • Study of a small pancreas region	Used by many laboratories
Pancreas slices	Small intact sections of living pancreatic tissue with exocrine and endocrine structure preserved	• Preserves microenvironment architecture • Avoids islet isolation process • Allows for study of interaction between endocrine and exocrine compartments	• Islet/pancreas blood flow and innervation are not maintained • Material is limited • Culture duration is limited	339,454,477,478
Isolated islets *in vitro*	Endocrine pancreas (islets) enzymatically and physically separated from exocrine pancreas for study	• Enriches for endocrine compartment of pancreas • Islet structure relatively intact • Can be processed in multiple ways for several techniques	• Heterogeneity of human islets (variable islet size in single preparation and variable purity between preparations) • Islet vascularization and innervation are not maintained • Limited supply; unpredictable availability • Culture duration is limited	479,480 Review: 481
***In vivo* transplantation (mice)**	Human islets engrafted into immunodeficient mice	• Islets can be studied in a dynamic *in vivo* environment • Permits longer-term studies • Anterior chamber of the eye (ACE) site allows for *in vivo* imaging of graft	• Hormones from endogenous mouse islet cells may affect studies • Glycemic set point of mouse is different than that of humans	482,483 ACE: 484–486 Reviews: 487,488
Pseudoislets	Three-dimensional organoids that combine islet cell populations to generate structures resembling native islets	• Allows for efficient genetic manipulation and even distribution of molecules (*e.g.*, virus) to all cells • Composition (proportions of cell types within islet) can be manipulated prior to reaggregation • Uniformity of resulting pseudoislets (composition and size)	• Potential effects of initially breaking cell-cell connections • Not clear how closely pseudoislets resemble primary islets • Variability between pseudoislet formation techniques/protocols • See also: limitations for isolated islets	465,489–494 Review: 495
Stem cell-derived insulin-producing cells and other islet cells	*In vitro* differentiation of undifferentiated embryonic SCs (ESCs) or induced pluripotent SCs (iPSCs) into β-like or other islet cells	• Controlled source of cells for study • Allows for development related questions • iPSCs can be individualized	• Not clear how closely SC-derived islet cells resemble primary islet cells • Heterogeneity between protocols, reagents, and cells produced • ESC source ≠ iPSC	β cells: 398,399,401,405,407,496; α cells: 408 Applications: 110,372,497 Reviews: 498–503
Immortalized cell lines	*e.g.*, EndoC; immortalized human β cell line derived from fetal pancreatic tissue	• Amenable to manipulation (gene knockdown, chemical treatment, CRISPR, etc.) • Single cell line reduces heterogeneity between experiments • Some versions allow for cell growth to be arrested	• Not clear how closely cell lines resemble primary islet cells • Difficult to propagate/culture	504–506

Table adapted from Walker, Saunders, et al., 2021[1].

Table 2. Structural and functional changes to pancreatic islets in disease

Diabetes Type	Islet/Pancreas Structure	Islet Function	Underlying Genetics	Key References
T1D	• Drastic loss of β cell mass • Disordered islet cell organization • Immune cell infiltration • Abnormal extracellular matrix • Smaller pancreas with reduced acinar cell number	• Significant loss of insulin secretion • Possible β cell dysfunction during disease development • Evidence of nearly normal insulin secretion by residual β cells • Evidence of α cell dysfunction; impaired response to hypoglycemia	• Polygenic; some known heritability • Very strong HLA loci association • Other SNPs identified by GWAS are largely related to immune system	40,76,80,312,313,507,508 Reviews: 299,509–511
T2D	• Islets appear relatively normal early in disease • β cell mass variable depending on disease duration • Thickened islet capillaries and increased vessel density • Amyloid deposits in many, but not all, donors • Macrophage infiltration	• Reduced insulin secretion, particularly relative to demand (insulin resistance) • Evidence of α cell dysfunction; failure of glucagon suppression with meal	• Polygenic; some known heritability • SNPs identified by GWAS are largely related to islet cells • Many SNPs related to non-coding enhancer regions	49,327,331,333,338–340,349,350,512–516 Reviews: 71,321,417,510,517–519
GDM	• Largely unknown • Potential defect in compensatory β cell expansion	• Insufficient insulin secretion	• Polygenic; large overlap with T2D • Majority of loci related to β cell function • GDM-specific: *HKDC1*, *BACE2*	364,520 Reviews: 363,366,521
MODY	• Variable depending on exact mutation; see text • Case reports have described phenotypes including decreased β cell mass, impaired pancreatic morphogenesis, pancreatic hypoplasia	• Variable depending on exact mutation; see text • Case reports have described progressive β cell dysfunction due to insulin secretory defects and/or glucose sensing defects	• Monogenic • Mutations to *HNF4α*, *GCK*, *HNF1α*, *PDX1*, *HNF1β*, *NEUROD1* constitute MODY 1-6, respectively • Other mutations identified, including those in *KLF11*, *CEL*, *PAX4*, *INS*, *BLK*, *ABCC8*, *KCNJ11*	373,522–531 Reviews: 368,532,533
Neonatal diabetes	• Variable depending on exact mutation; see text • Case reports have described phenotypes including pancreatic agenesis, pancreatic hypoplasia and $CHGA^+$, $hormone^-$ cells	• Variable depending on exact mutation; see text	• Monogenic; most commonly caused by mutations to *KCNJ11* or *ABCC8* • Other genes implicated include *FOXP3*, *GATA4*, *GATA6*, *GCK*, *HNF1β*, *INS*, *NEUROG3*, *PAX6*, *PDX1*, *PTF1A*, *RFX6*	128,129,377,378,534–538 Reviews: 374–376,539
PHHI	• Diffuse: disorganized islets; abnormal β cells in all portions of pancreas; evidence of β and δ cell transcriptional abnormalities • Focal: abnormal β cell lesions; increased β cell proliferation	• Insulin hypersecretion resulting in severe hypoglycemia, caused by absent or dysfunctional K_{ATP} channel • Tumor development due to imbalance between imprinted genes mapped to 11p15 (focal only)	• Diffuse: mutation in *ABCC8* or *KCNJ11* • Focal: paternally inherited *ABCC8* or *KCNJ11* mutation **and** region-specific loss of maternal 11p15 alleles	380,540–545 Reviews: 379,381,542,546,547

CFRD	• Increased immune cell infiltration of exocrine pancreas • Extensive fibrosis and fat infiltration (exocrine and peri-islet area) • Islet loss/dysmorphia	• *In vivo* insulin insufficiency likely due to islet loss • Remaining islets have similar function to normal islets *in vitro*	• Monogenic • Mutations to *CFTR* gene disrupt protein synthesis (Class I/VI), processing (Class II), or function (Class III/IV)	384,548,549 Reviews: 383,550–552
Post-transplantation diabetes	• Largely unknown • Possible β cell morphologic changes • Impaired insulin granule formation	• Impaired insulin secretion, particularly related to certain immunosuppressive agents	• Polygenic; large overlap with T2D	387–389,553–556 Reviews: 385,386,557

CFRD, cystic fibrosis-related diabetes; GDM, gestational diabetes; GWAS, genome-wide association study; MODY, mature-onset diabetes of the young (monogenic diabetes); PHHI, persistent hyperinsulinemic hypoglycemia of infancy; SNP, single nucleotide polymorphism; T1D, type 1 diabetes; T2D, type 2 diabetes.

Table adapted from Walker, Saunders, et al., 2021[1].

CHAPTER II:
MATERIALS AND METHODS

Some methods in this chapter have been adapted from Dai, Walker et al. 2020[558], Dai, Walker et al. 2020[559], Walker, Haliyur et al. 2020[560], Shrestha, Saunders, Walker et al.[561], Haliyur, Walker, et al. (manuscript in preparation), and Walker, Saunders, Rai et al. (manuscript in preparation).

Experimental Model and Subject Details

Animals

Immunodeficient 10-12-week old NOD-*scid*-*IL2rγ*^{null} (NSG) male mice were used for human islet transplantation studies. Animals were maintained by Vanderbilt Division of Animal Care in group-housing in sterile containers within a pathogen-free barrier facility housed with a 12hr light/12hr dark cycle and access to free water and standard rodent chow. All animal procedures were approved from by the Vanderbilt Institutional Animal Care and Use Committees.

Primary cell cultures

Primary human islets were cultured in CMRL 1066 media (5.5 mM glucose, 10% FBS, 1% Pen/Strep, 2 mM L-glutamine) in 5% CO_2 at 37°C for 0-24 hours prior to reported studies.

Human specimens

Pancreata and islets from normal donors and donors clinically diagnosed with T1D or T2D were obtained through a partnership with the International Institute for Advancement of Medicine (IIAM), National Disease Research Interchange (NDRI), Integrated Islet Distribution Program (IIDP), Alberta Diabetes Institute (ADI), Human Pancreas Analysis Program (HPAP) and Network for Pancreatic Organ Donors with Diabetes (nPOD). In diseased pancreatic organs as well as a subset of non-diabetic donors, pancreata from the same donor was processed for both islet isolation and tissue for histology (described below). These donors were all screened for criteria reflective of a representative pancreas including limited ICU/hospital stay, absence of pancreatitis, and no history of congestive heart failure or end stage renal disease. A number of non-diabetic human islets were also obtained through IIDP or ADI. Donor information for islet studies in this Dissertation are shown in **Table 3**. Donor information for pancreatic tissue studies in this Dissertation are shown in **Table 4**. Human kidney sample was provided by Dr. Agnes Fogo, Vanderbilt University Medical Center. The Vanderbilt University Institutional Review Board declared studies on de-identified human pancreatic specimens does not qualify as human subject research.

Methods

Human pancreatic islet procurement

Pancreas processing and islet isolation were performed by Rita Bottino at Allegheny Health System or Imagine Pharma. Pancreata from normal, T1D-diagnosed, and T2D-diagnosed donors were received within 18 hours from cross clamp and maintained in cold preservation

solution on ice until processing. Pancreas was then cleaned from connective tissue and fat, measured and weighed. Prior to islet isolation, multiple cross-sectional slices of pancreas with 2-3 mm thickness were obtained from the head, body and distal tail. Pancreatic slices were further divided into four quadrants and then either snap frozen or processed for cryosections.

Tissue specimens processed for cryosections were fixed in 0.1 M phosphate buffered saline (PBS) containing 4% paraformaldehyde (Electron Microscopy Sciences) for 3 hours on ice with mild agitation, washed in four changes of 0.1 M PBS over 2 hours, equilibrated in 30% sucrose/0.01 M PBS overnight and embedded in Tissue-Plus O.C.T. compound (Fisher Scientific).

For islet isolation, depending on the size of pancreatic duct, 18G or 22G catheters were inserted into the main pancreatic duct (one catheter towards head and the other one towards tail). Accessory duct and main pancreatic duct were clamped at the points where sections were collected to prevent leakage of collagenase solution during infusion. Collagenase solution consisting of collagenase NB1, (1600 U/isolation, Crescent Chemical), neutral protease NB1 (200U/isolation, Crescent Chemical), and DNase I (12000U/isolation, Worthington Biochemical Corporation) was pre-warmed to 28ºC and delivered intraductally using a Rajotte's perfusion system and then maintained at 37ºC for approximately 20min. The inflated tissue was then transferred to a Ricordi's chamber apparatus for combined mechanical and enzymatic digestion, which was maintained at 36ºC for 5-15 minutes prior to warm and cold collection. The digest was incubated in cold RPMI media (Mediatech) supplemented with heat inactivated 10% Fetal Calf Serum (Life Technologies) for 1 hour on ice. If post-digestion tissue pellet was larger than 2 mL and islets were distinguishable from exocrine tissue by dithizone staining (Sigma), a purification step consisting of density gradient (Biocoll, Cedarlane) centrifugation on a COBE 2991 Cell Processor (Gambro-Terumo) was used to separate islets from exocrine tissue. Islets were re-suspended in CMRL 1066 medium (Mediatech) supplemented with 10% heat-inactivated Fetal Calf Serum (Life Technologies), 100 units/mL Penicillin/0.1mg/mL Streptomycin (Life Technologies), 2 mmol/L L-glutamine (Life Technologies).

On average, the islet-enriched fraction contained 90,000 islet equivalents (IEQs), typically with a purer fraction (>50%) and a less pure fraction (>30%). Islets were cultured for 12 – 24 hours and then shipped from Pittsburgh to Vanderbilt University and/or other collaborators including the University of Massachusetts for further analysis following shipping protocols developed by IIDP. Upon arrival at Vanderbilt University, human islets were cultured in CMRL1066 media (5.5 mM glucose, 10% FBS, 1% Pen/Strep, 2 mM L-glutamine) in 5% CO_2 at 37°C for 0-24 hours prior to reported studies.

Traditional Immunohistochemical Analysis

Immunofluorescence of pancreas was performed on 5-μm cryosections from multiple blocks from head, body and tail regions. Kidneys bearing islet transplants were collected and then 5-μm cryosections of each graft were labeled for immunofluorescence. Immunolabeling of pseudoislets were performed on islet whole mounts and/or with islets embedded in collagen IV gels sectioned at 8-μm and was performed as previously described[562].

Briefly, cryosections were air dried and then either post-fixed with 1% paraformaldehyde in 10mM PBS for 10 minutes before permeabilization, or immediately permeabilized in 0.2% Triton-X in 10nM PBS. After permeabilization sections were washed three times in 10nM PBS for 3-5 minutes each, then blocked in 5% normal donkey serum in 10mM PBS for 60-90 in a humidified chamber at room temperature. Sections were incubated overnight with primary antibodies diluted in antibody buffer (0.1% Triton-X, 1% BSA in 10nM PBS) in a humidified chamber at 4°C, then washed three times with in 10mM for 10 minutes each. Sections were then incubated with secondary antibodies prepared in antibody buffer for 90 minutes in a humidified chamber protected from light, at room temperature. Sections were treated with DAPI (5 mg/mL stock diluted 1:50,000 in 10mM PBS) for 10 minutes, and then washed three times in 10mM PBS for 15 minutes each. Slides were mounted using SlowFade Gold antifade reagent (Invitrogen Molecular Probes) and sealed with fingernail polish prior to imaging.

Primary antibodies to all antigens and their concentrations are listed in **Table 5** and were visualized using the appropriate secondary antibodies listed in **Table 6**. Apoptosis was assessed by TUNEL stain (Millipore, S1675). Amyloid was visualized using a 2-minute incubation in Thioflavin S (0.5% w/v; #T-1892, Sigma, St. Louis, MO) followed by a brief wash in 70% ethanol. Digital images were acquired with a Zeiss LSM880 (Carl Zeiss), or FV3000 (Olympus) laser scanning confocal microscope, a Leica DMI6000B fluorescence microscope equipped with a Leica DFC360FX digital camera (Leica), a BX41 fluorescence microscope(Olympus), or Fluorescent ScanScope (Aperio).

Quantification of cytoplasmic or nuclear expression of markers was quantified using HALO software (Indica Labs) with a cytonuclear algorithm (HighPlex FL v3.2.1 or Cytonuclear v3) or my manual counting through MetaMorph 7.1 imaging software (Molecular Devices). Quantification of area or density measurements was performed using HALO with a classifier algorithm or with thresholding using MetaMorph 7.1. Endocrine cell mass was quantified by using the ratio of hormone positive cells as identified by cytonuclear algorithm within the entire pancreatic section from multiple blocks representing the head, body, and tail region.

CODEX Multiplexed Imaging

CODEX imaging and analysis was performed in collaboration with Diane Saunders in the Powers & Brissova group. Antibodies were purchased preconjugated from Akoya Biosciences or purchased from other vendors and conjugated using the CODEX Conjugation Kit (Akoya Biosciences) or through Leinco Technologies, Inc. (St. Louis, MO, USA). See **Table 7** for a complete list of CODEX antibodies and sources. 10-µm lightly fixed pancreas sections (4% PFA as described previously[563]) were mounted onto 22x22 mm glass coverslips (Electron Microscopy Sciences) coated in 0.1% Poly-L-lysine (Sigma). Coverslips were handled with bent-tip tweezers (Fine Science Tools) and stained with the CODEX Staining Kit (Akoya Biosciences) in uncoated 6-well tissue culture plates (VWR) per manufacturer instructions. Fluorescent oligonucleotide-conjugated reporters were combined with Nuclear Stain and CODEX Assay Reagent (Akoya Biosciences) in light-protected 96-well plates sealed with foil (Akoya Biosciences) according to 27-plex, 11 cycle experimental plan. Automated image acquisition

and fluidics exchange were performed using the Akoya CODEX® instrument and CODEX® Instrument Manager (CIM) v1.29 driver software (Akoya Biosciences) integrated with a BZ-X800 epifluorescent microscope (Keyence). Tissue was hydrated in 1X CODEX buffer (10X CODEX Buffer diluted in Milli-Q water) and hybridization/stripping of the fluorescent oligonucleotides was performed using dimethyl sulfoxide (Sigma). After loading of coverslip into stage insert, tissue was visualized with Nuclear Stain diluted 1:1000 in PBS and imaging area was set using BZ-X800 viewing software (Keyence), specifying the center point and tile number. All images were acquired using a CFI plan Apo I 20x/0.75 objective (Nikon) with 30% tile overlap and 5 z-planes (1.5 µm/z).

Following image acquisition, a “WashTissue” cycle was performed via CIM driver and coverslip was removed from stage insert. To visualize amyloid, a modified Thioflavin S staining protocol (**described above**) was performed via incubations of coverslip in 6-well plates. Coverslips were then washed once in 1X CODEX Buffer and reloaded into microscope stage insert in same orientation as previously imaged. Nuclear stain was applied as described previously, exposure time was set at 10-20ms for Cy2/A488 channel, and image acquisition was performed using the “AddCycle” function of the CIM driver.

We captured a total of 16 regions from 6 ND and 10 T2D donors (average 50 mm^2 tissue/donor). Image alignment, stitching, background subtraction, and deconvolution were performed using the CODEX® Processor v1.7.0.6 (Akoya Biosciences; see https://help.codex.bio/codex/processor/technical-notes for details). Individual channel images (TIFF files) were imported into HALO® software v3.1 (Indica Labs) for all analyses as described below.

Groups of 6-8 channels were combined using the “Fuse Channels” function in HALO and nuclear and amyloid stains from the appended cycle were registered with other channels using the “Image Registration” function. Tissue and islet areas were annotated by hand to exclude regions that were out of focus or had poor stain quality. Islets (estimated diameter ≥50 µm) were annotated based on DAPI, CHGA, and ThioS channels. Cell segmentation and cell type annotations were performed using the HALO HighPlex FL v3.2.1 module with consistent cytonuclear parameters (nuclear contrast threshold 0.456, maximum cytoplasm radius 0.48). Due to marker intensity variability among donor samples, thresholds were manually set for each marker and donor. Unless otherwise noted, cells were counted positive for a given marker if minimum intensity was reached in 50% of cytoplasm area (see **Figure 46A** for complete list of markers, abbreviations, and cell types). For cells with more variable morphology, positivity was also counted for nuclear area (30%: ARG1, CD11c, CD14, CD163, CD206, CD31, CD34, CD45, HLA-DR, IBA1, KRT, MCAM), Proliferating cells were counted only if minimum 60% of nuclear area met Ki67 intensity threshold. Extracellular matrix (COL-IV) and amyloid deposits (ThioS) were measured by random forest classification algorithm (HALO Tissue Classifier module) and expressed as positive area as percentage of total islet area. For spatial analyses, ThioS or CD31 area classifications were converted to an annotation layer. A nearest neighbor algorithm (HALO Spatial Analysis module) was applied to obtain average distance of endocrine cells to islet capillaries ($CD31^+$ region). Infiltration analysis was used to calculate proximity of various

cell types to amyloid, with ThioS annotation set as the interface layer. Infiltration was first performed for all cells within a 50 μm radius (5 10-μm zones), then for cells of a given phenotype to ultimately express prevalence as % total cells in each zone.

Fluorescence-Activated Cell Sorting (FACS) of human α and β cells

Human α and β cells sorting was performed in collaboration with the Vanderbilt Flow Cytometry Core (D. Flaherty and K. Weller). Human islets were dispersed using a modified protocol as described previously[564]. Briefly, 0.025% trypsin was used to disperse cells and reaction was quenched with modified RPMI medium (10% FBS, 1% Penn/Strep, 5 mM glucose). Cells were washed in the same medium and counted on a hemocytometer, then transferred to FACS buffer (2 mM EDTA, 2% FBS, 1X PBS). Indirect antibody labeling was completed via two sequential incubation periods at 4C, with one wash in FACS buffer following each incubation. Primary (HPi1, HPa3, NTPDase3) and secondary antibodies, listed in **Table 8**, have been characterized previously and used to isolate high-quality RNA from α- and β-cells[99,220,565]. Appropriate single color compensation controls were run alongside samples. Prior to sorting, propidium iodide (0.05 ug/100,000 cells; BD Biosciences) was added to samples for non-viable cell exclusion. Flow analysis was performed using an LSRFortessa cell analyzer (BD Biosciences), and a FACSAria III cell sorter (BD Biosciences) was used for FACS. Analysis of flow cytometry data was completed using FlowJo 10.1.5 (Tree Star). Gating strategy is shown in **Figure 44A.**

Measurement of islet endocrine cell populations by flow cytometry

Intracellular flow cytometry was performed by David Harlan and colleagues at the University of Massachusetts Medical School. Islet dissociation and intracellular antibody staining used a previously described protocol[566]. Anti-insulin (Gallus Immunotech), anti-chicken allophycocyanin, (Jackson ImmunoResearch), anti-glucagon (Sigma-Aldrich) conjugated with Zenon Pacific Blue (Invitrogen), and anti-somatostatin (LSBio) conjugated with Zenon Alexa Fluor 488 (Invitrogen) were used to stain β, α, and δ cells, respectively (**Table 8**). Dissociated islet cell preparations were analyzed using a BD Biosciences FACS Aria II Cell Sorter (University of Massachusetts Medical School Flow Core Laboratory). Cellular debris was eliminated from islet preparations using a forward scatter versus side scatter size gate.

Isolation of islet T cells

Islet T cell isolation was performed by Sally Kent and colleagues at the University of Massachusetts Medical School. One hundred hand-picked whole islets were dissociated and immediately stained with viability dye and T cell markers, which were used to detect T cell populations by flow cytometry as previously described[567]. The gate was set for single cells, viable cells, and CD45+ cells. All CD45+ cells were interrogated for either CD3+ T cells and CD19+ B cells. The CD3+ T cells were further evaluated for CD4+ and CD8+ cell subpopulations. The gating protocol is summarized in **Figure 52.** All primary antibodies are listed in **Table 8**.

RNA isolation, cDNA synthesis for quantitative RT-PCR

Total RNA was extracted from human islet grafts or pseudoislets using an RNAqueous RNA isolation kit (Ambion, Austin, TX). RNA quality control and quantity assessment (QC/QA) was

performed using Bioanalyzer instrument in the Vanderbilt Function Genomics Shared Resource (FGSR) core lab. cDNA was synthesized using High Capacity cDNA Reverse Transcription Kit (Applied Biosystems, 4368814) according to the manufacturer's instructions. Quantitative PCR (qPCR) was performed using TaqMan assays and reagents from Applied Biosystems (Foster City, CA) as described previously [24,568,569]. Primers used are listed in **Table 9**. SYPL1, SV2A, and CHDA were used for control genes in the immunosuppressive drug study. 18S and ACTB were used in parallel for control genes in the Dapagliflozin (DAPA) study. ACTB was used in the pseudoislet study. Relative changes in mRNA expression calculated by the comparative ΔCt method using Applied Biosystems Stepone Plus System.

Assessment of pancreatic islet function in vitro by macroperifusion

Islet perifusions were performed either by Powers and Brissova research group or Vanderbilt's Islet Procurement and Analysis core. Function of islets from diseased donors and normal controls (**Table 3**) were studied in a dynamic cell perifusion system at a perifusate flow rate of 1 mL/min[570]. The effluent was collected at 3-minute intervals using an automatic fraction collector. Insulin and glucagon concentrations in each perifusion fraction were measured by hormone assays below. Area under the curve (AUC) above baseline hormone release was calculated with the trapezoidal method in GraphPad Prism 8.0. Islets were then lysed with acid-ethanol solution to extract the total hormone content. Insulin and glucagon from supernatants and islet extracts were quantified using the aforementioned assays.

Assessment of pseudoislet function in vitro by static incubation

DAPA experiments. Human islets were cultured overnight in CMRL media at 37°C 5% CO2. The next day 15 size matched islets were pre-cultured for 1 hour with or without 500 nM DAPA in 5.6 mM glucose containing DMEM media with 0.1% BSA. Islets were then cultured for 1 additional hour in DMEM media with 0.1% BSA and the 3.3 mM or 16.7 mM glucose with or without 500 nM DAPA and media and islets were collected for analyses.
Pseudoislets. Pseudoislets (10-20 IEQs/well) were placed in 2 mL of DMEM (media, 2mM glucose) of a 12-well plate (351143, Corning) and allowed to equilibrate for 30 minutes and then were transferred to media containing the stimuli of interest for 40 minutes. Media from this incubation was assessed for insulin and glucagon by assays below.

Microperifusion platform

The microperifusion platform (**Figures 37** and **38**) is based on a previously published microfluidic device with modifications[571]. Design modifications were incorporated using SolidWorks 2018 3D computer-aided design (CAD) software. Microfluidic devices were machined, according to the CAD models, using a computer numerical controlled milling machine (MDX-540, Roland) from poly(methyl methacrylate) workpieces. To reduce the optical working distance, through-holes were milled into the culture wells and a #1.5 glass coverslip was bonded to the bottom component of the microfluidic device using a silicone adhesive (7615A21, McMaster-Carr). Custom gaskets were fabricated using a two-part silicone epoxy (Duraseal 1533, Cotronics Corp) and bonded into the top component of the device using a specialized polyester adhesive (PS-1340, Polymer Science). The two components of the microfluidic device are assembled in a commercially available device holder (Fluidic Connect PRO with 4515

Inserts, Micronit Microfluidics), which creates a sealed system and introduces fluidic connections to a peristaltic pump (Instech, P720) though 0.01" FEP tubing (IDEX, 1527L) and a low volume bubble trap (Omnifit, 006BT) placed in the fluid line just before the device inlet to prevent bubbles from entering the system (see **Figure 38B** for microperifusion assembly).

Fluid dynamics and mass transport modeling

Mathematical modeling of perifusion systems was performed by Ashu Agarwal and Matthew Ishahak at the University of Miami. Two-dimensional (2D) finite element method (FEM) models, which incorporate fluid dynamics, mass transport, and islet physiology, were developed for the macroperifusion and microperifusion platforms and implemented in COMSOL Multiphysics Modeling Software (Release Version 5.0). Fluid dynamics were governed by the Navier-Stokes equation for incompressible Newtonian fluid flow. Convective and diffusive transport of oxygen, glucose, and insulin were governed by the generic equation for transport of a diluted species in the chemical species transport module. Islet physiology was based on Hill (generalized Michaelis-Menten) kinetics using local concentrations of glucose and oxygen, as previously described[572,573]. The geometry of the macroperifusion platform was modeled as the 2D cross-section of a cylindrical tube with fluid flowing from bottom to top (**Figure 38D**). The geometry of the microperifusion platform was modeled as a 2D cross-section of the microfluidic device with fluid flow from left to right (**Figure 38E**). In both the macroperifusion and microperifusion models, 5 islets with a diameter of 150 μm (5 IEQs) were placed in the flow path. FEM models were solved as a time-dependent problem, allowing for intermediate time-steps that corresponding with fraction collection time during macro and microperifusion. A list of the parameters used in the computational models is provided (**Table 10**).

Assessment of pseudoislets by microperifusion

The microperifusion apparatus was contained in a temperature-controlled incubator (37°C) fitted to a Zeiss LSM 880 (Zeiss Microscopy Ltd, Jena, Germany) or Olympus FV3000 (Olympus Corporation, Tokyo, Japan) laser-scanning confocal microscope (**Figure 38B**). Pseudoislets (approximately 25 IEQs/chamber) were loaded in a pre-wetted well, imaged with a stereomicroscope to determine loaded IEQ, and perifused at 100 μL/min flow rate with Krebs-Ringer buffer containing 125 mM NaCl, 5.9 mM KCl, 2.56 mM $CaCl_2$, 1 mM $MgCl_2$, 25 mM HEPES, 0.1% BSA, pH 7.4 at 37°C. Perifusion fractions were collected at 2-minute intervals following a 20-minute equilibration period in 2 mM glucose using a fraction collector (Bio-Rad, Model 2110) and analyzed for insulin and glucagon concentration assays below.

Hormone assays

Insulin, glucagon, and somatostatin were measured by radioimmunoassay (RIA) (human insulin, RI-13K, Millipore; glucagon, GL-32K, Millipore; somatostatin: RK-060-03, Phoenix Pharmaceuticals), enzyme-linked immunosorbent assay (ELISA) (Human insulin, 10-1132-01, Mercodia or 80-ISNHU-E01.1, Alpco; mouse insulin, glucagon, 80-INSMSU-E01, Alpco; 10-1281-01, Mercodia), or Homogeneous Time Resolved Fluorescence (HTRF) assay (glucagon, 62CGLPEH, Cisbio). Assays were selected based on current protocols of the Islet Procurement and Analysis core.

Pseudoislet formation

Human islets were handpicked to purity and then dispersed with 0.025% HyClone trypsin (Thermo Scientific) for 7 minutes at room temperature before counting with an automated Countess II cell counter or manually by hemacytometer. Cells were then resuspended in appropriate volume of Vanderbilt pseudoislet media to allow for seeding into wells at 2000 cells per 200 µL each well of CellCarrier Spheroid Ultra-low attachment microplates (PerkinElmer) or 50 µL per drop in GravityPLUS™ Hanging Drop System (InSphero). In ultra-low attachment plates, pseudoislets were allowed to reaggregate for 6 days before being harvested and studied. For InSphero plates, drops were spun down into collecting reservoir on the 3rd day and 150 µL fresh media was added before allowing to fully reaggregate up to day 6. Full protocol used is available as a supplemental item in Walker, Haliyur et al[560].

Adenovirus

Adenoviral vectors CMV-mCherry (VB180905-1046uck), CMV-hM4Di-mCherry (VB180904-1144bbp), CMV-hM3Dq-mCherry (VB160707-1172csx) were constructed by VectorBuilder Inc (Chicago, IL) and adenovirus was prepared, amplified, and purified by the Human Islet and Adenovirus Core of the Einstein-Sinai Diabetes Research Center (New York, NY) or Welgen Inc (Worcester, MA). Adenovirus for scramble and targeted shRNA were tagged with mCherry or mKate2 under the CMV promoter and shRNA driven by a U6 promoter and were prepared, amplified and purified by Welgen, Inc. Titers were determined by plaque assay. Ad-CMV-GCaMP6f was purchased from Vector Biolabs (Catalog #1910, Malvern, PA). Dispersed human islets were incubated with adenovirus at a multiplicity of infection of 500 for 2 hours in Vanderbilt pseudoislet media before being spun, washed, and plated.

In vitro calcium imaging

GCaMP6f biosensor was excited at 488 nm and fluorescence emission detected at 493 – 574 nm. Images were acquired at 15-µm depth every 5 seconds using a 20x/0.80 Plan-Apochromat objective. Image analysis was performed with MetaMorph v7.1 software (Molecular Devices, San Jose, CA) or CellSens (Olympus). Pseudoislets in the field of view (3-7 pseudoislets/field) were annotated using the region of interest tool. The GCaMP6f fluorescence intensity recorded for each time point was measured across annotated pseudoislet regions and normalized to the baseline fluorescence intensity acquired over the 60 seconds in 2 mM glucose prior to stimulation.

Human islet transplantation

Surgical transplantation of human islets into the kidney capsule were performed by Greg Poffenberger of the Powers & Brissova group. Human islets were transplanted under the kidney capsule of male immunodeficient NOD.Cg-*Prkdc*^{scid}*Il2rg*^{tm1Wjl}/Sz (NSG) mice[574] age 12-18 weeks. Between 1000-2000 islet equivalents per mouse were transplanted beneath the kidney capsule of NSG mice. Islets were allowed to engraft for 2 weeks before beginning experiments.

Tacrolimus (TAC), Sirolimus (SIR), Ex-4, and DAPA administration

Two weeks after human islet transplantation, TAC (0.25 mg/kg/day, NDC 0469-3016-01, Astellas Pharma US, Inc., Northbrook, IL) or saline was delivered by micro-osmotic pumps (Alzet 1004) implanted in recipient NSG mice. Mice were divided equally and randomly between

treatment groups. SIR (0.2 mg/kg, NDC 0008-1030-06, Pfizer, New York, NY) or saline was given by intraperitoneal injection every 72 hours. Saline delivered via osmotic pump vs IP injection had no effect on glucose, insulin levels, morphology or cell composition of grafts and as such, we combined into one control group for data analysis in the immunosuppressive study. Blood concentrations of TAC and SIR were measured by Vanderbilt Diagnostic laboratories. Ex-4 (24nmol/kg/day, California Peptide Research, Inc., Napa, CA) or 1x PBS was also delivered by micro-osmotic pumps (Alzet 1004) as previously described[568]. For the DAPA study, 2 mg/kg daily oral dosing achieved clinically relevant levels and was used. Details on DAPA measurement in mouse serum are described below.

DAPA measurements

DAPA measurements in mouse serum were performed by Wade Calcutt in the Vanderbilt University Mass Spectrometry Core Facility. Sample analyses were carried out using an Acquity UPLC system (Waters Corp., Milford, MA) interfaced with a TSQ Quantum triple-stage quadrupole mass spectrometer (Thermo, San Jose, CA) equipped with a standard APCI ion source. Quantitation was based on SRM in negative ion mode (dapagliflozin: m/z 408 $\rightarrow$ 330, CE 14 V; tolbutamide (internal standard) IS: m/z 269 $\rightarrow$ 106, CE 21 V). Calibration curves were constructed by plotting peak area ratios (dapagliflozin / tolbutamide) against analyte concentrations for a series of eight spiked plasma standards, ranging from 0.05 µM to 50 µM dapagliflozin. A weighting factor of 1/C2 was applied in the linear least-squares regression analysis to maintain homogeneity of variance across the concentration. A Waters Atlantis dC18 analytical column (2.1 mm x 50 mm, 3 µm) was used for all chromatographic separations. Mobile phases were made up of 0.2% propionic acid in (A) H_2O and in (B) CH_3CN. Gradient conditions were as follows: 0–1 min, B = 5%; 1–5 min, B = 5–100%; 5–6.5 min, B = 100%; 6.5–7.0 min, B = 100–5%; 7–11 min, B = 5%. Plasma samples (50 µL) were spiked with tolbutamide (5 µL), lightly vortexed, allowed to stand at room temperature for 15-20 min, and deproteinized with 150 µL of cold acetonitrile. Samples were then vortexed and placed on ice for 10-15 min. Precipitated proteins were removed by centrifugation (10,000 x g, 20 min, 5°C). The clear supernatant (150 µL) of each sample was transferred to a clean microcentrifuge tube and evaporated to dryness under a gentle stream of nitrogen gas. The residue was reconstituted in 100 µL H_2O/ CH_3CN (3:1), vigorously vortexed, and transferred to a 200-µL silanized autosampler vials equipped with Teflon-lined bonded rubber septa.

Assessment of glucose tolerance and stimulated serum insulin and glucagon

Intraperitoneal glucose tolerance tests were performed with 2g/kg glucose after a 6 hour fast with blood glucose measurements at 0', 15', 30', 60', 90', and 120', as previously described[569]. For glucose-stimulated insulin secretion (GSIS), the mice were fasted for 6 hours and then injected intraperitoneally with glucose/arginine (2g/kg) or glucose alone (2g/kg). Blood samples were obtained before (0') and after (15') injection. In Ex-4 experiments the mice were injected with Ex-4 (100µg/kg) 30 minutes before GSIS. Total glucagon (Mercodia, 10-1271-01), mouse insulin (Alpco, 80-INSMSU-E01), and human insulin (Alpco, 80-ISNHU-E01.1) were analyzed by ELISA and also expressed as a ratio to blood glucose levels.

Measurement of total graft insulin or glucagon content

Transplanted human islet grafts were carefully separated from host mouse kidney. The grafts were transferred to 1.5ml Eppendorf tube and cut to 2-3 pieces using a sharp scalpel. 0.25 ml acid alcohol (0.1ml of concentrated HCl into 11ml of 95% ethanol) was added to the Eppendorf. After a 48-hour incubation at 4^{o}C, the supernatant was collected and stored at -80^{o}C. Insulin and glucagon content in graft extracts were diluted at least 1:1000 and measured by ELISA as above.

Electron microscopy

Electron microscopy was performed by Chunhua Dai in the Powers & Brissova group. Ultrastructure of β and α cells was studied by transmission electron microscopy as previously described[569]. The mice were perfused with PBS first for 5 minutes and followed by fixing solution (2.5% gluteraldehyde in 0.1M cacodylate buffer) for 20 minutes. Mouse kidney with transplanted human islet grafts were removed and continued to fix for 1 hour at room temperature. Human grafts were removed and kept in fixing solution at 4^{p}C overnight. The samples then were delivered to Vanderbilt EM core for embedding and sectioning and subsequently imaged on the Philips/FEI Tecnai T12 microscope at various magnifications.

Human islet graft bulk RNA-sequencing

RNA sequencing and analysis of islet grafts was performed at the HudsonAlpha Institute for Biotechnology in Hunstville, AL, by Dr. Nripesh Prasad. A minimum of 500 nanograms of total RNA (RNA isolation as above) was used for downstream RNA-seq applications. Polyadenylated RNAs were isolated using NEBNext Magnetic Oligo d(T)25 Beads. The NEBNext mRNA Library Prep Reagent Set for Illumina (New England BioLabs Inc., Ipswich, MA, USA) was then used to prepare individually bar-coded next-generation sequencing expression libraries as per manufacturer's recommended protocol. Library concentration was assessed using the Qubit 2.0 Fluorometer, and the library quality was estimated by utilizing a DNA 1000 Chip on an Agilent 2100 Bioanalyzer. Accurate quantification for sequencing applications was determined using the qPCR-based KAPA Biosystems Library Quantification Kit (Kapa Biosystems, Inc., Woburn, MA, USA). Paired-end sequencing (100 million, 100-bp, paired-end reads) was performed on an Illumina HiSeq2500 sequencer (Illumina, Inc., San Diego, CA, USA). Post-processing of the sequencing reads from RNA-seq experiments for each sample was performed using HudsonAlpha's unique in-house RNA-seq data analysis pipeline. Briefly, quality control checks on raw sequence data for each sample were performed using FastQC (Babraham Bioinformatics, Cambridge, UK). Raw reads were mapped to the reference *hg19* using TopHat v2.0. The alignment metrics of the mapped reads were estimated using SAMtools. Aligned reads were imported to the commercial data analysis platform AvadisNGS (Strand Scientifics, CA, USA). After quality inspection, the aligned reads were filtered on the basis of read quality metrics; reads with a base quality score of less than 30, alignment score of less than 95, and mapping quality of less than 40 were removed. Remaining reads were then filtered on the basis of their read statistics; missing mates, translocated, unaligned, and flipped reads were removed. The reads list was then filtered to remove duplicates. Samples were grouped and transcript abundance was quantified for this final read list using Trimmed Means of M-values (TMM) as the normalization method. Output data utilized for all subsequent comparisons were

summarized as normalized expression values generated by AvadisNGS. For RNA-seq analyses, p-value of the differentially expressed gene list was estimated by z-test using Benjamini Hochberg corrections of 0.05 for false-discovery rate. Differential expression of genes was further refined on the basis of fold changes (using the default cut-off ≥ ±1.5) observed in comparisons between defined conditions. DAVID v6.8 analysis was performed on the differentially expressed gene list of 1.5x fold change[575]. This data has been deposited in the GEO repository (GSE140230).

T2D FACS-purified α and β cell and whole islet RNA isolation and sequencing

Library preparation and sequencing of samples was performed at MedGenome (Foster City, CA). RNA was extracted from sorted α and β cells using the Invitrogen RNAqueous-Micro Total RNA Isolation kit (Thermo Fisher #AM1931). TURBO DNA-free (Ambion) was used to treat any trace DNA contamination. RNA was quantified by Qubit Fluorometer 2.0 and RNA integrity was confirmed (RIN >7) by 2100 Bioanalyzer (Agilent). Amplified cDNA libraries were constructed using SMART-seq v4 Ultra low Input RNA-kit (Takara) and sequencing was performed on an NovaSeq platform (Illumina) using paired-end reads (100 bp) and 25 million reads per sample.

Analysis was performed in collaboration with Dr. Steve Parker and Vivek Rai at the University of Michigan. Raw RNA-seq reads were processed using FastQC (v0.11.8) for broad quality assessment based on the following parameters: (1) base quality score distribution, (2) sequence quality score distribution, (3) average base content per read, (4) GC distribution in thereads, (5) PCR amplification issue, (6) overrepresented sequences, (7) adapter content. Based on the quality report of fastq files, sequence reads were trimmed using fastq-mcf (v1.05) and cutadapt (v2.5) to only retain high quality sequence for further analysis. The paired-end reads were aligned to the GRCh37/hg19 human reference with GENCODE v19 gene annotation using STAR splice-aware aligner (v2.5.4b; --outSAMUnmapped Within KeepPairs)[576].

Fragments mapping to features type in GENCODE v19 gene annotation were counted using featureCounts from Subread package[577]. The gene list was pruned to contain only protein-coding genes mapping to autosome and chrX, resulting in a total of 20,260 genes. Libraries were assessed using comprehensive quality metrics generated by QoRTs[578] as well as computed derived metrics. Briefly, on the top of QoRTs reported metrics, (1) 5'-3' gene coverage bias (as the ratio of coverage values at the 90%-ile and 10%-ile of the coverage distribution), (2) Kolmogorov-Smirov test statistic between cumulative gene diversity of each library relative to median distribution of all libraries within each cell type and standardized to a mean of 0 and standard deviation of 1 to yield a z-score, (3) number of reads mapped mapped to *Xist* and *SRY* genes, (4) average number of reads mapped to chrM, and (5) transcript integrity number (TIN)[579] were computed for each library. The labeled sex of donors was matched against the gene expression quantified for sex genes to rule out any sample swaps or mislabeling. Principal components for TPM normalized count matrix were computed for each cell type in order to detect potential outliers.

Differential gene expression analysis was performed between T2D and non-diabetic samples for each cell type individually using DESeq2[580]. In order to minimize potential effects of known and

unknown confounding factors, known covariates were included in the DESeq2 model as well accounted for unknown covariates using RUVseq latent variable approach[581]. Briefly, the following multi-step process was followed. (1) remove genes from the raw count matrix which had less than 10 reads in fewer than 25% of the samples for that cell type. (2) first-pass differential expression analysis using DESeq2 with Age, Sex, BMI, and Batch as known covariates. The output result was filtered for genes that were non-significant i.e., not differentially expressed between T2D and non-diabetic samples and had p-value > 0.5. These genes were used as "control" or "empirical" genes for RUVSeq::RUVg function to estimate latent variables accounting for variation in the data not attributed to disease status. (3) The latent variables estimated from the RUVseq run were then used as additional covariates (on the top of Age, Sex, BMI, and Batch where applicable) for the second run of DESeq2. The output results from DESeq2 were filtered for 1% FDR to generate the final list of genes differentially expressed between T2D and ND for each cell type. For each cell type, functional enrichment analysis was performed using RNA-enrich[582] with an FDR threshold of 5%. Terms were condensed using the RelSim function in REVIGO[583] with similarity parameter set to 0.5 and visualized in semantic space using an.xgmml file imported into Cytoscape software[584] v3.8.2. Combined analysis of DE genes (fold change ≥1.5 or ≤-1.5; $p<0.01$) was performed using Metascape[585]. Metascape's heuristic algorithm samples the 20 top-score clusters, selects up to the 10 best scoring terms (lowest p-values) within each cluster, and connects terms pairs with Kappa similarity above 0.3. The resulting network was exported as a .cys file and visualized using Cytoscape, with the most representative term name in each cluster selected manually.

Weighted Gene Correlation Network Analysis (WGCNA)[586] was adopted to create networks from the gene expression data. Briefly, genes were first filtered following the same rule established in Differential Gene Expression where only genes that had at least 10 reads in at least 25% of the samples for each cell type were retained. Raw counts were then processed using varianceStabilizedTransformation function in DESeq2 package and used removeBatchEffect from limma R package[587] to adjust for effects of age, sex, and BMI while protecting for disease status in the design matrix. The normalized and batch corrected count matrix was then used as input to blockwiseModules to create a "signed hybrid" network with "bicor" as the correlation function. The power (k) parameter was selected such that the scale free topology fit reached at least 80% fit. To examine cell type modules associated with quantitative traits of interest, a linear regression-based framework was utilized: (1) inverse normalization of the raw quantitative trait, (2) adjustment for Age, Sex, and BMI by linear regression, and (3) computation the spearman rank correlation between residuals and eigengene of all modules.

Single cell library preparation and sequencing

Sorted or dispersed islet cell samples were resuspended in 0.04% BSA/1X PBS at a density of 630-1,200 cells/µl and then loaded in triplicate (approximately 10,000 cells/replicate) on 10x Chromium chips (PN# 1000009) to ensure consistent results. Gel Bead in Emulsion (GEM) generation and barcoding were performed on the 10x Chromium Controller according to the manufacturer's instructions (10x Genomics Single Cell 3' Library and Gel bead Kit v2 #220104). Immediately after GEMs were generated, samples were transferred to a 0.2ml TempAssure

PCR 8-tube strip (USA Scientific #14024700), capped, and placed into a thermocycler (Bio-Rad T100™ Thermal Cycler) for reverse transcription. After incubation, the GEMs were broken, and pooled cDNA proceeded to cleanup using Silane magnetic beads (10x Genomics #2000048) to remove leftover reagents. cDNA was then amplified through 10 cycles of PCR and cleaned using SPRIselect beads (Beckman Coulter # B23318). Resulting cDNA (average 45 ng/replicate) was checked for quality by Qubit dsDNA HS Assay Kit (Thermo Fisher Scientific #Q32854) and Agilent Bioanalyzer High Sensitivity Kit (Agilent #5067-4626). Final libraries were constructed according to manufacturer's instruction and underwent 14 cycles of PCR amplification after sample index addition, yielding ~953ng and average library size of 486bp. Final libraries were sequenced with a Novaseq sequencer (Illumina) using paired-end reads (100 bp) to average depth of ~146,000 reads per cell.

scRNA-seq alignment, processing, quality control, and analysis

Alignment to reference transcriptome (GRCh38-1.2; gene annotation provided by 10x Genomics) and unique molecular identifier (UMI)-based gene expression quantification was obtained following the Cell Ranger analysis pipeline (v2.1). The "Aggr" function was used to aggregate transcript counts and normalize read depth across 5 islet preparations and their technical replicates, producing one single gene-cell (feature-barcode) matrix. Further data preprocessing and clustering was performed using Seurat version 3.1[588]. Cells with 200-4,000 detected genes and <10% mitochondrial gene expression were retained, and only genes expressed in ≥3 cells were considered for further analysis. Gene expression was normalized for each cell by library size and log-transformed using a size factor of 10,000 molecules per cell. For feature selection, 2,000 highly variable genes were selected using function "FindVariableFeatures." The data was further centered and scaled to zero mean and unit variance implemented in the "ScaleData" function using parameter "vars.to.regress" to regress out mitochondrial gene expression. Cells co-expressing the insulin (*INS*) and glucagon (*GCG*) genes above log expression of 6.5 and 5 respectively, as well as cells expressing *INS* or *GCG* in addition to any other cell type gene marker, were removed as doublets (see **Table 11** for cell type markers used). Transcript counts from lysed cells (ambient mRNA/background RNA) were estimated and genes identified from empty droplets (droplets without cells) using DropletUtils package[589]. Using the raw gene-barcode matrix (Cell Ranger v3.1), UMI threshold of 100 and below were considered ambient transcripts. About ~200 genes were identified as ambient genes and their expression level was noted to remove from the original gene barcode matrix in order to account for transcript stemming from lysed cells. The principal component analysis (PCA) was performed using previously determined 2,000 high variable genes as input. An elbow plot, which ranks the principal components (PCs) based on percent variance per PC, was considered to determine the number of PCs to use for downstream graph-based clustering. "FindNeighbors" and "FindClusters" functions were used with 20 PCs as input for cluster generation and resolution at 0.6. Finally, UMAP dimension reduction was used for cluster visualization.

For comparisons to other single cell RNA-seq experiments, raw gene count matrices were extracted from existing single cell RNA-seq datasets[590–592] and further analyzed using the R package Seurat version 3.1 as described above.

Single cell electrophysiology and gene expression

Patch-seq data was accessed from published data[592] *in collaboration with Dr. Joan Camunas and Dr. Patrick MacDonald.* Two-hundred hand-picked islets per donor were dissociated to single cells using enzyme-free Hanks'-based Cell Dissociation Buffer (Thermo Fisher Scientific, Cat# 13150-016) or Hanks' Balanced Salt Solution and StemPro accutase (ThermoFisher Scientific, Cat# A11105-01) and cultured in 5.5 mmol/L glucose DMEM with L-glutamine, 110 mg/L sodium pyruvate, 10% FBS, and 100 U/mL penicillin/ streptomycin for 1-3 days. Media were then changed to bath solution containing (in mM): 118 NaCl, 20 TEA, 5.6 KCl, 1.2 $MgCl_2$•6 H_2O, 2.6 $CaCl_2$, 5 HEPES, and either 1, 5 or 10 glucose (pH 7.4 with NaOH) in a heated chamber (32–35^{o}C). For whole-cell patch-clamping, fire polished thin wall borosilicate pipettes coated with Sylgard (3-5 MOhm) contained intracellular solution with (in mM): 125 Cs-glutamate, 10 CsCl, 10 NaCl, 1 $MgCl_2$•6H2O, 0.05 EGTA, 5 HEPES, 0.1 cAMP, and 3 MgATP (pH 7.15 with CsOH). Electrophysiological measures were collected using a HEKA EPC10 amplifier and PatchMaster Software (HEKA Instruments, Lambrecht/Pfalz, Germany). We measured cell size as total membrane capacitance. Membrane fusion was stimulated with a series of ten 500 ms depolarizations from -70 to 0mV and normalized to initial cell size. Early and late exocytotic responses reflect plasma membrane fusion of the readily releasable and reserve granules, respectively, while total exocytosis was taken as a measure of exocytotic capacity. In β cells early Ca^{2+} currents reflect mixed L- and P/Q-type currents, while late Ca^{2+} currents reflect primarily P/Q-type currents. The integrated current over a 500 ms depolarization is a measure of Ca^{2+} charge entry and used for normalization of exocytosis to Ca^{2+} influx. Finally, we measured the peak and voltage-dependence of half-inactivation of Na+ currents since these make important contributions to cellular excitability.

Immediately following recordings, the patch pipette was withdrawn and replaced with a wide-bore (0.2-0.5 MOhm) collecting pipette containing lysis buffer without ERCC mix. Cells were then collected bygentle suction and visual confirmation, and then transferred into 8-strip PCR tubes containing 4mL lysis buffer (with ERRC spike-in) on ice and stored at -80^{o}C until cDNA and library preparation. cDNA and sequencing libraries were generated using the SmartSeq-2 protocol as previously described[593]. For patch-seq cells, we first assembled the 8-strip tubes into 96-well plates for increased throughput (Bio-Rad, RC9601 and MSA5001). mRNAs were primed with an anchored oligo-dT and reverse transcribed using an LNA-containing template switching oligo, followed by PCR amplification (21 cycles). Libraries were then generated from the amplified cDNA by tagmentation with Tn5. Libraries were sequenced either in a NextSeq 500 or NovaSeq platform (Illumina) using paired-end reads (75 bp) to an average depth of 1 million reads per cell.

DNA and Whole Exome Sequencing

Genotyping was performed by Dr. Louis Philipson and colleagues at the University of Chicago. DNA was extracted from snap-frozen donor tissue using Wizard Genomic DNA purification kit (Promega, A1120). DNA sequencing was performed as previously described[594,595] using a custom designed next-generation sequencing (NGS) targeted panel that includes 148 genes implicated in monogenic forms of diabetes (neonatal diabetes and MODY), insulin resistance, lipodystrophy, obesity, rare syndromic forms of diabetes, and diabetes candidate genes[596]. All

targeted sequencing results from the atypical T1D donor are listed in **Table 12.** The T1D genetic risk score (GRS) was calculated from 10 variants known to be associated with T1D[597].

Whole-exome sequencing was performed using the Agilent SureSelect Clinical Research Exome Kit (Agilent Technologies) on Illumina NextSeq technology with 150- bp paired end reads and mean depth of coverage over 150X. Variants with a global population frequency >1% in ExAC were excluded. Variants were filtered for relevance to human diabetes using diabetes-related keywords with Online Mendelian Inheritance in Man (OMIM) and Human Gene Mutation Database (HGMD). All variants were interpreted according to the American College of Medical Genetics (ACMG) guidelines. The top 20 variants were assessed for pathogenicity and clinical phenotype and the top nine are reported in **Table 13**.

Statistics

Specific statistical tests used for each dataset are described in the figure legends and text for clarity. Statistical comparisons were performed using Prism v8 software (GraphPad, San Diego, CA) or in RStudio. A p-value less than 0.05 was considered significant. Data were expressed as mean ± standard error of mean.

Table 3. Donor information for islet studies

Donor ID	Age	Sex	BMI	Disease + Duration	Cause of Death	Tissue Source	Isolation Center	Study
08785748	46	M	24.3	---	Head Trauma	IIDP	U Penn	ISD; T2D
08784318	43	M	29.6	---	Head Trauma	IIDP	U Penn	ISD; T2D
08774468	44	F	23.8	---	CVA	IIDP	U Penn	ISD; DAPA; T2D
DON61	55	M	35.6	---	CVA	AHN	AHN	ISD
08930707	55	M	27.8	---	CVA	IIDP	U Illinois	ISD; T2D
DON75	16	M	23	---	Overdose	AHN	AHN	ISD; DAPA
08768702	59	F	22	---	CVA	IIDP	U Wisconsin	ISD; DAPA; T2D
08769130	37	M	27.6	---	CVA	IIDP	U Wisconsin	ISD; DAPA
HPAP004	24	F	32.2	---	Anoxia	HPAP	U Penn	ISD
DON160	15	M	25.1	---	Head Trauma	AHN	AHN	ISD
08769035	43	M	35	---	CVA	IIDP	S California	ISD
08768699	24	F	32.2	---	Anoxia	IIDP	U Penn	DAPA
DON120	19	M	20.1	---	Head Trauma	AHN	AHN	DAPA
08617638	49	M	34	---	CVA	IIDP	S California	DAPA; Pseudo; T2D
R237	61	M	19.7	---	N/A	ADI Islet Core	ADI Islet Core	DAPA
08768998	35	M	24.3	---	CVA	IIDP	S California	DAPA
08611143	32	M	26.2	---	Anoxia	IIDP	U Wisconsin	DAPA
08776514	48	F	29.2	---	CVA	IIDP	U Penn	DAPA
08776508	53	F	25.4	---	N/A	IIDP	U Penn	DAPA
08784601	51	F	21.2	---	CVA	IIDP	U Penn	DAPA
08775095	61	M	42.1	T2D-8y	CVA	IIDP	S California	DAPA
ABIC495	47	M	31.3	T2D-3y	CVA	AHN	AHN	DAPA; T2D
ADBI307	59	M	27.5	T2D-6y	CVA	AHN	AHN	DAPA; T2D
ADDA138	51	M	31.1	T2D-3y	Head Trauma	AHN	AHN	DAPA; T2D
ADLE098	60	M	38.3	T2D-1y	Head Trauma	AHN	AHN	DAPA; T2D
DON78	19	F	23.8	---	CVA	AHN	AHN	DAPA
08774213	20	M	21.7	---	Head Trauma	AHN	AHN	DAPA
08769829	35	M	28.5	---	Head Trauma	AHN	AHN	DAPA
08930762	68	M	24.9	---	CVA	IIDP	U Illinois	DAPA
DON308	35	M	24.7	---	Head Trauma	AHN	AHN	Pseudoislet
08619527	28	M	34.7	---	Head Trauma	IIDP	SL	Pseudoislet
10861888	58	F	36.6	---	Anoxia	IIDP	S California	Pseudoislet; T2D
11046361	57	M	35.9	---	Stroke	IIDP	SL	Pseudoislet; T2D
11106978	20	F	36.9	---	Head Trauma	IIDP	SL	Pseudoislet
11578698	57	M	25.8	---	Stroke	IIDP	SL	Pseudoislet
12713942	41	M	23.5	---	Stroke	IIDP	SL	Pseudoislet
10490796	53	F	26.3	---	Anoxia	IIDP	SL	Pseudoislet
10516338	52	F	26.9	---	Stroke	IIDP	SL	Pseudoislet
R252	26	F	25.4	---	N/A	ADI Islet Core	ADI Islet Core	Pseudoislet
R253	57	M	25.5	---	N/A	ADI Islet Core	ADI Islet Core	Pseudoislet
R260	73	F	26.9	---	N/A	ADI Islet Core	ADI Islet Core	Pseudoislet
R264	44	M	33.7	---	N/A	ADI Islet Core	ADI Islet Core	Pseudoislet; T2D
R282	57	M	26.4	---	N/A	ADI Islet Core	ADI Islet Core	Pseudoislet
R286	41	M	20.3	---	N/A	ADI Islet Core	ADI Islet Core	Pseudoislet
R306	22	F	21.1	---	N/A	ADI Islet Core	ADI Islet Core	Pseudoislet
R309	47	F	27.4	---	N/A	ADI Islet Core	ADI Islet Core	Pseudoislet
R314	31	F	30.3	---	N/A	ADI Islet Core	ADI Islet Core	Pseudoislet
R318	54	M	20.5	---	N/A	ADI Islet Core	ADI Islet Core	Pseudoislet
R323	60	F	24.9	---	N/A	ADI Islet Core	ADI Islet Core	Pseudoislet
R340	36	M	23.3	---	N/A	ADI Islet Core	ADI Islet Core	Pseudoislet
HPAP022	39	F	34.76	---	Anoxia	HPAP	U Penn	Pseudoislet
HPAP035	35	M	26.91	---	Anoxia	HPAP	U Penn	Pseudoislet
AHGV031	51	F	22.057	---	ICH	IIAM	AHN	Pseudoislet
AGHY243	19	M	20.96	---	Anoxia	OPO	U Penn	Pseudoislet
R310	25	M	26.4	---	N/A	ADI Islet Core	ADI Islet Core	Pseudoislet
AHG3262	58	F	31.07	---	CVA	OPO	U Penn	Pseudoislet
DON184	14	F	24.13	---	Anoxia	OPO	U Penn	scRNA-seq

DON185	39	F	34.76	---	Anoxia	OPO	U Penn	scRNA-seq
08768781	50	M	22.4	---	CVA	IIDP	U Penn	scRNA-seq
08768783	59	F	32.3	---	CVA	IIDP	U Wisconsin	scRNA-seq
R232	66	F	18.5	---	CVA	ADI Islet Core	ADI Islet Core	scRNA-seq
AIBT467	19	M	29.142	---	Head Trauma	IIAM	AHN	RFX6
AIAQ288	22	M	35.706	---	Head Trauma	IIAM	U Penn	RFX6
17277513	43	F	36.5	---	CVA	IIDP	S California	RFX6
AHLA313	47	M	32.78	---	Anoxia	OPO	U Penn	RFX6
18021384	56	M	24.2	---	Anoxia	IIDP	SL	RFX6
17528599	60	**M**	29.9	---	Anoxia	IIDP	U Penn	RFX6
ACHM315	55	M	35.565	---	CVA/ICH	IIAM	AHN	T2D
ADBN085	19	M	27.2	---	Head Trauma	NDRI	AHN	T2D
ADD3367	20	M	27.765	---	Head Trauma	NDRI	AHN	T2D
AFEL051	24	M	20.8	---	Anoxia, Drug Intoxication	OPO	AHN	T2D
ACKV075	26	F	35.9	---	Anoxia	IIDP	U Penn	T2D
ABIT067	32	F	39.4	---		IIDP	U Wisconsin	T2D
AEDI259	19	M	20	---	Head Trauma	NDRI	AHN	T2D; Atypical T1D
AEDZ192	19	M	21.154	---	Anoxia	NDRI	AHN	T2D; Atypical T1D
ADBD275A	35	F	23.6	---	Anoxia	IIDP	U Penn	T2D
AFCU134	39	F	34.76	---	Anoxia, Drug Intoxication	OPO	AHN	T2D
AFEF080	55	F	24.242	---	CVA/ICH	OPO	AHN	T2D
AFES372	52	M	29.2	---	ICH	OPO	AHN	T2D
AFG1440	45	F	29.752	---	Anoxia, CVA	OPO	AHN	T2D
AFJJ008	42	M	32.2	---	Anoxia, Drug Intoxication	OPO	AHN	T2D
AFL5294	35	M	24.691	---	Head Trauma, CVA/ICH	OPO	AHN	T2D
AGBA390	48	M	24.567	---	Anoxia, CVA	OPO	AHN	T2D
AGKS491	59	M	32.686	---	Head Trauma, CVA/ICH	IIAM	AHN	T2D
AHAD144	46	F	32.885	---	CVA/ICH	IIAM	AHN	T2D
11791244	47	M	36.1	---	CVA/ICH	IIDP	S California	T2D
11633049	48	M	38.8	---		IIDP	U Wisconsin	T2D
ACKB319	49	F	31.6	---	CVA	IIDP	U Penn	T2D
ADBQ038	50	M	30.2	---	CVA	IIDP	U Illinois	T2D
ADFR455	53	M	31.1	---	Anoxia	IIDP	U Wisconsin	T2D
10252228	55	F	35.7	---		IIDP	U Wisconsin	T2D
R265	64	M	37.6	---		ADI Islet Core	ADI Islet Core	T2D
R200	65	M	27.1	---	Unknown	ADI Islet Core	ADI Islet Core	T2D
ABHQ115	49	F	33.8	T2D-3y	CVA/ICH	IIAM	AHN	T2D
ABIQ254	66	F	32.78	T2D-3y	CVA/ICH	IIAM	AHN	T2D
ABKD062	61	F	31.2	T2D-4y	CVA/ICH	NDRI	AHN	T2D
ACIA085	64	M	33.168	T2D-5y	Head Trauma, ICH	IIAM	AHN	T2D
ADC1496	40	F	43.066	T2D-0y	CVA/ICH	IIAM	AHN	T2D
ADIX484	50	M	32.9	T2D-4y	CVA/ICH	NDRI	AHN	T2D
AEDN413	42	M	41.975	T2D-0y	CVA/ICH	IIAM	AHN	T2D
AEJR177	43	M	36.056	T2D-1y	Head Trauma	IIAM	AHN	T2D
AFCM451	37	F	49.766	T2D-5y	Anoxia, CVA	IIAM	AHN	T2D
AFFT486	59	M	36.89	T2D-0y	CVA/ICH	IIAM	AHN	T2D
AFI2364	53	M	30.116	T2D-7y	Anoxia	OPO	AHN	T2D
AFKE426	52	M	33.599	T2D-7y	CVA/ICH	IIAM	AHN	T2D
AGAH468	43	M	37.326	T2D-6y	CVA/ICH	IIAM	AHN	T2D
AGAL381	52	F	21.9	T2D-10y	CVA/ICH	NDRI	AHN	T2D
AGJU173	52	F	29.2	T2D-0y	CVA/ICH	IIAM	AHN	T2D
ACGI428	22	M	25.7	T1D-8y	Anoxia	IIAM	AHN	Atypical T1D
ABJG028	7	M	26.6	---	Respiratory Arrest	NDRI	AHN	Atypical T1D
ABIU320	8	F	16.1	---	ICH	IIAM	AHN	Atypical T1D

ADHM183	8	M	17.2	---	Anoxia	NDRI	AHN	Atypical T1D
AADK480	9	M	15.5	---	Head Trauma	NDRI	AHN	Atypical T1D
ABHF310	11	M	18.3	---	Anoxia	IIAM	AHN	Atypical T1D
AEFZ087	16	M	23.2	---	Head Trauma	IIAM	AHN	Atypical T1D
ACCZ181	19	M	34.1	---	Head Trauma	IIDP	U Wisconsin	Atypical T1D

M, Male; F, Female; IIDP, Integrated islet distribution program; ISD, Immunosuppressive drug; T2D, Type 2 diabetes; DAPA, dapagliflozin; AHN, Allegheny Health Network; CVA, cerebrovascular accident (stroke); ICH, intracranial hemorrhage; ADI, Alberta Diabetes Institute; OPO, organ procurement organization; NDRI, national disease research interchange; IIAM, international institute for the advancement of medicine; SL, Scharp lacy; N/A, not available.

Table 4. Donor information for histology

Donor ID	Age	Sex	BMI	Disease + Duration	Cause of Death	Tissue Source	Study
ACEZ011	20	M	19.442	---	Head trauma	IIAM	Transcription Factors; aT1D
ABI2259	35	M	26.852	---	Head trauma	IIAM	Transcription Factors; T2D
ACHM315	55	M	35.565	---	CVA/ICH	IIAM	T2D
ADBN085	19	M	27.2	---	Head Trauma	NDRI	T2D
ADD3367	20	M	27.765	---	Head Trauma	NDRI	T2D
AEDI259	19	M	20	---	Head Trauma	NDRI	T2D
AEDZ192	19	M	21.154	---	Anoxia	NDRI	T2D
AFCU134	39	F	34.76	---	Anoxia, Drug Intoxication	OPO	T2D
AFEF080	55	F	24.242	---	CVA/ICH	OPO	T2D
AFES372	52	M	29.2	---	ICH	OPO	T2D
AFFN281	52	M	28.09	---	Head Trauma	OPO	T2D
AFG1440	45	F	29.752	---	Anoxia, CVA	OPO	T2D
AFJJ008	42	M	32.2	---	Anoxia, Drug Intoxication	OPO	T2D
AFL5294	35	M	24.691	---	Head Trauma, CVA/ICH	OPO	T2D
AGBA390	48	M	24.567	---	Anoxia, CVA	OPO	T2D
AGKS491	59	M	32.686	---	Head Trauma, CVA/ICH	IIAM	T2D
AHAD144	46	F	32.885	---	CVA/ICH	IIAM	T2D
ABHQ115	49	F	33.8	T2D-3y	CVA/ICH	IIAM	T2D
ABIC495	47	M	31.3	T2D-3y	CVA/ICH	IIAM	T2D
ABIQ254	66	F	32.78	T2D-3y	CVA/ICH	IIAM	T2D
ABKD062	61	F	31.2	T2D-4y	CVA/ICH	NDRI	T2D
ACIA085	64	M	33.168	T2D-5y	Head Trauma, ICH	IIAM	T2D
ADBI307	59	F	27.548	T2D-6y	CVA/ICH	IIAM	T2D
ADC1496	40	F	43.066	T2D-0y	CVA/ICH	IIAM	T2D
ADDA138	56	M	30.973	T2D-3y	Head Trauma	NDRI	T2D
ADIX484	50	M	32.9	T2D-4y	CVA/ICH	NDRI	T2D
ADLE098	60	M	38.302	T2D-1y	CVA/ICH	IIAM	T2D
AEDN413	42	M	41.975	T2D-0y	CVA/ICH	IIAM	T2D
AEJR177	43	M	36.056	T2D-1y	Head Trauma	IIAM	T2D
AFCM451	37	F	49.766	T2D-5y	Anoxia, CVA	IIAM	T2D
AFFT486	59	M	36.89	T2D-0y	CVA/ICH	IIAM	T2D
AFHT091	54	M	38.28	T2D-0.66y	Head Trauma	IIAM	T2D
AFI2364	53	M	30.116	T2D-7y	Anoxia	OPO	T2D
AFKE426	52	M	33.599	T2D-7y	CVA/ICH	IIAM	T2D
AGAH468	43	M	37.326	T2D-6y	CVA/ICH	IIAM	T2D
AGAL381	52	F	21.9	T2D-10y	CVA/ICH	NDRI	T2D
AGJU173	52	F	29.2	T2D-0y	CVA/ICH	IIAM	T2D
ACGI428	22	M	25.7	T1D-8y	Anoxia	IIAM	Atypical T1D
ADHM183	8	M	17.2	---	Anoxia	NDRI	Atypical T1D
AEDI259	19	M	20.1	---	Head Trauma	NDRI	Atypical T1D
AEDZ192	19	M	21.2	---	Anoxia	NDRI	Atypical T1D
AACS476	10	M	19.3	---	Head Trauma	NDRI	Atypical T1D
ACEZ381	24	M	35.5	---	Head Trauma	IIAM	Atypical T1D
ABI2259	35	M	26.8	---	Head Trauma	IIAM	Atypical T1D
ACHM315	55	M	35.6	---	CVA	IIAM	Atypical T1D

M, Male; F, Female; T2D, Type 2 diabetes; AHN, Allegheny Health Network; CVA, cerebrovascular accident (stroke); ICH, intracranial hemorrhage; OPO, organ procurement organization; NDRI, national disease research interchange; IIAM, international institute for the advancement of medicine.

Table 5. Primary antibodies for immunohistochemistry

Antigen	Species	Source	Catalog #	Dilution
ARX	Sheep	R&D Systems	AF7068	1:2000
C-peptide	Mouse	DSHB	GN-ID4	1:2000
Caveolin-1	Rabbit	Abcam	ab2910	1:2000
CD31	Mouse	BD Pharmingen	550389	1:100
CD45	Mouse	BD Pharmingen	347460	1:100
Collagen-IV	Rabbit	Rockland	600-401-106S	1:1000
GFP	Chicken	Abcam	ab13970	1:1000
Glucagon	Rabbit	Cell Signaling	2760s	1:200
Glucagon	Mouse	abcam	Ab10988	1:200
Iba1	Rabbit	Wako	019-19741	1:500
Insulin	Guinea pig	Dako	A0564	1:1000
Ki67	Rabbit	Abcam	ab15580	1:1000
MAFA	Rabbit	Novus	NBP1-00121	1:250
MAFB	Mouse	R&D Systems	MAB3810	1:1000
MAFB	Rabbit	Roland Stein	N/A	1:3000
mCherry	Rabbit	Abcam	ab167453	1:1000
NKX2.2	Mouse	DSHB	74-5A5	1:1000
Nkx6.1	Rabbit	BCBC/P. Serup	N/A	1:2000
SGLT2	Rabbit	Novus Biologicals	NBP1-92384	1:100
SGLT2	Rabbit	abcam	Ab-58298	1:100
Somatostatin	Goat	Santa Cruz	sc7819	1:500
PAX6	Rabbit	Covance	PRB-28P-100	1:5000
PDX1	Rabbit	C. V. E. Wright	N/A	1:5000
pS6 Ser 235/236	Rabbit	Cell Signaling	4858s	1:500
pS6 Ser 240/244	Rabbit	Cell Signaling	5364s	1:500
VEGFR2	Goat	R&D Systems	AF644	1:2000

DSHB – Developmental Studies Hybridoma Bank (University of Iowa)

Table 6. Secondary antibodies for immunohistochemistry

Host Species	Primary Ab Species	Fluorophore	Source	Catalog #	Dilution
Donkey	Chicken	Cy2	Jackson Immunoresearch	703-225-155	1:500
Donkey	Goat	Cy2	Jackson Immunoresearch	705-225-147	1:500
		Cy3	Jackson Immunoresearch	705-165-147	1:500
		Cy5	Jackson Immunoresearch	705-175-147	1:200
Donkey	Guinea pig	Cy2	Jackson Immunoresearch	706-225-148	1:500
		Cy3	Jackson Immunoresearch	706-165-148	1:500
		Cy5	Jackson Immunoresearch	706-175-148	1:200
Donkey	Mouse	Cy2	Jackson Immunoresearch	715-225-150	1:500
		Cy3	Jackson Immunoresearch	715-165-150	1:500
		Cy5	Jackson Immunoresearch	715-175-150	1:200
Donkey	Rabbit	Cy2	Jackson Immunoresearch	711-225-152	1:500
		Cy3	Jackson Immunoresearch	711-165-152	1:500
		Cy5	Jackson Immunoresearch	711-175-152	1:200
Donkey	Rat	Cy2	Jackson Immunoresearch	712-225-153	1:500
		Cy3	Jackson Immunoresearch	712-165-153	1:500
		Cy5	Jackson Immunoresearch	712-175-153	1:200

Table 7. CODEX antibodies

Antigen	Clone	Conjugation	Source (catalog #)	Dilution	Reporter
CD45	HI30	Akoya	Akoya (4150003)	200	Alexa488-RX001
CD8	SK1	Akoya	Akoya (4150004)	100	Alexa488-RX004
CD38	HB-7	Akoya	Akoya (4150007)	200	Alexa488-RX007
Pan-Cytokeratin	AE-1/AE-3	Akoya	Akoya (4150020)	500	Alexa488-RX019
HLA-DR	L243	Akoya	Akoya (4250006)	300	Atto550-RX026
CD31	WM59	Akoya	Akoya (4250009)	400	Atto550-RX032
Ki67	B56	Akoya	Akoya (4250019)	600	Atto550-RX047
CD34	561	Akoya	Akoya (4250020)	200	Atto550-RX035
E-cadherin	4A2C7	Akoya	Akoya (4250021)	200	Atto550-RX014
CD3	UCHT1	Akoya	Akoya (4350008)	100	Cy5-RX015
CD4	SK3	Akoya	Akoya (4350010)	100	Cy5-RX021
CD11c	S-HCL-3	Akoya	Akoya (4350012)	100	Cy5-RX027
Glucagon	K79bB10	Custom	Abcam (ab10988)	400	Alexa488-RX016
C-peptide	C-PEP-01	Custom	ThermoFisher (MA1-19159)	200	Alexa488-RX031
Ghrelin	883622	Custom	R&D (MAB8200)	400	Alexa488-RX040
CD163	GHI/61	Custom	BioLegend (333602)	200	Alexa488-RX043
MCAM (CD146)	P1H12	Custom	BioLegend (361002)	100	Alexa488-RX046
β-Tubulin	TUJ1	Leinco	BioLegend (801201)	150	Atto550-RX017
Somatostatin	7G5	Custom	Novus (NBP2-37447)	400	Atto550-RX020
Arginase I	Polyclonal	Custom	Novus (NBP1-32731)	200	Atto550-RX029
Pancreatic polypeptide	548416	Custom	R&D (MAB62971)	600	Atto550-RX041
CD14	HCD14	Custom	BioLegend (325602)	100	Cy5-RX024
α-Amylase	Polyclonal	Leinco	Abcam (ab35414)	100	Cy5-RX030
IBA1	EPR16589	Custom	Abcam (ab221790)	200	Cy5-RX033
Chromogranin A	LK2H10+PHE5+CGA/414	Custom	Novus (NBP2-34674)	800	Cy5-RX036
Collagen IV	EPR20966	Leinco	Abcam (ab226485)	50	Cy5-RX042
CD206	15-2	Custom	BioLegend (321102)	200	Cy5-RX045

Table 8. Antibodies for flow cytometry and sorting

	Antigen		Species	Source	Catalog #	Dilution
Primary	CD39L3 (NTPDase3)		Mouse (IgG)	gift of J. Sévigny	N/A	1:50
	HIC0-4F9 [Biotin] (HPi1)		Mouse (IgG)	Novus	NBP1-18872B	1:100
	HIC3-2D12 (HPa3)		Mouse (IgM)	gift of P. Streeter	N/A	1:100
	Insulin		Chicken	Gallus Immunotech	ABI	1:10
	Glucagon-Pacific Blue		Mouse	Sigma Aldrich	G2654	1:600
	Somatostatin-AlexaFlour 488		Mouse	LS Bio	LS-C169129-100	1:200
	CD45		Mouse	BD BioSciences	560178	1:100
	CD3		Mouse	BD BioSciences	555334	1:100
	CD19		Mouse	BD BioSciences	555412	1:25
	CD4		Mouse	BD BioSciences	555346	1:25
	CD8		Mouse	BD BioSciences	561953	1:25
Secondary	**Fluorophore**	**Host**	**Primary Ab**	**Source**	**Catalog #**	**Dilution**
	APC	Donkey	Chicken	Jackson Immuno	703-136-155	1:25
	APC	Goat	Mouse (IgG)	BD Pharmingen	550826	1:500
	BV421–Strep	--	--	BD Pharmingen	563259	1:500
	PE	Goat	Mouse (IgM)	Jackson Immuno	115-116-075	1:1000

Table 9. Primers for qRT-PCR

Gene Symbol	Catalog #
18S	Hs99999901_s1
ABCC8	Hs01093761_m1
ACTB	Hs99999903_m1
CACNA1D	Hs00167753_m1
CHGA	Hs00900370_m1
GCG	Hs01031536_m1
GCK	Hs01564555_m1
INS	Hs02741908_m1
KCNJ11	Hs00265026_s1
KCNK16	Hs00259530_m1
MAFA	Hs01651425_s1
MAFB	Hs00534343_s1
MTOR	Hs00234508_m1
NFATC1	Hs00542678_m1
NFATC2	Hs00905451_m1
NFATC3	Hs00190046_m1
NFATC4	Hs00190037_m1
NKX6.1	Hs00232355_m1
PDX1	Hs00236830_m1
RFX6	Hs00941591_m1
RPS6	Hs04195024_g1
RPS6KB1	Hs00356367_m1
RPTOR	Hs00375332_m1
SLC5A2	Hs00894642_m1
SV2A	Hs01059458_m1
TFRC	Hs00951083_m1

Table 10. Computational Modeling Parameters

	Parameter	Macroperifusion	Microperifusion
Fluid Dynamics	Fluid	Water	
	Density	993 kg/m^3	
	Dynamic Viscosity	$7x10^{-4}$ Pa/s	
	Inlet Velocity	$2.13x10^{-4}$ m/s	$3.34x10^{-2}$ m/s
Mass Transport	Diffusion Coefficient, Glucose in Fluid	$9x10^{-10}$ m^2/s	
	Diffusion Coefficient, Glucose in Islets	$3x10^{-10}$ m^2/s	
	Diffusion Coefficient, Oxygen in Fluid	$3x10^{-9}$ m^2/s	
	Diffusion Coefficient, Oxygen in Islets	$2x10^{-9}$ m^2/s	
	Diffusion Coefficient, Insulin in Fluid	$1.5x10^{-10}$ m^2/s	
	Diffusion Coefficient, Insulin in Islets	$0.5x10^{-10}$ m^2/s	
	Oxygen Concentration	0.2 mol/m^3	
Islet Physiology	Number of Islets	5	
	Radius	$7.5x10^{-5}$ m	
	Maximum Oxygen Consumption Rate	-0.034 $mol/s/m^3$	
	Maximum Glucose Consumption Rate	-0.028 $mol/s/m^3$	
	Insulin Release Rate Constant	$3x10^{-3}$ 1/s	
	Maximum First Phase Insulin Secretion Rate	$10x10^{-5}$ $mol/s/m^3$	
	Maximum Second Phase Insulin Secretion Rate	$1.8x10^{-5}$ $mol/s/m^3$	

*Parameters in center apply to both perifusion systems

Table adapted from Walker, Haliyur et al. 2020[560].

Table 11. Markers used for cell type annotation in scRNA-seq.

Cell type	Gene marker(s)
α cell	*GCG*
β cell	*INS*
δ cell	*SST*
γ cell	*PPY*
ε cell	*GHRL*
Acinar	*PRSS1*
Ductal	*KRT19*
Stellate	*PDGFRB, COL1A1*
Endothelial	*PECAM1*
Immune	*HLA-DRA*

Table adapted from Shrestha, Saunders, Walker et al.[561]

Table 12. DNA sequencing of 22yM donor with 8 years of T1D for variants associated with monogenic diabetes.

Donor	Gene	Chr	Transcript ID (NCBI)	Nucleotide	Amino Acid Change	dbSNP ID	MAF	POLY Score
22yM, 8yrs T1D	*CDKN1C*	11	NM_000076.2	c.543_554del	p.Ala191_Pro194del	NA	0	0
	CYP27B1	12	NM_000785.3	c.963+7T>G	-	NA	0	0
	EIF2AK3	2	NM_004836.5	c.-201A>G	-	rs144057685	0.005	0
	FBN1	15	NM_000138.4	c.3294C>T	p.Asp1098Asp	rs140587	0.005	0
	GCK	7	NM_000162.3	c.209-8G>A	-	rs144798843	0.001	0

Chr – chromosome, MAF – Minor allele frequency; DNA isolated from pancreatic sample of donor was subjected to DNA sequencing covering coding regions and splice junctions of 148 genes associated with monogenic diabetes (3).

Table 13. Variants associated with diabetes arising from whole exome sequencing of 22yM donor with 8 years of T1D

Donor	Gene	Transcript ID (NCBI)	Nucleotide	Amino Acid Change	Zygosity	Allele Frequency (gnomAD)	SIFT
22yM 8yrs T1D	*ABCC9*	NM_005691.3	c.3594G>A	Met1198Ile	heterozygous	0.0071%	Tolerated
	COL6A5	NM_153264.6	c.2006T>G	Val669Gly	heterozygous	0.5300%	Deleterious
	EPG5	NM_020964.3	c.3280G>A	Gly1094Ser	heterozygous	0.0250%	Tolerated
	OAS1	-	c.812A>T	Tyr271Phe	heterozygous	0.0016%	Tolerated
	PPIP5K2	NM_001345875.2	c.3325A>G	Ile1109Val	heterozygous	0.0920%	Tolerated
	SLC2A4	-	c.811C>T	Arg271Trp	heterozygous	0.0000%	Deleterious
	SOS1	-	c.2593T>G	Leu865Val	heterozygous	0.0000%	Deleterious
	UCP1	-	c.169G>A	Gly57Ser	heterozygous	0.0290%	Tolerated
	ZZEF1	-	c.8785C>G	Leu2929Val	heterozygous	0.0510%	Deleterious

SIFT–Sorting Intolerant From Tolerant; Donor DNA underwent whole-exome sequencing. Variants were filtered for relevance to human diabetes using key words with the top nine variants reported here.

CHAPTER III:
ASSESSMENT OF THERAPEUTICS ON HUMAN ISLETS IN AN IN VIVO SYSTEM

Some text and data in this chapter have been adapted from Dai, Walker, et al., 2020[558], and Dai, Walker, et al., 2020[559].

Chapter introduction

Many pharmaceuticals have effects on pancreatic islets and glucose homeostasis. Some have proven to be effective in treating diabetes while others have different primary indications but development or worsening of diabetes is a consequential side effect[598–601]. Given the central role of the islet in glucose homeostasis and diabetes, understanding how human islets respond to different therapeutic treatments is of great interest. To address this question, in vitro culture in the presence of the therapeutic of interest is a common approach; however, these studies have inherent limitations. To extend and complement these findings, we have developed a transplantation model of human islets into immune-deficient mice[574] with dosing regimens designed to achieve clinically relevant drug levels. This approach has several advantages including 1) assessment in a dynamic in vivo environment that more closely mimics the clinical situation and 2) assessment for much longer time points than is possible with islets in culture. This chapter describes how we have used this approach to address two key questions: 1) how immunosuppressive drugs relate to the development of post-transplantation diabetes mellitus and whether this can be alleviated and 2) how the diabetes medication dapagliflozin, an SGLT2 inhibitor, affects islets. These studies have led to important insight into the pathogenesis of post-transplantation diabetes mellitus and how we might approach the rational design of clinical trials to reduce the incidence as well as into the mechanism of action of islet effects from SGLT2 inhibitors.

Tacrolimus- and sirolimus-induced human β cell dysfunction is reversible and preventable

Introduction

The development of effective immunosuppressive agents has enabled organ and cell transplantation to become a life-saving medical achievement. However, a number of potential adverse events following transplantation threaten the health of both the patient and the graft, including post-transplantation diabetes mellitus (PTDM)[602]. PTDM affects between 7-74% of transplantation patients (with the variance typically being attributed to center-specific differences in pre-transplant screenings and diagnostic tests)[603]. Furthermore, the risk for PTDM progressively increases in the post-transplantation period with PTDM incidence increasing linearly with time[604]. PTDM is associated with reduced graft function, increased graft loss, and increased patient mortality, making it both a common and significant complication[605]. In PTDM, both reduced insulin secretion and impaired insulin action through the development or worsening of insulin resistance have been proposed as mechanisms[603]. The pathogenesis of PTDM is likely multifactorial and shares T2D genetic risk factors[603,606]. Since treatment with immunosuppressive agents tacrolimus (TAC) and sirolimus (SIR) is associated with PTDM[607–

[610], elucidating the effect of these immunosuppressive agents on human β cells may aid the understanding of the pathophysiology and progression of PTDM.

TAC inhibits calcineurin, a calcium/calmodulin-dependent phosphatase which controls activation of the nuclear factor of activated T cells (NFAT) transcription factors. Calcineurin inhibition leads to immunosuppression by preventing T cell activation and cytokine production[611]. The calcineurin/NFAT pathway is also active in other cell types, and inhibition in these cells is thought to mediate the various toxicities of TAC[611]. In pancreatic β cells, calcineurin/NFAT signaling is thought to positively regulate insulin secretion and, in juvenile human islets, β cell proliferation[568,612]. Furthermore, TAC treatment has been shown to increase β cell apoptosis in cultured human islets[613,614].

In contrast, SIR inhibits mechanistic target of rapamycin (mTOR), a key regulator of cell metabolism, growth and proliferation[615]. Inhibition of mTOR leads to immunosuppression by preventing T and B cell expansion[616]. Like the calcineurin/NFAT pathway, mTOR signaling is crucial in many cell types, and its inhibition has adverse effects, including disruption of glucose homeostasis. In insulin-sensitive tissues, SIR treatment disrupts insulin signal transduction, causing insulin resistance[603,617]. In mouse islets and human islets in vitro, SIR treatment reduces insulin secretion and decreases β cell survival and proliferation[618,619].

While both TAC and SIR appear to have effects on β cells, existing studies have largely been performed in vitro or in murine models and have used a wide range of drug doses and treatment schedules that may not be clinically relevant. Importantly, mouse islets show a number of key differences to human islets including in their stress response, proliferation rates, and both basal and stimulated insulin secretion[21,24,569]. In addition, studies of human islets in vitro have been limited to a few days, not mimicking the clinical situation in humans. Thus, findings from prior studies are difficult to translate to patients with PTDM. We therefore sought to clarify the β cell effects of TAC or SIR treatment using human islets in an in vivo transplant model that mimics the clinical setting and drug exposure. Here, we show that TAC or SIR treatment at clinically relevant levels leads to β cell dysfunction related to multiple islet effects. We also demonstrate that TAC- or SIR-induced β cell effects are reversible, and that they can, at least partially, be prevented with concurrent glucagon-like peptide-1 (GLP-1) receptor agonist treatment.

Results

Tacrolimus and sirolimus impair insulin secretion from human β cells at clinically relevant levels in vivo

To investigate immunosuppressive drug exposure in a system that would mimic the human islet response in vivo, we used a human islet transplant model in the immunosuppressed NOD.Cg-*Prkdc*^{scid}*Il2rg*^{tm1Wjl}/Sz (NSG) mouse which have deficiencies in both innate and adaptive immunity[574]. We first examined the pharmacokinetics of TAC and SIR in the NSG mouse, and defined dosing regimens that achieved therapeutic drug levels [TAC, 5 to 20 ng/mL[620]; SIR, 5-20 ng/mL[621]]. Surprisingly, the half-life of TAC in the NSG mouse is much shorter than in humans (2 hours versus 12 hours); thus, we utilized 0.25mg/kg/day delivered by an implanted osmotic pump to achieve clinically relevant levels (**Figure 12A**) For SIR treatment, we found that drug

clearance varied drastically between mouse strains, highlighting the importance of robustly characterizing dosing regimens in each model when studying these drugs in mice. Ultimately, 0.2mg/kg of SIR delivered via IP injection every 72 hours achieved clinically relevant concentrations in the NSG mouse (**Figure 12B**). These doses are much lower than used in prior studies which did not report levels of these drugs and raises questions about the clinical relevance and translational potential of prior findings.

Two weeks following engraftment of human islets, mice began treatment with TAC, SIR, or saline for 4 weeks (**Figure 12C**). Human islet preparations were analyzed for viability, purity, and function by perifusion analysis; only islets which passed stringent quality control were used for subsequent studies[570]. We verified targeting of the mTOR pathway by showing that SIR treatment drastically reduced ribosomal protein S6 phosphorylation at two critical motifs, 235/236 and 240/244 in human grafts (**Figure 13A-13D**). Interestingly, TAC also decreased S6 phosphorylation.

Both TAC-treated and SIR-treated mice showed impaired glucose handling by glucose tolerance testing (GTT) with SIR treatment showing greater impairment, likely reflecting SIR-induced insulin resistance[617] (aggregate: **Figure 12D-12E**; individual donors: **Figure 14**). Mice treated with TAC had no change in fasting blood glucose while mice treated with SIR showed a slightly higher fasting blood glucose (**Figure 12F**). As changes in blood glucose likely reflect impact on endogenous mouse organ systems and human islet grafts, we evaluated function of the grafts by measuring serum insulin levels using a human-specific insulin assay and normalizing these to the glucose level of the mouse. In fasted mice, SIR treatment did not affect human insulin or the insulin/glucose ratio while TAC treatment decreased human insulin and the insulin/glucose ratio (**Figure 12G-12H**; individual donors: **Figure 15**).

After glucose-arginine stimulation, human islets in both TAC and SIR treatment groups secreted less insulin compared to saline-treated animals (**Figure 12I-12K**; individual donors: **Figure 15**). SIR-treated mice had both higher blood glucose and human insulin than TAC-treated mice. To assess for direct effects on islets, we cultured human islets in vitro with clinically relevant doses of TAC or SIR (20 ng/mL) for 1, 24, and 48 hours and found that after 48 hours of exposure, insulin secretion was inhibited at both basal (5.6mM) and high (16.7mM) glucose (**Figure 16**). These results indicate that at clinically relevant levels, both SIR and TAC directly affect human β cells in vivo by impairing insulin secretion in the stimulated and/or fasted state and that this could be a significant contributor to PTDM.

Tacrolimus and sirolimus treatment do not affect β cell proliferation or apoptosis in vivo

To investigate mechanisms underlying the human β cell dysfunction induced by TAC or SIR treatment, we harvested islet grafts for analysis. As both the calcineurin and mTOR pathway are involved in the regulation of β cell mass[568,612–614,619], we analyzed β cell proliferation by Ki67 but found low proliferation rates (<0.5%) with no differences between treatment groups (**Figure 17A, 17C**). Likewise, we assessed for apoptosis by the TUNEL assay; however, apoptotic β cells in the grafts were extremely rare with no difference between treatment groups (**Figure**

17B, 17D), indicating that neither TAC nor SIR treatment for 4 weeks at clinically relevant doses affect β cell proliferation or apoptosis in human islets in vivo.

Tacrolimus and sirolimus treatment increase amyloid formation and macrophages in human islet grafts

Amyloid deposition in islets, an important pathologic feature in type 2 diabetes, may be a cause or a hallmark of dysfunctional islets[347]. Because transplanted human islets form amyloid deposits and this is exacerbated by stressors such as insulin resistance[569], we assessed the grafts for amyloid deposition. Interestingly, we found that individual donors varied greatly in the degree of amyloid deposition seen and thus report values normalized to the saline-treated control. We found that TAC or SIR treatment increased amyloid deposition in the transplanted human islets (**Figure 18A-18B** normalized; **Table 14** non-normalized data points), supporting the concept of TAC- and SIR-induced β cell dysfunction. Surprisingly, both SIR and TAC treatment also increased the number of CD45+ cells within the graft area (**Figure 18C-18D**); these cells were primarily macrophages (as marked by IBA1) and of human origin (human-specific CD45), indicating that these are likely islet resident macrophages (**Figure 18E-18F**). Islet macrophages play both supportive and detrimental roles within the islet depending on the context[622–624]. The functional effects of TAC or SIR treatment on islet resident macrophages have not been studied; however, there is evidence that inhibition of the mTOR or NFAT pathways can activate resident macrophages as opposed to the well-characterized suppression seen in T cells[625–628]. Furthermore, amyloid deposits can stimulate islet macrophages to produce IL-1β which can inhibit β cell function[361,362].

Tacrolimus and sirolimus treatment disrupt insulin processing and β cell granule formation and lead to broad transcriptional dysregulation

To assess for structural alterations in the human β cell, we analyzed the grafts by electron microscopy and found fewer β cell insulin granules in TAC- and SIR-treated grafts (**Figure 19A-19B),** suggesting that TAC- or SIR-induced dysfunction is related to impaired mature insulin granule formation, a critical process in coordinated insulin release.

To examine the transcriptional consequences of TAC or SIR treatment, we assessed grafts by RT-PCR for the expression of genes encoding key molecules involved in β cell metabolism (*INS*, *GCK*, *SLC2A1*), β cell enriched transcription factors (*PDX1*, *MAFA*, *MAFB*, *NKX6.1*), the NFAT family (*NFATC1-4*), and mTOR signaling (*MTOR, RPTOR, RPS6KB1, RPS6*) (**Figure 20A-20D**). There were no changes in any of these transcripts in TAC- or SIR-treated grafts.

To obtain a broad view of the transcriptional landscape, we then performed unbiased RNA-sequencing of the human islet grafts (**Figure 20E-20F**). Gene set pathway analyses of differential gene expression by DAVID[575] within TAC- or SIR-treated grafts revealed enrichment of multiple gene lists related to three broad categories: extracellular matrix, ion/calcium flux, and peptide processing (**Figure 19C-19E**). Alterations in the extracellular matrix are consistent with the increased amyloid deposits and immune infiltration and associated increases in inflammatory-related transcripts across both TAC and SIR treatment groups (**Figure 20G-20H**). Dysregulation of genes related to the handling of calcium and other ion flux, suggests impaired

signal transduction related to stimulated insulin secretion. Finally, alteration of genes related to key insulin processing events such as cleavage at dibasic sites and the formation of disulfide bonds suggests a defect in mature insulin formation. To test this, we analyzed fasting human proinsulin levels in TAC- and SIR-treated mice (**Figure 19F**). We found elevated human proinsulin/insulin ratios, a marker of β cell stress and an early event in the progression of β cell dysfunction[629].

In sum, these data indicate that both TAC and SIR at clinically relevant doses do not affect regulation of β cell proliferation but have broad effects on human islets, including impaired insulin secretion, impaired insulin processing and β cell granule formation, and an increase in amyloid deposition.

Human β cell dysfunction reverses after 4-week withdrawal of TAC or SIR

To determine if TAC- or SIR-induced β cell dysfunction is reversible, we treated mice transplanted with human islets (two independent donors) with TAC or SIR for 4 weeks then withdrew treatment and assessed β cell function (**Figure 21A**). The ability to withdraw treatment and monitor islet function highlights the value of this model as this would not be possible in humans treated with these agents following organ or cell transplantation. With 4 weeks of TAC or SIR treatment, we saw impaired human graft function as before (**Figure 21B-21E**; **Figure 22A-22D**; **Figure 23B, 23D-23G).** However, 4 weeks after withdrawal of treatment, we saw a complete normalization of both glucose handling as well as human β cell function in both fasted and stimulated states (**Figure 21F-21I**; **Figure 22E-22H**; **Figure 23C, 23H-23K**). This suggests that dysfunction induced by TAC or SIR is not permanent and highlights that human β cells can recover normal function if such stressors are removed.

Following withdrawal of TAC or SIR, grafts were harvested and analyzed. Compared to grafts from the same treatment group after 4 weeks of treatment, amyloid deposition was higher in the saline-treated control grafts, was stable in TAC-treated grafts, and was lower in SIR-treated grafts (**Figure 21J-K**). Thus, after 4 weeks of withdrawal from treatment, amyloid deposition in grafts was similar between all treatment groups. Overall, these data indicate that these markers of islet dysfunction can normalize if the treatment is stopped and suggest that amyloid deposits may be cleared if islet insults are removed.

Exendin-4 treatment protects human β cells from TAC-induced dysfunction and partially ameliorates SIR-induced dysfunction

While it is helpful to know that the effects of TAC and SIR on human islets can be reversed with withdrawal, these drugs are indispensable in achieving chronic immune suppression in transplant patients. Thus, withdrawal of therapy is not a viable option. To assess ways to protect human islets from drug-induced dysfunction, we cotreated mice bearing human islets from two independent donors with either TAC or SIR and Exendin-4 (Ex-4), a glucagon-like peptide-1 (GLP-1) receptor agonist (**Figure 24A**). GLP-1, an incretin hormone released by the L-cells of the intestine, acts through G_s-coupled GLP-1 receptors on β cells to activate multiple signaling pathways including the calcineurin/NFAT pathway[630]. This signaling acts to potentiate stimulated

insulin secretion and also promote young human β cell proliferation[568]. GLP-1 receptor agonists are used clinically in individuals with T2D and have an excellent safety profile.

The addition of Ex-4 improved glucose handling in both TAC and SIR treated groups (**Figure 24B-24C**). Since GLP-1 signaling is primarily active in β cells in the setting of elevated glucose, we focused on stimulated graft function. We found that TAC+Ex-4 treatment improved stimulated human insulin and insulin/glucose ratio compared to TAC treatment alone and that these reached levels comparable to islet-graft function in mice never receiving TAC (**Figure 24D-24F**). In comparison to SIR treatment alone, SIR+Ex-4 treatment led to slightly improved insulin/glucose ratio (**Figure 24D-24F**). Taken together, this indicates Ex-4 is able to completely rescue TAC-induced β cell dysfunction and partially rescue SIR-induced β cell dysfunction.

Analysis of amyloid deposition within the grafts revealed that TAC+Ex-4-treated grafts had significantly less amyloid than TAC alone and was similar to that of control grafts (**Figure 24G-24H**). SIR+Ex-4 cotreatment showed a partial reduction in amyloid deposition compared to SIR treatment alone (**Figure 24G-24H**). Overall, these data are consistent with the functional improvements and demonstrate that TAC- and SIR-induced effects on human islets and amyloid formation can, at least partially, be prevented.

Discussion

Understanding the effect of immunosuppressive agents on human islets would help elucidate the pathogenesis of PTDM. To study this, we transplanted human islets into immunodeficient mice and treated the mice with clinically relevant levels of two commonly used immunosuppressive agents, TAC and SIR. Using this model, we identified several major molecular alterations related to this dysfunction, including reduced β cell granules, elevated proinsulin, and increased islet amyloid deposition, which have not been previously reported for β cell dysfunction related to immunosuppressive agents. Furthermore, gene pathway enrichment analysis of RNA-seq data revealed that TAC- or SIR-induced broad dysregulation of peptide processing, ion and calcium flux, and extracellular matrix maintenance. Together, these data provide new mechanistic insight into TAC- and SIR-induced dysfunction as it relates to PTDM.

With this model, we also demonstrated that TAC and SIR-induced dysfunction can be reversed with withdrawal of the drug and prevented with co-treatment with the GLP-1 agonist Ex-4, important findings with clinical implications. Ex-4 and TAC, at least in part, target similar pathways with TAC inhibiting calcineurin while GLP-1R signaling in the β cell has been shown to lead to calcineurin activation[568]. Our data suggest that β cell activation of calcineurin through the GLP-1R can overcome inhibition by TAC and thus prevent the insulin secretory deficit though we cannot rule out contribution from additional pathways. Ex-4 and SIR target different pathways, and we noted a partial improvement in human β cell health and function. It is possible that targeted mTOR activation in human β cells may be an effective approach of protecting human β cells from SIR-induced dysfunction.

This study differs from prior reports on the impact of TAC or SIR on islets[613,614,619] in that we studied human islets in vivo and used dosing regimens that achieved clinically relevant levels,

thus avoiding toxicity-related effects. In this setting, TAC and SIR affect human β cell function without altering β cell proliferation or death. This adds to a growing body of literature highlighting differences in how human islets respond in vivo versus in vitro, including in their ability to proliferate, differentiate, and respond to metabolic stressors such as hyperglycemia or dyslipidemia[569,631–635]. Thus, these results highlight that in vitro may not always reflect in vivo mechanisms and emphasize the value of studying human islets in a transplantation model.

Our model has a number of advantages, including allowing for studies that would not be possible in humans while still being able to assess human β cells in a complex, in vivo environment. This approach also allows for a comprehensive assessment that takes into account both direct actions of TAC or SIR on the grafts as well as indirect actions such as SIR-induced insulin resistance. While our model allowed for longer treatment periods than in vitro studies, transplant patients are typically on life-long immunosuppression and some develop PTDM years after transplant. It is unclear if TAC or SIR exposure over this length of time would have additional effects than what we observed and whether this would be reversible. Another caveat to our approach is that the transplantation procedure may add stress to the islets that would not be present in the pancreas *in situ* during the development of PTDM. To minimize this, we allowed the islets to engraft for 2 weeks before starting drug treatment, giving the islets time to recover. Further, while the immunosuppressed mouse is the best model to study human islets in vivo, TAC and SIR may have additional indirect effects on human islets by impacting the systemic immune system that are not reflected in our model. Finally, even though we performed all experiments with multiple independent donors, it is possible that the genetic and epigenetic variation of human islet donors could play a role in susceptibility to these drugs and PTDM.

PTDM is a major complication after all solid organ and cell transplantation, but clear treatment guidelines for long-term management or prevention are lacking[602]. Studies evaluating GLP-1-based therapies in PTDM are limited but indicate that short-term GLP-1 administration can improve insulin secretion[636]. Furthermore, small retrospective analyses have shown that sitagliptin, a DPP-4 inhibitor which boosts endogenous GLP-1 levels by preventing its breakdown, is safe and efficacious in treating PTDM[603]. Our data provide a strong rationale for cotreatment with a GLP-1-based agonist and suggest that clinical trials might test whether GLP-1 agonist treatment may be beneficial in patients treated with TAC or SIR.

In summary, we highlight that TAC- or SIR-induced human islet dysfunction is both reversible with withdrawal of treatment and, at least partially, preventable with cotreatment with a GLP-1R agonist. These studies highlight the importance of both calcineurin/NFAT and mTOR pathways in human β cell function and suggest that activation of these pathways specifically in β cells may be a useful approach to reduce the incidence of PTDM.

Dapagliflozin does not directly affect human α or β cells

Introduction

Blood glucose levels, which are normally tightly controlled through coordination of multiple organ systems, are elevated in T2D. Sodium-dependent glucose cotransporter 2 (SGLT2)

inhibitors such as dapagliflozin (DAPA) are important medications in the treatment of T2D and lower blood glucose by preventing glucose reabsorption by the kidney thereby promoting glucosuria. DAPA treatment also decreases insulin secretion from pancreatic islet β cells and improves muscle insulin sensitivity, thought to be a consequence of lower blood glucose[637,638]. Interestingly, initiation of DAPA treatment is also associated with a transient rise in glucagon from pancreatic islet α cells which may partially counteract the glucose-lowering benefits[637,638].

While the metabolic benefits of DAPA are clear, it remains controversial whether the effects of DAPA on glucagon secretion are due to direct effects on α cells. Previous studies of DAPA on cultured human islets have been conflicting. Partly this is because the DAPA concentrations used have been outside the therapeutic window (100-200 ng/ml; 250-500 nM)[639–641] calling into question the clinical relevance of the findings. For example, very low concentrations of DAPA (10 nM, below therapeutic range) increased glucagon secretion under high glucose (11 mM), but decreased glucagon secretion under low glucose (1 mM)[642]. In contrast, high concentrations of DAPA (12.5 μM, above therapeutic range) increased glucagon secretion in a subset of donor human islets under low and moderate glucose (1 and 6 mM) but had no effect under high glucose (15 mM)[643,644]. Moreover, recent studies have contended that SGLT2 is not expressed in islet cells and argued that SGLT2 inhibitors do not directly affect islet hormone secretion in rodent models[645,646].

Importantly, human islets show key differences from rodent islets including their endocrine cell composition and arrangement, gene expression (including of glucose transporters), glucose set-point, and both basal and stimulated insulin and glucagon secretion[22,24–26,568,569]. We therefore sought to clarify the effects of clinically relevant levels of DAPA on human islets both in vitro and in an in vivo transplant model that mimics the clinical setting and drug exposure. Here, we show that SGLT2 expression in human islets is extremely low and that DAPA does not directly affect insulin or glucagon secretion from the human islet.

Results

SGLT2 expression in the human islet is extremely low

To characterize SGLT2 (gene name *SLC5A2*) expression, we first performed immunofluorescence analyses of human and mouse kidney sections, finding robust SGLT2 staining in the kidney cortex (**Figure 25A-25B**). However, protein expression in both human and mouse islets was undetectable using the same antibody under the same conditions (**Figure 25C-25D**). In order to directly compare staining, we analyzed sections from human islets transplanted under the renal capsule of immunodeficient mice. While staining in the mouse kidney was robust, we could not detect any signal from the adjacent human islet graft (**Figure 25E**). At the transcript level, *SLC5A2* expression in whole islets was detectable but at levels 1600-fold lower than in human kidney (**Figure 25G**). Since SGLT2 expression may change in the diabetic state where inhibitors are used clinically, we also analyzed T2D islet grafts for SGLT2 staining and again could not detect signal within the graft (**Figure 25F**). Further, there was no difference in *SLC5A2* expression in T2D islets compared to non-diabetic islets (**Figure 25H**). Together, these data suggest that SGLT2/*SLC5A2* is not expressed in human islet cells to a significant degree, if at all.

DAPA treatment does not directly affect glucagon or insulin secretion in vitro

We next sought to clarify direct effects of therapeutic levels of DAPA on human islets in vitro using an acute exposure model (**Figure 26A**). We selected 500 nM DAPA (within the therapeutic range of total DAPA) and performed experiments in albumin-containing media to mimic the clinical situation where a majority of DAPA is bound by albumin[639–641]. We cultured human islets from four different islet preparations at basal glucose (5.6 mM) for 1 hour before transferring islets to low (3.3 mM) or high glucose (16.7 mM), chosen to be reflective of biological fasted and fed states. In this system, insulin secretion from β cells was unchanged at either high or low glucose by DAPA treatment (**Figure 26B-26C**). Similarly, glucagon secretion from α cells was also unchanged at either low or high glucose (**Figure 26D-26E**). Thus, these data suggest acute DAPA exposure does not directly affect human islet cell function.

Acute DAPA treatment in vivo mildly increased glucagon secretion

To investigate the effects of DAPA on human islets in a dynamic *in vivo* environment, we used a human islet transplant model in the immunocompromised NOD.Cg-*Prkdc*^{scid}*Il2rg*^{tm1Wjl}Sz (NSG) mouse[574]. First, we defined DAPA pharmacokinetics in the NSG mouse without transplanted human islets and found that 2 mg/kg daily oral dosing resulted in DAPA blood levels within the therapeutic window (**Figure 27A**). DAPA was cleared from the blood within 24 hours as similarly reported in human and did not accumulate in blood over several days of treatment (**Figure 27B-27C**). Further, after one-week treatment blood glucose levels were reduced and stimulated mouse glucagon levels were elevated, mirroring clinical data and indicating effective treatment (**Figure 27D-27H**).

Having established the appropriate dosing, we then transplanted human islets under the kidney capsule of NSG mice and repeated this across four different donor islet preparations. Following two weeks to allow engraftment, mice began treatment with DAPA (**Figure 28A**). After one week of DAPA treatment, we assessed graft function by measuring serum human insulin levels using a human-specific insulin assay and also measured total serum glucagon in the fasted state and after glucose stimulation. We found that mice treated with DAPA had similar fasting blood glucose and fasted levels of human insulin and total glucagon (**Figure 28B-28D**). While mouse and human glucagon cannot be distinguished due to 100% sequence identity, mouse glucagon levels from experiments without transplanted human islets are ~1/3 of that seen in those with transplants; thus, the majority of glucagon measured comes from the human islet grafts (**Figure 27E** and **28D**). After glucose stimulation, blood glucose was lower in the DAPA-treated group, indicating effective treatment (**Figure 28E**). Human insulin was also lower in the DAPA-treated group as expected given the lower blood glucose (**Figure 28F**). When normalized to the glucose level of the mouse, human insulin levels were unchanged with DAPA treatment (**Figure 28G**). Additionally, total glucagon was elevated in the DAPA group (**Figure 28H-28I**), demonstrating that this human islet transplant model recreates the transient elevations in glucagon secretion seen when initiating DAPA treatment in patients.

Chronic DAPA treatment in vivo did not affect the human islet graft function

To assess for longer term effects of DAPA treatment, we continued treatment with DAPA for an additional 3 weeks (**Figure 28A**). After 4 total weeks of DAPA treatment, there were no differences in fasted blood glucose, fasting total glucagon levels, or fasting human insulin levels (**Figure 28J-28L**). After glucose stimulation, DAPA-treated mice again had lower blood glucose (**Figure 28M**). Human insulin levels were lower in DAPA-treated animals but not different when corrected for the lower blood glucose (**Figure 28N-28O**). Interestingly, glucagon levels were no longer elevated in DAPA-treated mice (**Figure 28P-28Q**). In total, these data suggest that prolonged DAPA treatment with clinically relevant dosing does not alter glucagon secretion from human α cells.

Human islet grafts show no effects of DAPA treatment

With an in vivo model which recreates the clinical situation, we next analyzed the human islet grafts to investigate for direct effects of DAPA on human islets (**Figure 28A**). The ability to harvest the graft and perform detailed molecular studies on the human islets highlights the additional value provided by this model. We extracted total hormone from the grafts and found no difference in insulin or glucagon content with DAPA treatment (**Figure 29A-29B**), suggesting that glucagon and insulin synthesis and processing were not affected by DAPA treatment. To assess for ultrastructural alterations in the human α and β cell, we analyzed control and DAPA-treated grafts by electron microscopy but found equal numbers of both β and α cell granules (**Figure 29C-29F**). Furthermore, β and α cell proliferation (**Figure 29G-29H**) and apoptosis (**Figure 29I-29J**) were very low and unchanged in both DAPA-treated and control groups, suggesting that DAPA does not impact endocrine cell mass. Finally, islet amyloid deposition, a marker of islet stress and dysfunction, was not changed with DAPA treatment (**Figure 29K-29L**). Together, these data do not support a direct role for clinically relevant levels of DAPA in islet cell function

Discussion

Inhibitors of SGLT2, including DAPA, are common medications in the treatment of T2D with numerous benefits on whole body metabolism, but it has been unclear if these inhibitors act directly on the pancreatic islet, particularly α cells. To study this, we investigated the expression of SGLT2/*SLC5A2* and the effects of DAPA on hormone secretion in human islets in vitro and in vivo after transplantation into mice. *SLC5A2* transcript was multiple orders of magnitude lower than levels detected in the human kidney, and SGLT2 was undetectable in islets using the same antibody that readily detected expression in the kidney and has been used previously[643,644]. Further, neither *SLC5A2*/SGLT2 were altered in the T2D state. Functionally, acute DAPA treatment at therapeutic levels in vitro did not alter insulin or glucagon secretion at low or high glucose. In vivo, DAPA treatment led to lower blood glucose and proportionally lower human insulin levels. Total glucagon levels were elevated after one week of treatment but returned to normal levels after four weeks of treatment. Finally, molecular analysis of the human islet graft demonstrated that insulin and glucagon content, α and β cell granules, α and β cell proliferation and apoptosis, and amyloid deposition in human islet grafts were not changed with DAPA treatment.

This study differs from prior reports on DAPA's effect on the islet in several ways. For in vitro studies, we treated human islets with 500 nM DAPA to remain within the therapeutic window. Use of different DAPA concentrations may explain the dissimilarities seen from other studies where effects could be due to off target effects on ion channels or other glucose transporters[646]. Consistent with this notion, a recently published dose-response curve for DAPA reported that stimulation on glucagon secretion in vitro is not seen until DAPA levels are significantly above the range of levels seen in humans treated with DAPA[644].

Furthermore, while static in vitro studies (including ours) can be helpful to isolate direct islet effects, they are not fully reflective of the clinical situation where islets are vascularized and dynamically respond to glucose and other nutrients as well as endogenous hormones which modulate both β and α cell function. In this study, investigating human islet function in a context where DAPA's primary actions on the kidney change blood glucose allows for study in the appropriate context and appreciation of both direct and indirect actions. We found that DAPA had no effect in the fasted state when glucose levels are lower and thus SGLT2 is less active in the kidney. After glucose stimulation, blood glucose levels become elevated, but mice with DAPA treatment showed lower blood glucose, reflective of reduced ability of the kidney to resorb glucose. At this lower blood glucose level, we observed proportionally lower insulin, and elevation in glucagon with acute DAPA treatment. Because the effects of DAPA on insulin and glucagon secretion were not observed in vitro or in vivo in the fasted state but only in vivo with glucose stimulation, these effects are likely indirect and related to the dynamic in vivo environment. This is consistent with a recent multivariate analysis which concluded that glucose changes were the main determinant of the changes in glucagon secretion seen with SGLT2 inhibition[647].

Finally, a major advantage of our model is the ability to harvest the human islet graft and perform molecular analyses to assess for effects of DAPA on the islet, studies that cannot be performed in clinical research. For example, a recent study in mice showed that luseoglifozin, also an SGLT2 inhibitor, can stimulate mouse β cell proliferation in certain contexts[648]; however, our data indicates that this is unlikely to be the case for human β cells. Additionally, islet stressors such as dyslipidemia or treatment with immunosuppressive drugs can lead to evidence of poor islet health through the formation of amyloid[558,569], but this was not observed with DAPA treatment. Overall, the lack of discernible evidence of these effects on the islet graft further argues that DAPA does not directly act on the human islet.

There are limitations to our study. Principally, in vivo one is unable to differentiate glucagon that originates from endogenous mouse α cells from that which comes from engrafted human α cells due to 100% sequence identity. To address this, we performed parallel studies on mice without engrafted human islets and found that glucagon levels were ~1/3 what they were in mice with engrafted human islets, suggesting a majority of the detected glucagon originates from human α cells. Further, our in vitro studies are not hindered by this limitation and also show no direct effects on the human islet. Additionally, a recent study suggested SGLT2 inhibitors may act on δ cells within the islet if exogenous insulin is added[649]. While our data does not suggest that

SGLT2 is expressed in δ cells, we did not measure somatostatin secretion and thus do not know if DAPA has effects on δ cells in our system that did not include exogenous insulin.

In sum, we conclude that DAPA does not have direct effects on human islet function, but rather the transient effects on human α cell function are secondary to the acute glucose lowering of DAPA through increased renal glucose excursion. Future studies should focus on how α cells sense acute glycemic changes and establish chronic glycemic set points as well as how these systems may be altered in the diabetic state.

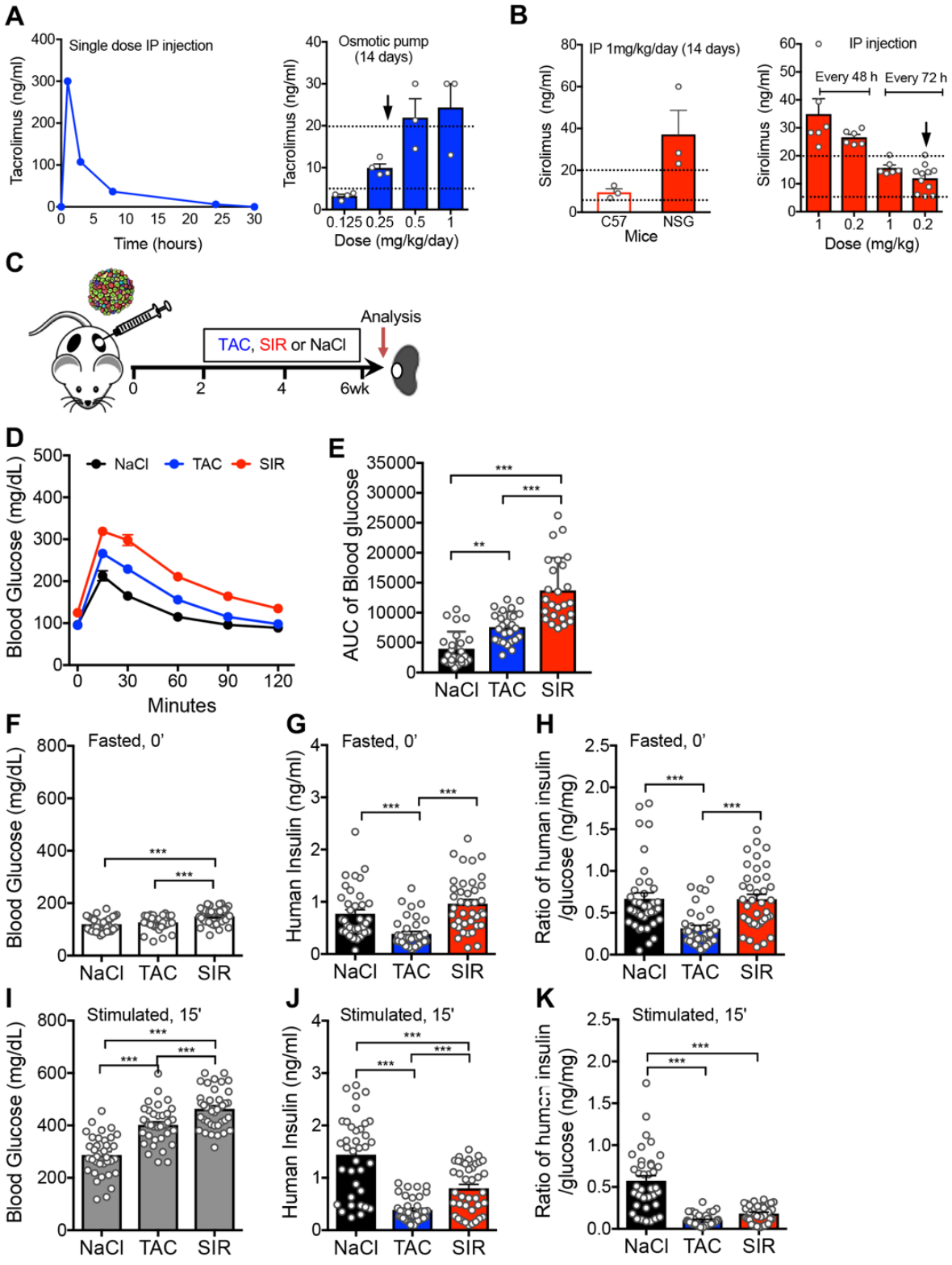

Figure 12. TAC and SIR treatment impairs β cell function of human islets in vivo.
(**A**) Time course of TAC blood levels with single dose (0.25mg/kg) injection in NSG mice to establish drug half-life and TAC dosing regimen. **(B)** Comparison of the SIR blood levels in C57BL/6 and NSG mice (n=3/group) and SIR dosing regimen. Trough levels for A and B in NSG

mice after 14 days treatment with various doses and interval times. Dotted lines indicate clinical therapeutic dose ranges and black arrows indicate doses chosen for this study. **(C)** Schematic of in vivo experimental design. **(D-E)** Glucose tolerance test (GTT) in mice after 4 week-treatment and area under curve (AUC) calculations (E; n=25 samples/treatment from 5 donors; individual donor data shown in **Figure 14**). **(F-K**) Fasted (6h) and 15' after glucose and arginine stimulation blood glucose (**F, I),** human insulin levels **(G, J)** and human insulin:blood glucose ratio **(H, K)** (n=37-39 samples/treatment from 7 donors; individual values and donor data shown in **Figure 15**). * $p<0.05$, ** $p<0.01$; *** $p<0.001$. Error bars indicate SEM. One-way ANOVA followed by Tukey multiple comparisons test was used for analysis of statistical significance. Figure adapted from Dai, Walker et al. 2020[558].

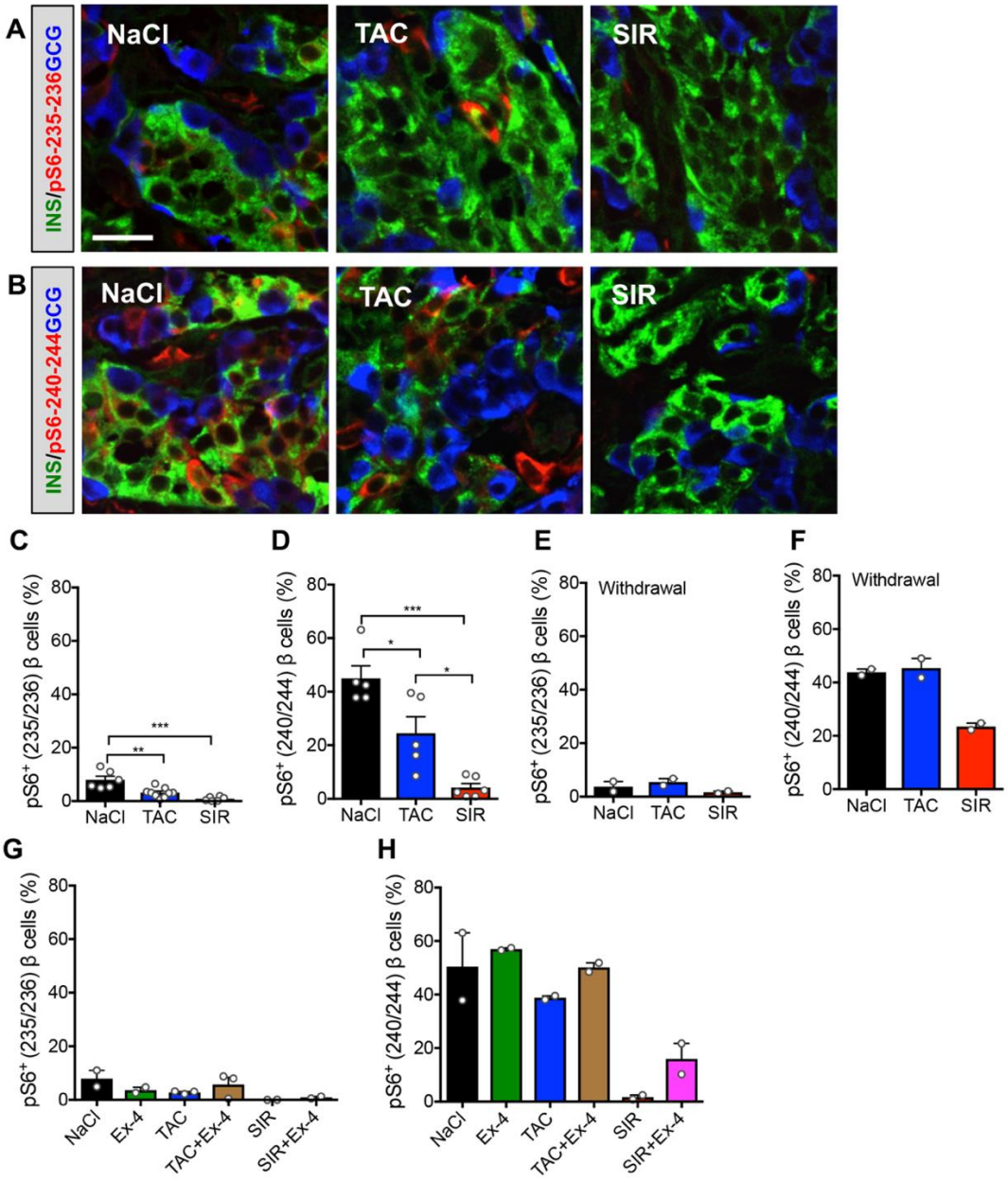

Figure 13. Related to Figure 12. TAC and SIR treatment reduces S6 phosphorylation in human grafts.

(A-B) Representative images of human grafts labeled with INS (green), pS6235/236 or 240/244(red), GCG (blue). Scale bar=20 mm and applies to all images in (A) and (B). **(C-D)** % of positive pS6 β cells in human grafts (n=6-9 grafts/treatment from 3 donors) (**E-F**) % of positive pS6 β cells in human grafts after 4 weeks withdrawal (n=2 grafts/treatment from one donor). (**G-H**) % of positive pS6 β cells in human grafts with Ex-4 cotreatment (n=2-3 grafts/treatment from one donor) * p<0.05, ** p<0.01, *** p<0.001. Data represent mean ± SEM. One-way ANOVA was used for analysis of statistical significance. Figure adapted from Dai, Walker et al. 2020[558].

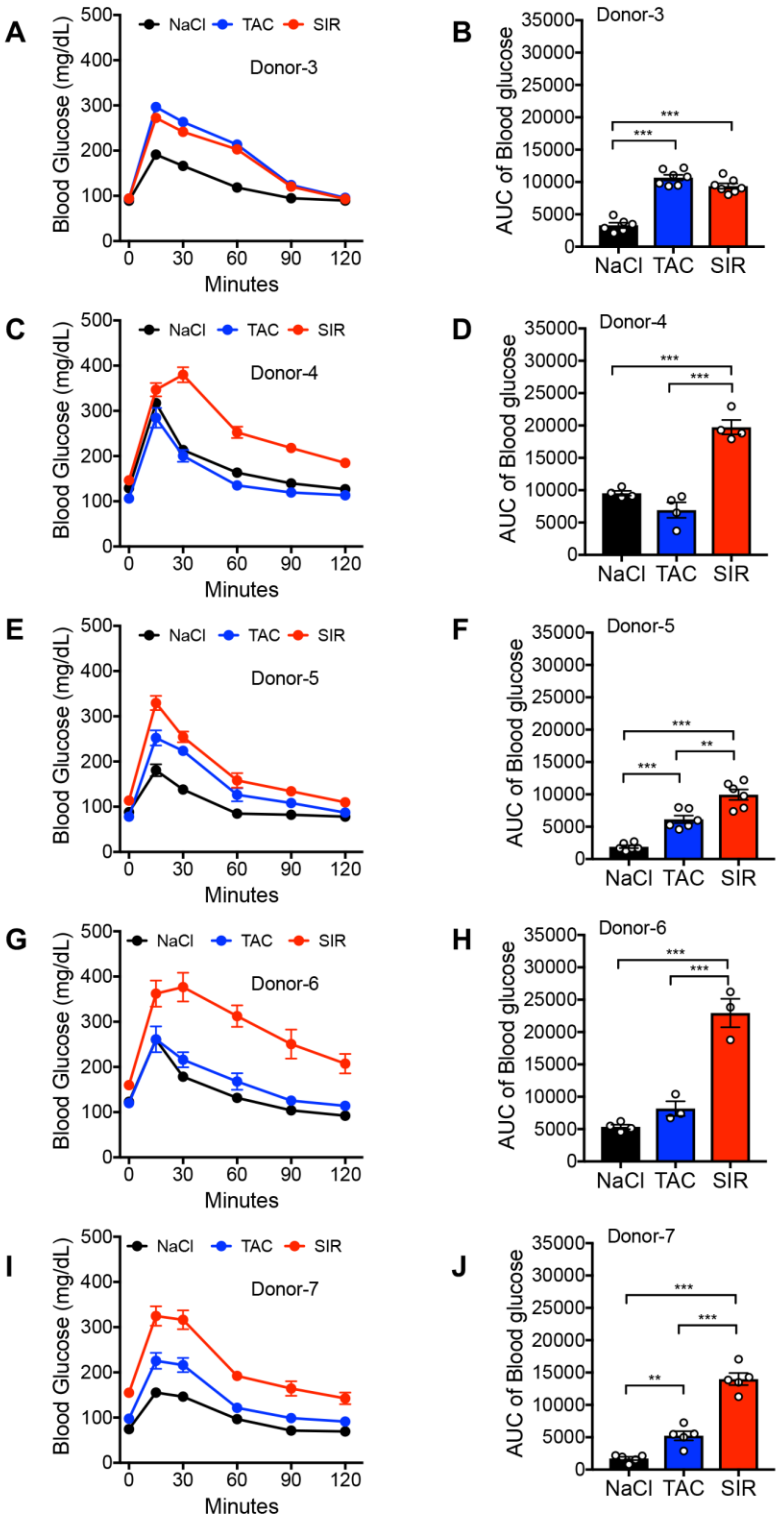

Figure 14. Related to Figure 12. Glucose tolerance test by individual donor in mice transplanted with human islets.

(A-J) GTT (**A,C,E,G,I)** or AUC (**B,D,F,H,J**) shown by donor; corresponds to **Figure 12D-12E**. n=3-7 samples/treatment/donor. Figure adapted from Dai, Walker et al. 2020[558].

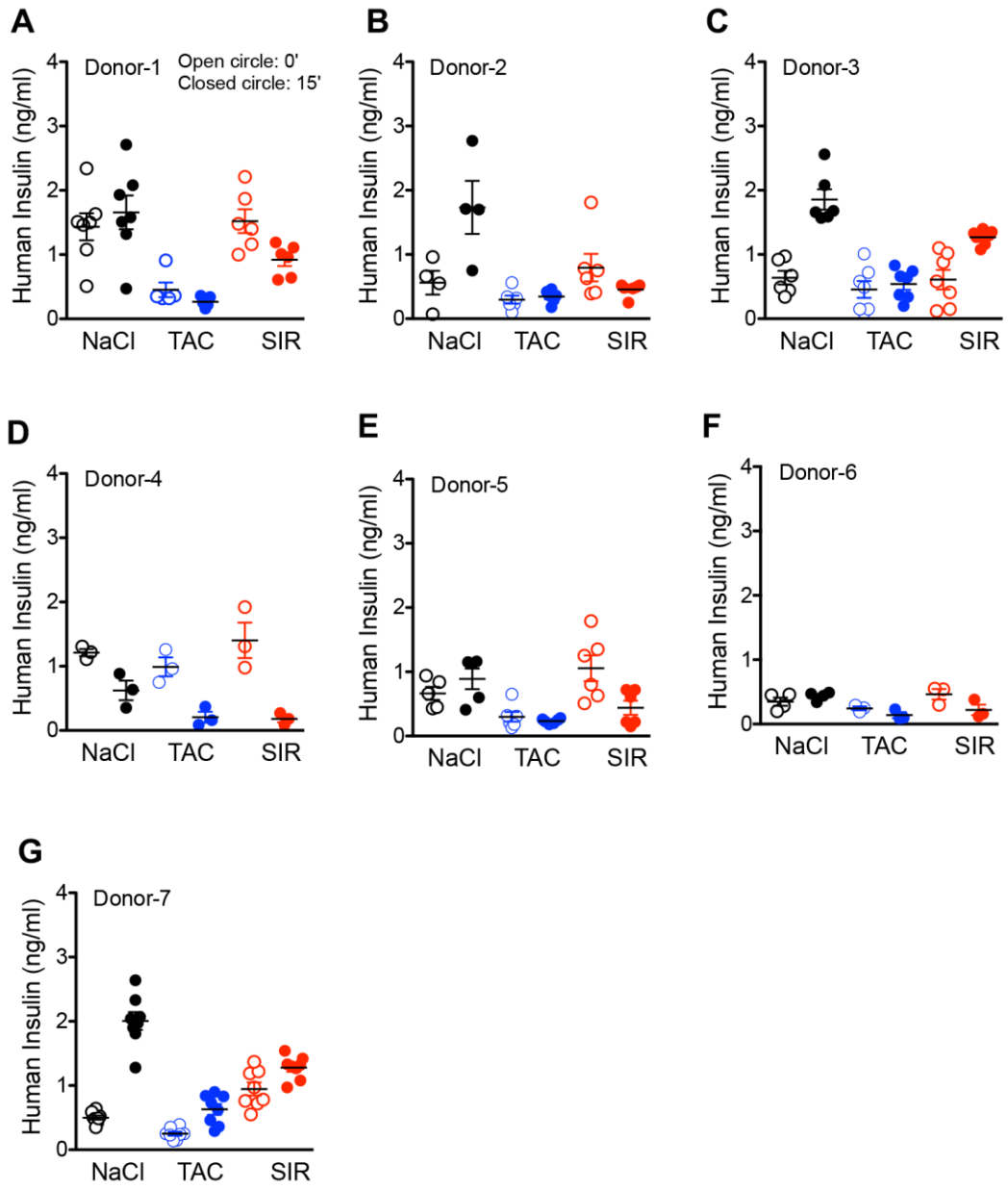

Figure 15. Related to Figure 12. Effects of TAC and SIR treatment for 4 weeks.
(**A-G**) Data corresponds to **Figure 12G,12J**. Human insulin levels before and after stimulation from individual donors with TAC or SIR treatment for 4 weeks. n=3-8 serum samples /treatment /donor. Figure adapted from Dai, Walker et al. 2020[558].

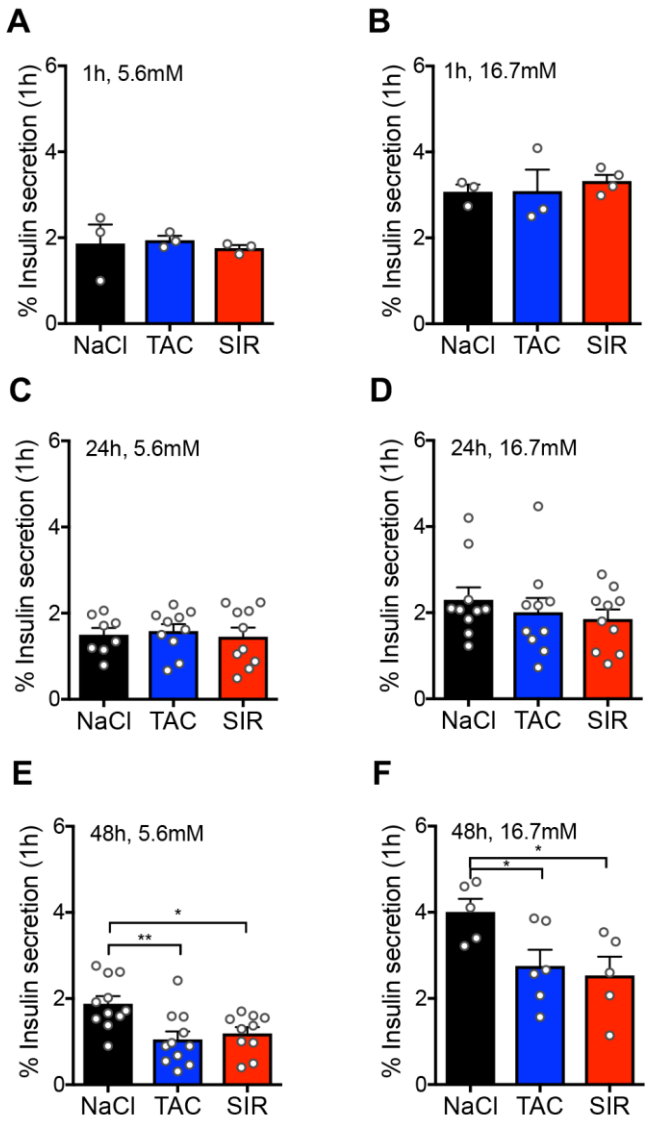

Figure 16. The effect of TAC and SIR on human β cell function in vitro.
(A-F) Insulin levels after human islets cultured with TAC or SIR for 1 hour (**A-B**, n=3 samples/treatment), 24 hours (**C-D**, n=8-10 samples/treatment), or 48 hours (**E-F**, n=10-11 samples/treatment) with 5.6mM or 16.7mM glucose. * $p<0.05$, ** $p<0.01$. Data represent mean ± SEM. One-way ANOVA was used for analysis of statistical significance. Figure adapted from Dai, Walker et al. 2020[558].

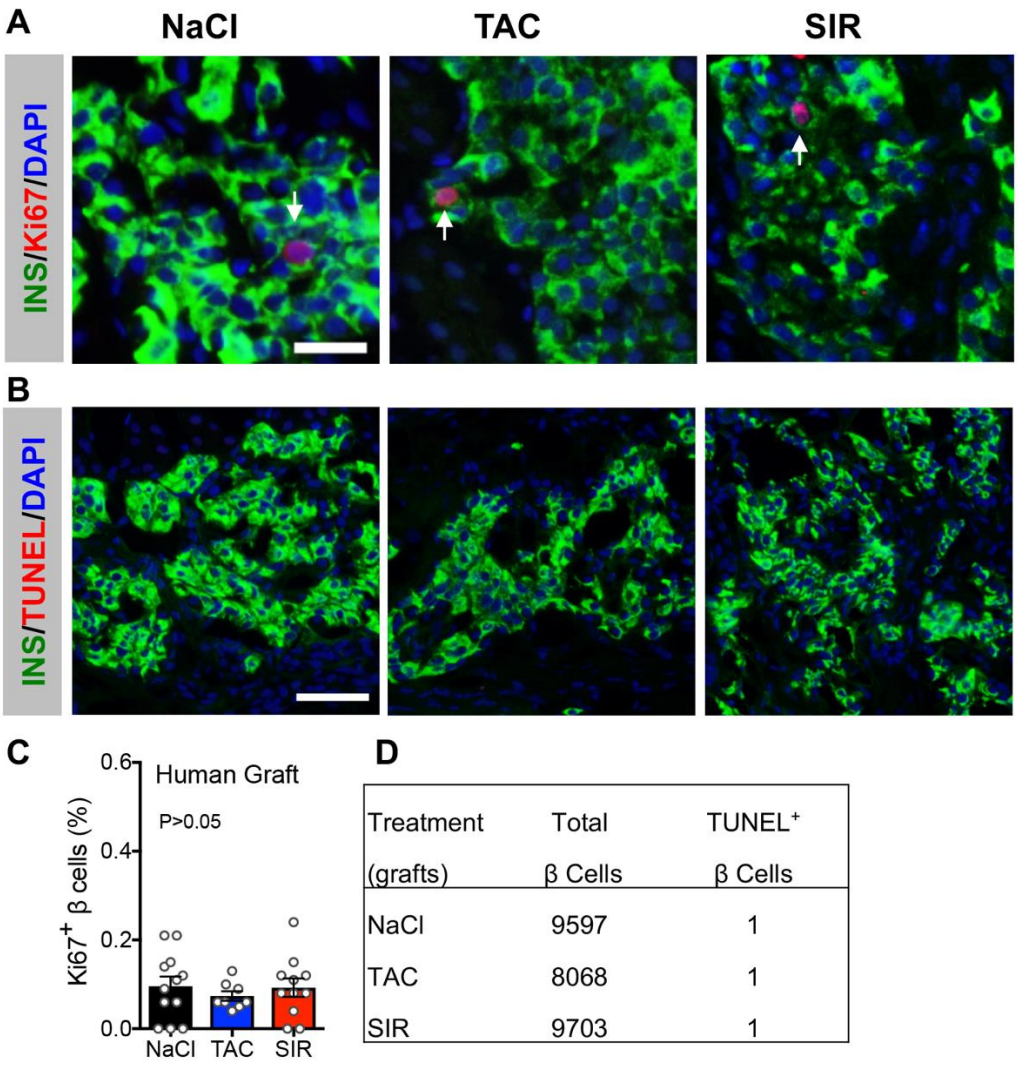

Treatment (grafts)	Total β Cells	TUNEL⁺ β Cells
NaCl	9597	1
TAC	8068	1
SIR	9703	1

Figure 17. TAC or SIR treatment do not change *in vivo* human β cell proliferation or apoptosis.

(**A**) Representative images of Ki67 assay in human grafts after 4 weeks treatment with insulin (green), Ki67 (red), and DAPI (blue). Arrows showed Ki67 positive β cells. Scale bar: 25 μm applies to all images in (A). (**B**) Representative images of TUNEL assay in human grafts after 4 weeks treatment with insulin (green), TUNEL (red), and DAPI (blue). Scale bar: 50 μm applies to all images in (B). (**C**) Percentage of Ki67 positive β cells in transplanted human grafts (n=8-12 grafts/treatment). (**D**) Quantification of TUNEL positive β cells. Data represent mean ± SEM. One way ANOVA was used for analysis of statistical significance. Figure adapted from Dai, Walker et al. 2020[558].

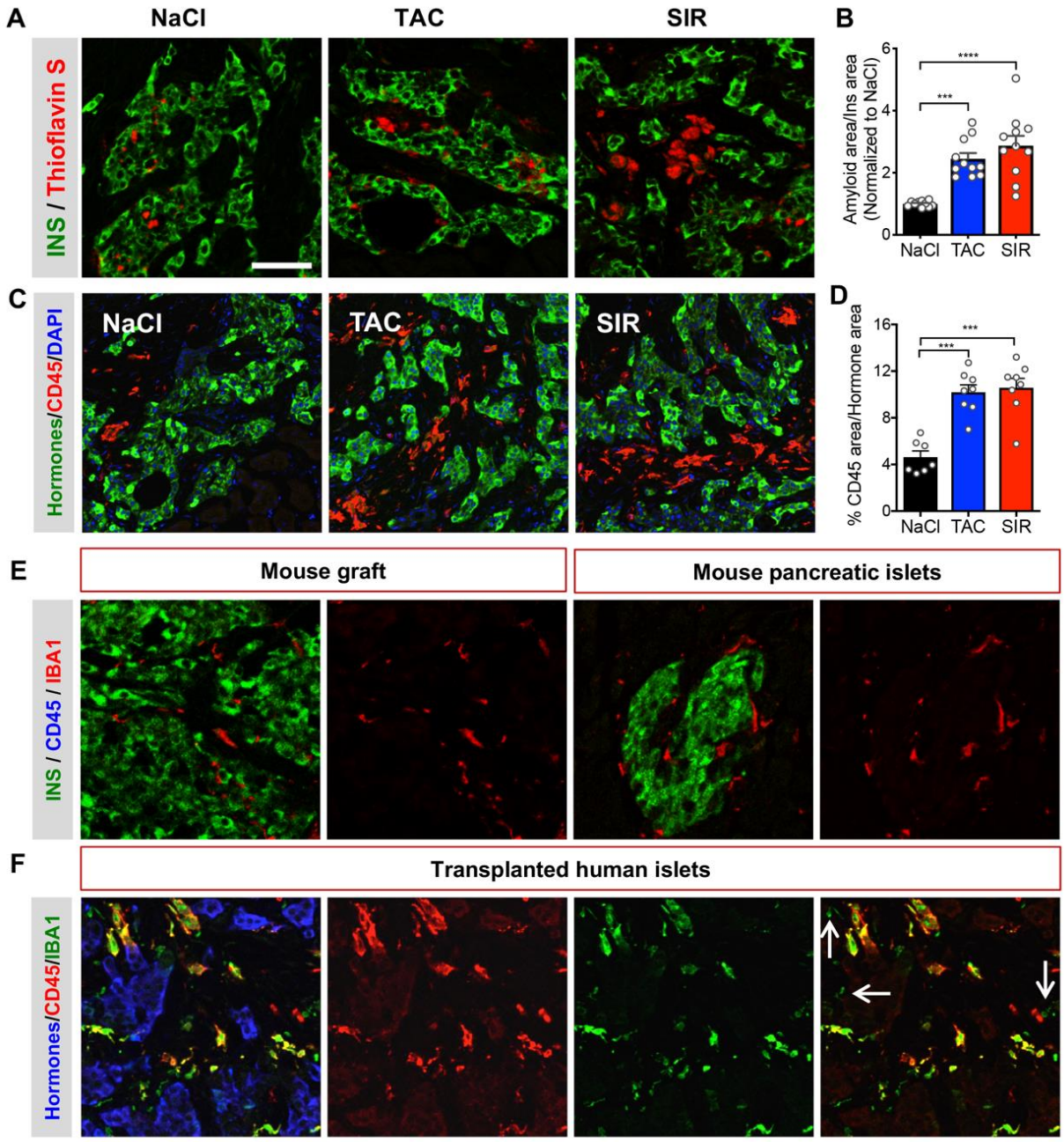

Figure 18. TAC and SIR increase amyloid formation and human-derived CD45⁺ cells in human islets grafts.

(**A**) Representative images of amyloid deposits, indicated by thioflavin S (red), in human grafts labeled with insulin (INS, green) and (**B**) quantification of thioflavin S area/insulin area normalized to the NaCl-treated ratio for that donor to account for donor differences (n=10-11 grafts/treatment from 5 donors, each point represents one graft with 5-6 sections analyzed per graft). See **Table 14** for raw amyloid/insulin area data. Scale bar: 50 µm applies to all amyloid images. (**C**) Representative images of CD45⁺ cells in human grafts with green (INS, GCG, SOM), red (CD45) and blue (DAPI) and (**D**) quantification % of CD45 area after TAC and SIR treatment for 4 weeks (B, n=7-8 grafts/treatment from 3 donors). (**E**) Images showing

macrophages in mouse grafts or mouse pancreatic islets, green (INS), red (IBA1, antibody reacts with human and mouse macrophages), blue (CD45, reacts only to human tissue, negative in both mouse graft and mouse pancreatic islet). (**F**) Macrophages in human graft derived from human (co-labeled CD45 and IBA1, yellow) and mouse (IBA1 only, green, pointed with arrows): blue (INS, GCG, and SOM), red (CD45), green (IBA1). Figure adapted from Dai, Walker et al. 2020[558].

Table 14. Percent of Amyloid/insulin area per graft – non-normalized data

	----------4 week treatment----------						4 week withdrawal		
	NaCl	TAC	SIR	Ex-4	TAC+Ex-4	SIR+Ex-4	NaCl	TAC	SIR
Donor 3	0.48	1.40	1.23						
	0.43	1.64	1.55						
		1.50	1.51						
Donor 4	0.32	0.69	0.50	0.23	0.38	0.21			
Donor 5	2.85	5.00	7.62	2.52	1.82	6.26			
	2.50	6.16	8.46	2.03	2.53	4.67			
					1.87	3.37			
Donor 6	0.38	0.83	0.84				0.32	0.52	0.31
	0.28	0.71	0.71				0.49	0.42	0.37
Donor 7	1.17	2.34	2.86				1.93	2.68	2.57
	0.95	2.05	3.83				2.05	2.49	3.06
	1.08	1.98	5.38						

Thioflavin S area expressed at a percent of insulin area for 5-6 sections per graft shows varying baseline amyloid formation by donor. Data from columns 1-3 (donors 3-7) is included in **Figure 18**, columns 1-3 and 7-9 for donors 6 and 7 is included in **Figure 21**, and columns 1-6 for donors 4 and 5 is included in **Figure 24**. Table adapted from Dai, Walker et al. 2020[558].

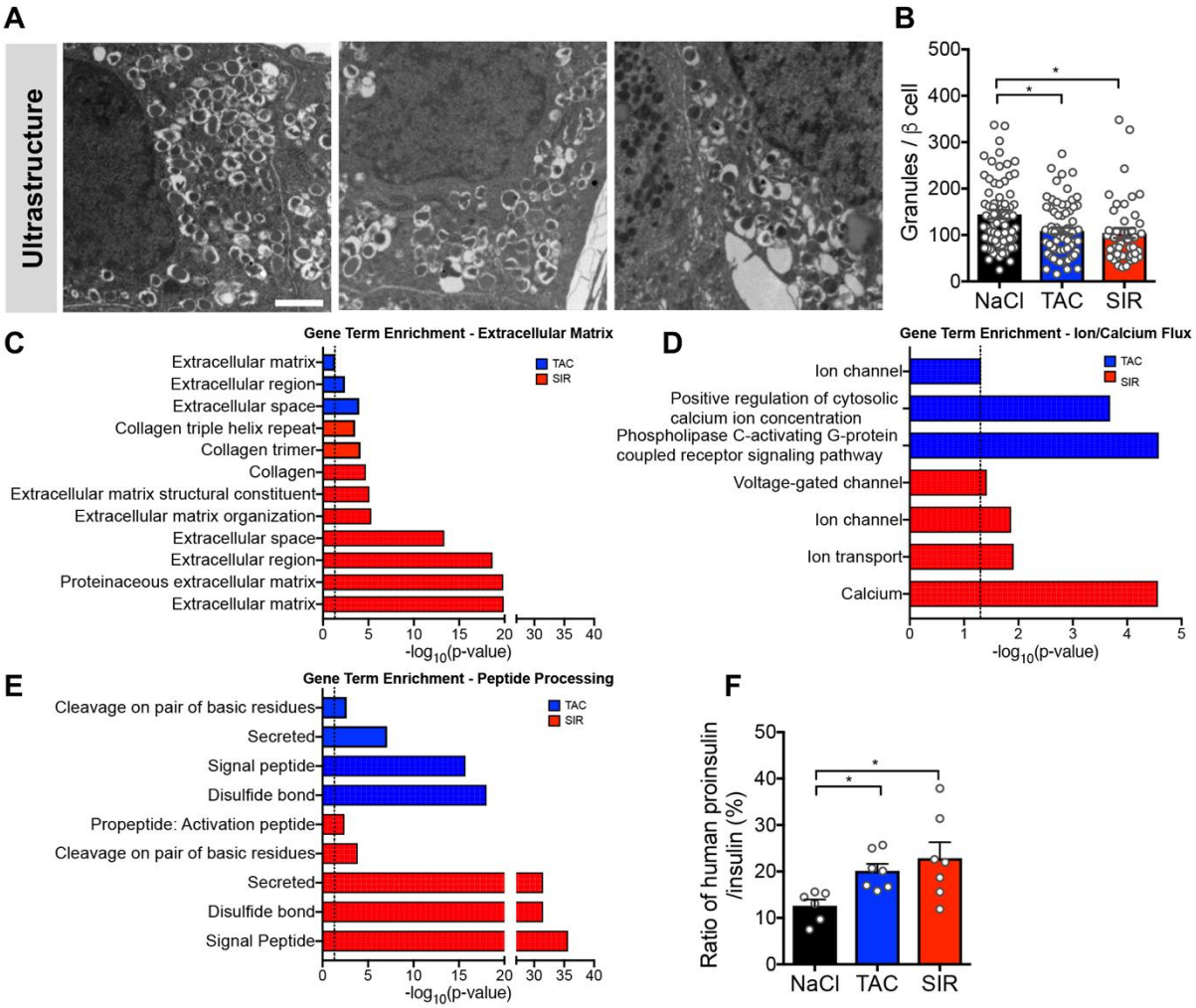

Figure 19. TAC and SIR reduce β cell insulin granules and induce broad transcriptional dysregulation.

(**A**) Representative EM images of β cells and quantification (**B**) of granules per β cell in human grafts from each drug treatment. Scale bar: 1 µm, applies to all EM images. (**C-E**) DAVID gene set enrichment for terms related to extracellular matrix (**C**), ion/calcium flux (**D**), peptide processing (**E**). Note that the x-axis scale is different in panel F. P-value plotted are the Benjamini Hochberg corrections of 0.05 for false-discovery rate and dotted line shows -$\log_{10}$(0.05). (**F**) Ratio of human proinsulin/insulin (NaCl, n=6; TAC, n=7; and SIR, n=7 fasted samples from donor 7). * p<0.05, ** p<0.01; *** p<0.001. Error bars indicate SEM. One-way ANOVA followed by Tukey multiple comparisons test was used for analysis of statistical significance. Figure adapted from Dai, Walker et al. 2020[558].

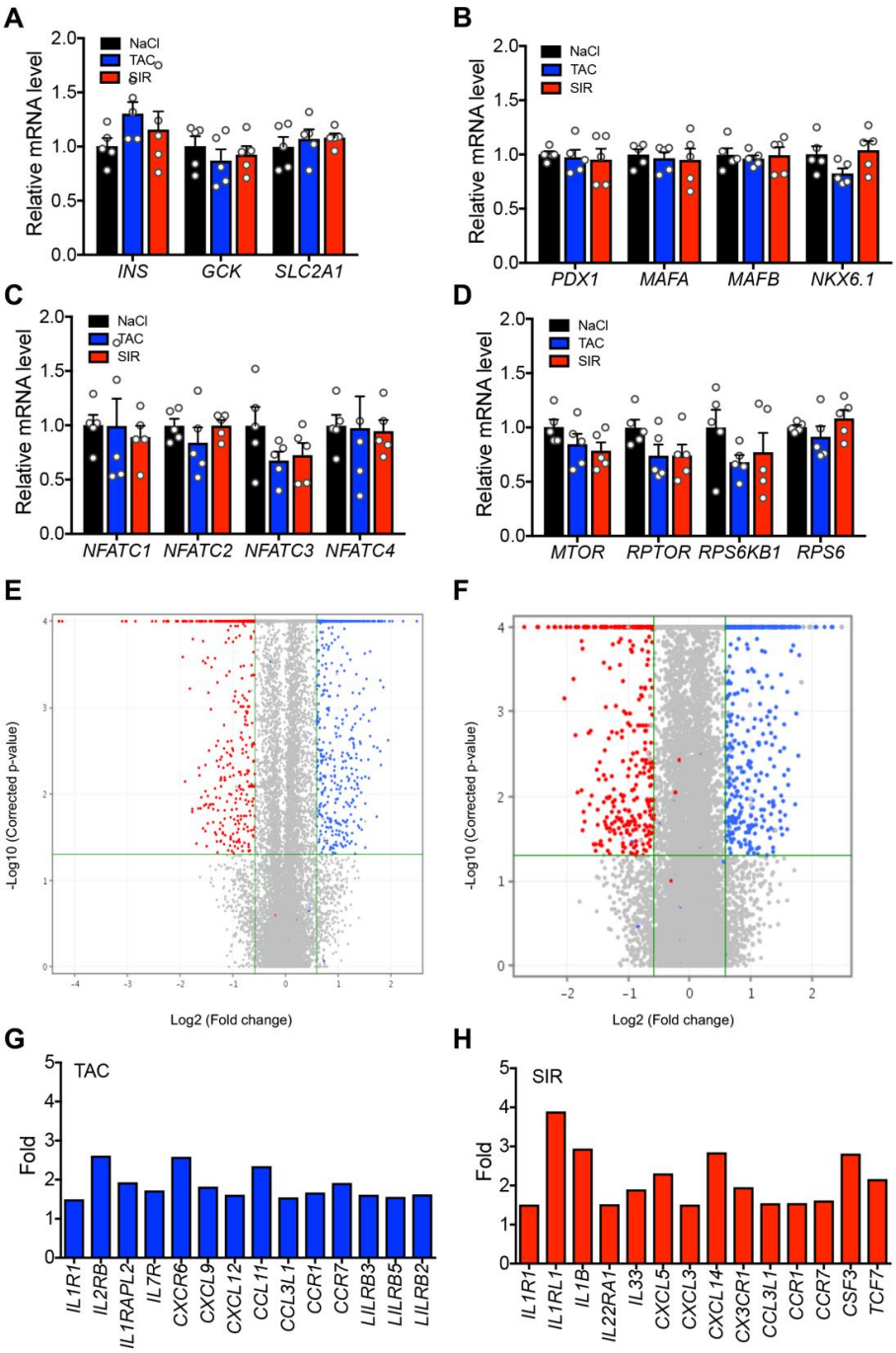

Figure 20. Gene expression in human grafts measured by real time quantitative RT-PCR and RNA-seq.

(A-D) Genes are grouped by (**A**) β cell metabolism, (**B**) β cell enriched transcription factors, (**C**) the NFATC family, and (**D**) mTOR signaling. n=5 grafts/treatment. (**E-F**) Volcano plots of RNA-seq data, TAC vs PBS (**E**) and SIR vs PBS (**F**). RNA-seq data from human graft samples. (**G-H**) Fold change transcripts related to inflammation stimulated by TAC (**G**) and SIR (**H**) compared to control group (n=5 samples from 2 donor transplantations). Figure adapted from Dai, Walker et al. 2020[558].

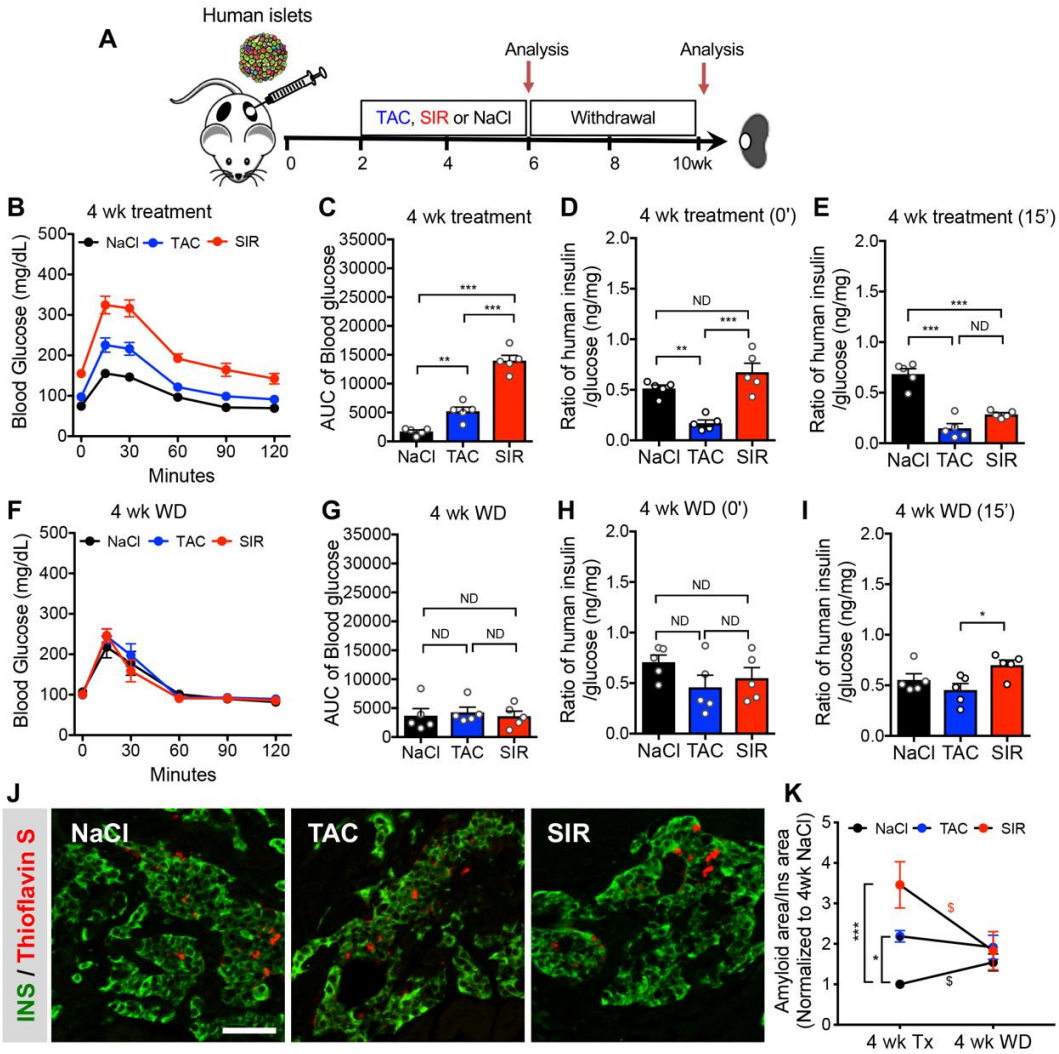

Figure 21. Impaired β cell function by either TAC or SIR normalizes after 4 weeks of withdrawal.

(A) Schematic of experimental design. Mice were given NaCl, TAC or SIR for 4 weeks followed by withdrawal (WD) for 4 weeks. (**B-C, F-G**) GTT and AUC after treatment with TAC or SIR for 4 weeks (**B-C**) or 4 weeks after withdrawal (**F-G**). (**D-E, H-I)** Human insulin:blood glucose ratios at 0' and 15' of glucose-arginine stimulation after 4 weeks treatment (**D-E**) and then 4 weeks after withdrawal (**H-I);** n=5 samples/treatment from one donor. See **Figure 22** for individual blood glucose and human insulin measurements. See **Figure 23** for data from a second donor which is shown separately due to significantly different baseline human insulin. (J-**K**) Representative images of amyloid after 4 weeks drug withdrawal (**J**) and quantification of amyloid burden after 4 weeks treatment and after 4 weeks withdrawal (**K**; n=4-5 grafts/treatment from 2 donors, 2-3 grafts per donor, each donor normalized to 4 week treatment with NaCl – see **Table 14** for raw data). Amyloid data is plotted differently from Figure 12 or 24 to show dynamic nature of this process. Scale bar: 50 µm applies to all amyloid images. * p<0.05, ** p<0.01, *** p<0.001. Error bars indicate SEM. One-way ANOVA followed by Tukey multiple comparisons test was used for analysis of statistical significance. Unpaired t-test was used to compare 4-week treatment to 4-week withdrawal within a group: $<0.05. Figure adapted from Dai, Walker et al. 2020[558].

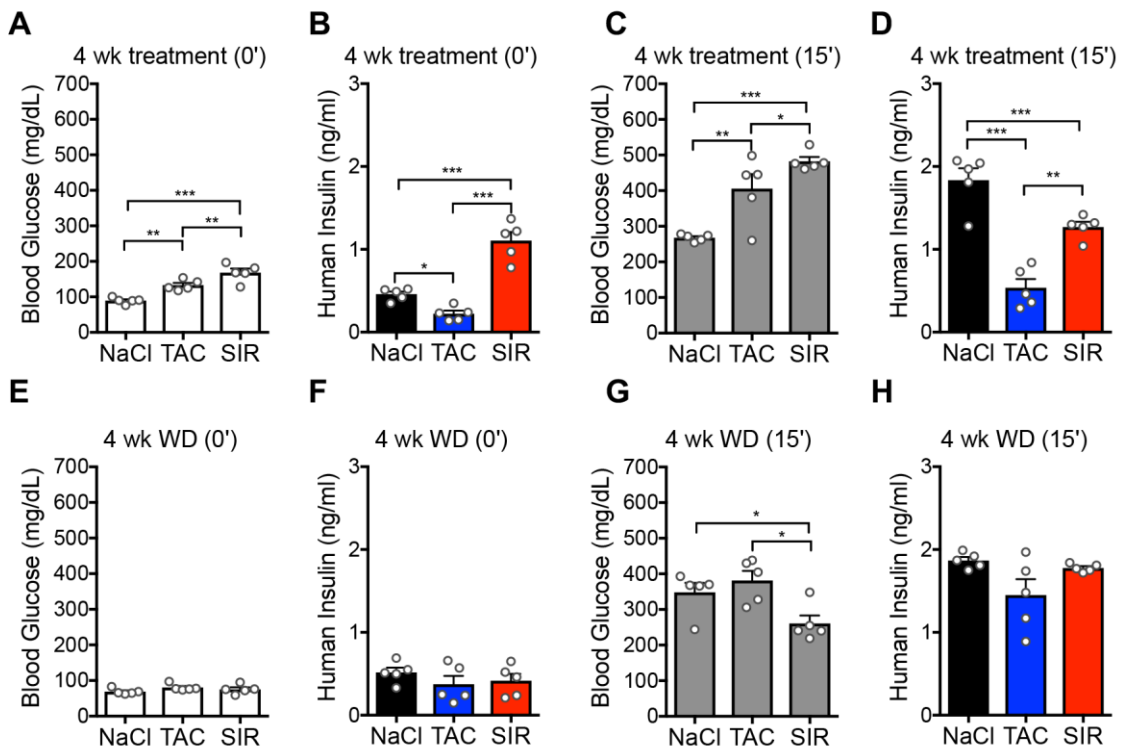

Figure 22. Related to Figure 21. The changes of blood glucose and human insulin levels induced by TAC or SIR are reversed after 4 weeks of withdrawal.

(A-H) Fasted and stimulated blood glucose and human insulin analyses after 4 weeks of drug treatment (**A-D**; corresponds to **Figure 21D-21E**). Fasted and stimulated blood glucose and human insulin analyses after 4 weeks drug withdrawal (**E-H**; corresponds to **Figure 21H-21I**). * p<0.05, ** p<0.01, *** p<0.001. Data represent mean ± SEM. One-way ANOVA was used for analysis of statistical significance. Figure adapted from Dai, Walker et al. 2020[558].

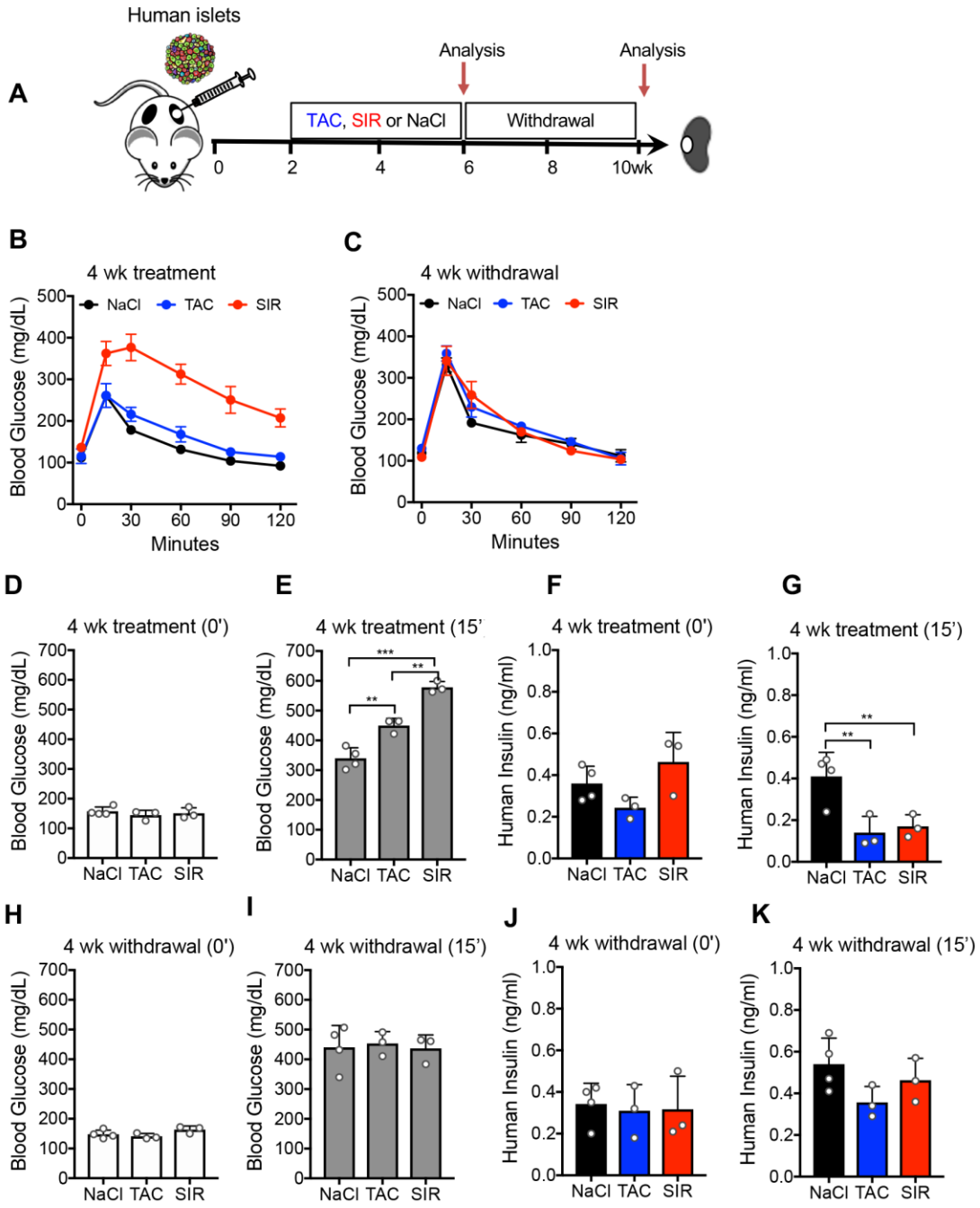

Figure 23. Related to Figure 21. Impaired β cell function by either TAC or SIR normalizes after 4 weeks of withdrawal.

(A) Schematic of experimental design. Mice were given NaCl, TAC or SIR for 4 weeks followed by withdrawal for 4 weeks. (**B-C)** GTT after treatment with TAC or SIR for 4 weeks (**B**) or 4 weeks after withdrawal (**C**). (**D-K**) Blood glucose and human at 0' and 15' of glucose-arginine stimulation after 4 weeks treatment (**D-G**) and then 4 weeks after withdrawal (**H-K**). n=3-4 samples/treatment. * $p<0.05$, ** $p<0.01$, *** $p<0.001$. Data represent mean ± SEM. One-way ANOVA was used for analysis of statistical significance. Figure adapted from Dai, Walker et al. 2020[558].

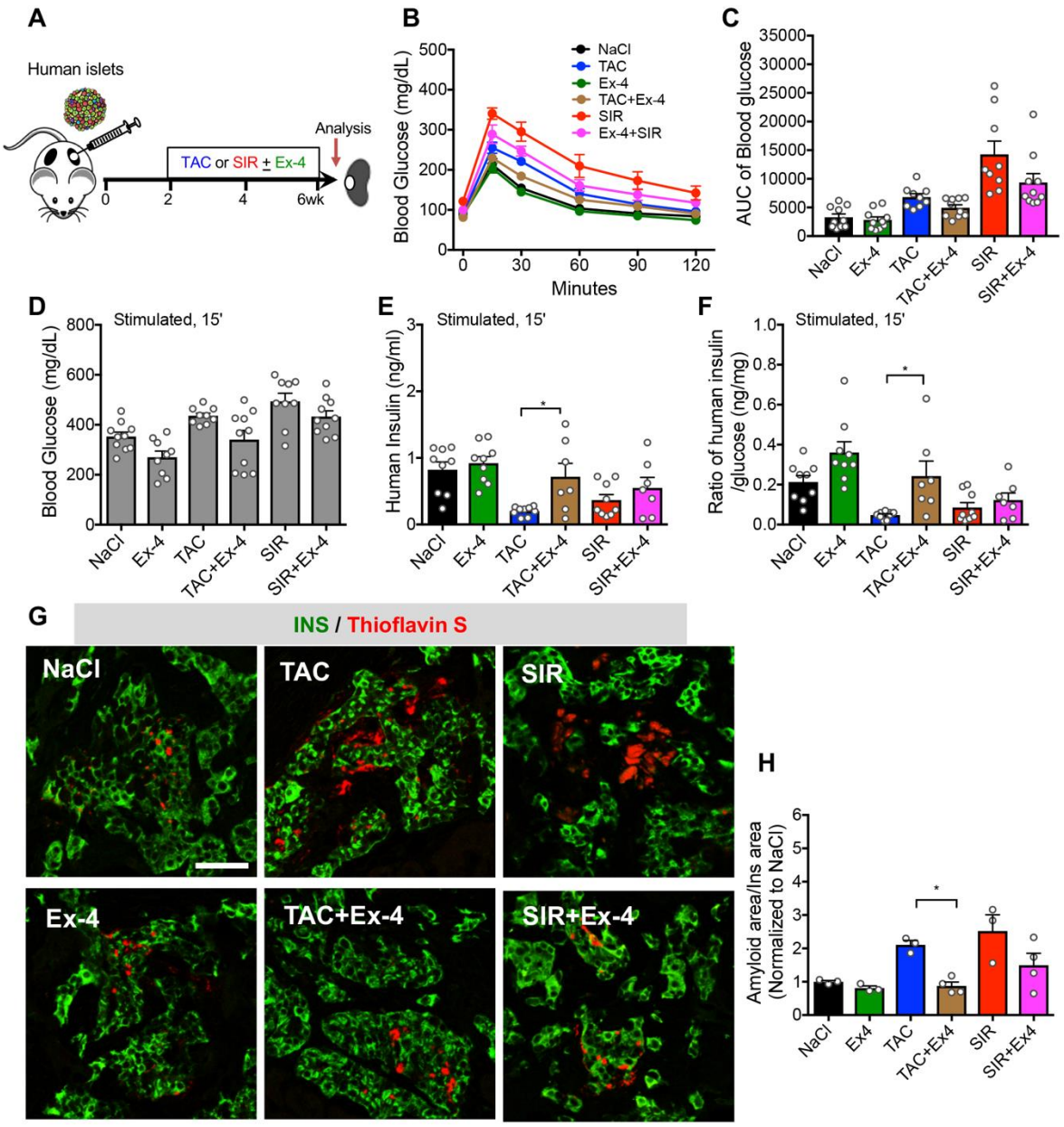

Figure 24. Ex-4 treatment can protect β cells from drug-induced dysfunction.
(A) Schematic of experimental design with TAC +Ex-4 or SIR + Ex-4 cotreatment for 4 weeks. (**B-C**) GTT and AUC after treatment with TAC or SIR with or without Ex-4 for 4 weeks. (**D-F**) Blood glucose, human insulin, and human insulin:blood glucose ratios at 15' after glucose-arginine stimulation (n=7-10 samples/treatment from 2 donors). Representative images (G) of amyloid after 4 weeks of treatment and quantification (H; n=3-4 grafts/treatment from 2 donors. - see **Table 14** for raw data). Scale bar: 50 μm applies to all amyloid images. * $p<0.05$, ** $p<0.01$, *** $p<0.001$. Data represent mean ± SEM. One-way ANOVA followed by Tukey multiple comparisons test was used for analysis of statistical significance. For ease of viewing, we highlight only the differences between NaCl vs. Ex-4, TAC vs TAC+Ex-4, or SIR vs SIR+Ex-4

within panels C-F and H. Full statistical comparisons are shown in **Table 15**. Figure adapted from Dai, Walker et al. 2020[558].

Table 15. Full statistical analysis of Figure 24C-24F and 24H

	AUC	Blood Glucose	Human Insulin	H Ins/Glucose Ratio	Amyloid /Ins area
NaCl vs Ex-4	ns	ns	ns	ns	ns
NaCl vs TAC	ns	ns	**	*	ns
NaCl vs TAC+Ex-4	ns	ns	ns	ns	ns
NaCl vs SIR	***	**	ns	ns	*
NaCl vs SIR+Ex-4	**	ns	ns	ns	ns
Ex-4 vs TAC	ns	***	***	***	*
Ex-4 vs TAC+Ex-4	ns	ns	ns	ns	ns
Ex-4 vs SIR	***	***	*	***	**
Ex-4 vs SIR+Ex-4	**	***	ns	**	ns
TAC vs TAC+Ex-4	ns	ns	*	*	*
TAC vs SIR	**	ns	ns	ns	ns
TAC vs SIR+Ex-4	ns	ns	ns	ns	ns
TAC+Ex-4 vs SIR	***	**	ns	ns	**
TAC+Ex-4 vs SIR+Ex-4	ns	ns	ns	ns	ns
SIR vs SIR+Ex-4	ns	ns	ns	ns	ns

Groups compared by One-way ANOVA followed by Tukey multiple comparisons test. ns $p>0.05$, * $p<0.05$, ** $p<0.01$, *** $p<0.001$. Table adapted from Dai, Walker et al. 2020[558].

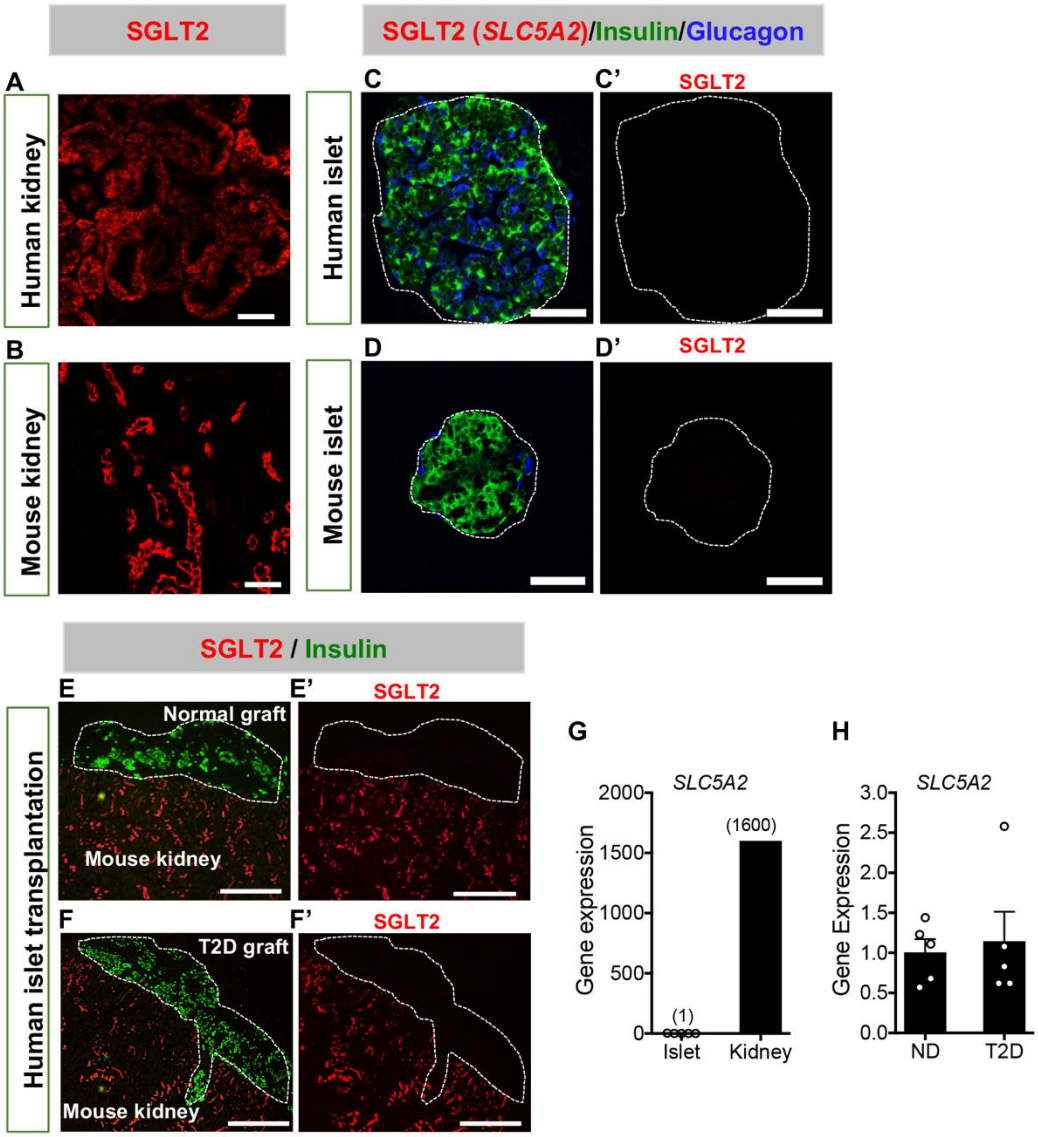

Figure 25. SGLT2/*SLC5A2* expression is extremely low in mouse and human islets. (**A-F***)* Representative images of immunostaining for SGLT2 expression in human (**A**) and mouse (**B**) kidney, human (**C**) and mouse (**D**) pancreatic islets, and transplanted normal (**E**) or T2D (**F**) human islet grafts under the mouse kidney capsule, allowing us to visualize mouse kidney and human islet tissue on the same section. C', D', E' and F' show only immunostaining for SGLT2. Scale bar in A ,B, C, C', D, and D': 50mm. Scale bar in E, E', F, F': 100mm. Green: insulin (guinea pig anti-insulin, Dako), blue: glucagon (mouse anti-glucagon, abcam), red: SGLT2 (rabbit anti-SGLT2, Novus). SGLT2 staining was confirmed with a second independent antibody (rabbit anti-SGLT2, abcam; images not shown). See supplemental table 2 for detailed antibody information. (**G**) Expression of *SLC5A2* mRNA (encodes SGLT2) in human pancreatic islets (n=5 donors) and human kidney cortex (n=1) measured by qRT-PCR. (**H**) Expression of *SLC5A2* mRNA in age-matched normal (ND, 44-59 years old, n=5) and T2D human pancreatic islets (47-61 years old, n=5) measured by qRT-PCR. p=0.7377. Student's t-test was used for analysis of statistical significance. Figure adapted from Dai, Walker et al. 2020[559].

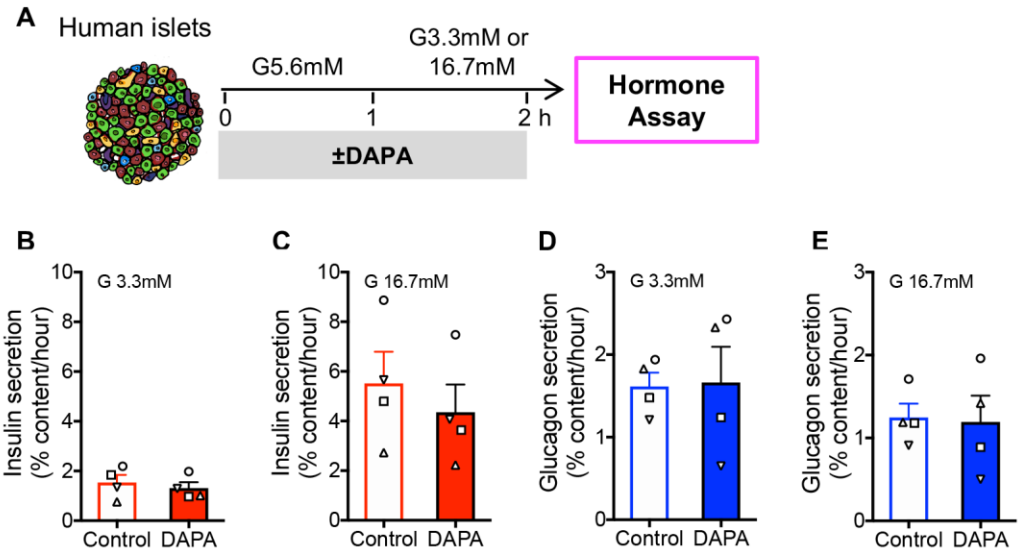

Figure 26. DAPA treatment does not affect α or β cell function in human islets in vitro. (**A**) Schematic design of acute DAPA treatment of human islets in vitro. After one hour with or without DAPA treatment in basal (5.6 mM) glucose, islets were transferred to low (3.3 mM) or high (16.7 mM) glucose for one hour. Low and high glucose media and islet extract was collected and analyzed for insulin and glucagon. (**B-E**) Insulin and glucagon secretion in low or high glucose with or without DAPA. Each data point corresponds to one donor (with symbols matched across panels; n=4 donors total) that is an average of multiple technical replicates. Student's t-test was used for analysis of statistical significance; $p > 0.05$. Figure adapted from Dai, Walker et al. 2020[559].

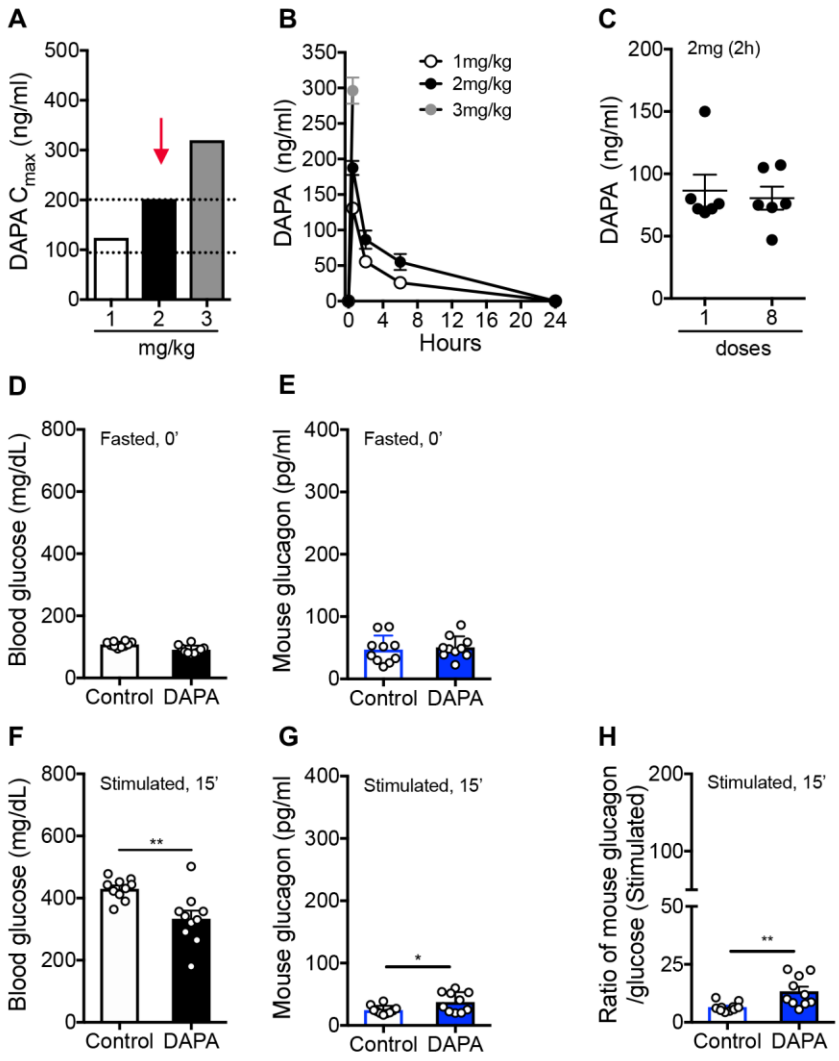

Figure 27. Effects of DAPA treatment on insulin and glucagon secretion in vivo and effect of DAPA in NSG mice without transplanted human islets.

(**A-C**) Pharmacokinetics of DAPA treatment by oral gavage in the NSG mice. (**A**) dose-dependent plasma C_{max} with the dotted lines representing the clinical therapeutic dose range, (**B**) time course of DAPA absorption and clearance, (**C**) accumulation across repeated dosing. Red arrow in (A) indicates the dose we used in the study. (**D-J)** NSG mice without human islet transplanted received DAPA treatment for 1 week. The mice were fasted for 6 hours and blood glucose (**D,H**), and mouse glucagon (**E, I)**, were measured at 0' or 15' after glucose challenge (2g/kg glucose delivered i.p.).Y-axes have been set to match Figure 28 and allow for comparison. Data also expressed as ratio of stimulated and mouse glucagon to blood glucose (**E**). ** $p<0.01$. Student's t-test was used for analysis of statistical significance. Figure adapted from Dai, Walker et al. 2020[559].

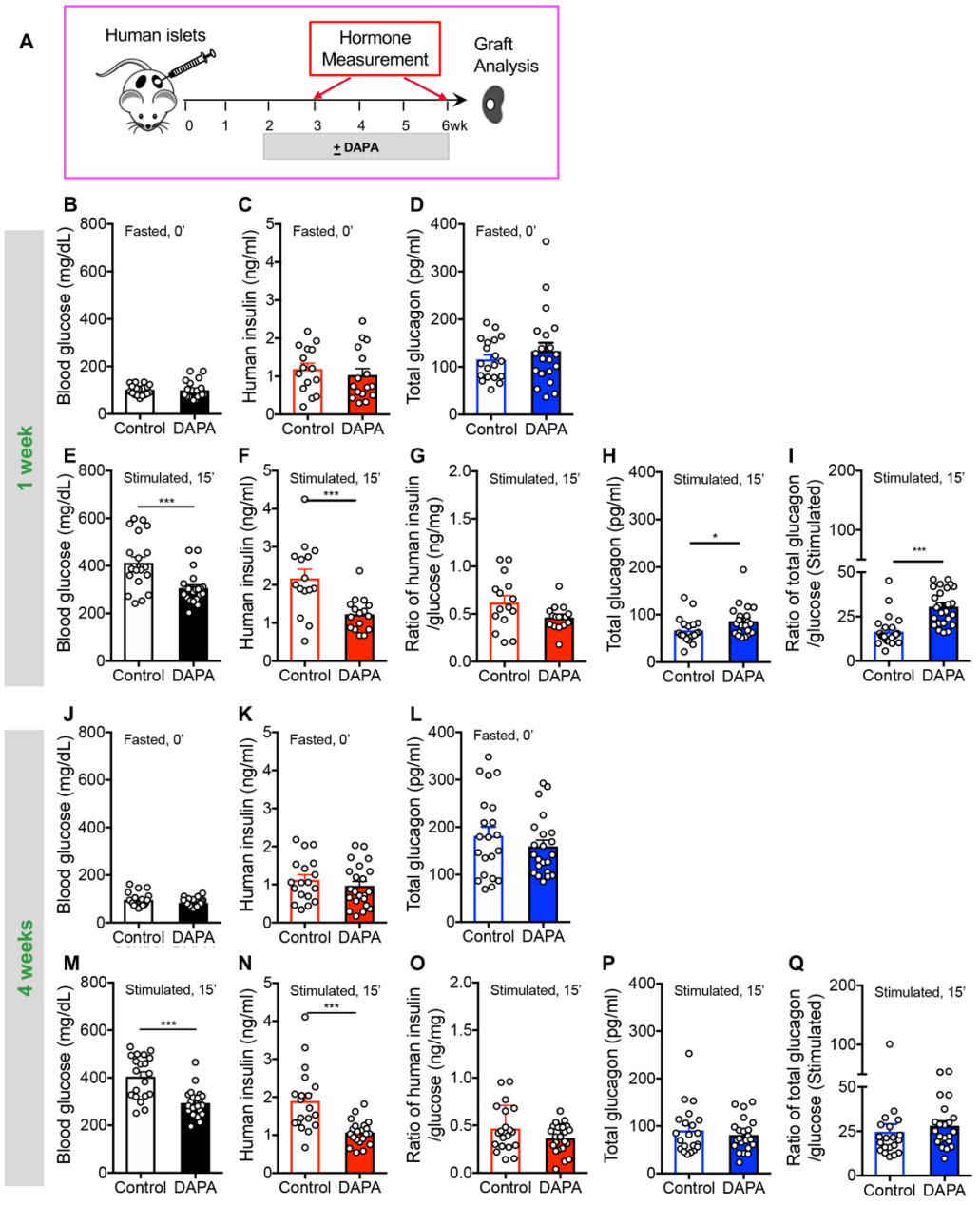

Figure 28. Effects of DAPA treatment on insulin and glucagon secretion in vivo.
(**A**) Schematic design of DAPA treatment on human islets in vivo. The mice were daily given DAPA (2mg/kg/day) by oral gavage for 4 weeks with graft function measured after 1 week of treatment (**B-I**) and 4 weeks of treatment (**J-Q**). Basal (6h fasted, 0'; **B**) and stimulated blood glucose (2 g/kg glucose delivered i.p., Stimulated, 15'; **E**), human insulin (**C, F**), total glucagon (**D, H**) from the mice treated for 1 week with DAPA. Basal and stimulated blood glucose (**J, M**), human insulin (**K, N**), and total glucagon (**L, P**) after 4 weeks treatment. For both 1 and 4 week treatment, data also expressed as ratio of stimulated human insulin (**G, O**) and total glucagon (**I, Q**) to blood glucose. Each dot represents a serum sample from a single mouse with transplanted human islets. * $p<0.05$, *** $p<0.001$. Student's t-test was used for analysis of statistical significance. Figure adapted from Dai, Walker et al. 2020[559].

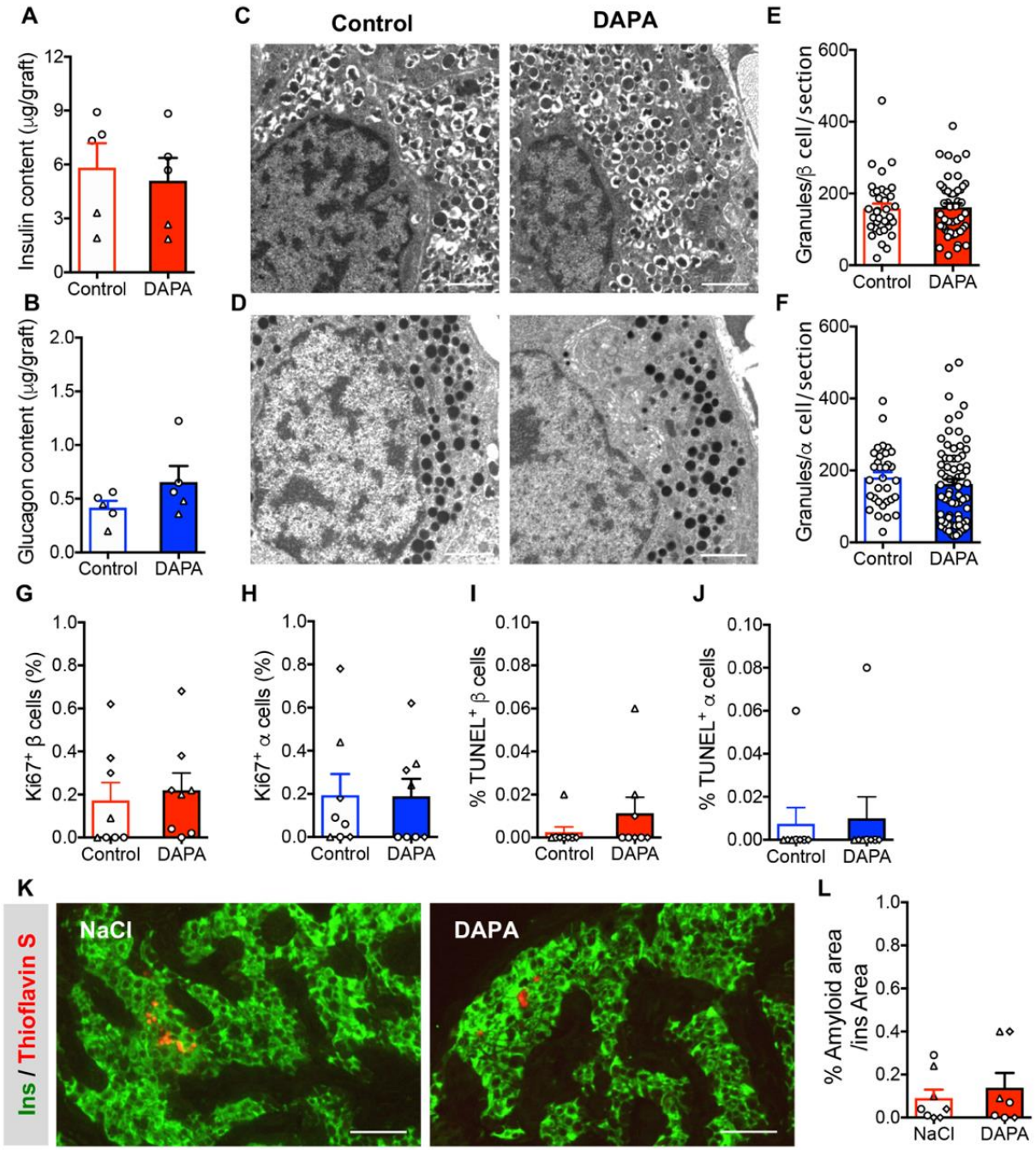

Figure 29. DAPA does not alter insulin or glucagon content, human α or β cell granule number, proliferation, apoptosis, or amyloid deposition in human grafts.
(**A, B**) Insulin and glucagon content of human islet grafts (n=5 grafts from 2 donor transplantations, symbols matched across panels). (**C-F**) Representative EM images of human transplanted beta (**C**) and alpha cells (**D**) (x6500) with or without DAPA treatment and quantification of granules in β (**E**) and α cells (**F**); each dot represents a section of a beta or alpha cell from two islet grafts of one donor for control and DAPA treatment. (**G, H**) Percent of

Ki67 positive β and α cells (antibodies used: guinea pig ani-insulin, Dako; mouse anti-glucagon, abcam; rabbit anti-Ki67, abcam). (**I, J**) Percent of TUNEL positive β and α cells (antibodies used: guinea pig anti-insulin, Dako; rabbit anti-glucagon, Cell Signaling; TUNEL assay, Millipore-S7165). (**K**) Representative images of amyloid deposits in human grafts labeled with insulin (green) and thioflavin S (amyloid, red) and quantification of amyloid area (**L**). Scale bar: 50 μm. n=8 grafts from 3 donor transplantations, symbols matched across panels G-J, L. Student's t-test was used for analysis of statistical significance; $p > 0.05$. Figure adapted from Dai, Walker et al. 2020[559].

CHAPTER IV:
HUMAN PSEUDOISLET SYSTEM TO STUDY ISLET PHYSIOLOGY

Some text and data in this chapter have been adapted from Walker, Haliyur et al., 2020[560].

Introduction

Pancreatic islets of Langerhans, small collections of specialized endocrine cells interspersed throughout the pancreas, control glucose homeostasis. Islets are composed primarily of β, α, and δ cells but also include supporting cells such as endothelial cells, nerve fibers, and immune cells. Insulin, secreted from the β cells, lowers blood glucose by stimulating glucose uptake in peripheral tissues, while glucagon, secreted from α cells, raises blood glucose mainly through its actions in the liver. Importantly, β and/or α cell dysfunction is a key component of all forms of diabetes mellitus[357,594,595,650–657]. Thus, an improved understanding of the pathways governing the coordinated hormone secretion in human islets may provide insight into how these may become dysregulated in diabetes.

In β cells, the central pathway of insulin secretion involves glucose entry via glucose transporters where it is metabolized inside the cell, resulting in an increased ATP:ADP ratio. This shift closes ATP-sensitive potassium channels, depolarizing the cell membrane and opening voltage-dependent calcium channels where calcium influx is a trigger of insulin granule exocytosis[94]. In α cells, the pathway of glucose inhibition of glucagon secretion is not clearly defined with both intrinsic and paracrine mechanisms proposed[234,249,253]. Furthermore, gap junctional coupling and paracrine signaling between islet endocrine cells and within the 3D islet architecture are critical for islet function, as individual α or β cells do not show the same coordinated secretion pattern seen in intact islets[168,200,201,276,281]. How these coordinated cellular responses relate to the islet cellular composition is not known but the absence of β cells in the T1D islet has been hypothesized to contribute to α cell dysfunction in T1D[594].

The 3D islet architecture, while essential for function, presents experimental challenges for mechanistic studies of intracellular signaling pathways in primary islet cells. Furthermore, human islets show a number of key differences from rodent islets including their endocrine cell composition and arrangement, glucose set-point, and both basal and stimulated insulin and glucagon secretion, highlighting the importance of studying signaling pathways in primary human cells[22,24–26].

To study signaling pathways in primary human islet cells within the context of their 3D arrangement, we developed an integrated approach that consists of: 1) human pseudoislets closely mimicking native human islet biology and allowing for efficient genetic manipulation; and 2) a microfluidic system with the synchronous assessment of intracellular signaling dynamics and both insulin and glucagon secretion. Using this experimental approach, we demonstrate differences in G_q and G_i signaling pathways between human β and α cells. We further extend the system to cellular manipulation of the pseudoislet to resolve cell-type specific intracellular signals and investigate drivers of pseudoislet aggregation.

Results

Human pseudoislets resemble native human islets and facilitate virally mediated manipulation of human islet cells

To establish an approach that would allow manipulation of human islets, we adapted a system where human islets are dispersed into single cells and then reaggregated into pseudoislets[493,494,658–660] (**Figure 30A**). To optimize the formation and function of human pseudoislets, we investigated two different systems to generate pseudoislets, a modified hanging drop system[661,662] and an ultra-low attachment microwell system. We found both systems generated pseudoislets of comparable quality and function (**Figures 31A** and **31B**) and thus combined groups for comparisons between native islets and pseudoislets. A key determinant of pseudoislet quality was the use of a nutrient- and growth factor-enriched media (termed Vanderbilt pseudoislet media).

Pseudoislet morphology, size, and dithizone (DTZ) uptake resembled normal human islets (**Figures 30B-30D**). Pseudoislet size was controlled to between 150-200 μm in diameter by adjusting the seeding cell density and thus resembled the size of an average native human islet. Compared to native islets from the same donor cultured in parallel using the same pseudoislet media, pseudoislets had similar insulin and glucagon content though insulin content was reduced in pseudoislets from some donors (**Figure 30E**). Endocrine cell composition was also similar with the ratio of β, α, and δ cells in pseudoislets unchanged compared to cultured native islets from the same donor (**Figures 30F** and **30G**).

As the primary function of the pancreatic islet is to sense glucose and other nutrients and dynamically respond with coordinated hormone secretion, we assessed the function of pseudoislets compared to native islets by perifusion. We used the standard perifusion (termed in the text also as macroperifusion) approach of the Human Islet Phenotyping Program of the Integrated Islet Distribution Program (IIDP; https://iidp.coh.org/) which has assessed nearly 300 human islet preparations. In this system, ~250 islet equivalents (IEQs) are loaded into a chamber and exposed to basal glucose (5.6 mM glucose; white) or various secretagogues (16.7 mM glucose, 16.7 mM glucose and 100 μM isobutylmethylxanthine (IBMX), 1.7 mM glucose and 1 μM epinephrine, 20 mM potassium chloride (KCl); yellow). Pseudoislet insulin secretion was very similar to that of native islets in biphasic response to glucose, cAMP-evoked potentiation, epinephrine-mediated inhibition, and KCl-mediated depolarization (**Figure 30H**). Pseudoislets and native islets also had comparable glucagon secretion, which was inhibited by high glucose, and stimulated by cAMP-mediated processes (IBMX and epinephrine) and depolarization (KCl) (**Figure 30I**). Compared to native islets on the day of arrival, pseudoislets largely maintained both insulin and glucagon secretion after six days of culture with the exception of a slightly diminished second phase glucose-stimulated insulin secretion and an enhanced glucagon response to epinephrine in cultured native islets and pseudoislets (**Figure 31C-31N**). These results demonstrate that after dispersion into the single-cell state, human islet cells can reassemble and reestablish intra-islet connections crucial for coordinated hormone release across multiple signaling pathways.

Interestingly, the islet architecture of both native whole islets and pseudoislets cultured for six days showed β cells primarily on the islet periphery with α cells and δ cells situated within an interior layer. Furthermore, the core of both the cultured native islets and pseudoislets consisted largely of extracellular matrix (collagen IV) and endothelial cells (caveolin-1) (**Figures 32A-32C**), likely reflective of the consequences of culture and the loss of shear stress along endothelial cells. The survival of intraislet endothelial cells in culture for an extended period of time could be due to the nutrient- and growth factor-enriched media. Additionally, the islet cell arrangement suggests that extracellular matrix and endothelial cells may facilitate pseudoislet assembly. Proliferation, as assessed by Ki67, was low in both native and pseudoislets with β cells below 0.5% and α cells around 1% (**Figures 32A** and **32D**). Similarly, apoptosis, as assessed by TUNEL, was very low (<0.5%) in pseudoislets and cultured human islets (**Figures 32A** and **32E**). Interestingly, endothelial cells appear to have greater turnover as evidenced by the presence of both Ki67 and TUNEL staining in the core of both native islets and pseudoislets (**Figure 32A**).

To assess markers of α and β cell identity in pseudoislets, we investigated expression of several key islet-enriched transcription factors by immunolabeling. The expression of β (PDX1, NKX6.1) and α cell markers (MAFB, ARX) as well as those expressed in both cell types (PAX6, NKX2.2) was maintained in pseudoislets when compared to native islets (**Figures 32F-32J**), indicating that the process of dispersion and reaggregation does not affect islet cell identity.

The 3D structure of intact islets makes virally mediated manipulation of human islet cells challenging due to poor viral penetration into the center of the islet. We adopted the pseudoislet system to overcome this challenge by transducing the dispersed single islet cells before reaggregation (**Figure 33A**). To optimize transduction efficiency and subsequent pseudoislet formation, we incubated with adenovirus for 2 hours in Vanderbilt pseudoislet media at a multiplicity of infection (MOI) of 500. Transducing pseudoislets with an adenovirus expressing a fluorescent reporter did not affect pseudoislet morphology or function and achieved high transduction efficiency of β and α cells throughout the entire pseudoislet (**Figures 34A-34E**). Interestingly, β cells showed a higher transduction efficiency (90%) than α cells (70%), suggesting that α cells may be inherently more difficult to transduce with adenovirus (**Figure 34B**).

Activation of G_i signaling reduces insulin and glucagon secretion

To investigate the value of this experimental approach, we sought to perturb expression of a single islet gene and then assess islet cell function. We chose to alter G-protein-coupled-receptor (GPCR) signaling in islet cells because GPCRs are known to modulate islet hormone secretion[663,664]. GPCRs, a broad class of integral membrane proteins, mediate extracellular messages to intracellular signaling through activation of heterotrimeric G-proteins which can be broadly classified into distinct families based on the G_α subunit, including G_i-coupled and G_q-coupled GPCRs[665]. An estimated 30-50% of clinically approved drugs target or signal through GPCRs, including multiple drugs used for diabetes treatment[666,667].

Studying GPCR signaling with endogenous receptors and ligands can be complicated by a lack of specificity—ligands that can activate multiple receptors or receptors that can be activated by multiple ligands. To overcome these limitations, we employed the DREADD technology[668]. DREADDs are GPCRs with specific point mutations that render them unresponsive to their endogenous ligand. Instead, they can be selectively activated by the otherwise inert ligand, clozapine-N-oxide (CNO), thus providing a selective and inducible model of GPCR signaling[668,669]. DREADDs are commonly used in neuroscience as molecular switches to activate or repress neurons with G_q or G_i signaling, respectively[670]. In contrast, there have been comparatively very few studies using DREADDs in the field of metabolism, but they have included investigating the G_q and G_s DREADD in mouse β cells and the G_i DREADD in mouse α cells[200,671]. The G_s-coupled DREADD has been reported to be leaky and have basal activation, and thus, we chose here to focus on the two most commonly used DREADDs, G_i and G_q, to demonstrate how this experimental approach can be utilized. To our knowledge, this is the first study to utilize this powerful technology in human islets.

To investigate G_i-coupled GPCR signaling, we introduced adenovirus encoding hM4Di (Ad-CMV-hM4Di-mCherry), a G_i DREADD, into dispersed human islet cells, allowed reaggregation into pseudoislets and then tested the effect of activated G_i signaling (**Figure 33A**). G_i-coupled GPCRs signal by inhibiting adenylyl cyclase, thus reducing cAMP, and by activating inwardly rectifying potassium channels (**Figure 33B**). Endogenous GPCRs which couple to G_i proteins include the somatostatin receptor in all islet cells as well as the α_2 adrenergic receptor in β cells [663,664]. CNO (10 μM) had no effect on insulin or glucagon secretion in mCherry-expressing pseudoislets (**Figures 34F** and **34G**), thus we compared the dynamic hormone secretion of hM4Di-expressing pseudoislets with and without CNO in response to a glucose ramp (2 mM glucose, 7 mM glucose, 11 mM glucose, 20 mM glucose; gray) and depolarization by KCl (20 mM; yellow) by perifusion. Activation of G_i signaling had clear inhibitory effects on insulin secretion by β cells at low glucose, which became more prominent with progressively higher glucose concentrations (gray shading; **Figures 33C-33E**). Furthermore, bypassing glucose metabolism by directly activating β cells via depolarization with potassium chloride did not overcome this inhibition by G_i signaling (yellow shading; **Figures 33C** and **33F**). Together these data demonstrate that in human β cells, G_i signaling significantly attenuates, but does not completely prevent, insulin secretion and that this effect, at least in part, occurs downstream of glucose metabolism.

The activation of G_i signaling also had inhibitory effects on glucagon secretion (**Figures 33G-33J**). We did not observe a substantial inhibition of glucagon secretion in the hM4Di and hM4Di+CNO group in response to glucose, but activation of G_i signaling with CNO caused a clear reduction in glucagon secretion, and secretion remained lower in the hM4Di+CNO group than control hM4Di pseudoislets. When stimulated with potassium chloride, pseudoislets with activated G_i signaling increased glucagon secretion but not to the level of controls. This demonstrates that the inhibitory effects of G_i signaling persist even if the α cell is directly activated by depolarization. Thus, in α cells, activation of G_i signaling reduces glucagon secretion across a range of glucose levels and when the cell is depolarized by potassium chloride.

Activation of G_q signaling greatly stimulates glucagon and somatostatin secretion but has both stimulatory and inhibitory effects on insulin secretion

G_q-coupled GPCRs signal through phospholipase C, leading to IP_3-mediated Ca^{2+} release from the endoplasmic reticulum (**Figure 35A**). Endogenous GPCRs which couple to G_q proteins in islets include the M_3 muscarinic receptor and the free fatty acid receptor FFA (also known as GPR40)[663,664]. To investigate G_q-coupled GPCR signaling, we introduced hM3Dq (Ad-CMV-hM3Dq-mCherry), a G_q DREADD, into dispersed human islet cells, allowed reaggregation, and assessed hM3Dq-expressing pseudoislets by perifusion. When CNO was added to activate G_q signaling, there was an acute increase in insulin secretion. However, this was not sustained as insulin secretion fell quickly back to baseline, highlighting a dynamic response to G_q signaling in β cells (**Figures 35B-35E**). Furthermore, continued G_q activation inhibited glucose-stimulated insulin secretion, suggesting that in certain scenarios, G_q signaling may override the ability of glucose to stimulate insulin secretion. These results highlight the value of assessing hormone secretion in the dynamic perifusion system. Finally, G_q activation reduced, but did not completely prevent, insulin secretion in response to direct depolarization with potassium chloride, indicating that the inhibitory effects cannot be overcome by bypassing glucose metabolism and suggesting that they occur downstream of the K_{ATP} channel. Together, these data indicate that activated G_q signaling can have both stimulatory and inhibitory effects on human β cells.

In contrast, activation of G_q signaling in α cells robustly increased glucagon secretion in low glucose and it remained elevated with continued CNO exposure during glucose ramp as well as in the presence of potassium chloride (**Figures 35F-35I**). This indicates that in contrast to the β cells, activation of G_q signaling in α cells robustly stimulates glucagon secretion and this response is sustained across a glucose ramp and during KCl-mediated depolarization.

Given the differing responses in β and α cells and the potential for paracrine signaling, we sought to measure somatostatin secretion and elucidate the effect of G_q activation in δ cells. The relatively low abundance of δ cells in the native islets and pseudoislets (approximately 5%) prevented detection of somatostatin in the perifusion and microperifusion experiments (below assay sensitivity), so we tested the effect of CNO in low (2 mM) and high (11 mM) glucose in the context of static incubation. In glucose alone, somatostatin secretion was below the assay detection limit in three out of the four donors tested; in contrast, activation of G_q signaling increased somatostatin secretion in both low and high glucose (**Figure 36A-36D**), showing that G_q signaling robustly stimulates δ cells.

Integration of pseudoislet system with genetically-encoded biosensor and microfluidic device allows synchronous measurement of intracellular signals and hormone secretion

While conventional macroperifusion systems, including the perifusion system used in this study reliably assess islet hormone secretory profiles[220,570,594,595,654], their configuration does not allow coupling with imaging systems to measure intracellular signaling. To overcome this challenge, we developed an integrated microperifusion system consisting of pseudoislets and a microfluidic device that enables studies of islet intracellular signaling using genetically-encoded biosensors in conjunction with hormone secretion (**Figures 37A** and **38A-38C**). The microfluidic device

(**Figure 38A**)[571] is made of bio-inert and non-absorbent materials with optimized design for nutrient delivery, synchronous islet imaging by confocal microscopy, and collection of effluent fractions for analysis of insulin and glucagon secretion. The microperifusion system uses smaller volumes, slower flow rates, and fewer islets than our conventional macroperifusion system (**Figures 38D-38F**).

To investigate the dual effects of activated G_q signaling on insulin secretion, we co-transduced pseudoislets with hM3Dq and GCaMP6f (**Figure 38C**), a calcium biosensor (Ad-CMV-GCaMP6f), as the G_q pathway conventionally signals through intracellular Ca^{2+} (**Figure 35A**). In the absence of CNO, hM3Dq-expressing pseudoislets had stepwise increases in GCaMP6f relative intensity as glucose increased, corresponding to increasing intracellular Ca^{2+} and highlighting the added value of the system (**Figure 37B; Supplemental Video 1**). This intracellular Ca^{2+} response to stepwise glucose increase was accompanied by increasing insulin secretion (**Figure 37C**), but the first phase of insulin secretion was not as clearly resolved as in the macroperifusion (**Figure 35B**).

Since there are differences in the design of the macro- and microperifusion systems, we used multiphysics computational modeling with finite element analysis[572,573] to model the insulin secretion dynamics of the two systems (**Figures 38H** and **38I**). This modeling accurately predicted the overall shape of each insulin secretory trace with the macroperifusion showing a "saw-tooth" pattern (**Figure 38H**) while the microperifusion had a more progressive increase (**Figure 38I**). Using this approach, we found that differences in the insulin secretory profiles were primarily due to the different fluid dynamics and experimental parameters between the two perifusion systems, especially the experimental time for each stimulus and the flow rate. Overall, this analysis demonstrates how perifusion parameters can impact insulin secretory pattern and indicates the strength of using complementary approaches. It also emphasizes the importance of validating new microperifusion devices[672,673] by comparing these with macroperifusion that have been used for many years by many laboratories.

When G_q signaling was activated with CNO, we again saw a transient stimulation of insulin secretion at low glucose followed by relative inhibition through the glucose ramp, while glucagon secretion from α cells was stimulated throughout the entire perifusion, independently of glucose concentration (**Figures 37C, 37D, 37G-37J**). Furthermore, the Ca^{2+} dynamics in response to G_q activation were consistent with the insulin secretory trace showing a rapid but short-lived increase in intracellular Ca^{2+}. Interestingly, the Ca^{2+} signal remained elevated above baseline but did not significantly increase with rising glucose (**Figures 37B, 37E** and **37F**; **Supplemental Video 2**). This indicates that the dual effects of G_q signaling on insulin secretion in β cells are largely mediated by changes in intracellular Ca^{2+} levels.

Human pseudoislets allow cellular manipulation to resolve cell-type specific signals

To manipulate individual cell types within the islet, we sought to combine our pseudoislet approach with advancements in techniques to purify live cell populations. We used fluorescence-activated cell sorting (FACS) with recently identified cell surface antibodies[220,674] to purify human α and β cell populations and then combined these cells to form pseudoislets of

2000 total cells that were only β cells, only α cells, or in a 50:50 ratio (**Figure 39A**). All three types of pseudoislets formed with similar size and morphology though we noted that α cell only pseudoislets appeared to form more quickly than other groups (**Figure 39B**). Enrichment of the desired cell type was confirmed by evaluating the insulin or glucagon content in these pseudoislets. Glucagon and insulin were undetectable in β cell only and α cell only pseudoislets respectively (**Figure 39C**). Further, mixed pseudoislets contained about half the insulin or glucagon content of the pseudoislets with only one cell type, in line with the seeing ratios (**Figure 39C**).

Combining both cellular and genetic manipulation in this system allows for cell specificity with viral delivery, a process that is currently inefficient or non-specific in human islet cells through other means. Using out microfluidic system, we resolved cell type-specific signaling, for example specifically isolating the β cell calcium signal from mixed pseudoislets (**Figure 39D**). This allows us to model pathogenic states (α cell only T1D-like pseudoislets) to investigate mechanisms of α cell dysfunction, an important feature of T1D[594]. We found that α cells showed minimal Ca^{2+} response despite robust glucagon secretion in response to low glucose and epinephrine in α cell only pseudoislets (**Figure 39E**), suggestive that signaling may instead be mediated through other second messengers such as cAMP.

Real-time monitoring of pseudoislet formation reveals role for α cells in pseudoislet aggregation

At birth, the cellular arrangement of many human islets resembles those of rodents – a β cell core surrounded by mantle of α and δ cells[27,30,675]. Postnatally, human islets undergo substantial cellular rearrangement to achieve the intermingled arrangement of adult islets[22,25]. How and why this shift occurs is largely unknown, but such dynamic changes likely impact the risk for and/or development of T1D and T2D. This cellular rearrangement coincides with the period when autoimmunity first appears. Further, as cells rearrange, they form important physical connections with each other including gap junctions to help synchronize β cell depolarizations across the islet as well as extracellular connections such as Eph-ephrin juxtracrine signaling[287,676]. As our pseudoislet approach uses clear ultra-low attachment microwells that is compatible with live cell imaging, this system is amenable to investigating processes by which islet cells arrange themselves.

Pseudoislet formation takes place over ~6 days (144 hours) during which the dissociated endocrine cells become progressively more compact and assume the islet-like spheroid shape (**Figure 40A**). To investigate how pseudoislets form more specifically, we utilized FACS-purified β and α cells; β cells were then transduced with a GFP-expressing adenovirus while α cells were transduced with an mCherry-expressing adenovirus to allow for specific cell type identification and tracking during pseudoislet formation (**Figure 40B**). To test how the absence of β cells affects pseudoislet formation, we plated some wells with combined β and α cells in a 50:50 ratio (1000 β cells and 1000 α cells) and others with all α cells (2000 α cells) and monitored their formation using confocal microscopy every 3 hours starting 24 hours after transduction to allow expression of the fluorescent protein (**Figure 40B**).

By 24 hours after plating, α cell only pseudoislets were more compact than the mixed pseudoislets (**Figure 40C**), suggesting that the α cells were able to more quickly form close cell-cell connections. Interestingly, in the mixed pseudoislets at 24 hours, α cells appeared to form distinct clusters with each other while β cells were evenly spread across the cell cluster (**Figure 40D**). These clusters remained throughout pseudoislet formation and appeared to help facilitate pseudoislet aggregation (**Supplemental Video 3**). Together, this data suggests there may be inherent signals in adult human α cells that encourage homotypic connections and may help explain the dynamic islet rearrangement seen in human islets as they mature.

Discussion

The three-dimensional multicellular human islet architecture, while essential for islet cell function presents experimental challenges for mechanistic studies of intracellular signaling pathways. Using primary human islets, we developed a pseudoislet system that resembles native human islets in morphology, cellular composition, cell identity, and dynamic insulin and glucagon secretion. This system allows for efficient cellular manipulation and virally mediated genetic manipulation in almost all cells in the pseudoislet. To evaluate the coordination between intracellular signals and islet hormone secretion, we developed an integrated system consisting of pseudoislets and a microfluidic device that enables studies of islet intracellular signaling using genetically encoded biosensors in conjunction with hormone secretion. We used this integrated approach to define new aspects of human islet biology by investigating GPCR signaling pathways using DREADDs and a calcium biosensor. Further, we combined the approach with FACS to manipulate the pseudoislet cellular composition. This allowed accurate cell-specific targeting to distinguish intracellular dynamics of islet endocrine cells to various stimuli and understand the pseudoislet formation process.

Despite α and β cells both being excitable secretory cells and sharing many common developmental and signaling components, this experimental approach allowed us to demonstrate similar and distinct responses to activation of GPCR signaling pathways, highlighting the uniqueness in each cell's molecular machinery. The activation of G_i signaling was inhibitory in β and α cells resulting in reduced insulin and glucagon secretion, respectively, and showed more substantial impact in β cells where this signaling blunted insulin response to both a glucose ramp and to KCl-mediated depolarization. Interestingly, direct KCl depolarization was not sufficient to overcome these inhibitory effects in either β or α cells, suggesting that reduced cAMP via the inhibition of adenylyl cyclase, in addition to cAMP-independent pathways[677], plays a role in both insulin and glucagon secretion. These results align well with recent studies in β cells suggesting cAMP tone is crucial for insulin secretion and observations in α cells highlighting cAMP as a key mediator of glucagon secretion[168,253,281,678].

The activation of G_q signaling showed major differences in β cells compared to α cells. In α cells, the activated G_q signaling elicited a robust and sustained increase in glucagon secretion in the presence of a glucose ramp and potassium chloride. In contrast, G_q signaling in β cells had a transient stimulatory effect in low glucose and then inhibitory effects on both insulin and intracellular Ca^{2+} levels with sustained activation during glucose ramp. Interestingly, previous

studies of acetylcholine signaling have also reported dual effects on Ca^{2+} dynamics in β cells depending on the length of stimulation[232]. This signaling was thought to be mediated through the muscarinic acetylcholine receptor M_3 (from which the hM3Dq DREADD is based). Overall, these results suggest a negative feedback or protective mechanism that prevents sustained insulin release from β cells in response to G_q signaling that is not active in α cells under similar circumstances.

There are limitations and caveats to the current study. First, our approach expressed the DREADD receptors in all cell types. Although we can distinguish the effects on islet α and β cells through their distinct hormone secretion, it is possible that complex paracrine signaling contributes to the results described here. Future modifications of this system could incorporate cell-specific approaches to target a particular islet cell type. Second, the DREADD receptors are likely expressed at higher levels than endogenous GPCRs. To mitigate this, we used the appropriate DREADD-expressing pseudoislets as our controls and were encouraged to see normal secretory responses in these control pseudoislets. Third, while there is some concern that CNO can be reverse-metabolized in vivo into clozapine which could potentially have off-target effects[679], this is unlikely in our in vitro system. We also verified that CNO had no effect on mCherry-expressing pseudoislets, making it unlikely that CNO itself is competitively inhibiting endogenous receptors in human islets. Fourth, we used a CNO concentration of 10 μM for all of our experiments, a standard concentration used for in vitro assays[200,680], but it is possible that islet cells may show dose-dependent effects. Finally, this is an in vitro study focused on acute functional effects of these pathways on human islets, and chronic in vivo studies of these pathways may show different results. For example, in mouse β cells, chronic in vivo activation of G_q pathways using the DREADD system lead to an increase in β cell function and mass[681] while inhibition of G_i signaling with β cell-specific pertussis toxin expression affected only function[682]. Future work could involve transplantation of DREADD-expressing pseudoislets into immunodeficient mice to study the effect of activating these pathways on human islets in vivo[568].

Overall, these findings demonstrate the utility of the pseudoislet system for the ability to manipulate human islets. Other approaches include inducible pluripotent stem cells that allow similar genetic manipulation and cellular control. However, it is unclear if these approaches create entirely normal human islet cells and protocols to form non-β islet cell types are not as well defined[683]. We show in this system that α and β cells in pseudoislets maintain their fully differentiated state as well as their dynamic responsiveness to glucose and other stimuli. Additionally, this approach allows for the study of all islet cells within the context of other cell types and 3D assembly. While our data suggest that breaking down and rebuilding the islet does not impair paracrine interactions, this could be further evaluated by looking at secretion in response to factors that exclusively rely on paracrine interactions such as ghrelin or certain amino acids[168,684,685].

Ultimately, the integration of the pseudoislet approach with a microfluidic perifusion system and live cell imaging provides a powerful experimental platform to gain insight into human islet biology and the mechanisms controlling regulated islet hormone secretion which currently limits the development of novel therapeutic approaches. Here, we focus on virally mediated gene

expression to alter signaling pathways, but this system could be adapted to accommodate technologies such as CRISPR. Further, cellular manipulation in the pseudoislet system will allow mechanistic studies of cellular arrangement and the physical, electrical, and paracrine interactions of different cell types in the islet microenvironment that govern overall islet function.

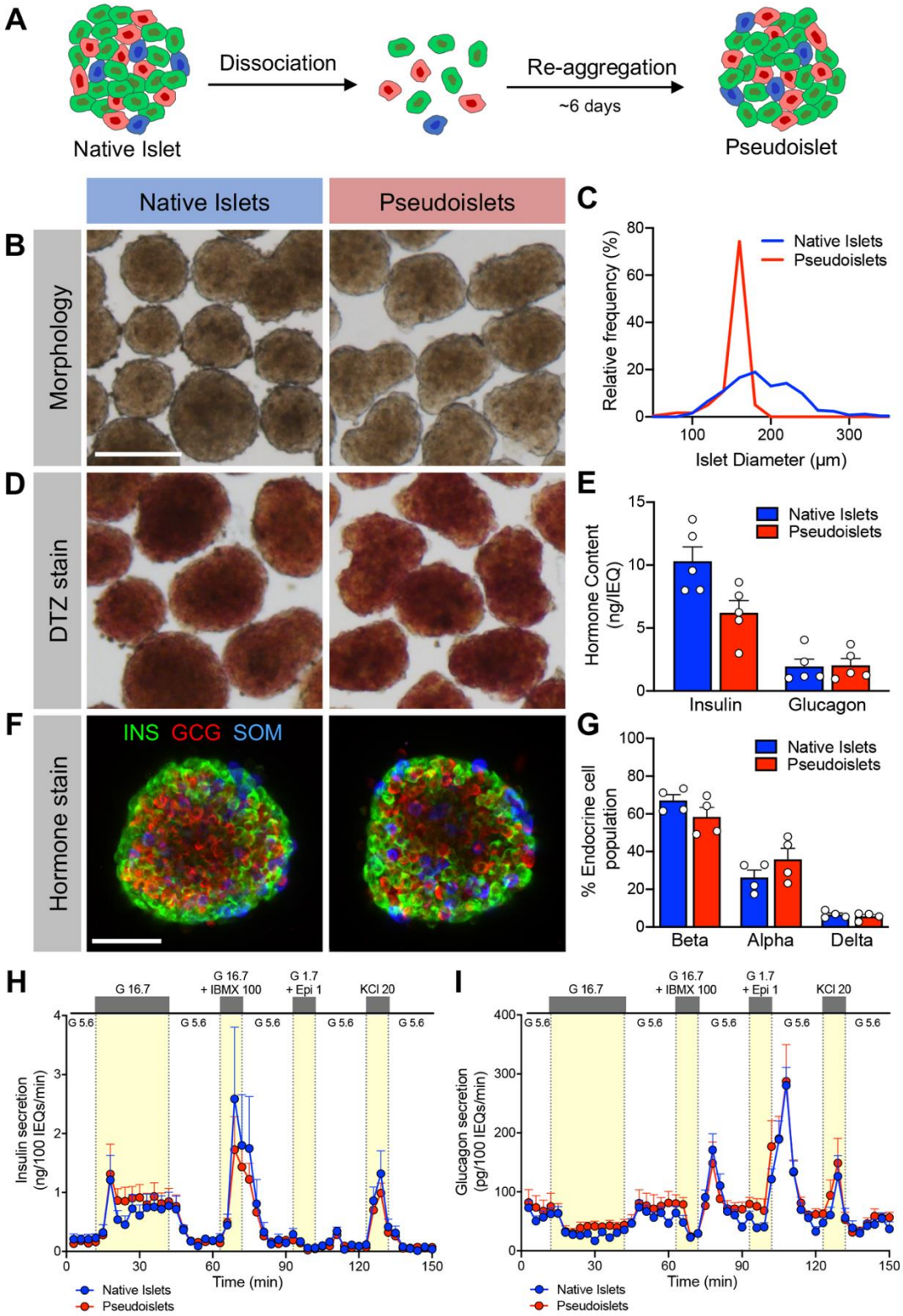

Figure 30. Pseudoislets resemble native human islets in morphology, cell composition, and function.

(**A**) Schematic of pseudoislet formation. (**B**) Bright-field images showing the morphology of native islets and pseudoislets. Scale bar is 200 μm and also applies to D. (**C**) Relative frequency

plot of islet diameter comparing hand-picked native islets to pseudoislets from the same donor. (**D**) Dithizone (DTZ) uptake of native islets and pseudoislets. (**E**) Insulin and glucagon content normalized to islet volume expressed in islet equivalents (IEQs); 1 IEQ corresponds to an islet with a diameter of 150 μm; n=5 donors; $p > 0.05$. (**F**) Confocal images of native islets and pseudoislets stained for insulin (INS; β cells), glucagon (GCG; α cells), and somatostatin (SOM; δ cells); scale bar is 50 μm. (**G**) Quantification of relative endocrine cell composition of native islets and pseudoislets; n=4 donors; $p > 0.05$. Insulin (**H**) and glucagon (**I**) secretory response to various secretagogues measured by perifusion of native islets and pseudoislets from the same donor (n=5). G 5.6 – 5.6 mM glucose; G 16.7 – 16.7 mM glucose; G 16.7 + IBMX 100 – 16.7 mM glucose with 100 μM isobutylmethylxanthine (IBMX); G1.7 + Epi 1 – 1.7 mM glucose and 1μM epinephrine; KCl 20 – 20 mM potassium chloride (KCl). Wilcoxon matched-pairs signed rank test was used to analyze statistical significance in E and G. Panels H and I were analyzed by 2-way ANOVA; $p > 0.05$. The area under the curve for each secretagogue was compared by one-way ANOVA with Dunn's multiple comparison test (**Figure 31E-31H** and **31J-31M**). Data are represented as mean ± standard error of the mean (SEM). Figure adapted from Walker, Haliyur et al. 2020[560].

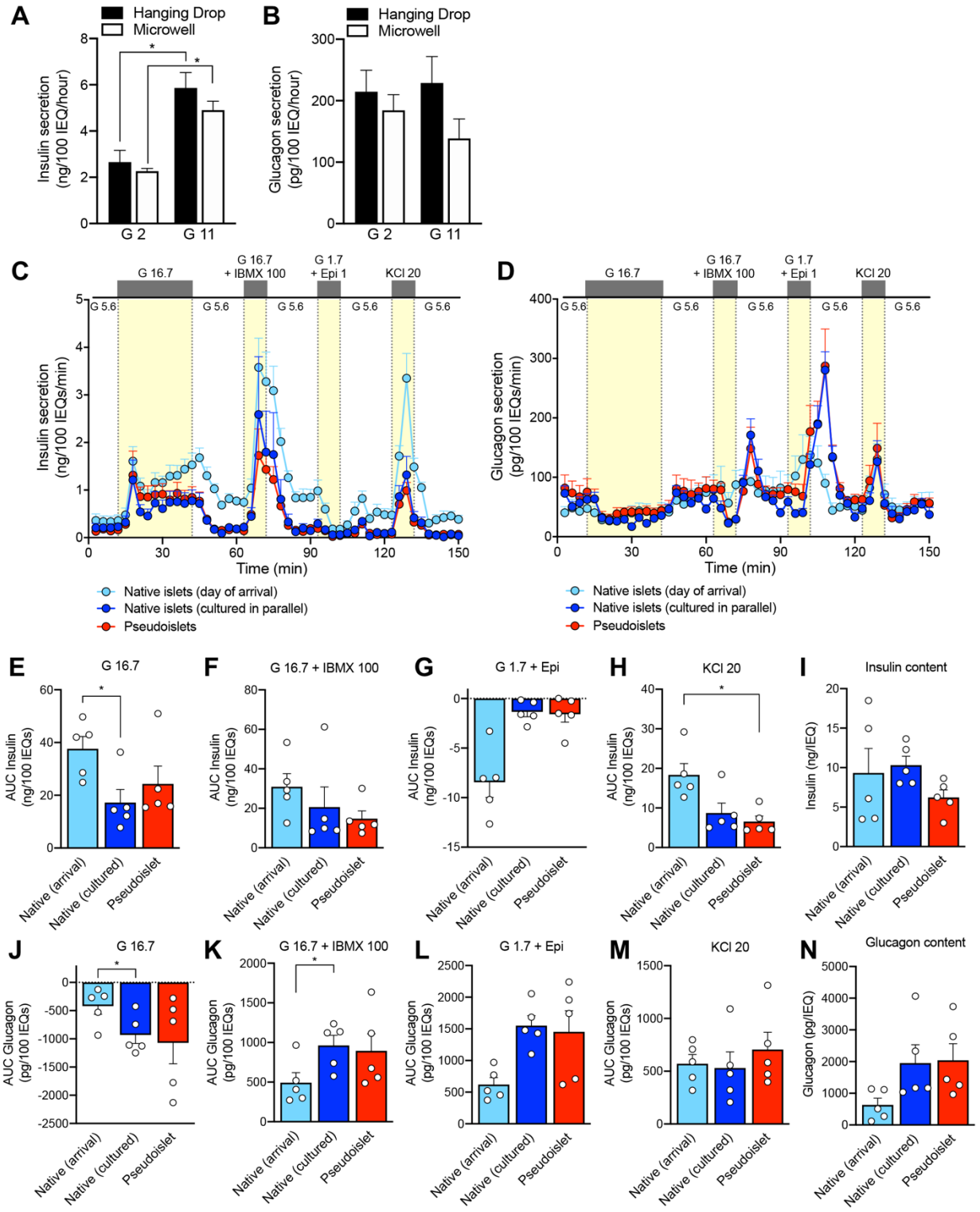

Figure 31. Related to Figure 30. Evaluation of hormone secretory responses in pseudoislet system.

Comparison of insulin (**A**) and glucagon secretion (**B**) by static incubation in pseudoislets made via modified hanging drop system (InSphero) versus ultra-low attachment microwell system

(Perkin Elmer); n=1 donor, 3 replicates, $p > 0.05$. Insulin (**C**) and glucagon secretion (**D**) was measured by macroperifusion in native islets on the day of arrival to Vanderbilt (light blue trace) was compared in the same donor with secretory response of native islets cultured for six days in Vanderbilt pseudoislet media (dark blue trace, also shown in **Figures 30H** and **30I**) and pseudoislets collected at the end of six day reaggregation period (red trace, also shown in **Figures 30H** and **30I**); n=5 donors; G 5.6 – 5.6 mM glucose; G 16.7 – 16.7 mM glucose; G 16.7 + IBMX 100 – 16.7 mM glucose with 100 µM isobutylmethylxanthine (IBMX); G1.7 + Epi 1 – 1.7 mM glucose and 1 µM epinephrine (Epi); KCl 20 – 20 mM of potassium chloride (KCl). (**E-N**) The area under the curve (AUC) of the insulin secretory responses to G 16.7 (**E**), G 16.7 + IBMX 100 (**F**), G 1.7 +Epi 1 (**G**), KCl 20 (**H**) and insulin content (**E**). The AUC of the glucagon secretory responses to G 16.7 (**J**), G 16.7 + IBMX 100 (**K**), G1.7 + Epi 1 (**L**), and KCl 20 (**M**), and glucagon content (**N**). One-way ANOVA with Dunn's multiple comparison test was used to analyze differences in panels E-N; *, $p<0.05$.). Figure adapted from Walker, Haliyur et al. 2020[560].

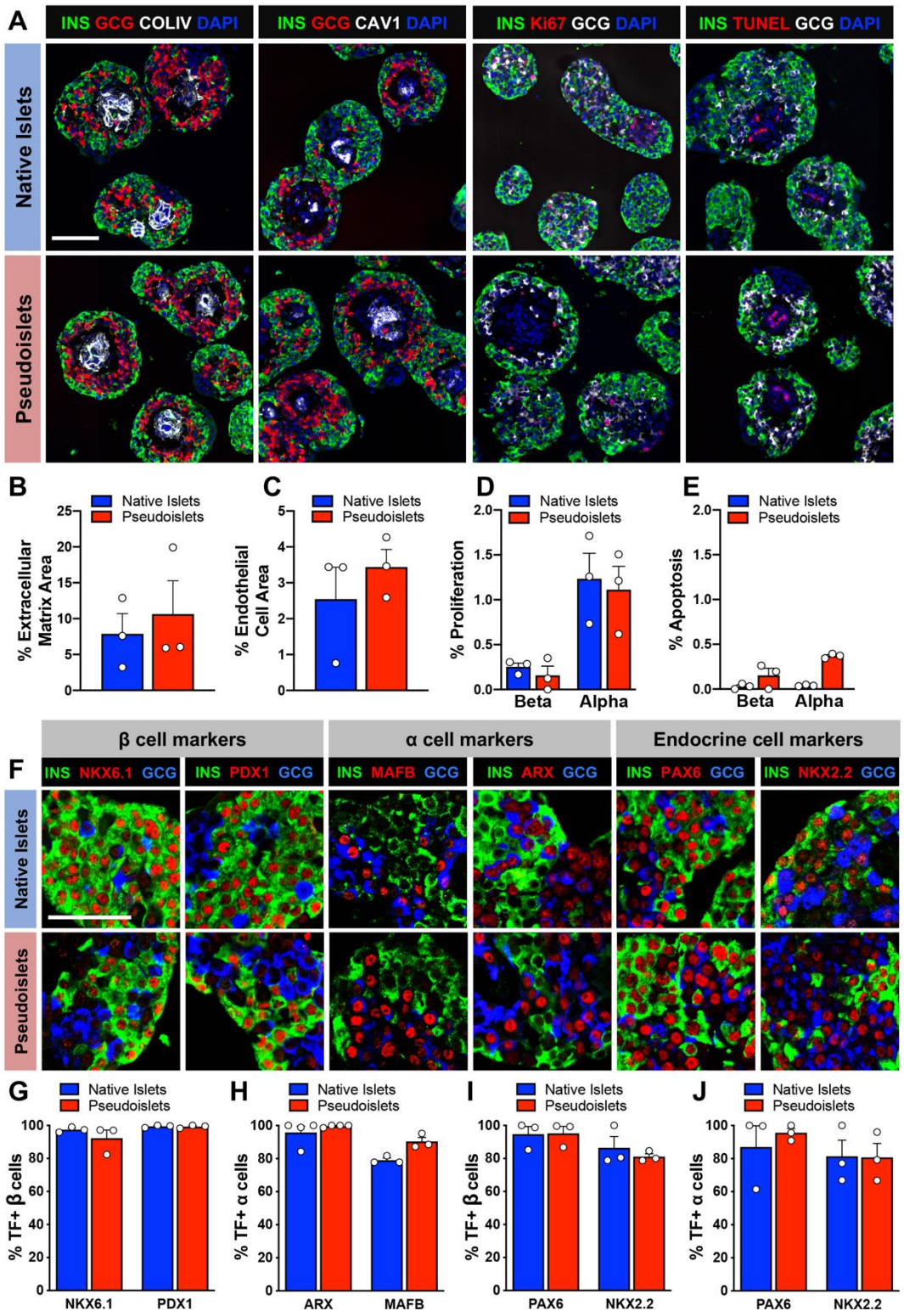

Figure 32. Pseudoislets resemble native human islets in proliferation, apoptosis, architecture, and express markers of α and β cell identity.

(**A**) Immunofluorescence visualization of labeling for insulin (INS; β cells) and (GCG; α cells) in combination with detection of proliferation (Ki67), apoptosis (TUNEL), extracellular matrix

(collagen IV, COLIV) and endothelial cells (caveolin-1, CAV1). Scale bar is 100 μm. (**B**) Quantification of β and α cell proliferation in native islets and pseudoislets; expressed as % INS+ or GCG+ cells expressing Ki67; n=3 donors; $p > 0.05$. (**C**) Quantification of β and α cell apoptosis by TUNEL assay; n=3 donors; $p > 0.05$. (**D**) Quantification of COLIV-expressing extracellular matrix; expressed as % COLIV+ area to INS+ and GCG+ cell area; n=3 donors; $p > 0.05$. (**E**) Quantification of endothelial cell area; expressed as % CAV1+ cell area to INS+ and GCG+ cell area; n=3 donors; $p > 0.05$. (**F**) Expression of transcription factors (TF) important for β cell identity (NKX6.1 and PDX1), α cell identity (MAFB and ARX), and pan endocrine cell identity (PAX6 and NKX2.2). Scale bar is 50 μm. (**G**) Quantification β cell identity markers in β cells of native islets and pseudoislets (n=3 donors/marker; $p > 0.05$). (**H**) Quantification of α cell identity markers in α cells of native islets and pseudoislets (n=3-4 donors/marker; $p > 0.05$). (**I-J**) Quantification of pan endocrine markers in β (**I**) and α (**J**) cells of native islets and pseudoislets (n=3 donors/marker; $p > 0.05$). Wilcoxon matched-pairs signed rank test was used to analyze statistical significance in panels B-E and G-J. Data are represented as mean ± SEM.). Figure adapted from Walker, Haliyur et al. 2020[560].

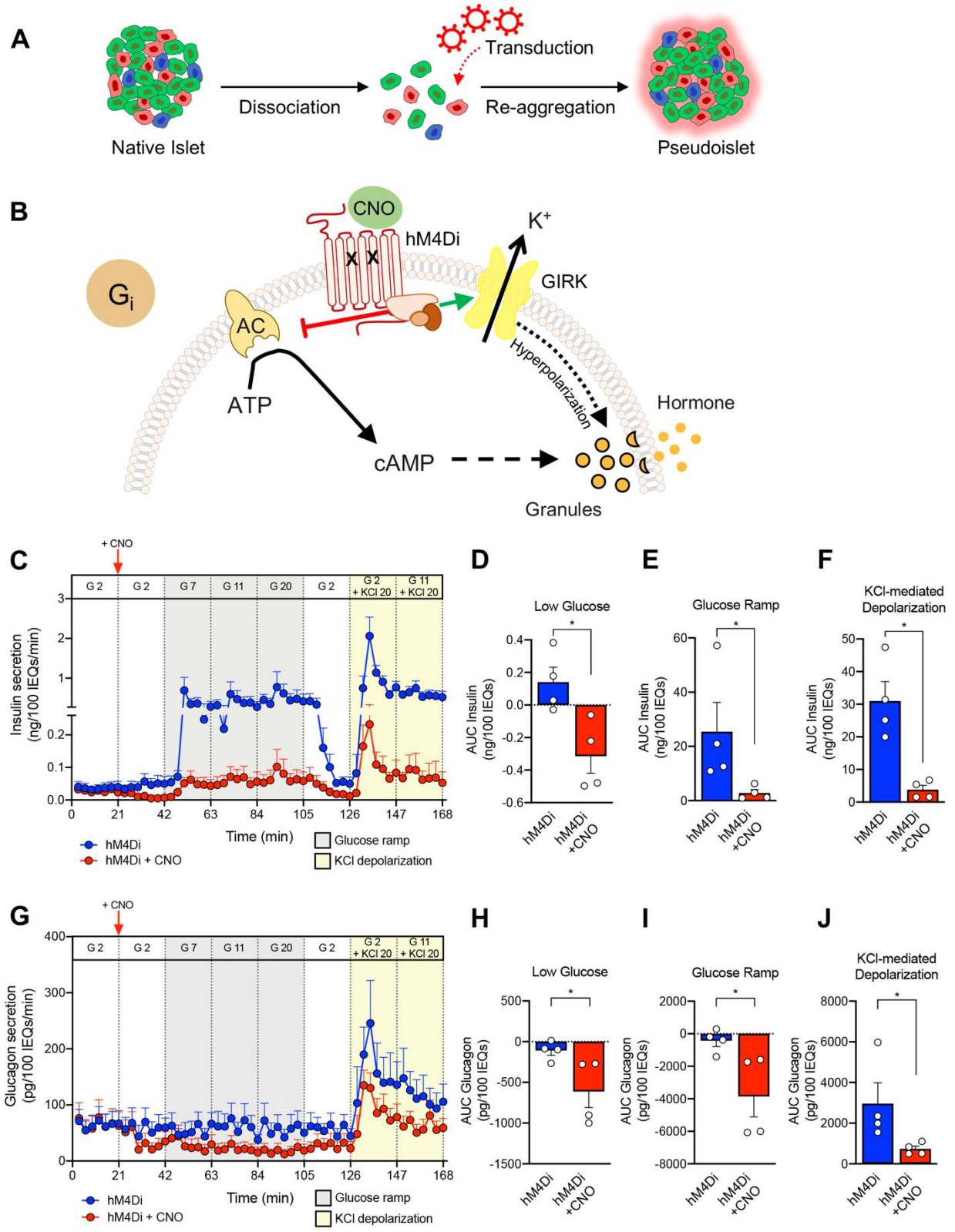

Figure 33. G_i activation reduces insulin and glucagon secretion.

(A) Schematic of incorporation of efficient viral transduction into pseudoislet approach. (**B**) Schematic of the G_i-coupled GPCR signaling pathway. CNO – clozapine-N-oxide, AC – adenylyl

cyclase, ATP – adenosine triphosphate, cAMP – cyclic adenosine monophosphate, GIRK – G protein-coupled inwardly-rectifying potassium channel, K^+ – potassium ion. (**C**) Dynamic insulin secretion assessed by macroperifusion in response to low glucose (G 2 – 2 mM glucose; white), glucose ramp (G 7 – 7 mM, G 11 – 11 mM, and G 20 – 20 mM glucose; grey) and KCl-mediated depolarization (KCl 20 – 20 mM potassium chloride in the presence of G 2 or G 11; yellow) in the absence (blue trace) or presence of CNO (red trace); n=4 donors/each. 10 µM CNO was added after the first period of 2 mM glucose as indicated by a vertical red arrow and then continuously administered for the duration of the experiment (red trace). Note the split of y-axis to visualize differences between traces at G 2 ± CNO. (**D-F**) Insulin secretion was integrated by calculating the area under the curve (AUC) for response to the low glucose (white), glucose ramp (gray), and KCl-mediated depolarization (yellow). Baseline was set to the average value of each trace from 0 to 21 minutes (before CNO addition). (**G-J**) Glucagon secretion was analyzed in parallel with insulin as described above. Insulin and glucagon secretory traces in panels C and G, respectively, were compared in the absence vs. presence of CNO by two-way ANOVA; ****, $p < 0.0001$ for both insulin and glucagon secretion. Area under the curve of insulin (**D-F**) and glucagon responses (**H-J**) to low glucose, glucose ramp, and KCl-mediated depolarization were compared in the absence vs. presence of CNO by Mann-Whitney test; *, $p < 0.05$. Data are represented as mean ± SEM.). Figure adapted from Walker, Haliyur et al. 2020[560].

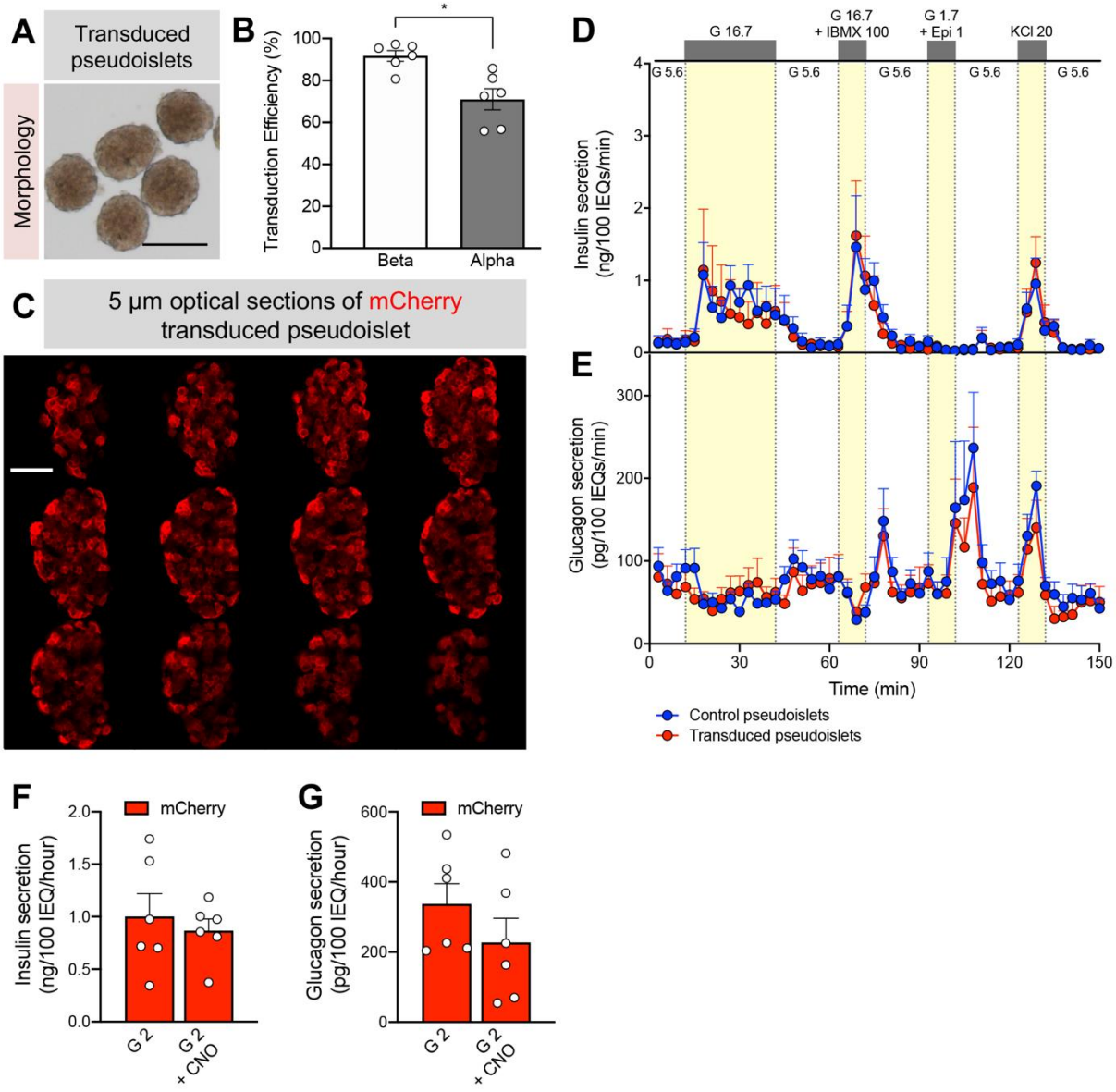

Figure 34. Related to Figure 33. Pseudoislet system allows for highly efficient transduction of human islet cells.

(**A**) Bright-field image of transduced pseudoislets. Scale bar is 200 µm. (**B**) Transduction efficiency of β and α cells in this system; *, $p < 0.05$. (**C**) Confocal image of mCherry-transduced pseudoislet showing optical sections taken every 5-µm to highlight transduced cells throughout the entire pseudoislet. Scale bar is 100 µm. Insulin (**D**) and glucagon (**E**) secretion in response to a series of β and α cell secretagogues measured by macroperifusion in control pseudoislets and pseudoislets transduced with m-Cherry virus from the same donor (n=3 donors). Insulin (**F**) and glucagon secretion (**G**) in mCherry-expressing pseudoislets measured in 2 mM glucose (G 2) with and without CNO (n=2 donors; n=3 replicates/donor; $p > 0.05$). Panels D and E were analyzed by 2-way ANOVA; $p > 0.05$. Panels F and G were compared by Mann-Whitney test.). Figure adapted from Walker, Haliyur et al. 2020[560].

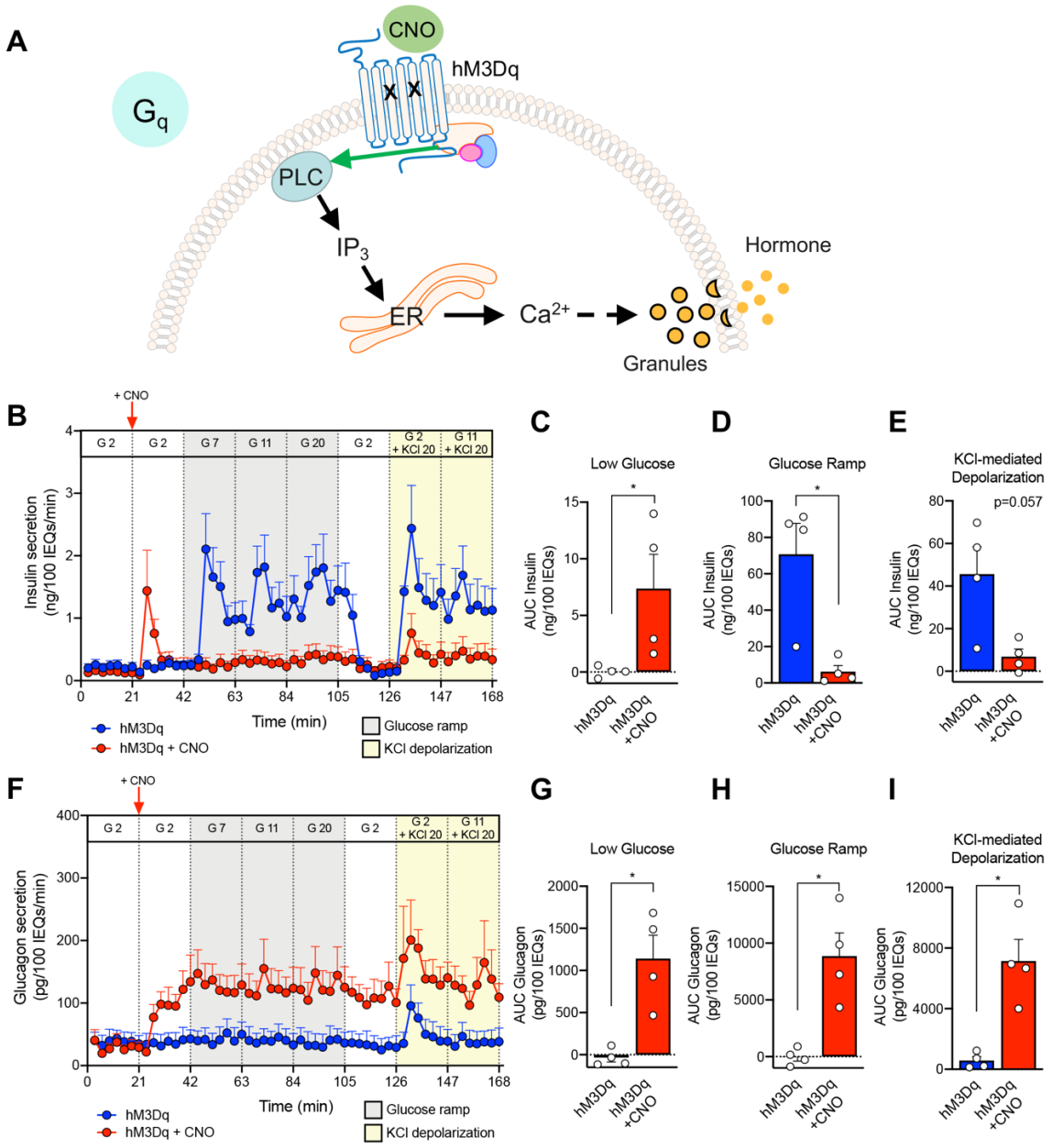

Figure 35. G_q activation stimulates glucagon secretion but has stimulatory and inhibitory effects on insulin secretion.

(**A**) Schematic of the G_q-coupled GPCR signaling pathway. CNO – clozapine-N-oxide, PLC – phospholipase C, IP_3 – inositol triphosphate, ER – endoplasmic reticulum, Ca^{2+} – calcium ion. (**B-E**) Dynamic insulin secretion was assessed by macroperifusion and analyzed as described in detail in Figure 33; n=4 donors/each. (**F-I**) Glucagon secretion was analyzed in parallel with insulin as described in Figure 33. Insulin and glucagon secretory traces in panels B and F, respectively were compared in the absence vs. presence of CNO by two-way ANOVA; ****, $p < 0.0001$ for both insulin and glucagon secretion. Area under the curve of insulin (**C-E**) and glucagon responses (**G-I**) to each stimulus were compared in the absence vs. presence of CNO by Mann-Whitney test; *, $p < 0.05$. Data are represented as mean ± SEM.). Figure adapted from Walker, Haliyur et al. 2020[560].

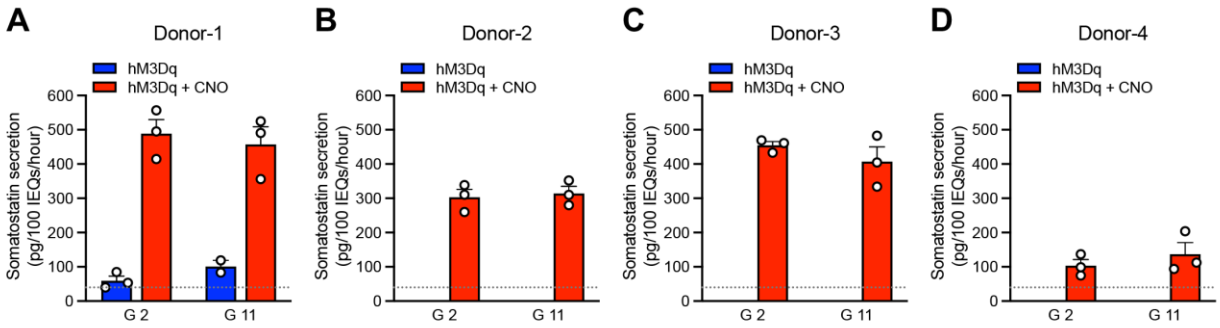

Figure 36. Related to Figure 35. Somatostatin secretion from hM3Dq-expressing pseudoislets by static incubation.

(**A-D**) Somatostatin secretion in static incubation experiments at low (G 2; 2 mM glucose) and high (G 11; 11 mM glucose) with and without activation of G_q signaling (±10 μM CNO) across 4 independent donors (3 biological replicates/condition/donor other than Donor-1, G 11 which has only 2 replicates). Gray dotted line represents the limit of the assay sensitivity; somatostatin secretion in G 2 and G 11 for Donors 2-4 were below the limit of detection.). Figure adapted from Walker, Haliyur et al. 2020[560].

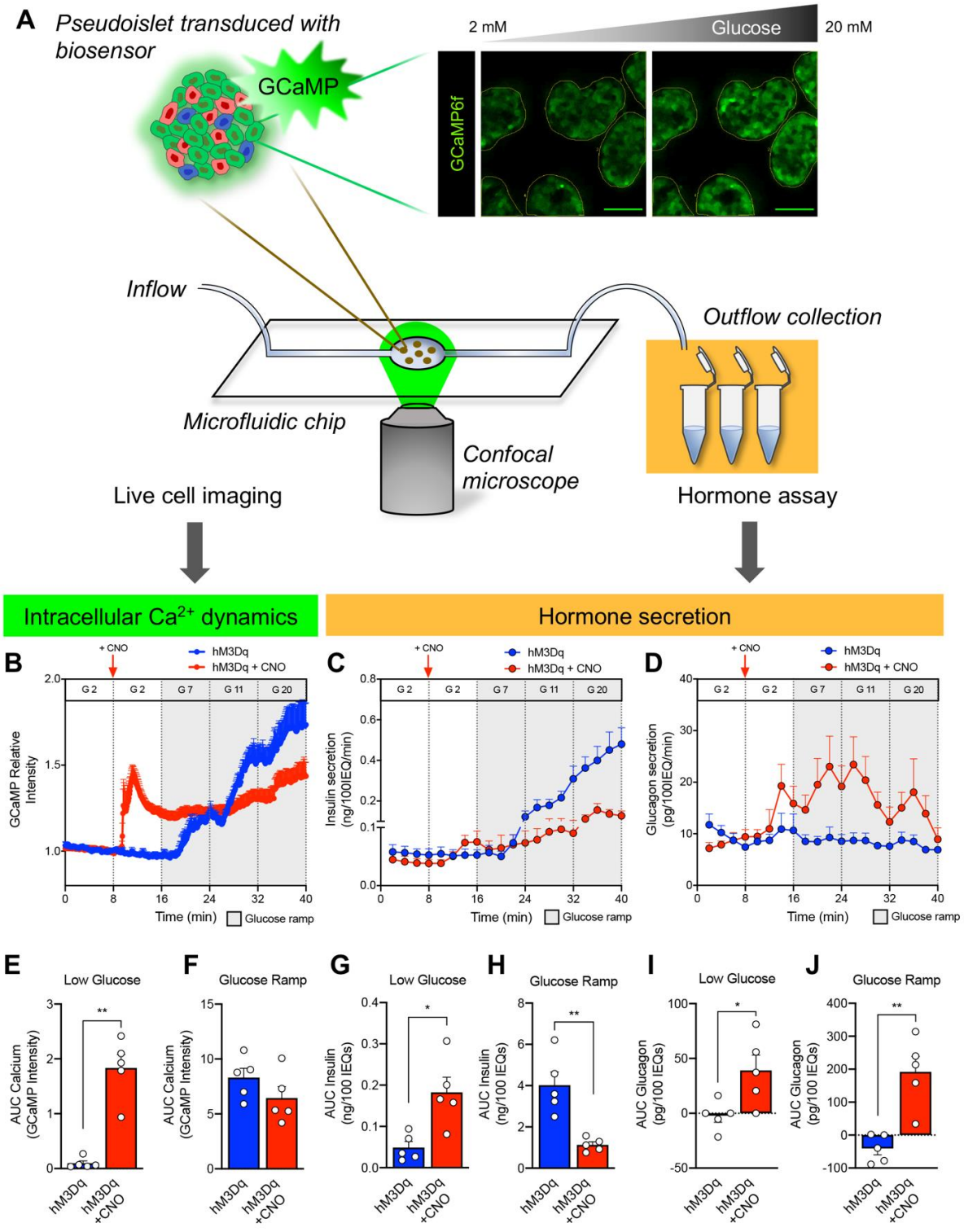

Figure 37. Pseudoislet system integrated with microfluidic device allows for co-registration of hormone secretion and intracellular signaling dynamics.

(**A**) Schematic of pseudoislet system integration with a microfluidic device to allow for synchronous detection of intracellular signaling dynamics by the genetically encoded GCaMP6f

biosensor and confocal microscopy, and collection of microperifusion efflux for hormone analysis. Dynamic changes in GCaMP6f relative intensity (**B**), insulin secretion (**C**), and glucagon secretion (**D**) assessed during microperifusion in response to a low glucose (G 2 – 2 mM glucose; white), glucose ramp (G 7 – 7 mM, G 11 – 11 mM, and G 20 – 20 mM glucose; grey) and in the absence (blue trace) or presence of CNO (red trace); n=3 donors/each. 10 µM CNO was added after the first period of 2 mM glucose as indicated by a vertical red arrow and then continuously administered for the duration of the experiment (red trace). See Supplemental Videos 1 and 2 for representative visualization of each experiment. Calcium signal (**E, F**) and insulin (**G, H**) and glucagon (**I, J**) secretion was integrated by calculating the area under the curve (AUC) for response to the low glucose (white) and glucose ramp (gray). Baseline was set to the average value of each trace from 0 to 8 minutes (before CNO addition). Calcium and hormone traces in panels B-D were compared in the absence vs. presence of CNO by two-way ANOVA; * $p < 0.05$ for calcium trace, **** $p < 0.0001$ for both insulin and glucagon secretion. Area under the curve of calcium (**E, F**), insulin (**G, H**) and glucagon responses (**I, J**) to low glucose and glucose ramp were compared in the absence vs. presence of CNO by Mann-Whitney test; *, $p < 0.05$, **, $p < 0.01$. Data are represented as mean ± SEM.). Figure adapted from Walker, Haliyur et al. 2020[560].

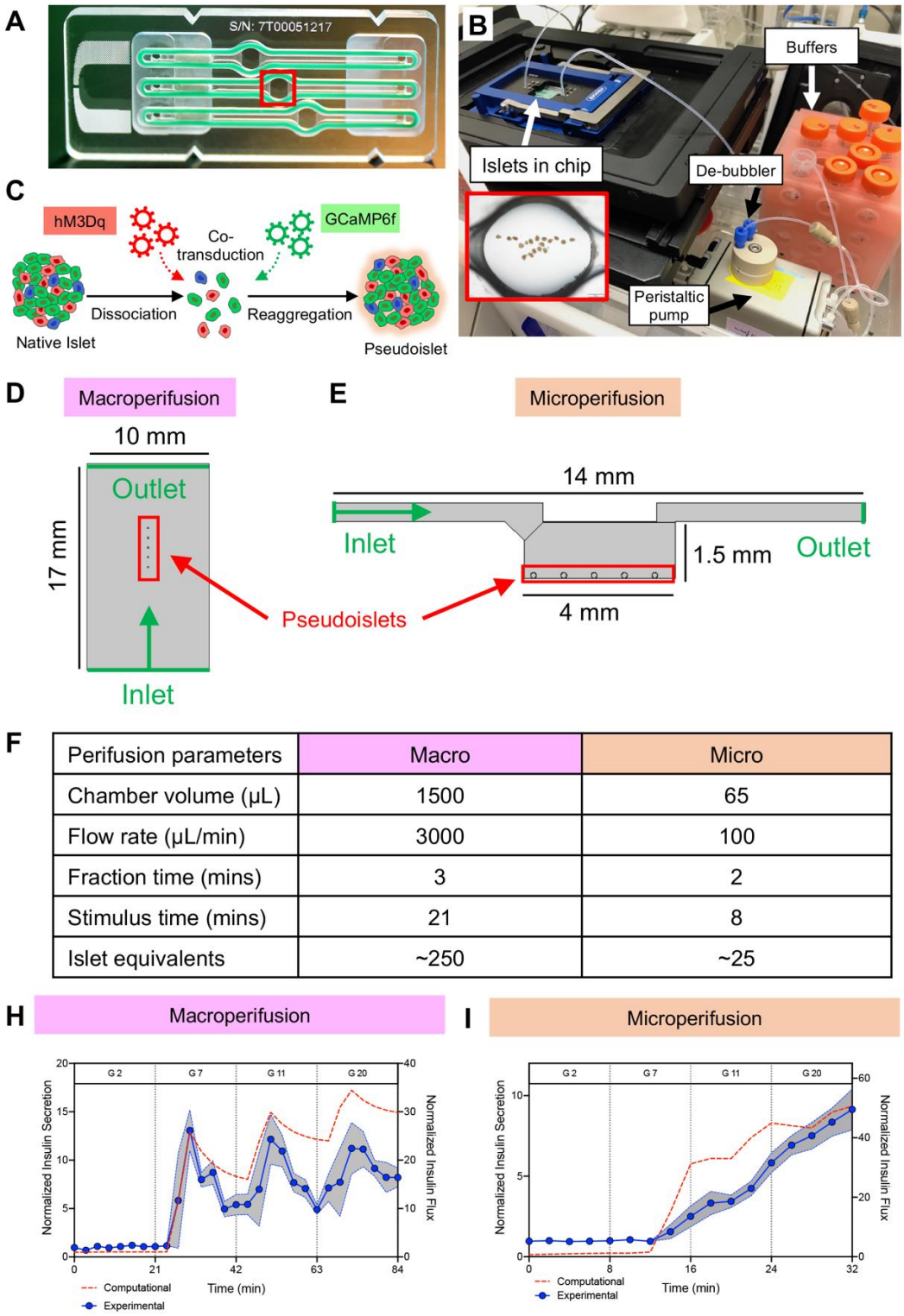

Perifusion parameters	Macro	Micro
Chamber volume (µL)	1500	65
Flow rate (µL/min)	3000	100
Fraction time (mins)	3	2
Stimulus time (mins)	21	8
Islet equivalents	~250	~25

Figure 38. Related to Figure 37. Microperifusion system assembly and fluid dynamic modeling of macro- and microperifusion.

(**A**) Picture of microfluidic device showing where islets are loaded and imaged (red box). There are three potential chambers to load islets, but in the current experimental layout, islets are

loaded only into one chamber. (**B**) Experimental set-up of the microfluidic device on the confocal microscope stage within incubator including peristaltic pump, de-bubbler, and perifusion buffers. (**C**) Schematic of experimental workflow with incorporation of genetically encoded biosensor into hM3Dq-expressing pseudoislets. Schematic of the macroperifusion (**D**) and microperifusion chamber (**E**) showing the path of fluid flow. (**F**) Key experimental parameters of macroperifusion and microperifusion system. (**H** and **I**) Comparison of normalized insulin secretion acquired experimentally versus predicted by modeling in macroperifusion (**H**) and microperifusion (**I**). Experimental insulin data was normalized to average value in 2 mM glucose. The gray region demonstrates the SEM comparing experimental insulin secretion data and insulin flux from COMSOL computational modeling in the macroperifusion system (**H**) and microperifusion system (**I**); G 2 – 2 mM, G 7 – 7 mM, G 1 – 11 mM, G 20 – 20 mM glucose. Figure adapted from Walker, Haliyur et al. 2020[560].

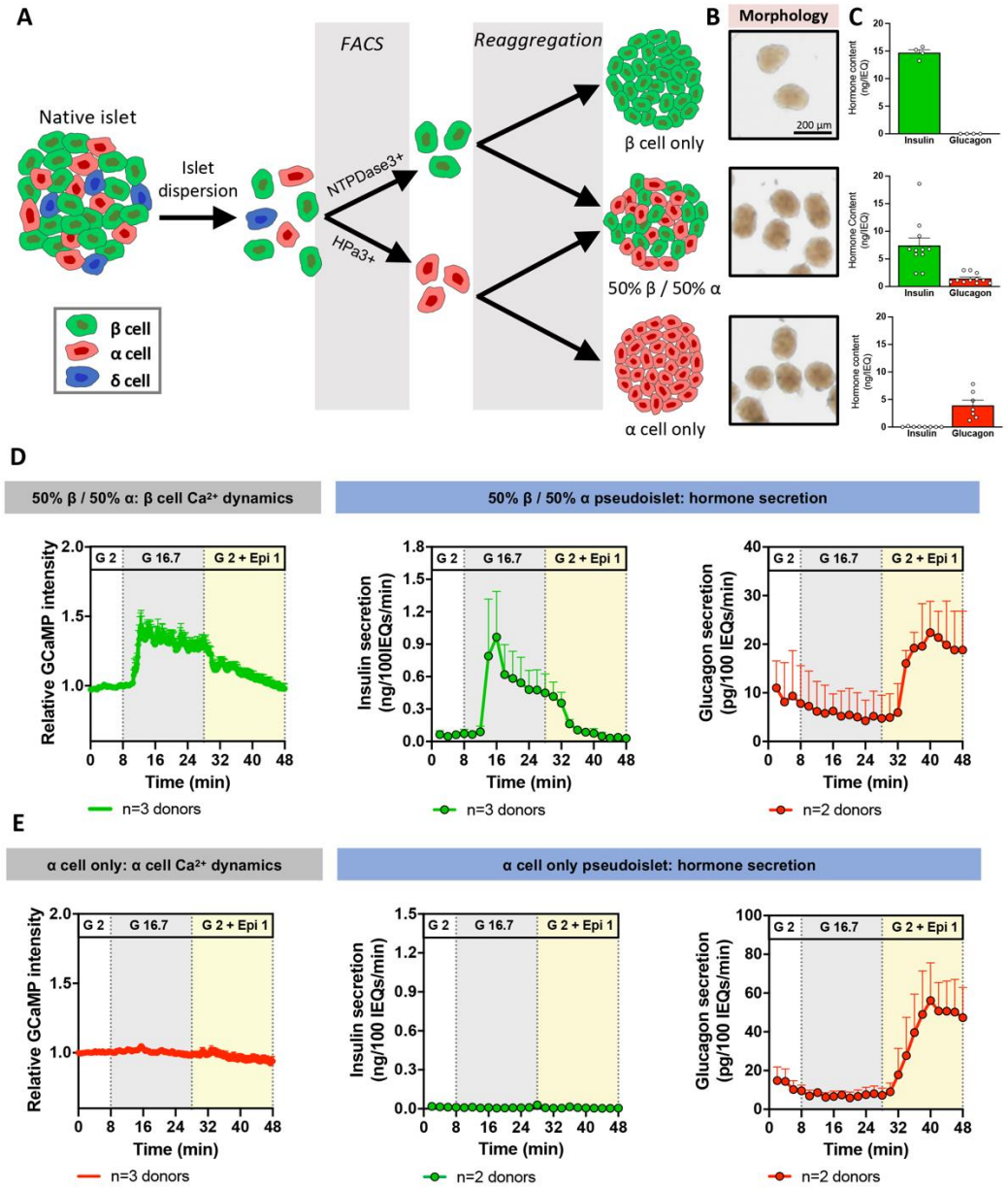

Figure 39. Cellular manipulation of pseudoislets allows tracking of intracellular signals from specific cells.

(**A**) Schematic of incorporation of recombination of FACS-purified β and α cells into pseudoislets with varied cell composition. (**B**) Bright-field images showing the morphology of native islets and pseudoislets. Scale bar is 200 µm and applies to all three images. (**C**) Insulin and glucagon content normalized to islet volume expressed in islet equivalents. For representation, values that were below the limit of detection of the insulin or glucagon assay are shown as 0. Dynamic changes in GCaMP6f relative intensity, insulin secretion, and glucagon secretion from 50% α / 50% β cell pseudoislets with β cells labeled with GCaMP6f (**D**) or α cell only pseudoislets (**E**) assessed during microperifusion in response to high glucose (G 16.7; gray) and low glucose (G 2) and epinephrine (yellow). Green traces indicate being reflective of β cells while red trace is reflective of α cells. Data are represented as mean ± SEM.

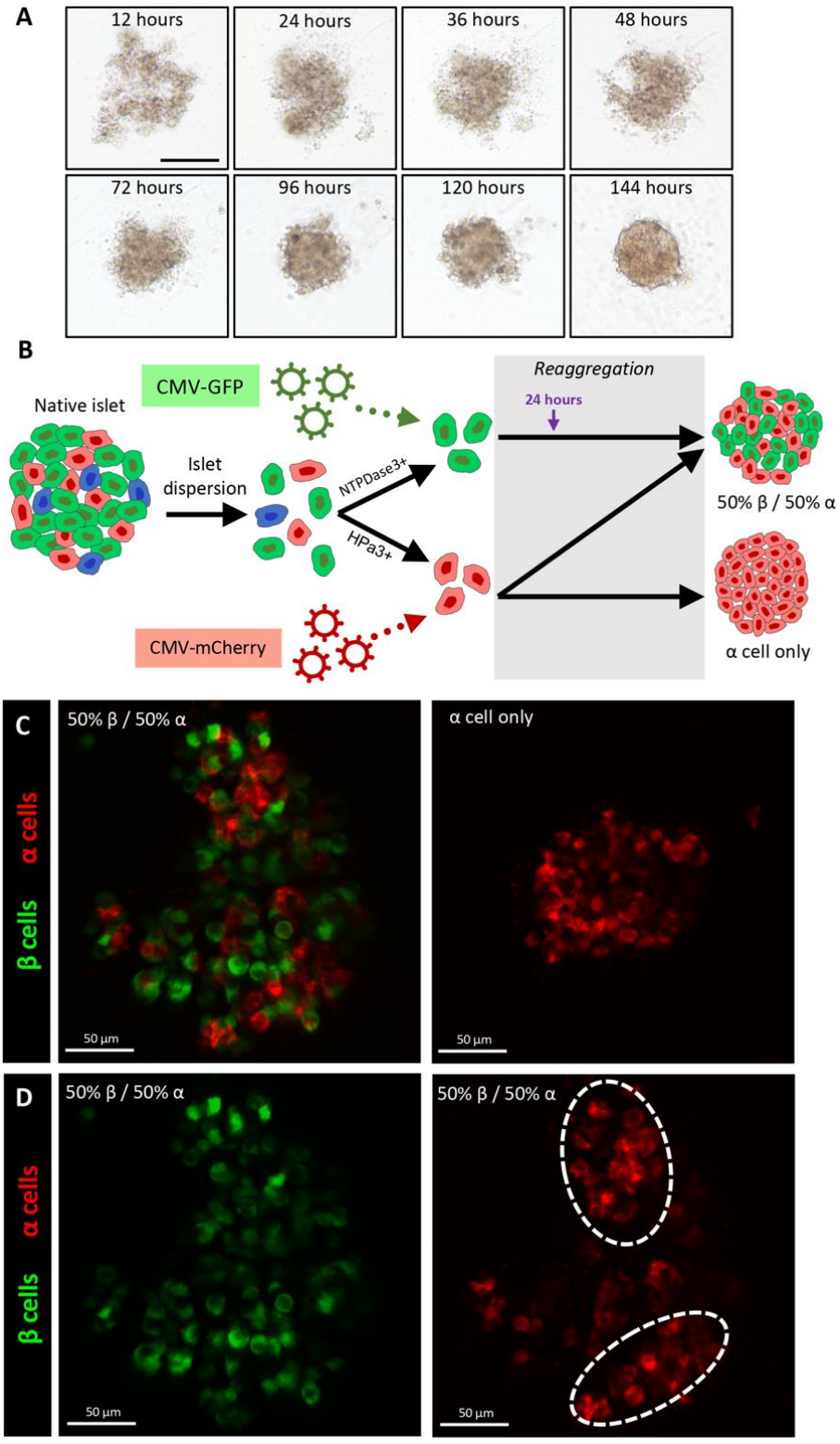

Figure 40. Real-time monitoring of pseudoislet formation reveals α cell role in pseudoislet aggregation.

(**A**) Bright-field images of pseudoislets forming at defined time intervals. Scale bar is 150 µm and applies to all images in the panel. (**B**) Schematic of sorted cell pseudoislets with α cells

labeled by mCherry and β cells labeled by GFP with subsequent imaging by confocal microscopy. (**C**) Maximum intensity projection of 50% β / 50% α cell pseudoislet and α cell only pseudoislet 24 hours after plating. Green is GFP from β cells and red is mCherry from α cells. (**D**) Individual channels of 50% β / 50% α cell pseudoislet image shown in C. Scale bar in images in C and D is 50 μm. See Supplemental Video 3 for time lapse of 50% β / 50% α cell pseudoislet formation.

CHAPTER V:
INTEGRATED ANALYSIS OF THE DIABETIC HUMAN PANCREAS

Some text and data in this chapter have been adapted from Haliyur, Walker, et al. (manuscript in preparation), and Walker, Saunders, Rai et al. (manuscript in preparation).

Chapter Introduction

The central role of the pancreatic islet in the pathogenesis of diabetes and differences between rodent and human islet biology highlight the need to robustly study the human pancreas. However, access to these organs, especially the pancreas from individuals with diabetes, is limited. Further, disease heterogeneity along with high genetic and environmental diversity highlight the complexity in interpreting findings from human donors. To address this, our group developed infrastructure to collect pancreatic tissue and islets from the same donor that can be processed and studied using numerous experimental approaches, along with the donor's de-identified medical record in order to place findings in the appropriate clinical context. This chapter describes two ways in which we have used this approach to further our understanding of human diabetes. First, we describe an integrative approach to robustly study the function, transcriptome and tissue architecture from isolated islets and pancreas from 20 donors with short-duration T2D to reveal early, disease-driving mechanisms in T2D. Second, we investigate an atypical pathobiological finding of substantial insulin secretion in a donor with presumed T1D and describe how we integrated studies of islets, tissue, and genetics to understand the etiology of their diabetes. These studies demonstrate both how integrated studies of small cohorts can reveal broad disease-driving mechanisms and how detailed studies of unique cases can reveal underappreciated disease heterogeneity. Ultimately, both types of approaches will be important in our quest to understand and better treat human diabetes.

Human β cell dysfunction in short-duration type 2 diabetes is defined by a disrupted islet microenvironment and RFX6-mediated transcriptional dysregulation

Introduction

Type 2 diabetes (T2D) mellitus is a common metabolic disease defined by abnormally elevated blood glucose levels, affecting more than 460 million individuals worldwide[686] and characterized by insufficient insulin secretion, insulin resistance, and increased hepatic glucose production[687]. Clinically, T2D is progressive with patients often initially able to control blood glucose levels with changes to diet and exercise but eventually moving to oral medications and ultimately requiring exogenous insulin[323,688,689]. Genetic and physiologic complexity result in T2D being clinically heterogeneous with likely multiple molecular pathways and time courses to reach hyperglycemia[690]; however, the majority of loci that have been identified through genome-wide association studies (GWAS) are presumed to result in perturbations to β cells, pointing to impaired insulin secretion as a key determinant for whether T2D develops and how quickly it progresses[691–693].

Pancreatic islets, vascularized and innervated mini-organs dispersed throughout the exocrine pancreas, are central in the control of glucose homeostasis. Islets are composed primarily of endocrine cells – α cells, which secrete glucagon; β cells, which secrete insulin; δ cells, which secrete somatostatin; pancreatic polypeptide (PP) or γ cells, which secrete PP; and ε cells, which secrete ghrelin – but also contain capillaries (endothelial cells and pericytes), neuronal projections, resident immune cells, and fibroblasts[1]. These cells act in coordination to exert hormonal control on glucose metabolism largely through insulin, which lowers blood glucose, and glucagon, which raises blood glucose. While impaired insulin secretion is a hallmark of diabetes, the contributions of systemic environment, local signals in the islet microenvironment, and intrinsic β cell genomic changes, as well as how these interact, are not precisely defined.

Postulated disease processes in T2D islets include β cell loss and/or dedifferentiation, endoplasmic reticulum (ER) stress, amyloid deposition, oxidative stress, glucotoxicity, lipotoxicity, and islet inflammation[342–347,623], processes that have been primarily studied in rodent models of T2D due to difficulty in obtaining and studying human pancreatic tissue[21,694]. Importantly, human islets show several key differences from mouse islets, including in endocrine and non-endocrine cell composition and arrangement, basal and stimulated insulin secretion, response to dyslipidemia and hyperglycemia, and expression of key islet-enriched transcription factors[21–25,569,695]. Thus, to precisely target and treat type 2 diabetes, it is critical to define the initiating conditions and triggers for impaired insulin secretion in human tissue.

We describe an integrative approach to robustly study the pancreas and isolated islets from 20 short-duration T2D donors. Our approach analyzed islet function both in *in vitro* and *in vivo* using a transplant system, the islet transcriptome by bulk RNA-sequencing (RNA-seq) from whole islets and from fluorescence-activated cell sorting (FACS)-purified β cells and α cells, and pancreatic tissue via traditional and multiplexed imaging approaches for a deep understanding of the T2D islet microenvironment. Integration of findings across these studies reveals that β cell dysfunction in short-duration T2D is defined by a disrupted islet microenvironment as well as RFX6-mediated transcriptional dysregulation, providing key insight into the pathogenesis of T2D.

Results

Identification, collection and processing of short-duration T2D donor pancreata

As T2D is a highly heterogeneous and progressive disease, an unfocused approach to study islets from individuals with T2D is likely to miss important biology. Further, with long-standing disease it becomes more difficult to decipher processes that are consequences of prolonged hyperglycemia versus those that are causative. Therefore, to identify early, disease-driving mechanisms in islets, we focused on short-duration T2D as determined by a combination of disease duration and treatment paradigm (**Figure 41A**). Organ donors were screened by a board-certified endocrinologist (A.C.P.) to identify donors that not only fit the short-duration criteria but were also 1) without significant co-morbidities that would confound data interpretation and 2) representative of “common” T2D in the general population in terms of age and BMI, to allow findings to be generalizable. Using this approach we collected 20 T2D pancreata from donors aged 37-66 years (mean 52 years) with an average T2D duration of 3.5

years (range 0-10 years) where 25% were managing with lifestyle changes only and 75% had begun some form of diabetes medical treatment; donors were of diverse ethnic background and as expected, BMI and HbA1C were elevated (**Figure 41A** for summary; **Table 3** for detailed information by donor). To comprehensively understand disease mechanisms, we both isolated islets and processed tissue blocks from each pancreas whenever possible, allowing integration of islet function through hormone secretion, cellular and molecular characterization of tissue architecture and microenvironment, and cell type-specific transcriptomic analysis in the same donors (**Figure 41B**). Non-diabetic donors (n=17) were also collected and processed for multi-modality study. Partnerships with the Integrated Islet Distribution Program (IIDP) and the Alberta Diabetes IsletCore provided additional non-diabetic isolated islets (n=20) that allowed better matching of donor characteristics such as age and BMI for specific comparisons and additional power in our analyses.

Despite similar insulin content, short-duration T2D islets show substantially reduced stimulated insulin secretion

To investigate β cell function in this cohort, we analyzed isolated islets from age- and BMI-matched T2D and ND donors (**Figure 42A-42B**) by dynamic perifusion system[570,594] using the standard perifusion approach of the Human Islet Phenotyping Program of the IIDP (https://iidp.coh.org/), which has assessed over 400 human islet preparations[696,697]. When normalized by islet volume, basal insulin secretion in T2D islets was slightly reduced (**Figures 1C** and **42C**) while stimulated insulin secretion was markedly reduced in response to high glucose, cAMP-evoked potentiation, and KCl-mediated depolarization (**Figures 41C-41F**). Both first and second phase of insulin secretion were affected but first phase showed a more substantial reduction (**Figures 42D-42E**). Inhibition of insulin secretion by low glucose and epinephrine was similar between ND and T2D islets (**Figures 42F**). Importantly, insulin content was not reduced in T2D islets and even trended higher than ND islets (**Figures 41G**). As such, normalization of secretion by islet insulin content showed concordant findings (**Figure 42G-42L**). Together, these data suggest that while short-duration T2D islets maintain their insulin production, β cells have defects at multiple steps of insulin secretory pathway, including those distal to glucose metabolism.

Our perifusion system additionally allows measurement of glucagon to investigate α cell function. In contrast to insulin secretion, no substantial differences in basal or stimulated glucagon secretion were observed in T2D islets when normalized by islet volume, though we did note a slightly slower return to baseline in the T2D trace after removal of stimulation (**Figures 41H-41K** and **42M-42N**). Glucagon content was similar between ND and T2D and as such, normalization by glucagon content showed consistent secretion dynamics (**Figures 41L** and **42O-42T**). While there is substantial evidence of dysregulated glucagon secretion in T2D, this data suggests such dysfunction is not a hallmark of *ex vivo* islets in the early stages of T2D.

Correlation of donor attributes to functional metrics highlighted a significant negative correlation between donor HbA1C and stimulated insulin secretion (**Figure 41M**), demonstrating a link between reduced β cell function ex vivo and degree of glucose control in the pateint. To test how the systemic environment contributes to β cell dysfunction in T2D islets, we transplanted

T2D or ND islets from a subset of donors into immunodeficient NSG mice (**Figure 41N**). After six weeks in a normoglycemic, non-insulin resistant *in vivo* environment, T2D islets secreted less human insulin than ND islets, especially after stimulation with glucose/arginine (**Figures 41O-41Q**, average per islet preparation; **42U-42W**, individual mice), consistent with *ex vivo* findings of impaired stimulated insulin secretion. In sum, these experiments highlight β cell dysfunction as a hallmark of early T2D that is sustained after transplantation into a normoglycemic, non-insulin resistant environment and suggests intrinsic β cell dysregulation and/or cellular and molecular alterations within the islet microenvironment are key features driving reduced insulin secretion.

Integrated transcriptome analysis of islets and FACS-purified α and β cells reveals broad transcriptional dysregulation

To investigate islet-autonomous changes in T2D, we undertook coordinated collection of β and α cells purified by FACS using well-characterized cell surface antibodies[220,565] as well as hand-picked isolated islets for RNA-sequencing (**Figures 43A** and **44A**). This approach allowed us to assess both the β and α cell-specific transcriptional landscape as well as global islet dysregulation in the short-duration T2D cohort. As this large collection of rare tissues spanned several years, we used a robust latent variable analysis[581] to isolate biological variation and then analyzed the dataset by both differential gene expression[580] and gene network analyses[586] (discussed beginning with Figure 50) (**Figures 43A**).

Comparing transcriptomic profiles from ND and T2D β cells revealed 352 differently expressed genes based on a strict false discovery rate (FDR) 1% threshold and >1.5 fold-change cutoff (**Figure 43B-43C**). Of note, genes such as *G6PC2*, which is involved in regulating glucose flux and is a major target of autoimmunity in T1D and *GLP1R*, the receptor for glucagon-like peptide 1 (GLP-1) and a key pharmacological focus for treating T2D, were expressed at lower levels in T2D β cells. In contrast, genes such as *FAIM2*, an inhibitor of apoptosis, *SLC38A5*, a sodium-dependent neutral amino acid transporter, and *TSPAN5*, a member of the tetraspanin family that modulates Ca^{2+} handling, were expressed at higher levels.

In α cells, 248 genes were significantly differentially expressed, including elevated expression of *PCSK1*, a prohormone processing enzyme that is typically not highly expressed in α cells but may be upregulated in states of stress and lead to alternative processing of preproglucagon[104,698] (**Figures 43D** and **44B**). Interestingly, T2D α cells showed reduced expression of *KLF11*, the MODY7 gene. While clearly critical for β cell function, KLF11's role in α cells is less understood. Still, the KLF11 protein has been detected in α cells[699] and single-cell RNA-seq datasets demonstrate higher *KLF11* expression in α cells compared to β cells (data not shown), indicating that there may be an unexplored role in α cells. Notably, KLF11 gene targets include a number of genes involved in lipid/cholesterol metabolism[700,701] and *LDLR* also has reduced expression in T2D α cells (**Figure 43D**).

In islets, 564 genes were significantly differentially expressed; this higher number than for sorted β or α cells may reflect greater cell type heterogeneity within the sample, emphasizing the valuable specificity of our sorted cell approach in parallel with appreciation of non-α or β cell

components in islet samples (**Figure 43E** and **44C**). Notably, *SSTR5*, the principal δ cell somatostatin receptor[702], was elevated in T2D islets and likely reflects changes in δ cell biology. Reduction in *ADAMTS4*, a matrix metalloproteinase, and elevation in *PCOLCE2*, a collagen endopeptidase, highlight dynamic modulation of the extracellular matrix within the islet microenvironment in short-duration T2D. Reduced expression of *CXCL8*, a chemokine that stimulates angiogenesis through vascular endothelial growth factor (VEGF)[703], further suggests altered signaling to non-endocrine cells within the islet.

To understand the biological context with which these genes are associated, we performed pathway analyses on differentially expressed genes and broadly visualized these pathways using REVIGO, a clustering algorithm that uses semantic similarity to collapse and group similar gene ontology (GO) terms[583]. T2D β cells were enriched for numerous metabolic pathways including glucose, amino acid, and fatty acid processes, as well as mitochondrial regulation, but also showed regulation of insulin secretion-related pathways including exocytosis, ion transport and protein secretion (**Figure 43F**). In aggregate, α cells did not show enrichment for as many pathways but did display terms related to amino acid and steroid signaling (**Figure 43G**). Additional pathways of interest in the α cell included those relating to ion handling as well as regulation of blood vessels. In islets, numerous cytokine signaling and immune terms were enriched, as were pathways related to ER processing and unfolded proteins that were less prominent in α or β cells (**Figure 43H**). Targeted investigation revealed central carbon metabolism pathways as substantially dysregulated in T2D β cells while T2D α cell dysregulation was more concentrated in intracellular signaling pathways (**Figure 43I**). Importantly, genes related to MODY, well known to play critical roles in β cell function, were significantly enriched in T2D β cell samples.

To understand how gene expression changes correlated across sample types, we grouped genes that were differentially expressed in at least one sample type based on their directional change in the other two cell types (**Figures 43J** and **44D**). The most common groups were situations where all three samples showed consistent directional change (000 or 111 representing reduced or elevated in T2D β, α, and islets, respectively), but interestingly, the next most common situation was β cells showing opposite regulation from α cells and islets (100 or 011), highlighting the importance of studying FACS-purified β cells rather than solely extrapolating signals from islets (**Figure 43J**). Pathway analyses of the combination gene lists with reduced expression across all samples (000) revealed metabolic pathways consistently enriched (**Figures 44E-44F**).

While only a minority of differentially expressed genes were shared across samples, a significant overlap in ontologies indicated that many of the same biological processes were dysregulated even if the exact same genes were not (**Figure 43K**). To appreciate these relationships, we applied a network visualization of enrichment across all three sample types. This revealed some β cell-specific clusters (vitamin metabolism) and islet-specific clusters (inflammatory pathways and protein misfolding), but many clusters were consistent across all three sample types (hormone secretion, lipid metabolism, and cilia organization) (**Figure 43L**). In sum, differential expression of sorted β and α cells and whole islets allows for detailed

appreciation of both cell-specific and islet-wide molecular changes in T2D, and integration of these analyses emphasizes how signals are enriched within various islet compartments.

Short-duration T2D donors do not show significant changes in endocrine cell mass or area but show shifts in endothelial cell phenotype

To understand the context in which these functional and transcriptomic changes to the β cell, α cell, and islet act, we comprehensively evaluated the pancreatic tissue architecture from our T2D cohort and compared them to ND controls. In order to achieve both breadth and depth in our analyses, we combined a high-throughput traditional immunohistochemistry (IHC) approach representing major anatomical pancreatic regions across the entire donor cohort with high-dimensional multiplexed imaging for special analysis of cellular phenotypes at the single-cell and individual islet level (**Figure 45A**). Through traditional IHC, we analyzed multiple sections from pancreatic head, body, and tail regions of 20 T2D and 11 age-matched ND donors. A subset of this cohort was further phenotyped with a 28-marker panel using co-detection by indexing (CODEX), which allows fluorescence-based imaging of large tissue sections, allowing us to analyze >370 mm^2 of pancreatic tissue and positively identify 2,983,608 cells with spatially-resolved specific cellular phenotypes defined by combined expression/exclusion of multiple markers (**Figure 46A**). We chose this multiplexed approach because unlike imaging mass cytometry or CyTOF[704,705], it does not destroy tissue and permits section retrieval for a subsequent application of chemical stains and deeper resolution of cellular relationships with acellular tissue components in a given tissue microenvironment.

To determine if changes in endocrine cell ratios contributed to reduced insulin secretion in T2D islets, we robustly evaluated β, α, and δ cell populations. Multiple analyses across the three pancreatic regions, including evaluation by area of stain and by cell identification within islet and within the entire pancreatic section, revealed that there was no loss of β cell mass or increase in α cell mass in short-duration T2D (**Figures 45B** and **46B-46F**). We additionally assessed for apoptosis using the TUNEL assay but found such cells to be exceedingly rare in both ND and T2D human endocrine cells (data not shown). Donor-to-donor variability, particularly in the ratio of β and α cells, was notable, underscoring the challenge in working with heterogeneous human tissues. Further, CODEX allowed us to thoroughly evaluate the endocrine compartment for all islet endocrine cell types simultaneously (including γ and ε cells), as well as to identify cells expressing only a panendocrine marker chromogranin A (CHGA) that has sometimes been used to define “dedifferentiated” β cells[706,707] (**Figures 45C-45D**). We found that $CHGA^+$/$hormone^-$ cells within our donor cohort were rare and not significantly changed in T2D (**Figures 45D** and **46H**). Thus, these data suggest that changes in endocrine cell mass, including loss of β cell mass, is not a substantial component in short-duration T2D. Instead, it points to reduction in β cell function as the predominant feature of this disease stage.

To define changes in the islet microenvironment that may contribute to β cell dysfunction, we next investigated islet non-endocrine components, of which islet capillary endothelial cells (ECs) were the most abundant (**Figures 45E** and **46I**). Additionally, pathway analysis from RNA-seq highlighted enrichment in processes controlling blood vessel size, particularly in α cells, as well as processes related to VEGF production, a primary regulator of islet capillary formation and

maintenance[562,708,709]. Therefore, we performed islet capillary morphometric analysis and found that while islet capillary density did not change, the area per capillary was reduced in the T2D cohort (**Figure 45G-45H**). This size reduction was accompanied by a corresponding increase in the average distance of endocrine cells to the nearest capillary in T2D islets (**Figure 45I**). Interestingly, the closer proximity of α and δ cells to capillaries as compared to β cells, in both ND and T2D islets, aligned with the concentration of blood vessel-related pathway enrichment in T2D α cells over β cells (**Figure 45I** and **45F**). To molecularly evaluate EC phenotypes, we investigated co-expression of CD34 and HLA-DR, markers which are present on subsets of $CD31^+$ ECs, and found that T2D ECs appeared to show a phenotypic shift defined by fewer ECs expressing CD34, a cell adhesion marker that is particularly prevalent in progenitor capillary ECs[710,711] (**Figure 45J-45K**). In sum, this data highlights a change in the structural and molecular phenotype of capillaries in the islet microenvironment that may contribute to islet dysfunction in T2D.

Amyloid deposition is heterogenous in short-duration T2D and associated with loss of endocrine cells and increase in immune cells

Although less abundant than endothelial cells, immune cells contribute to the islet microenvironment (**Figure 45E**) and are known to play important roles in islet homeostasis[712,713]. Of the islet immune cell repertoire, macrophages ($IBA1^+$) were the largest population with T cells the next most prevalent, while $CD45^+$ $CD38^+$ (presumably B and/or NK) cells were very rare; there were also some $CD45^+$ cells present that were not positive for another identifying immune marker in our panel (**Figures 47A-47B**). Intraislet macrophages were not changed but intraislet T cells ($CD45^+$ $CD3^+$) were significantly increased in T2D (**Figures 47C** and **48A**). Further characterization of macrophages based on phenotypic markers indicative of a more proinflammatory ($HLA\text{-}DR^+$) or anti-inflammatory (CD163 and/or $CD206^+$) state did not show a shift in macrophage phenotype in T2D (**Figure 48B**). The increase in T cells in T2D islets was represented across $CD4^+$ (helper), $CD8^+$ (cytotoxic), and $CD4^-$ $CD8^-$ (double negative) T cells but there was not substantial expression of the major histocompatibility class II (MHCII) receptor HLA-DR in these cells (**Figures 48C-48D**).

One hallmark of the islet microenvironment specific to T2D is amyloid deposition. In this short-duration cohort, 75% of donors had evidence of amyloid deposits, but there was a wide range in how many islets within a donor it was detected (**Figures 47D-47E**). Amyloid deposits were embedded in the predominantly acellular extracellular matrix (ECM) located in the islet perivascular regions (**Figure 48E**). Interestingly, sorted T2D β cells were enriched in ECM remodeling pathways, potentially suggesting dynamic changes within this compartment (**Figure 47F**). While aggregated amyloid deposits were clearly enriched in T2D islets, expression of *IAPP*, in contrast to *INS*, was strongly reduced in T2D β cells, suggesting that a post-transcriptional component to IAPP processing and/or folding may contribute to amyloid deposits (**Figures 47G** and **48F**). Interestingly, whole islets, but not sorted β cells, showed significant enrichment in pathways for ER stress and the unfolded protein response (**Figure 47H**). In aggregate, these data suggest that inappropriate processing of IAPP may lead to disruption of the perivascular ECM and activate cells responding to the improperly folded protein.

It was noteworthy that islets with and without amyloid were often in the same tissue section, sometimes very near each other (**Figure 48G**). Further, we noted that the degree of amyloid deposition could vary widely even in cases where amyloid prevalence was similar (**Figure 48H**). Therefore, to more precisely investigate the effects of amyloid on the islet microenvironment and cellular phenotypes and relationships, we pursued analyses on individual annotated islets. Cross-sectional islet cell number was not different between ND or T2D islets or when broken down by islets with or without amyloid (**Figure 49A-49B**). To ascertain if islets with amyloid had features distinct from other islets, we aggregated per-islet metrics across our multiplexed imaging panel and applied Uniform Manifold Approximation and Projection (UMAP)[714], a dimensionality reduction tool helpful for visualizing high-dimensional data (**Figures 47I** and **49C**). Interestingly, high amyloid islets (amyloid^{hi}) were a minority of the total islets but formed a distinct cluster which was retained after removing the amyloid metric feature from the data provided for UMAP (**Figures 47I-47J, 49D**), suggesting that features independent of amyloid distinguish these islets from amyloid-negative islets. The amyloid^{hi} cluster was comprised of multiple donors and showed disruptions in the prevalence of several markers compared to other islets (**Figure 49E**).

Higher amyloid burden negatively correlated with total endocrine and β cells in the islet (**Figures 47K-47L**) but did not alter the ratio within the endocrine compartment (**Figure 49F**), suggesting that amyloid causes nonspecific loss of all endocrine cell types to similar degrees. Among non-endocrine components of the islet, endothelial cell and pericyte abundance did not change, nor did area of collagen IV, a major component of the islet ECM (**Figures 47M-47N** and **49G**). In contrast, immune cell proportion was strongly positively correlated with the degree of amyloid deposition, which was represented by increases to both macrophages and T cells (**Figures 47N** and **49H**). The correlation of macrophages was attributable to macrophages expressing at least one phenotypic marker (HLA-DR, CD163, CD206), but did not suggest an overt phenotypic switch (**Figure 47O**). Both $CD8^+$ and $CD4^+$ T cells positively correlated with degree of amyloid, although the correlation was more substantial with $CD8^+$ T cells (**Figure 47P**). While overall endothelial cell abundance did not correlate with amyloid, there was a significant negative correlation with ECs expressing CD34, consistent with the phenotypic trends seen at the donor level, and significant positive correlations with HLA-DR^+ ECs, indicative of immune signaling in capillaries **Figure 49I-49J**).

Next, we investigated the spatial relationship of islet cells with amyloid deposits and found that non-endocrine cells, particularly macrophages and endothelial cells, were enriched near amyloid deposits, while endocrine cells did not show such enrichment (**Figures 47Q-47R** and **49K**). Pathway analysis of the transcriptome of these donors highlighted enrichment in pathways for cytokine production and signaling as well as for immune recruitment and migration, particularly in islet samples (**Figures 47S-47T**). Our tissue analyses suggest that these signals are likely related to amyloid-laden islets in T2D. Thus, amyloid deposits in T2D are associated with disruptions to the islet microenvironment leading to loss of islet endocrine cells, disruption of endothelial cell phenotype, and recruitment of macrophages and T cells.

Gene network analyses on sorted β cells identify disrupted cilia homeostasis and highlight RFX6 as a highly connected hub gene that is reduced in T2D β cells

To understand the key gene networks within β cells that are contributing to β cell dysfunction in short-duration T2D, we took transcriptomic profiles from our FACS-purified β cell samples and clustered genes based on expression patterns using weighted gene correlation network analysis (WGCNA)[586]. This approach took the >14,000 genes per sample that met our criteria for expression and identified 48 modules of highly correlated genes, providing a useful summary to explore the full array of transcriptomic data (**Figure 50A**). To identify modules most closely associated with T2D, we assessed enrichment in modules for genes differentially expressed (**Figure 50B**). Pathway analysis of these modules revealed three modules (modules 1, 5, and 7) whose genes were implicated in pathways related to different elements of carbohydrate, lipid, and amino acid metabolism (**Figure 50C**). Module 7 was additionally enriched for other signaling components that influence stimulated insulin secretion, including ion transport and cAMP signaling.

Module 6, by contrast, was primarily defined by enrichment in cilia genes (**Figure 50C**). This was consistent with differential expression analysis which showed significant enrichment for cilia terms across samples (**Figure 50D**). Thus, enrichment in module 6 indicates that the dysregulation leading to differential expression is highly correlated across samples. Comparison of these differentially expressed genes to a validated list of cilia-related genes, CiliaCarta[715], revealed a majority of high-quality cilia genes were expressed at higher levels in T2D compared to ND for both β and α cells. To investigate whether these changes at the transcript level translated to cellular alterations, we stained tissue sections from the same donors with cilia marker ARL13B (**Figure 50F**). Total cilia area within the islet was elevated in T2D tissue, attributable to a higher cilia density with unchanged cilia size (**Figure 50H**) and consistent with elevations in cilia transcripts.

Gene co-expression modules also provide opportunity to investigate correlation of transcriptomic profiles with additional parameters that would not otherwise be sufficiently powered. In this case, having perifusion metrics from the same donors allowed us to investigate β cell gene networks that track with elevated or reduced insulin secretion parameters, including basal secretion, integrated secretion to numerous stimuli, and islet insulin content (**Figure 50I**). This analysis revealed numerous interesting correlations but in particular, module 1, defined by metabolic pathways (**Figure 50C**), was the highest correlated module to insulin area under the curve for 16.7 glucose.

By correlating genes expression with the expression profile of the module eigengene, this network analysis allows the identification of “hub” genes that are disproportionately connected both within and across modules. This analysis on our network revealed numerous highly connected genes (**Figure 50J**). In particular, *RFX6*, an islet-enriched transcription factor, stood out as being highly connected both within its module and across modules. As a transcription factor, RFX6 is in a prime position to exert broad regulation of cellular processes and cell states. Additionally, *RFX6* is a member of module 1, which was both enriched for differentially expressed genes and showed the strongest correlation to high glucose-stimulated insulin

secretion. Further, not only is *RFX6* a highly connected gene, it is also one of the most reduced islet-enriched transcription factors at the transcript level in T2D β cells (**Figure 50K**). To determine if these changes extended to the protein, we assessed RFX6 expression by immunohistochemistry and found a reduction in T2D β cells (**Figure 50L-50M**). In sum, these data highlight RFX6 as a highly connected hub gene in β cells that is associated with insulin secretion and is significantly reduced at both the transcript and protein level in short-duration T2D.

Discussion

Our results highlight how integrated analyses of short-duration T2D isolated islets and pancreatic sections can provide molecular insight into disease-driving mechanisms of T2D. We highlight that *in vitro* these islets have defects in multiple steps of the insulin secretory pathway, including components distal to glucose metabolism, despite no change in insulin content. These defects were sustained after transplantation into a normoglycemic, non-insulin resistant environment. Further, β cell loss and dedifferentiation were not observed in our cohort, highlighting reduction in β cell function as the predominant feature of the early disease stage. In addition to β cell functional defects, the islet microenvironment was significantly altered; T2D islets had smaller islet capillaries, increased intraislet T cells, and heterogeneous amyloid deposition in a minority of islets. Within these amyloid^{hi} islets, there was a loss of endocrine cells and disruptions in non-endocrine cell composition or phenotype. Integrated transcriptomic analysis of sorted β and α cells and whole islets demonstrated transcriptional dysregulation in β cells that was concentrated in metabolic and hormone secretory pathways, while whole islets showed enrichment for pathways associated with the immune system and ER stress, emphasizing how signals are enriched in different compartments of the islet. From sorted β cells, *RFX6* was significantly reduced in T2D and emerged as a highly connected hub gene that is associated with insulin secretion, emphasizing its role in mediating β cell dysfunction in short-duration T2D.

The relative contribution of reduced β cell mass in T2D is subject to ongoing debate[650,716–719]. Numerous post-mortem studies have suggested a mild reduction in β cell mass in T2D[515,720–724], but there is significant overlap in β cell mass among T2D and normal individuals and several studies noted that such defects were most prominent in donors with increased disease duration or who were being treated with insulin. Our study demonstrates in the early stages of T2D, there is no loss of β cell mass and instead this stage is defined by significant β cell dysfunction. Further, while β cell dedifferentiation is not consistently defined, we show that loss of insulin immunoreactivity with retention of the pan-endocrine marker chromogranin A is not a significant hallmark of disease process at this stage. Given the immense difficulty in increasing human β cell mass, our data emphasizes the importance of early intervention to improve the function of the substantial β cell mass that remains. This is consistent with reports of rapid disease reversibility with bariatric surgery or severe caloric restriction in early T2D[725–730]. Our *in vivo* data indicates that such reversibility cannot be achieved simply through correction of glycemia or insulin sensitivity but rather that additional signals targeting the islet and/or β cell are needed.

While β cells are the ultimate source of insulin, they do not act in isolation. Indeed, individual β cells do not show the same dynamic secretion pattern seen in intact islets[144,145,168,201,276,676], highlighting that the larger islet microenvironment is crucial for coordinated islet function. Our study reveals that non-endocrine components of the islet, including the vascular system, immune system, and extracellular regions, show substantial alterations in short-duration T2D. The presence of these features prior to changes in islet endocrine composition suggests that non-endocrine cells play early and possibly causal roles in β cell dysfunction. These results also highlight a need to consider the full array of islet cells when pursuing β cell replacement as a therapy for diabetes.

Studies of endothelial cell-β cell interactions have revealed important roles in both physiology and pathophysiology, though mechanistic studies have largely been conducted in mouse islets, which have notable differences in vascularization compared to human islets, namely an increased capillary density[562,709,731]. While we observed β cell dysfunction in isolated islets without active blood flow, these islets do retain endothelial cells that could signal to β cells; further, islet transplants are revascularized by a combination of host and graft endothelial cells[732], thus local signals could contribute to the continued β cell dysfunction in this setting. Interestingly, our data also highlight that signaling between α cells and endothelial cells may be equally important, as α cells were positioned closer to capillaries than β cells and T2D α cells showed dysregulation of pathways related to blood vessel dynamics. Ultimately, newly developed techniques such as pancreas slice culture and transplantation into the anterior chamber of the eye[733–735], as well as improvements to endothelial cell culture *in vitro*[736], will provide an opportunity to investigate how these early phenotypic changes observed in endothelial cells may contribute to β cell dysfunction.

The significant enrichment of inflammatory pathways specifically in the transcriptome from whole islets suggested differences in immune cells in T2D, which was confirmed by our tissue-level observations of increased abundance of several types of T cells. Although autoreactive T cells are critical to the pathogenesis of T1D, the role of tissue resident T cells in normal islet physiology or in T2D is less clear and may be an interesting area for future investigation. Instead, most research into T2D-related islet inflammation has focused on intraislet macrophages[623]. While our results did show macrophages as the most abundant immune cell in the islet, they were not significantly enriched in short-duration T2D donors. Assessment of a select number of macrophage polarization markers did not reveal a phenotypic change though assessment of additional markers may help to clarify this. In contrast, at the islet level, increased amyloid strongly correlated with increased macrophages and these same islets showed loss of endocrine cells. Thus, while amyloid-laden islets were a minority of islets in this short-duration T2D cohort, our results add to a growing body of literature on the relationship of amyloid, immune, and endocrine cells[347,361,737,738].

One of the most consistent transcriptional findings across β cells, α cells, and islets was enrichment in pathways related to cilia. Primarily studied in mice, cilia contain a disproportionate concentration of GPCRs and through knockout studies have been shown to be critical in regulating glucose sensing, calcium influx, and paracrine signaling within the islet[739–741]. In our

cohort, a majority of cilia-related transcripts were elevated, differing from a previous report in T2D[742], but consistent with what we identified at the tissue level where we observed an increase of intraislet cilia. To our knowledge, the effect of increased islet cilia has not been examined but this could represent a compensatory process by which islet cells early in the disease are attempting to upregulate to mitigate deficits in β cell function.

Within the β cell, transcriptional dysregulation clearly plays an important role in impaired insulin secretion. Pathways related to metabolism of carbohydrates, lipids, and proteins, as well as peptide processing and vesicle exocytosis, were all enriched for differentially expressed genes specifically in T2D β cells, consistent with functional data showing impairments at multiple stages of the insulin secretory pathway. Gene network analyses revealed that *RFX6* was a highly connected hub gene that controlled gene expression within a module that was both enriched for differentially expressed genes and highly correlated to insulin secretory parameters. Further, RFX6 was reduced specifically in β cells at both the mRNA and protein level in our short-duration T2D donor cohort. In mice, Rfx6 has been shown to direct formation of β cells and is required in the adult β cell to maintain cell identity[743,744], while in an immortalized cell line, RFX6 has been shown to control insulin secretion by modulating calcium homeostasis[745]. Further, T2D GWAS loci are enriched in RFX6 binding motifs, linking reduced RFX6 action to genetic susceptibility for T2D[746]. Thus, future work should directly investigate the role of RFX6 in human β cells to link it to T2D as well as focus on how RFX6 is regulated in the β cell.

There are limitations to this study that suggest opportunities for future work. While we have taken great care to focus our organ collection efforts, the natural history of T2D makes precise determination of disease onset difficult. Analogous studies on pancreata from long-standing T2D would provide additional information and help determine which processes are more causal and which are consequences. Further, increasing donor number will allow for better appreciation of and investigation into T2D disease heterogeneity. Additionally, integration of additional studies such as electrophysiology, proteomics, or metabolomics would provide complementary information that might identify specific pathways within the broadly dysregulated cellular and metabolic categories revealed by our transcriptomic profiling. In this vein, consortia efforts such as the Human Pancreas Analysis Program (HPAP), Network for Pancreatic Organ donors with Diabetes (nPOD), and Human BioMolecular Atlas Program (HuBMAP), will be critical to obtain increased numbers of pancreata and perform detailed molecular characterization. Finally, since it is infeasible within this study to follow up on multiple interesting findings, mechanistic studies, ideally performed in human islets, will be necessary to complete our understanding of how these newly identified or further validated processes contribute to β cell dysfunction.

In sum, we highlight an innovative, multi-faceted approach to studying the human pancreas and islets in the context of disease. In this study, we generated substantial datasets encompassing T2D dynamic hormone secretion, islet, α and β cell transcriptome, and multiplexed imaging of the islet microenvironment, and we integrated these to provide a holistic view of short-duration T2D. Ultimately, we demonstrate that the initial defect in T2D is impaired β cell function, that

there are disruptions to endothelial and immune cells within the islet microenvironment, and that β cell transcriptional dysregulation at multiple points in the insulin secretory pathway is in part mediated by RFX6. Together, these data provide key insights into the molecular pathogenesis of T2D.

Integrated analysis of the pancreas and islets reveals unexpected pathobiological characteristics in 22-year-old male with presumed type 1 diabetes

Introduction

T1D is an autoimmune disease that results from selective destruction of insulin-producing beta cells. Classically, T1D presents during childhood or adolescence; however, a number of patients do not fit these typical criteria[747]. For example, T1D genetic risk scores (GRS) suggest T1D can develop within the first six-months of life[748] and that as much as 40% of T1D develops after the age of 30[597,749]. Beyond age of onset, phenotypic differences in timing to insulin dependence, residual C-peptide production, and seroconversion could result from variables such as environment, ethnicity and genetics[750]. Furthermore, clinical insulin deficiency can present as T1D but actually result from single gene variants[595,596].

As the pathogenic heterogeneity of T1D is increasingly being recognized[304], the concept of numerous endotypes, representing discrete, complex biological networks, responsible for the clinically observable T1D phenotype is emerging[751], yet precise definitions for these endotypes do not exist. Using infrastructure developed to study pancreatic tissue and islets from the same donor in conjunction with the redacted medical record, we report unexpected findings in the pancreatic islets and tissue of an individual with 8 years of clinical T1D and our approach to comprehensively assess pathobiological characteristics in this donor to determine whether clinical insulin deficiency resulted from type 1 diabetes.

Results

Clinical characteristics of donor and pancreas

As part of studies of the T1D pancreas, we obtained the pancreas from a Caucasian 22-year-old male (BMI: 25.7 kg/m2) with an 8-year history of T1D treated with Novolog and Lantus. The donor's average blood glucose was 295 mg/dL based on the HbA1C of 107 mmol/mol (11.9%). Low measured serum C-peptide (0.06 ng/mL) suggests relative and near absolute insulin deficiency but could reflect impaired insulin secretion related to critical illness at the time of sample collection[594]. The donor carried high-risk HLA haplotypes DR4 and DQ8, but all T1D-associated autoantibodies (mIAA, IA2A, GADA and ZnT8) were negative at time of death. No family history of diabetes was reported in the redacted medical chart. The pancreas weighed 59.1g, similar to other pancreata from individuals with T1D as observed by our group[317,318]. We processed the pancreas to obtain both tissue and isolated islets to allow integrated analyses. Islet isolation yielded 32,000 IEQs at 65% purity, with greater than 90% viability, similar to other type 1 donors[594].

Isolated islets showed insulin secretion and content comparable to non-diabetic donors

Isolated islets from this donor (**Table 3**) were compared to islets from individuals without diabetes (**Table 3**). Surprisingly, islets from the donor had robust, dynamic insulin secretion at levels similar to non-diabetic controls both when normalized by islet volume (islet equivalent: IEQ) and when normalized by % insulin content (**Figure 51A-51D**). This was unusual as typically recent-onset T1D islets only show similar insulin secretion when normalized by % insulin content[594]. Interestingly, glucagon secretion was similar to controls when normalized by IEQ although there was an elevated peak in response to cAMP-mediated potentiation, but this was substantially decreased when normalized by % glucagon content (**Figure 51E-51H**). These α cell findings are similar to studies of recent-onset T1D islets (<10y T1D duration) and were not described in the α cells from a donor with clinical insulin insufficiency due to HNF1A-associated monogenic diabetes[594,595]. Both insulin and glucagon content per IEQ were within ranges seen of islets from non-diabetic donors (**Figure 51I-51J**). Independent evaluation of isolated islet endocrine composition by flow cytometry (**Figure 51K**) was also in the range of normal, unusual for T1D of this duration[594].

Genetic analysis did not uncover monogenic causes of diabetes.

Because of the unexpected islet insulin content and absence of T1D-associated antibodies at the time of death, we sequenced the donor DNA for variants in 148 diabetes-related genes[596] and identified a heterozygous variant in the intronic region of glucokinase (GCK: c.209-8G>A, **Table 14**) now known to be non-pathologic. This concurred with our clinical assessment as heterozygous loss of function variants in GCK result in Maturity-Onset Diabetes of the Young 2 (MODY2) characterized by mild non-progressive hyperglycemia that does not require treatment[752] was inconsistent with the medical history of this donor. Further analysis of single nucleotide polymorphisms in HLA and non-HLA loci revealed a T1D genetic risk score of >75th percentile, which is reported to be indicative of T1D with 95% specificity and 50% sensitivity[597].

To further investigate diabetes related to a single gene variant, we performed whole-exome sequencing. All variants associated with diabetes were evaluated by keywords and assessed for pathogenicity and clinical phenotype, but no clear pathogenic variants in known genes related to beta cell identify or function were identified (**Table 15**). Interestingly, we did identify a previously unreported variant in SLC2A4 (c.811C>T), which encodes GLUT4, the insulin-regulated glucose transporter expressed primarily in adipocytes and striated muscle[753], that was predicted to be deleterious.

Investigation of pancreatic tissue identified cellular and molecular features of type 1 diabetes.

We next systematically analyzed the head, body and tail regions of the donor pancreas by immunofluorescence. This revealed 70.7% of islets reviewed (220 of 311 islets) contained at least one β cell, in contrast to tissue studied by our group from donors with less than 10 years of T1D (17.8±15.5%)[594] (**Figures 52A-52B**). Despite remnant β cells in most islets, in aggregate, the distribution of the proportion of β cells per islet was strongly shifted downward, which was not seen with α cells (**Figure 52B-52C**). Concordantly, β cell mass in this pancreas was lower than α cell mass and less than that seen in donors without diabetes (**Figure 52D**).

Given the remnant β cell mass, we next investigated islet immune cell infiltration. Despite no humoral immunity, 21 of 311 islets (7%) evaluated from eight blocks encompassing the pancreas head, body and tail regions demonstrated CD45+ infiltration with 15 or more CD45+ cells within the islet or at the islet periphery (**Figure 52E-52F**)[754]. Notably, degree of islet immune cell infiltration correlated with the proportion of islet β cells but not islet α cells (**Figure 52G**)[304]. To identify these immune cells, lymphocytes were sorted from 100 isolated pancreatic islets from the donor (**Figure 52H-52N**) with 6 CD4+ T cells, 20 CD8+ T cells, and 12 CD19+ B cells identified, similar to other samples with greater than 5 years duration of T1D[567].

With α cell dysfunction in isolated islets, we next looked for evidence of disordered gene expression recently described in T1D[594,755]. Evaluation of the pancreatic tissue showed misexpression of β-cell marker NKX6.1 transcription factor in a pattern similar to the T1D α cell. However, no appreciable change in donor α cell ARX or MAFB expression was noted (**Figure 53A-53B**).

Discussion

As part of studies of T1D pancreata, we report substantial β cell numbers and detectable in vitro β cell function comparable to donors without diabetes in isolated islets from an individual with clinical T1D for 8 years. These unexpected findings prompted us to search for single gene variants that contribute to heterogeneity in clinical insulin deficiency, however both targeted and whole-exome DNA-sequencing found no clear monogenic cause for diabetes. A deleterious variant in SLC2A4 was identified, yet GLUT4 defects are thought to be associated with insulin resistance[756], inconsistent with the donor's clinical presentation. Nonetheless, defects in insulin signaling could have contributed to the overall clinical picture. Histological analysis of pancreatic tissue revealed reduced β cell mass, insulitis, and molecular changes in α cells consistent with prior reports of T1D. Only by integration of pancreatic islet histology, function, and molecular analysis with thorough vetting of genetic studies using donor clinical information could we conclude that this donor's clinical insulin deficiency most likely resulted from immune-mediated loss of β cell mass, possibly on a background of reduced insulin action.

While the majority of T1D samples have nearly undetectable β cell mass by 10 years of disease, similar cases of substantial remnant β cell mass (>10% of control) despite years of T1D have been reported[304,757], however, near normal β cell numbers with preserved function in isolated islets was quite unusual. The discordant findings in β cell numbers from isolated islets compared to in situ analysis of pancreatic tissue is not fully understood. With increasing evidence recognizing T1D as a disease of the entire pancreas and reduced pancreas weight in this donor consistent with prior reports[317,318], it is possible islets as described in pancreata with reduced β cell mass, namely smaller and dysmorphic, may have been unintentionally lost during islet isolation leaving islets with preserved native architecture overrepresented. Other possibilities include causes of clinical insulin deficiency either unknown or not identifiable by post-mortem analysis alone.

Infrastructure for pancreatic organ donation and analysis of human T1D tissue, through consortia such as Human Pancreas Analysis Program (HPAP)[758], Human Islet Research

Network (HIRN) and Network for Pancreatic Organ Donors with Diabetes (nPOD)[304,759], have revealed marked heterogeneity in β cell mass at disease onset, insulitis, and persistence of insulin-producing β cells in long-standing disease. This heterogeneity may ultimately result from multiple, distinct biological mechanisms representing different endotypes, currently undefined, which act to produce the T1D clinical phenotype[751]. This could represent the potential for individually tailored therapies[760], highlighting the importance of thorough study of and reporting on unique pathobiological characteristics in T1D such as this one. Further, the findings reported here demonstrate that it is crucial to integrate studies from both isolated islets and histological evaluation during pancreatic tissue analysis. Continued use of this integrated approach in conjunction with mechanistic studies of human pancreatic tissue[560] will improve our understanding of this pathogenic heterogeneity.

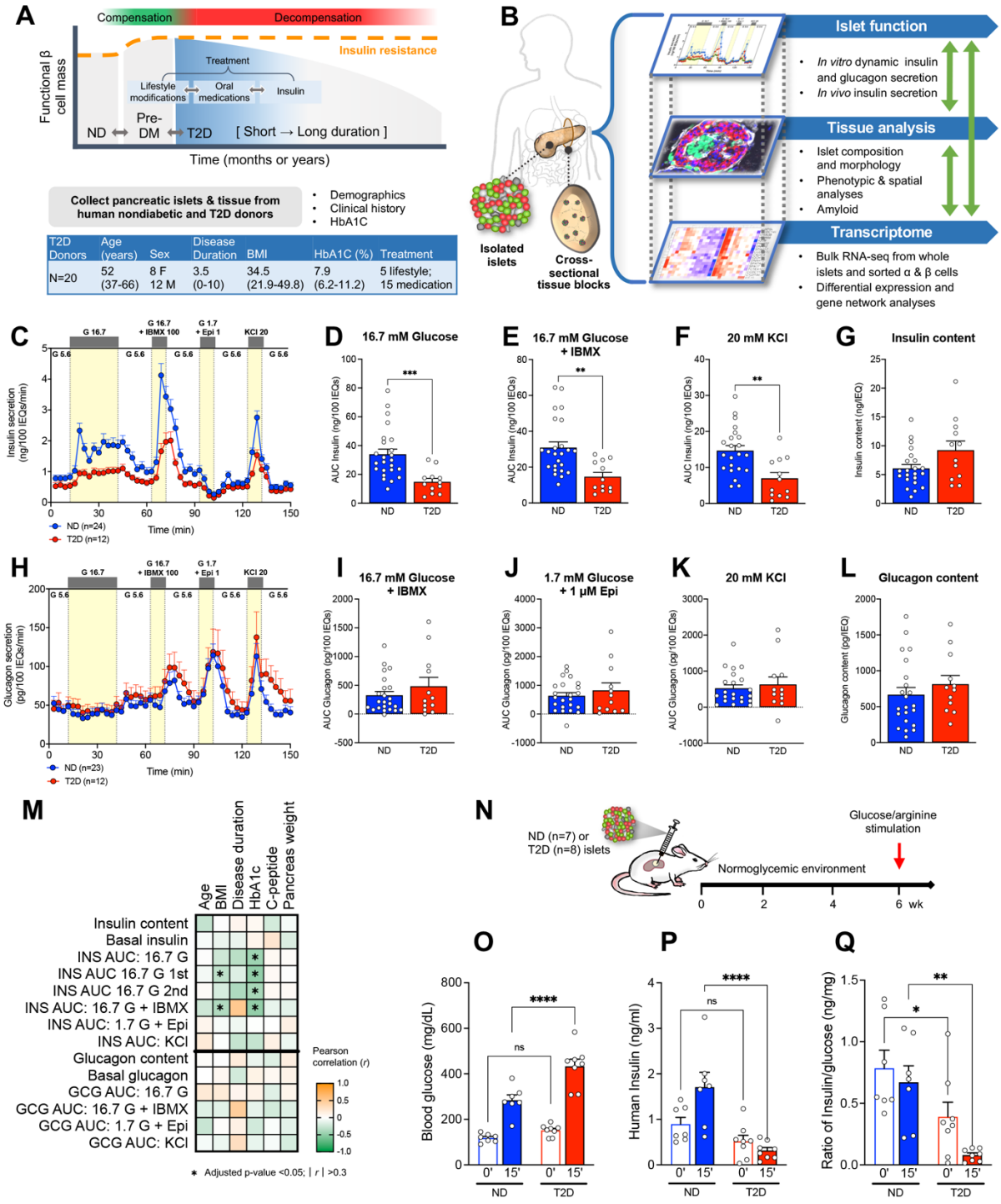

Figure 41. Integrated analysis of islet function, gene expression, and histology on a cohort of donors with short-duration T2D reveals substantially reduced stimulated insulin secretion *in vitro* and *in vivo* despite similar islet insulin content.

(A) Schematic of T2D progression and summary of clinical characteristics of T2D donors. **(B)** Schematic of experimental approach to integrate studies across islets and tissue. **(C)** Dynamic insulin secretory response to various secretagogues measured by perifusion in non-diabetic

(ND, n=24) and T2D islets (n=12) normalized to islet volume expressed by islet equivalents (IEQs); 1 IEQ corresponds to an islet with a diameter of 150 µm. G 5.6 – 5.6 mM glucose; G 16.7 – 16.7 mM glucose; G 16.7 + IBMX 100 – 16.7 mM glucose with 100 µM isobutylmethylxanthine (IBMX); G1.7 + Epi 1 – 1.7 mM glucose and 1µM epinephrine; KCl 20 – 20 mM potassium chloride (KCl). **(D-F)** Insulin secretion was integrated by calculating the area under the curve (AUC) for response to the secretagogues in yellow. Additional metrics from this trace are shown in **42C-42F** and normalization by islet insulin content is shown in **42G-42L**. **(G)** Total islet insulin content normalized to islet volume. **(H-K)** Dynamic glucagon secretory response **(H)** in the same perifusion system with integrated area under the curve analyses **(I-J)** to secretagogues in yellow. Additional metrics from this trace are shown in **Figure 42M-42N** and normalization by islet glucagon content is shown in **Figure 42O-42T**. **(L)** Total islet glucagon content normalized to islet volume. **(M)** Pearson correlation of perifusion metrics to clinical characteristics of donors. **(N)** Schematic of human islet transplantation and in vivo assessment of function. **(O-Q)** Fasted (6h) and 15' after glucose and arginine stimulation blood glucose **(O)**; human insulin levels **(P)** and human insulin:blood glucose ratio **(Q)**. Data are shown as donor average with 4-8 mice/donor. **Figure 42U-42V** shows data per each individual mouse. *p<0.05, **p<0.01, ***p<0.001, ****p<0.0001. Error bars indicate SEM. Panels **D-G** and **I-L** were analyzed by two-tailed t-test. Panels **O-Q** were analyzed by two-way ANOVA.

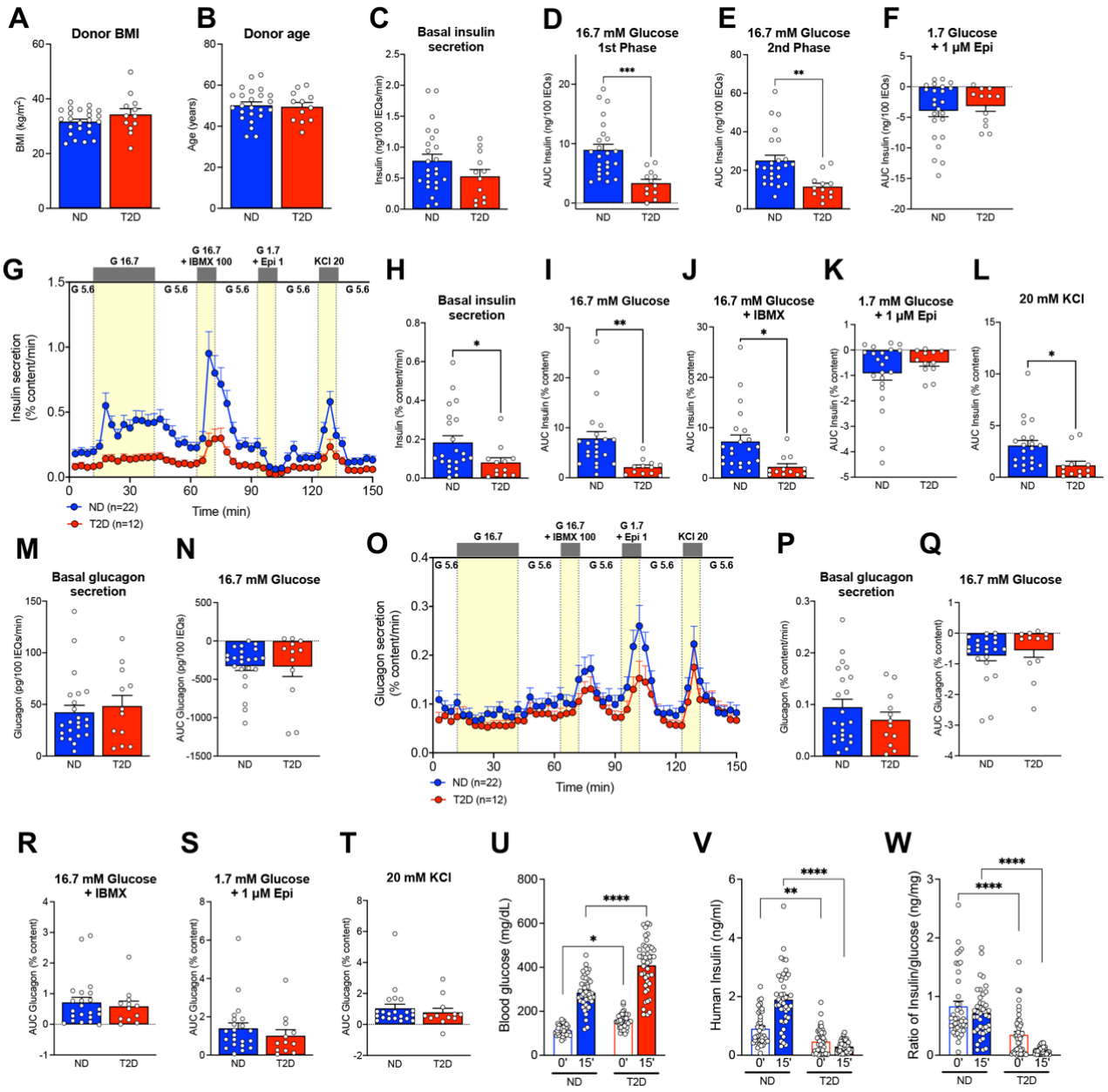

Figure 42. Related to Figure 41. Short-duration T2D islets show substantially reduced stimulated insulin secretion in vitro and in vivo despite similar insulin content.
(A-B) Matching of ND and T2D donor age **(A)** and BMI **(B)** for perifusion experiments. **(C)** Basal insulin secretion calculated as average of first three points of perifusion trace. **(D-E)** Integrated area under the curve breaking down the total 16.7 glucose response to the first phase (**D;** through minute 24) and 2nd phase (**E;** remainder of glucose stimulation). **(F)** Area "under" the curve calculated from trace baseline for inhibition with low glucose + epinephrine. **(G-L)** Dynamic insulin secretion and metrics equivalent to **Figure 41** but normalized by total insulin content. **(M)** Glucagon secretion at basal glucose calculated as average of first three points of perifusion trace. **(N)** Area "under" the curve calculated from trace baseline for inhibition with high glucose. **(O-T)** Dynamic glucagon secretion and metrics equivalent to **Figure 41** but normalized

by total glucagon content. **(U-W)** Fasted (6h) and 15’ after glucose and arginine stimulation blood glucose **(U)**, human insulin levels **(V)**, and human insulin:blood glucose ratio **(W)**. Data shown per each individual mouse. * p<0.05, **p<0.01, ***p<0.001, ****p<0.0001. Error bars indicate SEM. Panels **A-F**, **H-N**, and **P-T** were analyzed by two-tailed t-test. Panels U-W were analyzed by two-way ANOVA.

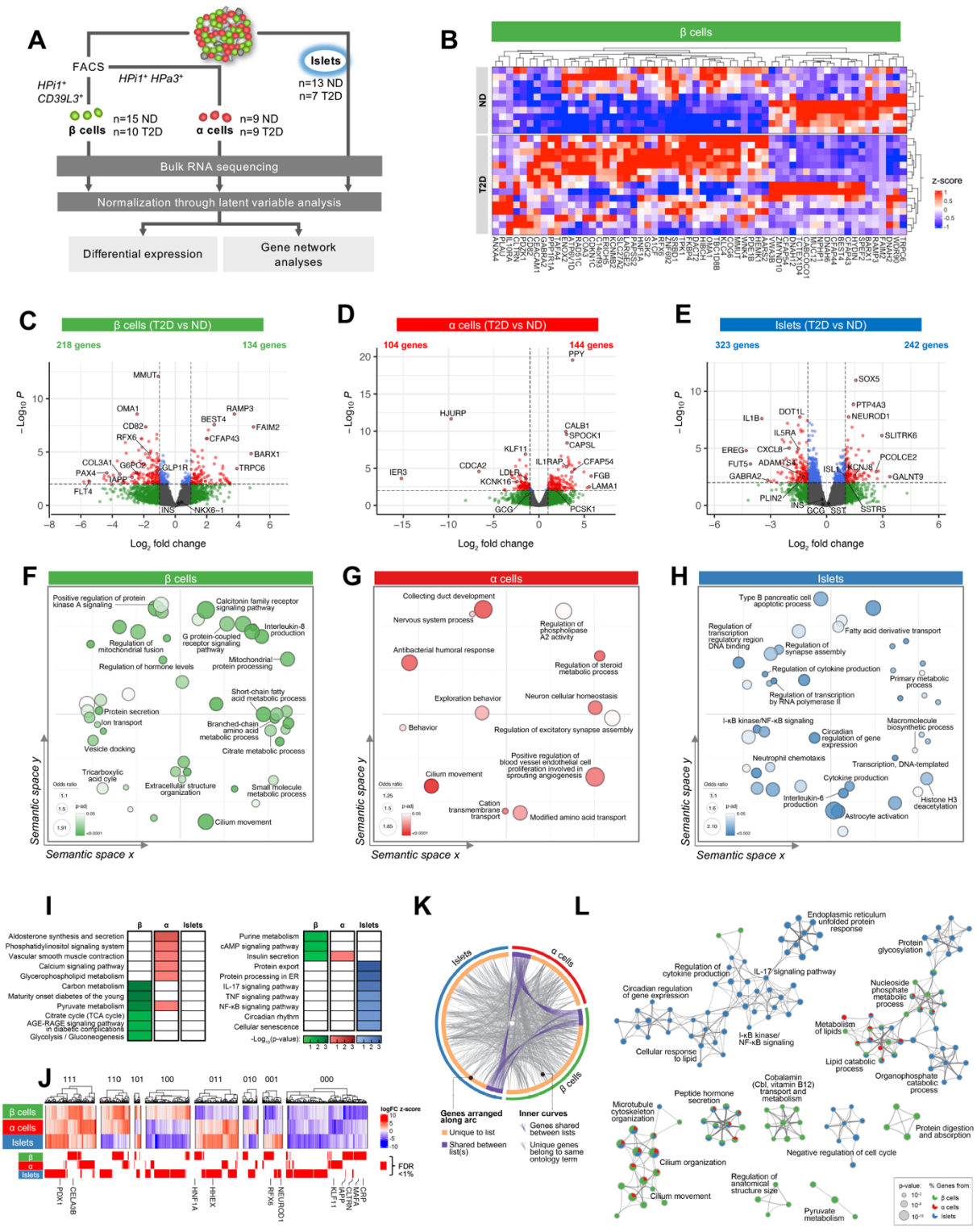

Figure 43. Integrated transcriptome analysis reveals numerous genes and pathways dysregulated in T2D.

(A) Schematic of sample collection and transcriptome analysis. **(B)** Heat map of most differentially expressed genes (by p-value) in T2D β cells. Congruent heat maps for α and islet

samples are shown in **Figure 44**. **(C-E)** Volcano plot illustrating differentially expressed genes between ND and T2D β cells (C), α cells (D), and (E) islets. Vertical lines denote fold-change cutoff (≥1.5) while horizontal line indicates p-value cutoff (0.01). Genes passing both thresholds are colored and some genes of interest are labeled. Numbers above plots indicate the number of genes downregulated (left) or upregulated (right). **(F-H)** Gene ontology terms obtained from RNA Enrich (FDR<0.05) were condensed using the RelSim function of Revigo (similarity=0.5) and plotted in semantic space to emphasize similarity. Dot size represents odds ratio and color represents p-value. Select terms are labeled. **(I)** Heat map depicting most enriched KEGG pathways (by p-value) for each sample type based on differentially expressed gene lists (FDR<0.01). **(J)** Heat map showing the shared and unique trends of differential gene expression across sample types, with each vertical group (dendogram) representing a specific combination of directionality across samples (1s correspond to positive fold-change and 0s to negative fold-change; digit order represents the direction in β, α, and islet samples, respectively). Red bars in bottom section highlight genes in each category that meet the FDR <0.01 threshold across samples. **(K-L)** Visualizations of overlap from all sample types at the gene and pathway levels for genes FC≥1.5 and FDR<0.01, analyzed by Metascape. Outer circle of Circos plot **(K)** represents the size of each sample list (β cells: 352 genes, green; α cells 248, red; islets 564, blue). The inner circle represents individual genes arranged along the arc. Genes in purple are shared between list(s) and are connected by purple curves, while genes unique to a list are shown in orange. Grey curves illustrate overlap between gene lists at the level of shared ontology terms (only those with <100 genes shown), where genes linked by a grey curve belong to the same enriched ontology term. **(L)** A heuristic algorithm was employed to select a subset of enriched terms (20 top-score clusters, with up to 10 best scoring/lowest p-value terms within each cluster), where terms with Kappa similarity >0.3 are connected by edges (thicker = higher similarity). Node size is proportional to p-value for term enrichment; pie slices represent the percentage of genes under the term that originated from the corresponding gene list.

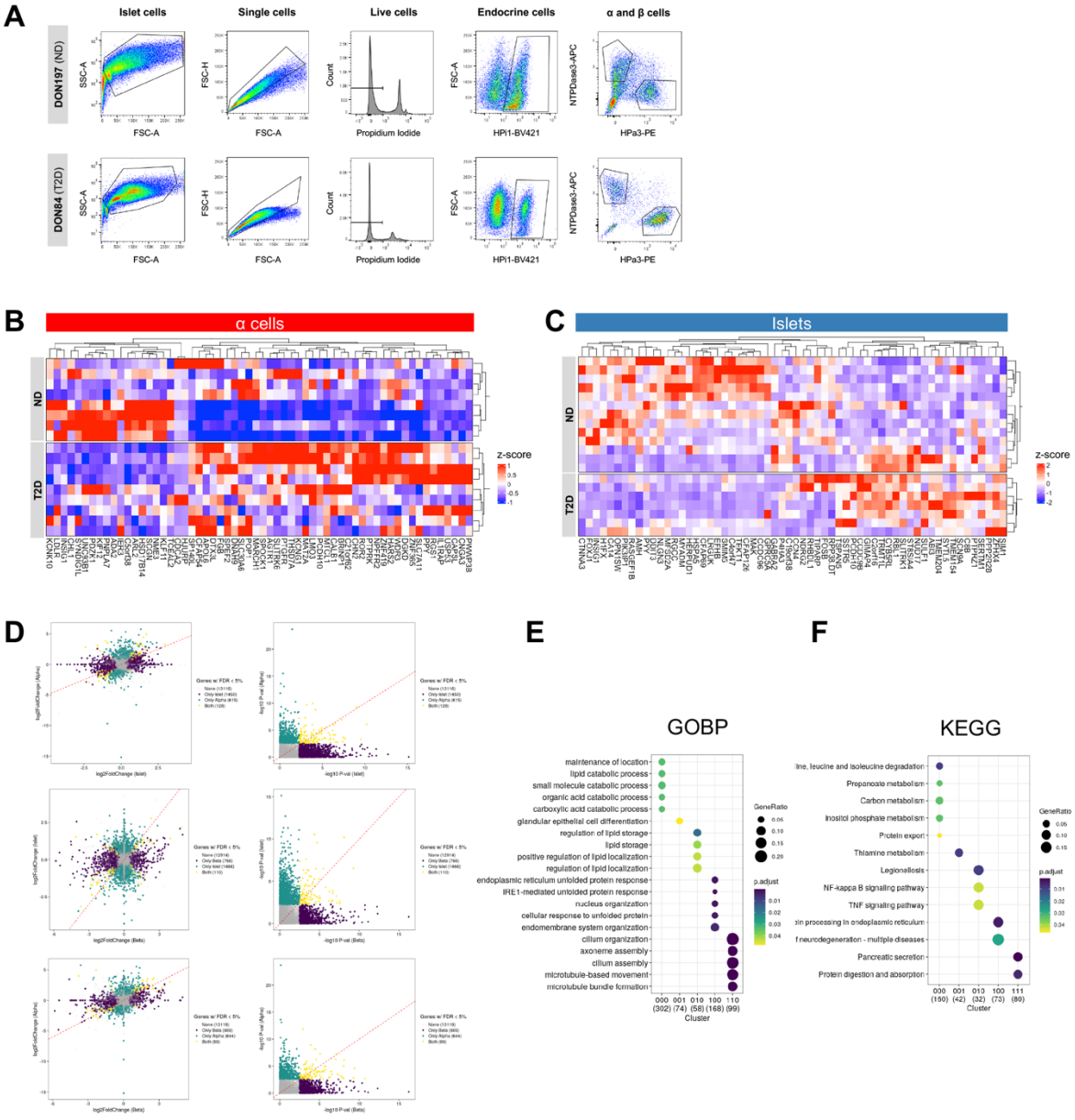

Figure 44. Related to Figure 43. Transcriptional analysis of sorted α and β cells and islets from ND and T2D donors.

(A) Gating strategy for sorted α and β cells identified by cell surface markers. Cell debris were excluded by forward scatter (FSC) and side scatter (SSC), single cells were identified by voltage pulse geometry (FSC-A v. FSC-H), and non-viable cells were excluded using propidium iodide (PI). Endocrine cell subpopulations were then isolated based on positivity for HPi1 (pan-endocrine marker) and additional positivity for HPa3 (α cells) or NTPDase3 (β cells). **(B-C)** Heat maps of the most differentially expressed genes (by p-value) in T2D α cells **(A)** and islets **(B)**. **(D)** Pairwise comparison of differentially regulated genes used to generate heat map shown in **Figure 43J**. **(E-F)** Pathway enrichment for sample clusters shown in **Figure 43J**, where α cell, β cell, and islet samples show regulation of genes in the same or opposite directions in T2D.

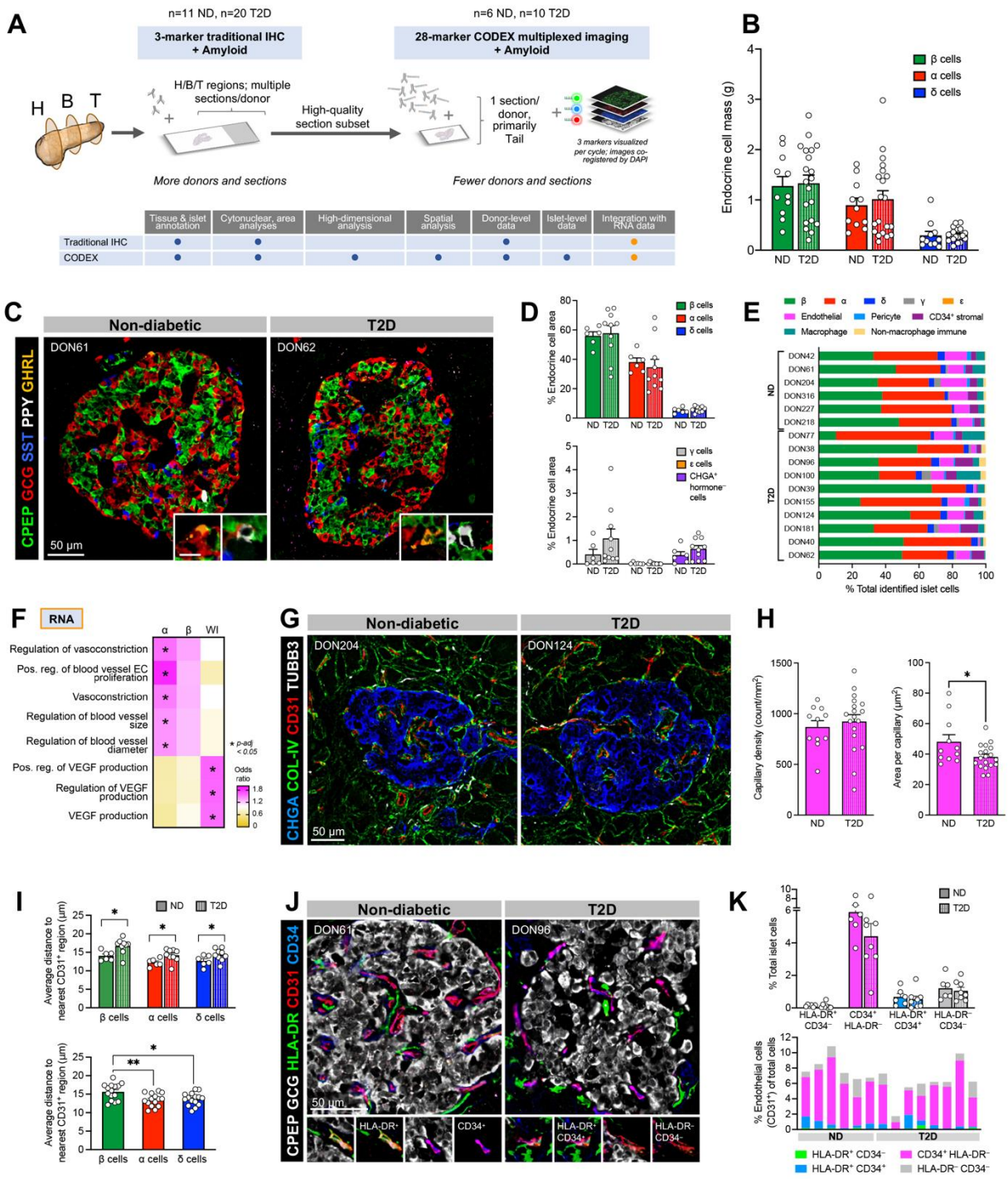

Figure 45. Integrated tissue analysis shows normal endocrine cell mass and endocrine cell composition in the short-duration T2D donor cohort but demonstrates alteration in intra-islet capillaries.

(A) Complementary approaches of traditional immunohistochemistry (IHC) and high content multiplexed imaging were applied to ND and T2D tissues to quantify single-cell phenotypes and their spatial relationships. **(B)** Cell counts of the most abundant endocrine cell populations determined by IHC were combined with pancreas weight to estimate endocrine mass (β, green;

α, red; δ, blue). **(C)** Representative islets captured by CODEX imaging. Scale bar, 50 μm. Insets show less abundant γ cells (pancreatic polypeptide, PPY; white) and ε cells (ghrelin, GHRL; orange); scale bar, 25 μm. **(D)** Cross-sectional area of each of the five endocrine cell types as assayed by CODEX. CHGA+/hormone$^-$ cells, while rare, were also quantified (purple bars). **(E)** Endocrine and non-endocrine islet cells were identified simultaneously using a 28-marker CODEX panel that allowed for labeling of endothelial cells (CD31; magenta), pericytes (MCAM; light blue), endothelial and stromal cells (CD34; purple), macrophages (IBA1; teal), and other immune cells (CD45; yellow). Each bar represents one donor (mean 42 islets and 7,322 cells per donor). **(F)** Heatmap showing select vascular-related GO terms from RNA Enrich for each RNA sample type; asterisks denote terms with FDR $p<0.05$. **(G)** Islet capillaries (CD31; red) are closely associated with neuronal projections (TUBB3; white) and extracellular matrix (collagen-IV, COL-IV; green). Scale bar, 50 μm. **(H)** The larger donor cohort was assessed by traditional IHC to visualize islet capillaries (caveolin-1). Capillary density (capillary count per mm^2 islet area) and area per capillary were quantified to describe islet vasculature. **(I)** Nearest neighbor analysis of CODEX images determined the average distance of each endocrine cell type to nearest capillary. Top bar graph, ND vs. T2D; bottom, cell type comparison independent of disease. **(J)** Representative CODEX images depicting phenotypes of endothelial cells (CD31; red) defined by single or dual positivity for HLA-DR (green) and CD34 (blue). Examples of each combination (HLA-DR+ only, CD34+ only, HLA-DR+ CD34+, and HLA-DR- CD34-) are shown in bottom panel. Scale bar, 50 μm. **(K)** Quantification of phenotypes shown in panel **J**, expressed as proportion of total islet cells (top graph) and showing donor breakdowns (bottom graph).

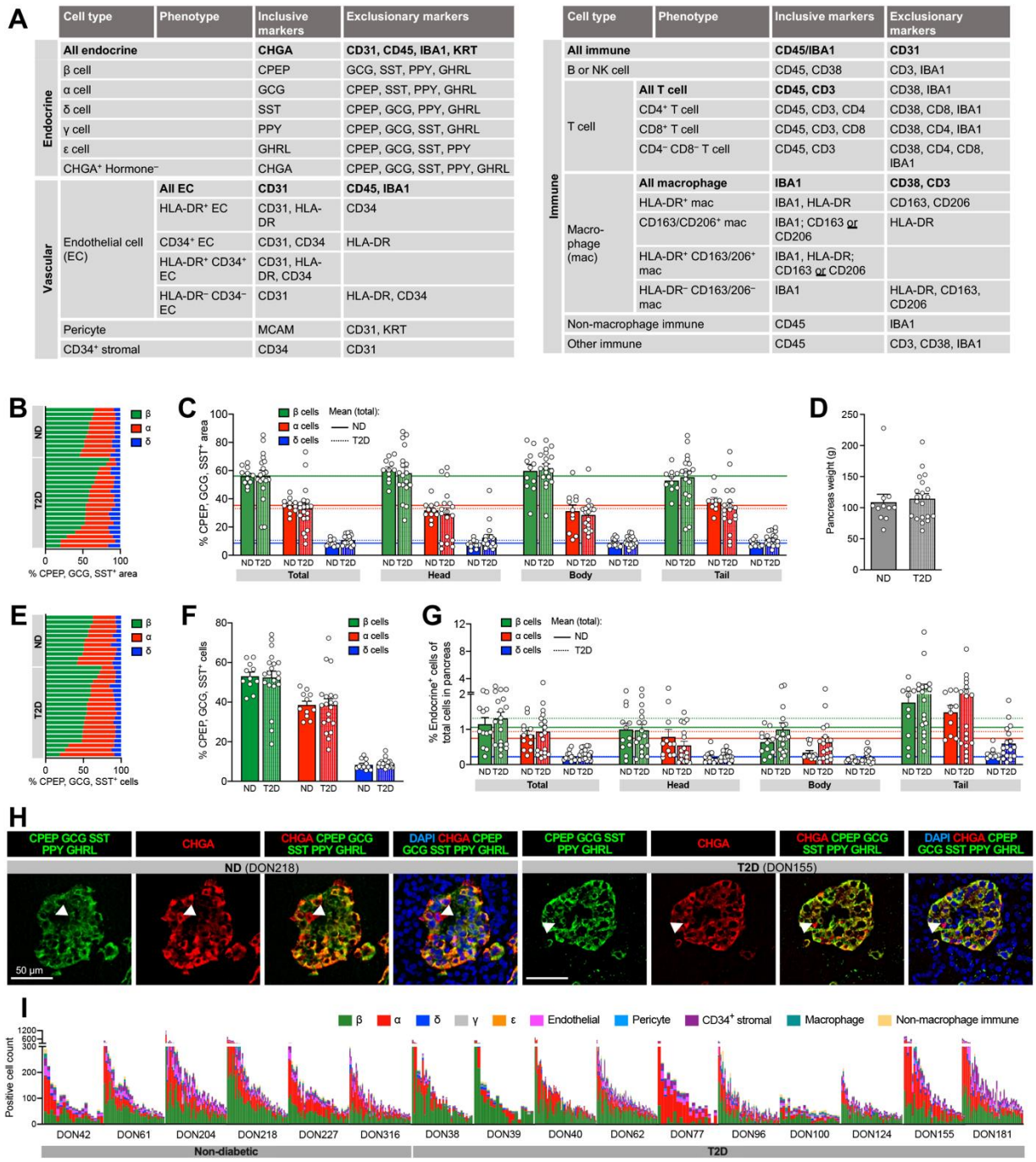

Figure 46. Related to Figure 45. Integrated tissue analysis reveals that endocrine cell abundance is not changed in the short-duration T2D donor cohort.

(A) Cell populations and phenotypes distinguished by the CODEX antibody panel. Positive and exclusionary marker(s) are listed for each major cell type. **(B-C)** Cross-sectional area of β cells (C-peptide; green), α cells (glucagon; red), and δ cells (somatostatin; blue) stratified by individual donor **(B)** or by pancreas region **(C)**. In panel **C**, each dot represents data from one donor (mean >0.75 mm^2 of β, α, or δ cell area analyzed/donor) and horizontal lines (solid, ND;

dotted, T2D) denote mean values for combined analysis (“Total”), enabling comparison of relative enrichment in specific pancreatic regions. **(D)** Pancreas weight measured during organ procurement; used to calculate endocrine cell mass in **Figure 45B**. **(E-G)** Cytonuclear quantification of endocrine cells stratified by individual donor **(E)**, expressed as a proportion of total endocrine population **(F)**, and expressed as percentage of total pancreatic cells (G). In panels **F-G**, each dot represents data from one donor (mean: >13,000 β, α, or δ cells identified from >575,000 pancreatic cells/donor); horizontal lines in panel **G** denote mean values for combined analysis (“Total”), enabling comparison of relative enrichment in specific pancreatic regions. **(H)** Representative images depicting rare cells positive for chromogranin A (red) but negative for all hormones (green) in both ND and T2D islets. Scale bars, 50 μm. Arrowheads denote CHGA+ hormone- cells. **(I)** Abundance of endocrine and non-endocrine cells in ND and T2D islets; each vertical bar is one islet and proportionally colored to represent cell composition. Islets are grouped by donor and ordered from largest (highest total cell number) to smallest. Corresponds to **Figure 45E**.

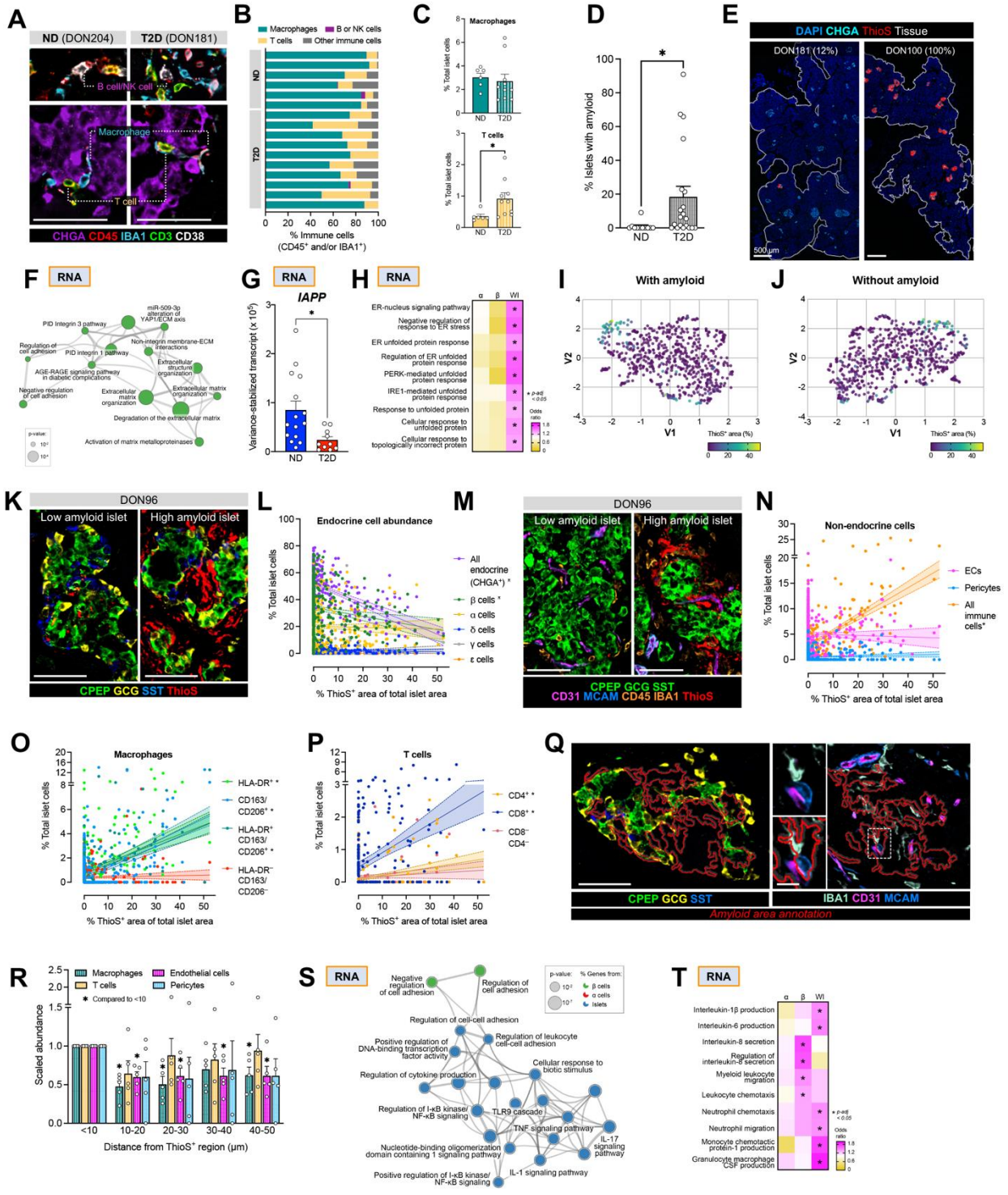

Figure 47. Heavy amyloid burden correlates with decreased endocrine cell abundance, altered endothelial cell phenotype, and increase in immune cells.

(A-C) Immune cells phenotyped by CODEX are shown in both ND and T2D islets (A) and subpopulations are quantified in panels B-C (unpaired t-test, $p<0.05$). Scale bar, 50 µm. **(D)** Assessment of amyloid prevalence [% total islets positive for Thioflavin S (ThioS) regions] in full ND/T2D cohort. **(E)** CODEX images depicting a range of amyloid-laden regions (red

annotations) in islets (chromogranin A, CHGA; cyan) of tissue cross-sections. Percentage in label refers to amyloid prevalence for the given donor. Scale bar, 500 μm. **(F)** Visualization of select pathways enriched for β cell genes (FC≥1.5 and p<0.01, ND vs T2D) generated using Metascape. Terms with Kappa similarity >0.3 are connected by edges, while node size is proportional to enrichment p-value. **(G)** Islet amyloid polypeptide (*IAPP*) RNA transcript is reduced in T2D β cells. **(H)** Heatmap showing select GO terms from RNA Enrich related to protein processing and unfolded protein response; asterisks denote terms with FDR p<0.05 in the respective sample type. **(I-J)** High-dimensional component analysis of islet cell composition, where each dot corresponds to one T2D islet imaged by CODEX. Dot color represents degree of amyloid burden (purple, no amyloid; green to yellow, high amyloid), highlighting the clustering of heavily amyloid-laden islets on the periphery of the clusters, even when amyloid is not used as an input parameter. **(K)** Representative images showing an islet with low amyloid (left) and a high amyloid burden (right) from the same tissue cross-section. Scale bar, 50 μm. **(L)** Scatterplot and linear regression illustrating the relationship between ThioS content (amyloid) and islet endocrine cell abundance at the level of individual islets, as assayed by CODEX. Asterisks denote a statically significant nonlinear slope (correlation) with amyloid. **(M)** Representative CODEX images of low- and high-amyloid islets highlighting vascular endothelial cells (CD31; magenta), pericytes (MCAM; light blue), and immune cells (CD45, IBA1; orange). Scale bars, 50 μm. **(N)** Scatterplot and linear regression of amyloid burden with cell populations depicted in panel M. **(O-P)** Macrophages **(O)** and T cells **(P)** are further stratified by combinatorial expression of various markers, with unique phenotypes significantly associated with amyloid. **(Q)** CODEX image showing the same islet in left and right panels, with ThioS stain (not pictured) indicated by red outline. Left panel shows endocrine cells; right panel shows perivascular and immune cells present at interface of the amyloid region. Scale bar, 50 μm in main panels and 10 μm in inset. **(R)** Quantification of spatial distribution of macrophages (teal bars), T cells (yellow), endothelial cells (magenta), and pericytes (light blue) in relation to ThioS+ regions. Each dot represents data from one donor; cell counts are expressed as percent of total cells within the concentric region (<10 μm from amyloid, 10-20 μm from amyloid, etc.) and scaled to abundance of <10 μm region to account for variability in overall population abundance between donors. **(S)** Magnification of select clusters depicted in **Figure 43L**, where Metascape employed a heuristic algorithm to represent pathway enrichment from differentially expressed genes in β cell, α cell, and islet RNA samples. Node size is proportional to p-value for term enrichment and color represents the corresponding gene list (sample type) from which the term originated. **(T)** Heatmap showing select GO terms from RNA Enrich related to protein processing and immune signaling; asterisks denote terms with FDR p<0.05 in the respective sample type.

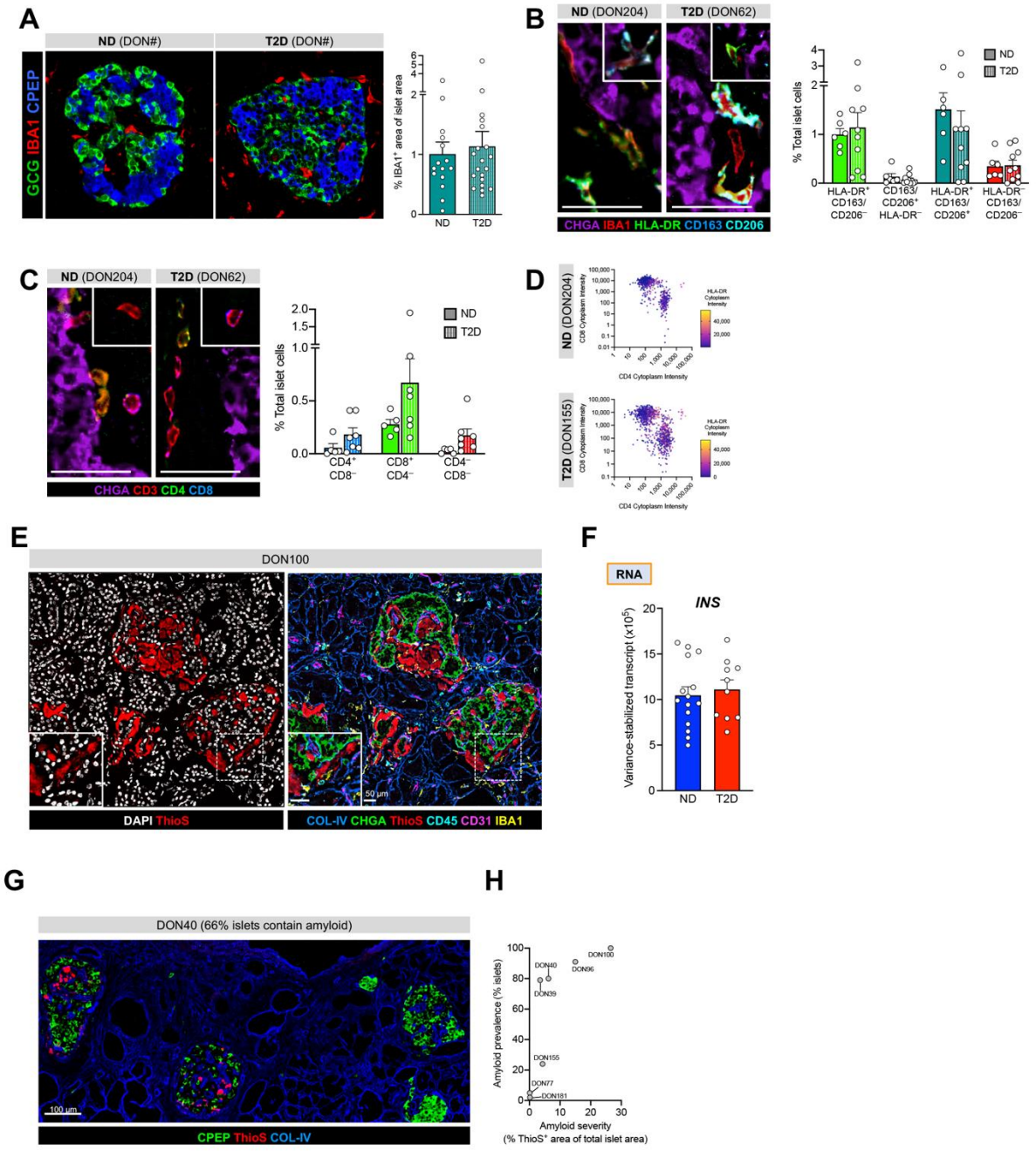

Figure 48. Related to Figure 47. Short duration T2D islets show increases in T cells and increased amyloid deposition.

(A) Representative images (left) and quantification (right) from traditional immunohistochemistry (IHC) detecting macrophages (IBA1; red) in ND and T2D islets. **(B-C)** A 28-plex marker panel enabled immune cell phenotyping by CODEX for macrophages (B) and T cells (C). Images show combinatorial marker expression in islet macrophages (IBA1^{+}) and T cells (CD3^{+}); insets do not correspond to the larger field of view but are included to illustrate phenotypic variety. Scale bars, 50 µm. Right panels quantify each phenotype as a percentage of total cell population. (**D**) Scatter plot showing CD4 and CD8 marker expression within CD3+ cells with

cells colored by expression level of HLA-DR. **(E)** CODEX image from a donor with high amyloid burden (all islets in section were positive for ThioS). Left panel illustrates the relatively acellular region of amyloid aggregates (white, nuclei; red, amyloid). Right panel illustrates the intricate extracellular matrix (collagen-IV, COL-IV; blue), along with remaining endocrine cells (chromogranin A, CHGA; green), vasculature (CD31; magenta), and resident immune cells (CD45, cyan, and IBA, yellow). Scale bars, 50 μm. **(F)** Insulin (*INS*) mRNA transcript is unchanged in T2D β cells. Corresponds to **Figure 47G**. **(G)** Correlation matrix of donor attributes and histological characteristics assayed by traditional immunohistochemistry (IHC), including amyloid prevalence. Asterisks denote statistically significant positive (orange) or negative (green) correlations between to variables. **(H)** Representative traditional IHC image showing proximity of amyloid-containing islets (left two islets shown in field of view) to those devoid of amyloid (right two islets). Scale bar, 100 μm. **(I)** Amyloid prevalence, as assayed by traditional IHC in pancreatic sections from multiple regions, is plotted with quantification of severity (percent of islet area positive for ThioS) as assayed by CODEX.

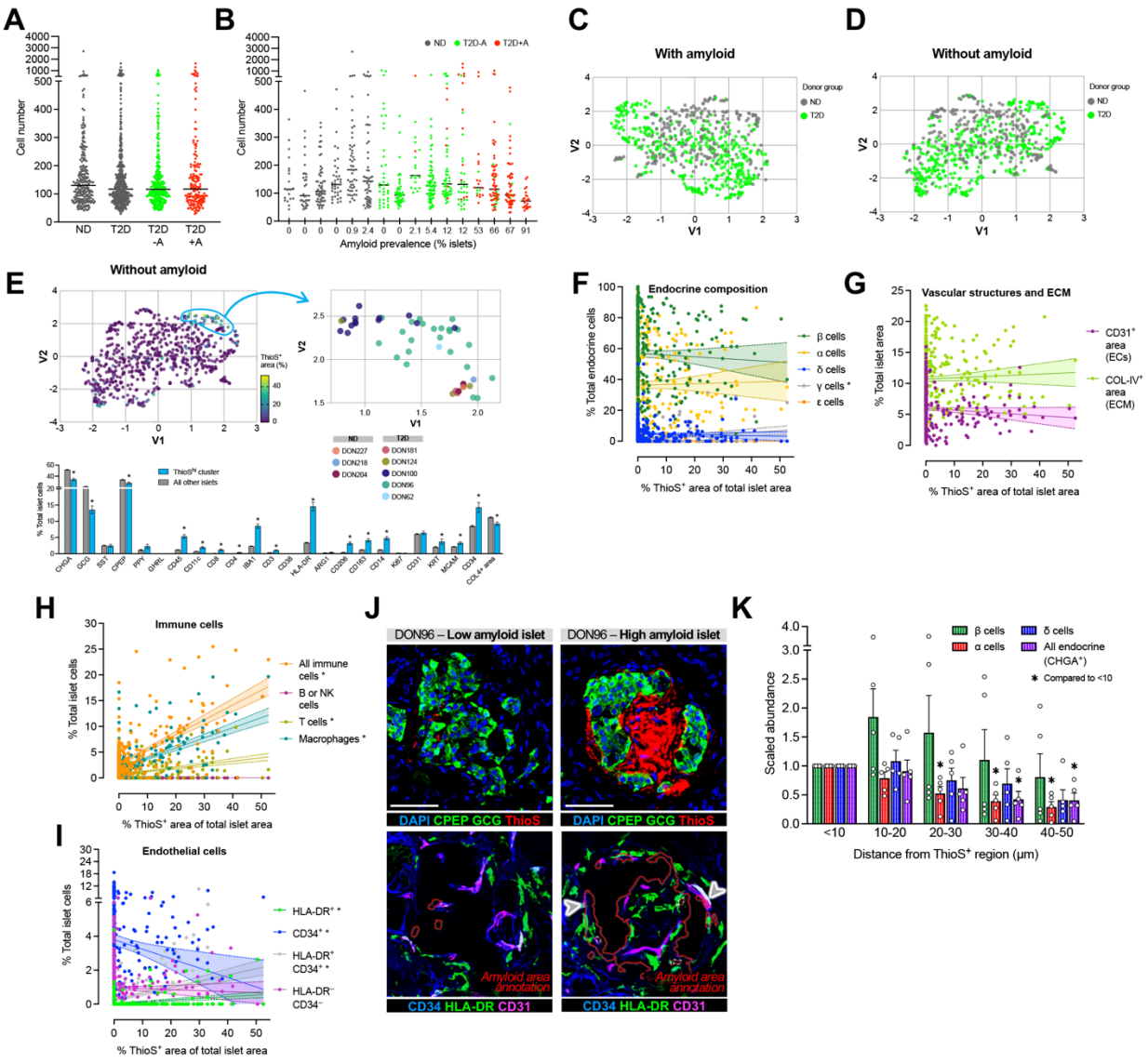

Figure 49. Related to Figure 47. Heavy amyloid burden correlates to decreased endocrine cell abundance, altered endothelial cell phenotype, and increase in immune cells.
(A-B) Distribution of islet size as assessed by cross-sectional cell number. Islets are grouped by disease and amyloid status (**A**) and by individual donor (**B**). "T2D" encompasses all islets from T2D donors and then the same islets are stratified by whether they are amyloid negative ("T2D-A") or amyloid positive ("T2D+A"). Islets containing amyloid are shown in red. **(C-D)** High-dimensional component analysis of islet cell composition, corresponding to data shown in Figure 4I-4J. Dot color indicates disease status. (**E**) Zoom in of high amyloid cluster of and representation of the donor islets which represent the cluster as well as average proportion of cell markers in that cluster versus all other islets. **(F-G)** Scatterplots showing association of amyloid burden with islet endocrine composition **(F)** and vascular and ECM compartments **(G)**. In panel **F**, individual endocrine cell populations are expressed as a percentage of total endocrine cells rather than percentage of total islet cells to normalize for the endocrine cell loss observed with increased amyloid (see **Figure 47L**). Asterisks denote a statically significant

nonlinear slope (correlation) with amyloid (ThioS). (H) Scatter plot and linear regression of all immune cells and then broken down into specific immune cell types showing association with amyloid burden. **(I-J)** Vascular phenotypes in low- and high-amyloid islets from the same donor, as assayed by CODEX. Top images panels show endocrine area (C-peptide and glucagon; green) co-registered with amyloid (ThioS; red). Bottom image panels are identical fields of view but show endothelial cells (CD31; magenta) and cell surface markers CD34 (blue) and/or HLA-DR (green). Amyloid area seen in top panels is annotated by red outline in bottom panels to enable visualization of vascular cells. Arrows point to endothelial cells co-expressing CD34 and HLA-DR in high-amyloid islet. Scale bars, 50 μm. The phenotypic shift of endothelial cells with amyloid is quantified in panel **I**. **(K)** Spatial distribution of endocrine cells in relation to ThioS+ regions, corresponding to data in **Figure 47R**. Each dot represents data from one donor; cell counts are expressed as percent of total cells within the concentric region (<10 μm from amyloid, 10-20 μm from amyloid, etc.) and scaled to abundance of <10 μm region to account for variability in overall population abundance between donors. Asterisks denote significant decrease in density compared to <10 μm of ThioS+ region.

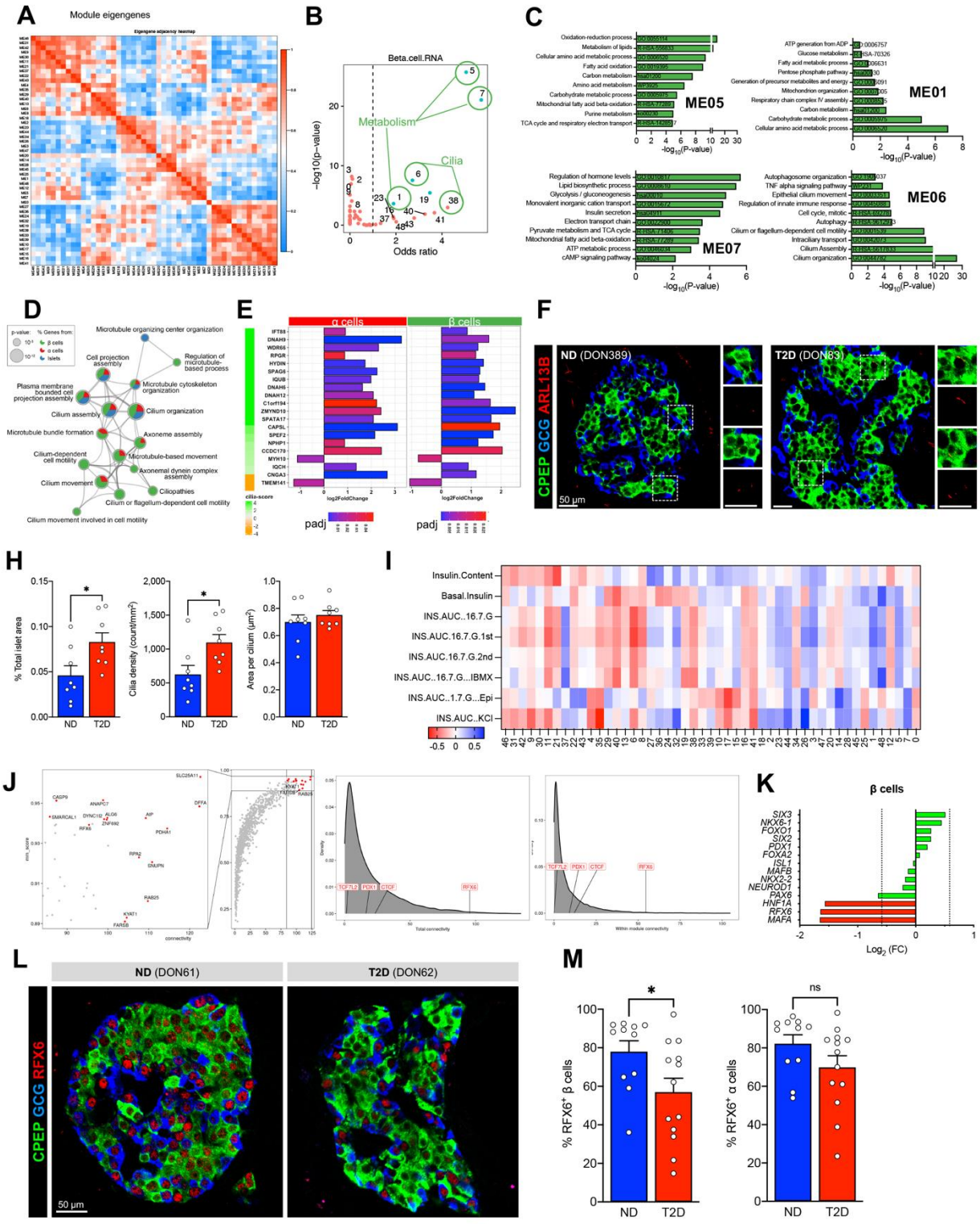

Figure 50. Gene network analyses on sorted β cell identify disrupted cilia homeostasis and highlight RFX6 as a highly connected hub gene that is reduced in T2D β cells.
(A) Heatmap of similarity between module eigengenes by Spearman correlation. **(B)** Scatterplot of enrichment for differentially expressed genes (FDR 1%) in module gene lists with annotation

of major categories. **(C)** Module exploration by pathway enrichment to identify defining features of unique modules. **(D)** Magnification of select clusters depicted in **Figure 43L**, where Metascape employed a heuristic algorithm to represent pathway enrichment from differentially expressed genes in β cell, α cell, and islet RNA samples. Node size is proportional to p-value for term enrichment and color represents the corresponding gene list (sample type) from which the term originated. **(E)** Fold change for differentially expressed genes in a validated database of genes related to cilia formation and homeostasis. Genes are ordered by CiliaCarta score (green-orange heatmap), with fold change plotted and bars colored by adjusted p-value (red-blue heatmap). **(F)** Confocal images of islet cilia in ND and T2D sections (CPEP, green; GCG, blue; ARL13B, red). Insets show individual cilia. Scale bars, 50 μm. **(H)** Quantification of cilia area, density, and size. **(I)** Heatmap of Spearman correlation of module eigengenes to insulin secretory functional parameters from Figure 1. **(J)** Module membership, total connectivity, and within module connectivity for each gene in WCGNA analysis with select genes called out. **(K)** Fold change of key islet-enriched transcription factors in FACS-purified β cells. Vertical line represents fold change of 1.5 and red color indicates meets threshold of FDR>0.01.
(L) Confocal images of RFX6 expression in ND and T2D sections (CPEP, green; GCG, blue; RFX6, red). Scale bar, 50 μm. **(M)** Quantification of % of β and α cells with nuclear positivity for RFX6 stain. * $p<0.05$. Error bars indicate SEM. Panels **H** and **M** were analyzed by two-tailed t-test.

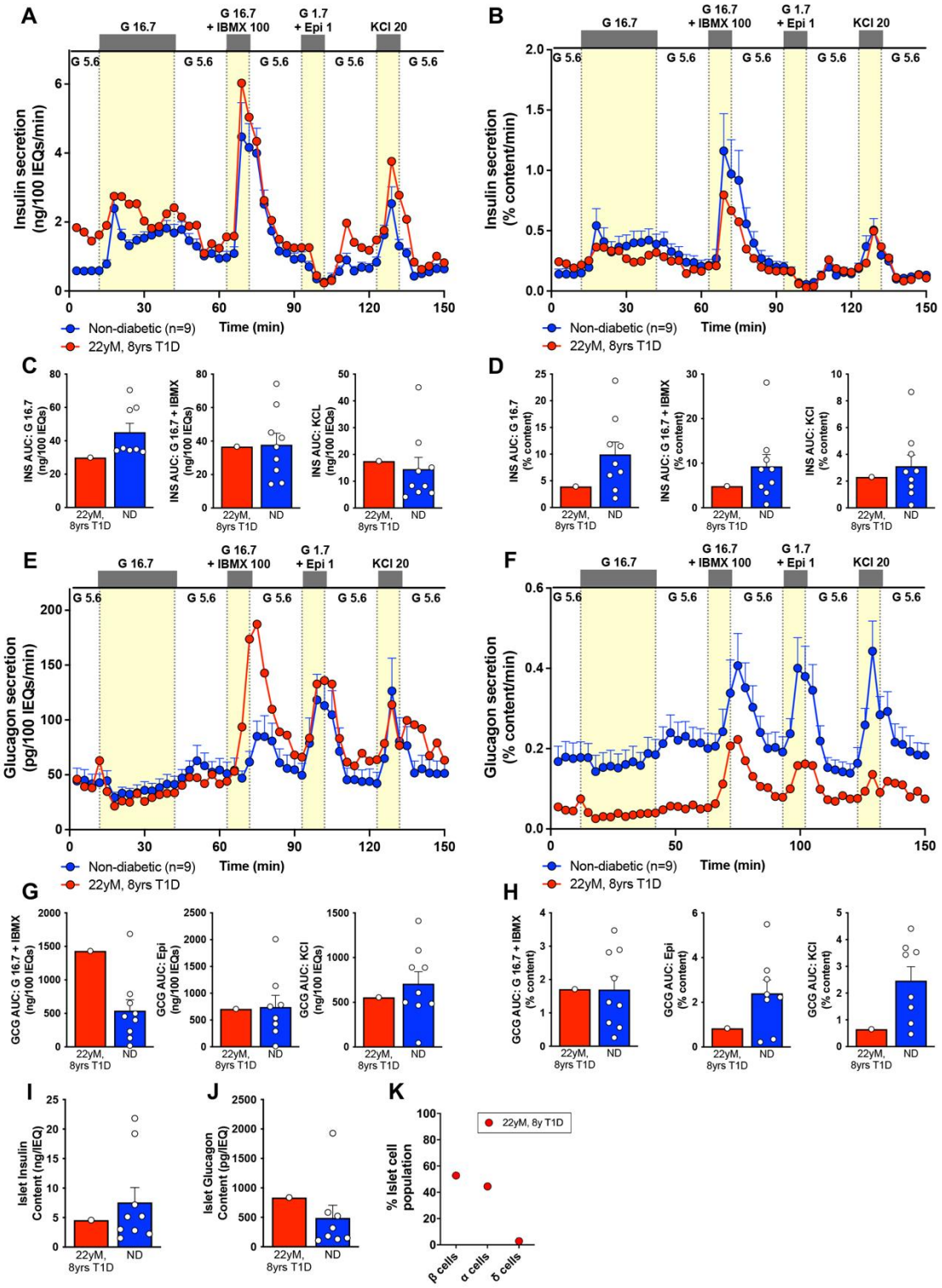

Figure 51. Pancreatic islets isolated from pancreas of 22-year-old donor with 8 years of type 1 diabetes (T1D) had surprising dynamic insulin secretion and substantial insulin content.

(**A-B**) Insulin secretion measured in islets isolated from 22yM-8y T1D (red) pancreas compared to controls without diabetes (blue) normalized to overall islet insulin cell volume as expressed by

islet equivalent (IEQ) (**A**) or by % insulin content (**B**); G 5.6 – 5.6 mM glucose; G 16.7 – 16.7 mM glucose; G 16.7 + IBMX 100 – 16.7 mM glucose + 100 μM isobutylmethylxanthine (IBMX); G 1.7 + Epi 1 – 1.7 mM glucose + 1 μM epinephrine; KCl 20 – 20 mM potassium chloride. (**C-D**) Integrated insulin secretion was calculated as area under the curve (AUC) for the following secretagogues G 16.7, G 16.7 + IBMX 100, and KCl 20 calculated from the IEQ trace (**C**) or the % content trace (**D**). (**E-H**) Glucagon secretion from the perifusion described in **A** normalized to IEQ (**E**) or % glucagon content (**F**) and integrated glucagon release as area under the curve from basal glucagon release for secretagogues G 16.7 + IBMX, G 1.7 + Epi 1, and KCl 20 for the IEQ trace (**G**) and % content trace (**H**). (**I-J**) Islet insulin (**I**) and glucagon (**J**) content compared to donors without diabetes. (**K**) Endocrine cell populations in dispersed isolated pancreatic islets from this donor contained 52.7% beta cells, 44.4% alpha cells, and 2.7% delta cells. Normal control islets collected by this method had a range of 53.4±2.6% beta cells, 38.5±2.7% alpha cells, and 7.5±0.9% delta cells[566]. Results of the non-diabetic samples are expressed as mean ± standard error of the mean.

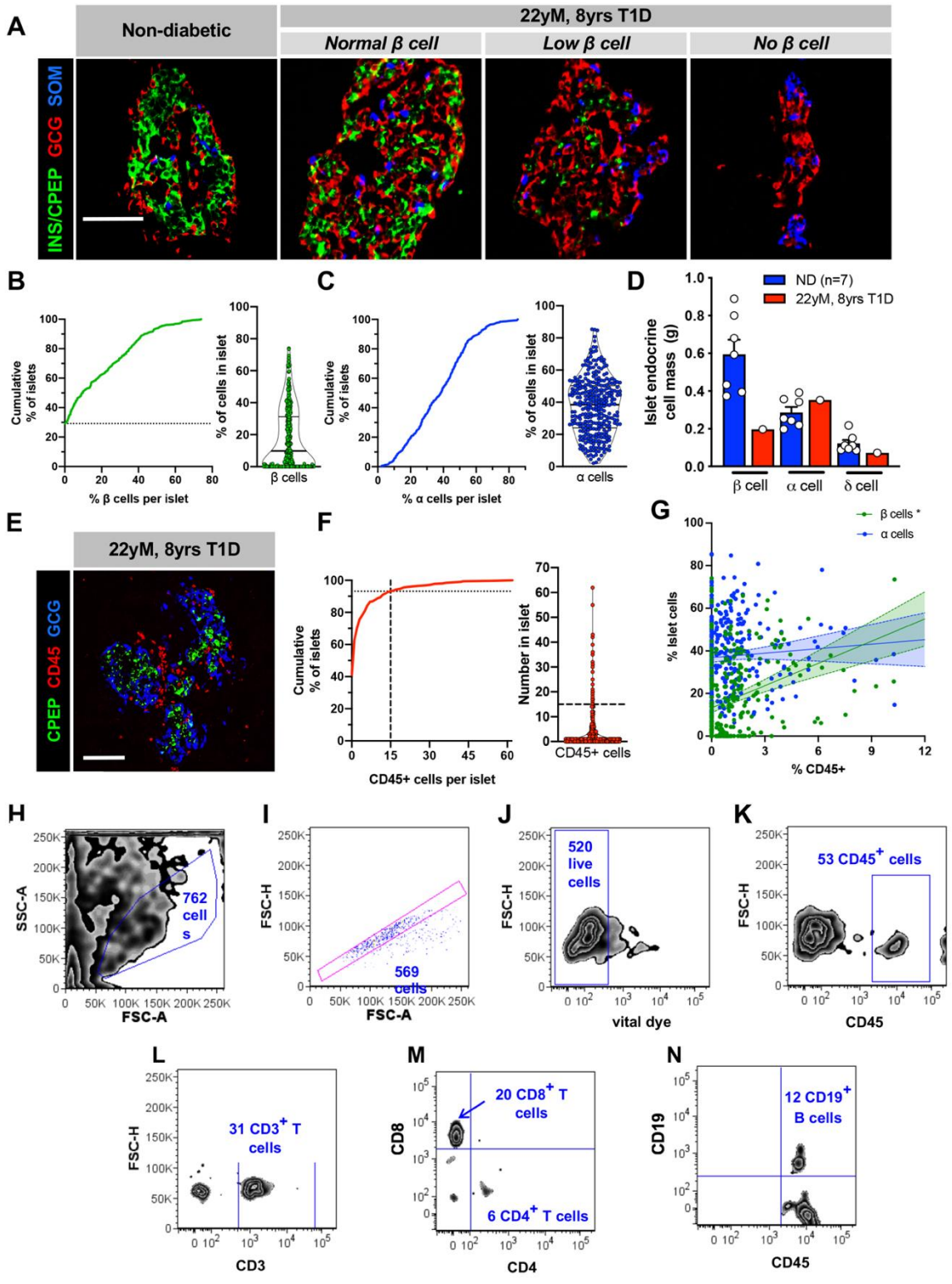

Figure 52. Histological evaluation of pancreatic tissue and islets reveals endocrine and immune characteristics of T1D.

(**A**) Expression of insulin (INS) or C-peptide (CPEP), glucagon (GCG), and somatostatin (SOM) in the donor's pancreatic tissue compared to a normal non-diabetic islet. Representative islets of

varying beta (β) cell numbers from donor are shown. Scale bar – 50 μm. (**B-C**) Cumulative distribution and violin plot of % beta cells (**B**, green) per islet, % alpha cells (**C**, blue). Dashed line in **B** denotes nearly 30% of islets were devoid of all beta cells. (**D**) Beta, alpha (α), and delta (δ) cell mass (grams) in donor pancreas compared to controls. Each data point represents the average mass across the combined pancreatic head, body and tail regions of each donor. (**E**) Representative islet (CPEP – green, GCG – blue) from donor showing significant immune cell (CD45 – red) infiltration. Scale bar – 50 μm in **E**. (**F**) Cumulative distribution and violin plot of number of CD45+ cells per islet. Intersection of dashed lines in **F** indicates approximately 7% of islets (n=311 islets evaluated) with 15 or greater CD45+ cells. (**G**) Correlation of % CD45+ cells versus % CPEP+ or % GCG+ cells in 311 islets reviewed from this donor analyzed by simple linear regression. (**H**) One hundred hand-picked whole islets from this donor were dissociated with enzyme and immediately stained with a viability dye and T-cell specific markers that were detected by flow cytometry. The lymphocyte gate was then gated for (**I**) single cells, (**J**) viable cells, and **(K**) CD45+ cells. These CD45+ cells were then interrogated for (**L**) CD3+ T cells, which were evaluated for the subpopulations of (**M**) CD8+ and CD4+ T cells, and for (**N**) CD19+ B cells.

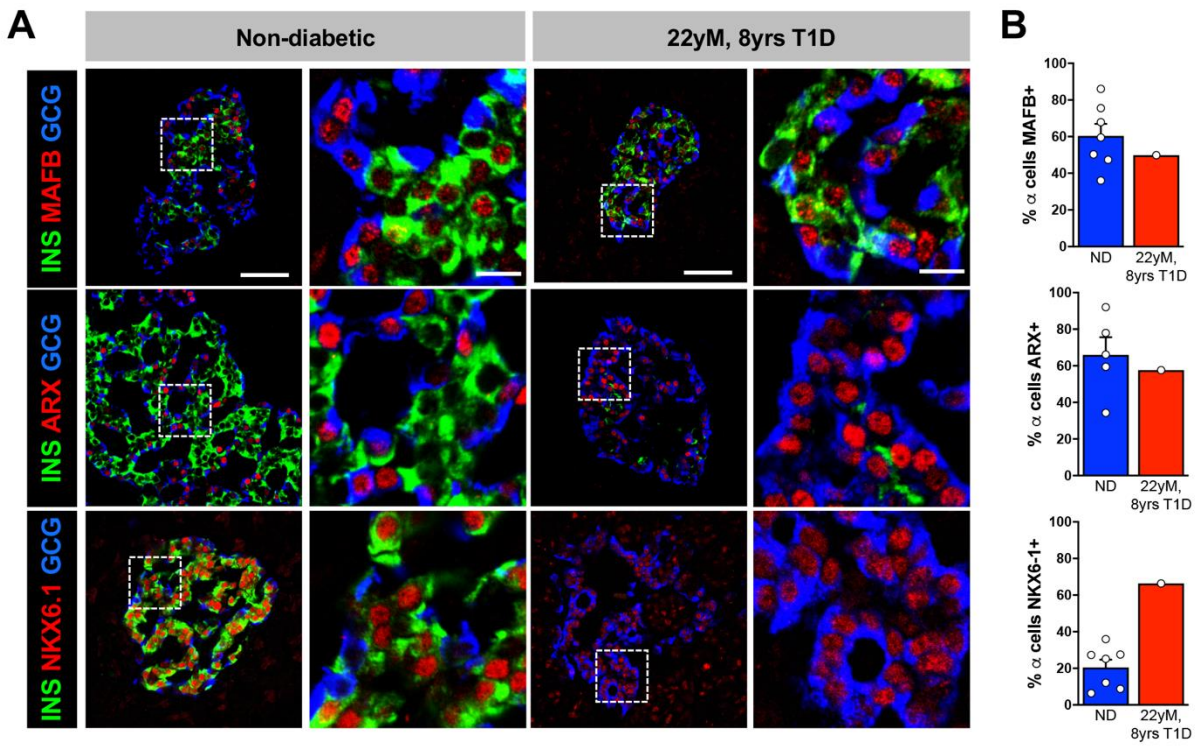

Figure 53. Alpha cells show misexpression of NKX6.1.
(**A-B**) Immunohistochemistry (**A**) for expression of nuclear markers MAFB, ARX, and NKX6.1 and quantified (**B**) compared to the appropriate controls. Scale bars in **A** represent 50 μm with corresponding inset scale bar 10 μm.

CHAPTER VI:
ROLE OF TRANSCRIPTION FACTORS IN α AND β CELL IDENTITY AND FUNCTION

Some text and data in this chapter have been adapted from Shrestha, Saunders, Walker et al.[561], and Walker, Saunders, Rai et al. (manuscript in preparation).

Introduction

Pancreatic islets are cell clusters dispersed throughout the pancreas, composed primarily of endocrine cells that coordinate glucose homeostasis. Islet β cells secrete insulin which acts to lower blood glucose and α cells secrete glucagon which acts to raise blood glucose. In addition to α and β cells, cooperative interaction of less prevalent endocrine cells (δ, γ, and ε) and non-endocrine cell populations in the islet microenvironment, including endothelial cells, macrophages, pericytes (stellate cells), nerve fibers, and immune cells, provide additional signals to modulate islet function[761]. Islet α and β cells are characterized by the precise expression of transcriptional and signaling machinery that allows sensing and integration of glucose, nutrient, and neurohormonal signals resulting in proportional hormone secretion. Importantly, pancreatic islet dysfunction through impaired insulin and/or glucagon secretion is a hallmark of most forms of diabetes[762–765]. Thus, identifying key factors and molecular pathways governing α and β cell identity and function is crucial to understanding, treating, and preventing diabetes.

One set of important molecules governing α and β cell identity and function are islet-enriched transcription factors (TFs) that have been shown to have important roles in both islet development as well as in the maintenance of the islet cell phenotype, particularly in mouse and islet-like cells derived from human stem cells[766–769]. Importantly, several islet-enriched TFs have species differences between human and mouse, highlighting the need to closely investigate transcription factors in human systems[770,771]. For example, members of the Maf transcription factor family show differences in cell type distribution and timing of expression[772,773]. Such TFs interact in complexes and networks to exert broad control over cellular processes, making them foundational regulators of cell states. In fact, in addition to their coordinated role in islet cell development, loss or misexpression of key TFs has been highlighted in numerous forms of diabetes[774–777].

Importantly, with advances in scientific methodologies, it has been increasingly recognized that islet cells are heterogeneous. This is particularly apparent in β cells, where recent work has shown human β cell heterogeneity in function[592], cell surface protein expression[778,779], and transcriptomic profile[780,781]. In contrast, heterogeneity within human α cells has been much less studied. Given the central role for islet-enriched TFs play in regulating cell states, potential heterogeneity in these TFs may represent distinct cellular states with broad implications for human islet biology and diabetes.

To investigate how heterogeneity of islet-enriched TFs in human islets relates to islet function, we focused on transcription factors that play important roles in islet cell development and

disease as suggested by existing bulk RNA-seq datasets, namely *ARX*, *MAFB*, *MAFA*, and *RFX6*[770,777,782,783]. To study ARX, MAFB, and MAFA, we generated a scRNA-seq dataset of over 40,000 islet cells from adult donors, which includes endocrine, immune, and endothelial cell populations, that is accessible through a user-friendly web portal. This dataset provided sufficient cell numbers to classify α and β cells into subgroups based on combinatorial *ARX*/*MAFB* and *MAFA*/*MAFB* expression, respectively, and allowed us to identify key correlates to α and β cell function. We further validated the existence of these cell populations within human pancreatic tissue *in situ* and linked *MAFA*/*MAFB* transcriptional heterogeneity of human β cells to their electrophysiological properties. To study RFX6, we utilized adenoviral delivery of shRNA to knockdown RFX6 in β cells of pseudoislets. This approach allowed us to directly study the effects of reduced *RFX6* expression on pseudoislet cell composition and function.

Results

Transcriptional and immunohistochemical profiling of human α and β cells suggests a role for key transcription factors ARX, MAFA, and MAFB in islet cell development and disease

Both *in vivo* and *in vitro* studies have helped identify TFs with cell-specific expression patterns in islets. In mouse α cells, Aristaless Related Homeobox (ARX) factor is essential for α cell differentiation and function, a finding which has been confirmed in human α cells[768,784–786]. Indeed, *ARX* transcripts are heavily enriched in α cells (**Figures 54A-54B and 55A-55B**)[772,787,788]. Of note, α cells from donors with type 1 diabetes (T1D) show decreased *ARX* expression compared to α cells from nondiabetic donors (ND) (**Figure 54C**), indicating that this factor may contribute to impaired glucagon secretion observed in T1D[594].

MAFA is a *bona fide* β cell factor exerting direct control over both insulin expression as well as key components of glucose-stimulated insulin secretion, and it is expressed relatively late in β cell development, making it a commonly used marker of fully mature β cells[789–791]. MAFA is thought to play a broadly similar role in adult mouse and human β cells, and existing RNA-seq datasets underscore its β cell specificity (**Figures 54A-54B** and **55A-55B**). MAFA is clearly present in adult β cells but its expression actually does not peak until several years after birth, as illustrated by previous histological studies[772] and transcriptomic profiles of β cells from fetal versus adult donors (**Figure 54D**)[782]. This increase in MAFA levels temporally correlates with the acquisition of increased glucose sensitivity[792–794], suggesting that MAFA plays a role in β cell maturation and function.

In contrast to ARX and MAFA, MAFB is expressed by both α and β cells (**Figures 54A-54B** and **55A-B**) and shows significant species differences: it is retained in human β cells during adulthood, while in rodents it becomes restricted to α cells in the early postnatal period[771]. Of note, the MAF factors are thought to be capable of forming both homo- and heterodimers[795], providing an opportunity for synergy between MAFA and MAFB in β cells. In α cells, MAFB is known to directly bind to the *GCG* promoter to regulate glucagon expression[796], rendering it an important regulator of α cell function. Like *ARX*, *MAFB* is reduced in α cells from donors with T1D (**Figure 54C**).

The unique and dynamic expression patterns of *ARX*, *MAFA*, and *MAFB* demonstrated by bulk RNA-seq (**Figures 54A-54D** and **55A-55B**) suggest that these TFs are linked to key aspects of α and β cell function. However, our analysis of their specific distribution in adult human pancreatic tissue revealed that not all α or β cells in a given islet express them (**Figures 54E** and **55C-55D**). Thus, to further understand the role of these TFs, we sought to determine the cell-to-cell variability that cannot be discerned from a pooled cell population profiled by bulk RNA-seq. Given the known importance of TFs in regulating cellular processes, we hypothesized that TF heterogeneity at the single cell level could define α or β cell subtypes with different functional properties.

scRNA-seq reveals heterogenous transcription factor expression in α and β cells

One major advantage of scRNA-seq is its ability to dissect heterogeneous cell composition within and across cell types. However, because some subpopulations are relatively rare, robust datasets are required to sufficiently characterize these populations. In this study, we obtained 44,953 high-quality single cell transcriptomes of hand-picked islets from n=5 healthy donors with robust dynamic insulin and glucagon secretion profiles characterized by perifusion to ensure healthy and functional cells were being assessed (**Table 3** and **Figure 56A**). Graph-based unsupervised clustering[588] reliably detected major endocrine cell types (α, β, δ) and also acinar, ductal, stellate, endothelial, and immune cells (**Figure 57A**). Clusters were annotated to identify cell types, including rare populations such as γ and ε, using markers listed in **Table 11** and identified cell types were represented in each donor (**Figure 56B**). Cell populations were confirmed by the specific expression of additional known identity markers (**Figure 57B**). Within cell types, the expected clustering by individual donor (**Figure 56C**) is apparent. To facilitate the exploration of this robust single cell dataset, we created an online application that allows one to browse single cell gene expression by both the cell type and donor (**Figure 56D**).

To investigate the cell-specific signatures of human α and β cells, we analyzed expression patterns of canonical islet-enriched TFs. *PAX6*, *RFX6*, *NEUROD1*, and *NKX2-2* were expressed in all endocrine cell types, whereas *PDX1*, *NKX6-1*, and *MAFA* were enriched in β cells, *IRX2* was specifically expressed in α cells, and *ARX* was expressed in α, γ, and ε cells, consistent with previous single cell studies[588,590,591] (**Figure 57C**). *PAX6*, *NEUROD1* and *MAFB* were among the most prevalent endocrine factors, expressed in >75% of both α and β cells (**Figure 57C**). Of particular interest, *MAFB* – known in humans to be expressed in both α and β cells – is also enriched in the immune cell population, which had been overlooked in previous studies due to low abundance of immune cells in isolated islets. Interestingly, we noticed that each of these key TFs had a bimodal distribution, meaning there was a clear subpopulation of cells without detectable expression of each factor (**Figure 57D**), consistent with our observations for MAFA, MAFB and ARX in pancreatic tissue (**Figure 54E**). Given the crucial role islet-enriched TFs play in islet cell identity and function, particularly when acting in TF regulatory networks, we thus hypothesized that combinations of key TFs would identify important islet cell subtypes.

Heterogeneity of ARX and MAFB expression in α cells by scRNA-seq predicts expression of key α cell functional genes

Since both ARX and MAFB are downregulated in α cells from donors with T1D[777], we tested the hypothesis that these factors cooperatively regulate α cell function. We first confirmed heterogeneous *ARX* and *MAFB* expression in α cells from all five donors (**Figure 58A**)**.** Of 24,248 total α cells, we identified populations of α cells without *ARX* or *MAFB* expression ("None;" 10%), populations expressing only *ARX* or only *MAFB* (4% and 48%, respectively), and a population co-expressing both *ARX* and *MAFB* ("Both;" 38%) that were relatively stable across all five donors (**Figure 58B**). For these four populations, we investigated expression of other islet-enriched TFs, α cell-enriched genes, and genes related to ion flux, glucose metabolism, vesicle trafficking, exocytosis and cell stress (**Figures 58C** and **59**). Interestingly, we observed that numerous α cell-enriched TFs (*RFX6*, *PAX6*, *NEUROD1*, *ISL1*, *IRX2*) and genes related to nutrient sensing or glucagon secretion (*ACLY*, *PKM*, *GSTA4*, *GPX3*, *G6PC2*, *KCTD12*, *KCNK16*, *KCNJ6*, *ABCC8*) were elevated in α cells co-expressing *MAFB* and *ARX* compared to the other populations, while genes related to cell stress (*DDIT*, *ATF4*) were highest in the "None" group, suggesting that presence of both factors may support increased metabolic activity and glucagon secretory capacity. To confirm these findings, we analyzed three additional scRNA-seq datasets of human islets that utilized different single cell technologies[590–592] and found the results to be consistent (**Figure 60A**).

We next asked whether *ARX*/*MAFB* heterogeneity existed at the protein level given the known differences that exist between transcript and protein expression[797]. To assess this, we performed immunohistochemical analysis of ARX and MAFB on pancreatic tissue sections from nondiabetic donors (**Figures 58D** and **60B**). Cells were classified by automated algorithm for "low" or "high" ARX and MAFB expression, setting an intensity threshold that remained consistent across all islets from a given tissue. By this measure, all four combinations of ARX/MAFB-expressing α cells were detected in each donor evaluated: ARX^{lo} $MAFB^{lo}$ (41%), ARX^{hi} $MAFB^{lo}$ (19%) ARX^{lo} $MAFB^{hi}$ (9%) and ARX^{hi} $MAFB^{hi}$ (30%) (**Figure 58E**). Taken together, our results indicate the presence of α cell subpopulations classified according to unique and conjunctional expression of ARX and MAFB and suggest that combined expression of these two markers likely identifies highly functional and mature α cells.

β cells co-expressing MAFA and MAFB exhibit characteristics of enhanced secretory function

Given the ability of MAFA and MAFB to heterodimerize[795] and the unique expression changes during β cell maturation[770,772,782], we hypothesized that MAFA and MAFB co-expression represents a unique subpopulation of human β cells. To test this, we resolved 11,034 β cells into subgroups that expressed only *MAFA* or only *MAFB* (4% and 52%, respectively), β cells that co-expressed both *MAFA* and *MAFB* ("Both;" 22%), and β cells with undetected expression of *MAFA* and *MAFB* ("None;" 21%) (**Figure 61A-61B**). We assessed these groups for the same set of key cellular identity and functional genes described above for α cells, and we saw a general trend of increased expression of key functional genes with dual *MAFA* and *MAFB* expression (**Figures 61C** and **62**). Specifically, numerous genes related to cell identity (*PDX1*, *PAX6*, *NEUROD1*, *ISL1*, *PCSK1*, *IAPP*), glucose metabolism (*ACLY*, *G6PC2*, *GPX3*), ion

channels (*ABCC8*, *KCNJ6*), and exocytosis (*VAMP2*, *SYT7*, *PCLO*, *TSPAN7*, *RGS9*, *FAM159B*, *BMP5*) were all increased in MAFA and MAFB co-expressing cells compared to other subgroups. In contrast, stress genes (*HSPA5*, *HERPUD1*, *DDIT3*, *ATF4*) were either significantly reduced in the co-expression group or significantly elevated in the "None" group. These expression patterns indicate that presence of both factors may be crucial for increased metabolic activity and insulin secretion. Analysis of three independent single cell studies of human islets utilizing other platforms[590–592] confirmed these results (**Figure 63A**). The presence of β cell MAFA/MAFB heterogeneity at the protein level ($MAFA^{lo}$ $MAFB^{lo}$, 46%; $MAFA^{hi}$ $MAFB^{lo}$, 8%; $MAFA^{lo}$ $MAFB^{hi}$, 29%; $MAFA^{hi}$ $MAFB^{hi}$, 16%) was validated by immunohistology in pancreatic sections, where cells representative of all four populations were identified in each of multiple non-diabetic donors (**Figures 61D-61E** and **63B**).

To determine whether the β cell subpopulation co-expressing *MAFA* and *MAFB*, enriched for numerous genes related to metabolism and hormone secretion, had functionally relevant consequences compared to other β cells, we utilized human Patch-seq data from Camunas *et al.*[592]. Transcriptomes from 194 β cells within this dataset (**Figure 64A**) showed high similarity with our larger dataset of 11,034 β cells (**Figures 61C**). In addition to producing an mRNA profile, the Patch-seq approach captures an electrophysiological profile of each cell, generating linked data on cell size, exocytosis, and ion channel currents. In agreement with transcriptome data, β cells that co-expressed both *MAFA* and *MAFB* showed increased electrophysiologic activity across several parameters including early exocytosis, early and late Ca^{2+} current, and late Ca^{2+} conductance when compared to cells that expressed *MAFA* only, *MAFB* only, or neither factor (**Figure 64B**). Of note, *MAFA*/*MAFB* co-expressing β cells are comparable in size to those expressing only one or neither factor, suggesting that neither the transcriptomic data nor the elevated electrophysiologic activity can be attributed to larger cells expressing more genes (**Figure 64B**). Thus, these data provide strong support that heterogeneous populations of β cells on the basis of combinatorial MAFA/MAFB expression exist and that co-expression of both factors marks β cells with elevated function.

RFX6 controls stimulated insulin secretion in human β cells

In results described in Chapter V of this Dissertation, RFX6 was highlighted as a highly connected and differentially regulated gene controlling transcriptional changes in short-duration T2D β cells. Therefore, we hypothesized that RFX6 is required for normal function of adult human β cells. In addition to the single cell studies highlighted above, a complementary approach to assess the role of transcription factors in human islet cell identity and function is to use genetic modification in the pseudoislet system described in Chapter IV of this Dissertation. Therefore, we approached this by using shRNA knockdown of RFX6 in human pseudoislets (**Figure 65A**).

Both scramble shRNA and RFX6 shRNA pseudoislets formed with similar size and morphology (**Figure 65B**). The mCherry fluorescent tag in the adenovirus was highly enriched in β cells (>90% of β cells transduced) compared to α cells (<50% of α cells transduced) within the pseudoislets of both groups (**Figure 65C**). The higher β cell transduction efficiency allowed for preferential targeting of β cells similar to T2D while leaving a majority of the α cells unaltered.

Indeed, β cell specific knockdown of *RFX6* was approximately 60% (**Figure 65D**). This reduction in *RFX6* did not lead to a reduced proportion of β cells in the pseudoislet as measurement by C-peptide immunolabeling (**Figure 65E-65F**), suggesting that at this time point (6 days), reduced RFX6 expression does not lead to β cell death or loss of β cell identity. In order to evaluate the effect of RFX6 knockdown on β cell function, we assessed dynamic insulin secretion in the presence of three secretagogues to which T2D islets had significantly blunted insulin response (high glucose, cAMP, and KCl). Similar to T2D islets, RFX6 shRNA pseudoislets showed reduced stimulated insulin secretion in response to all three stimuli compared to the scramble shRNA pseudoislets (**Figure 65G-65H**). These results highlight that RFX6 controls stimulated insulin secretion in human β cells and plays a critical role in T2D β cell dysfunction.

Discussion

Islet-enriched TFs are dysregulated in numerous important processes in islets and as such understanding how these transcription factors work in human α and β cells is of great value. By transcriptional profiling and assessment of protein expression at the single cell level, we found that several key islet-enriched TFs important for α and β cell maturity and function had a heterogenous expression pattern within normal adult human islet cells. To study this heterogeneity, we generated a large scRNA-seq dataset and stratified α and β cells based on differential or combined expression of key TFs (*ARX*/*MAFB* in α cells; *MAFA*/*MAFB* in β cells) that are thought to act cooperatively. We found that co-expression of these TF combinatorial pairs predicted greater expression of genes related to glucose metabolism, ion flux, and hormone secretion, including both known α and β cell functional markers and those not extensively studied in islets. Importantly, we identified subpopulations with TF heterogeneity at the protein level by spatial analysis of normal human tissue and demonstrated, using Patch-seq, greater electrophysiological activity in *MAFA* and *MAFB* co-expressing β cells. These results suggest that combinatorial expression of key islet TFs defines highly functional and mature α and β cells.

Though it is widely appreciated that numerous TFs act in protein complexes to regulate cellular identity and function, the significance of their heterogenous expression for maintaining identity and function has not been explored. Building on the strength of scRNA-seq to resolve cell heterogeneity, we explored numerous islet-enriched TFs and found bimodal distribution patterns that suggest the presence of unique combinatorial profiles. In this chapter, we investigated expression patterns of three TFs with known changes in islet cell development and diabetes: α cell-specific *ARX*, β cell-specific *MAFA*, and *MAFB*, which is expressed in both α and β cells and has a unique expression profile compared to rodent islets. Interestingly, other islet-enriched TFs, including *RFX6*, were consistently elevated in *ARX*/*MAFB* co-expressing α cells and *MAFA*/*MAFB* co-expressing β cells, supporting the concept of islet-enriched TFs acting in self-regulating networks, and making it likely that combinatorial profiles of other TFs will also reveal interesting populations with functional consequences. Larger datasets and network-based approaches considering additional TF combinations should be used to examine more complex expression patterns and how these patterns change in T1D and T2D islet cells.

Our data suggest that *ARX*/*MAFB* co-expressing α cells and *MAFA*/*MAFB* co-expressing β cells have elevated expression of functional genes compared to cells that express only one or neither factor. Nonetheless, elevated expression for certain genes in single TF-expressing populations (*e.g.*, *MDH2* and *KCNMA1* in *MAFB*-expressing β cells) may provide insight on how these individual TFs act in each cell type. Indeed, a comparison of our data to molecular studies of these TFs in mice or human stem cells reveals numerous similarities. For example, our data demonstrate that *MAFA*/*MAFB* co-expressing β cells are distinct from populations that express only a single TF which suggests that although these factors are related, they have distinct targets and roles within the β cell. This is consistent with a recent report showing that in mice, MAFB does not compensate for MAFA loss[772]. Further, our data highlight *MAFB* as playing a key role in defining both β and α cell identity, in line with a recent report where MAFB deletion in human embryonic stem cells disrupted the differentiation process for both β and α cells[798]. Thus, our approach highlights how transcription factor profiles at the single cell level can be used to predict transcriptional and functional consequences of genetic manipulation, emphasizing an immense power for large scRNA-seq datasets.

While there were not sufficient cells for robust statistical comparison of all subsets, it is interesting to note that the electrophysiological profile of the cells expressing neither MAFA nor MAFB was similar to those cells expressing only one of the factors, thus suggesting a specific benefit to having combined expression of both factors in adult human β cells that is not apparent with only one of the TFs. These findings have several implications given the unique timing of MAFA and MAFB expression in the human β cell and differ slightly from our transcriptional data that suggested more of a progressive increase with the double negative group showing the lowest expression, followed by single TF groups, and co-expressing cells having highest expression of genes related to hormone secretory function. Future investigation with larger functional datasets will be needed to further delineate these interesting findings as well as directly evaluate the role of MAFA, MAFB, and other enriched transcription factors in human islet cell hormone secretion.

One contribution to bimodal distribution of low-abundance transcripts like TFs is gene dropout, where a gene is detected only in a subset of cells due to low mRNA quantity. However, greater expression of functional genes in one subpopulation (often dual positive cells) suggests that dropout is not simply a stochastic event and could instead reflect cell activity or a biological process such as transcriptional bursting[799]. Further, we analyzed three additional scRNA-seq datasets of human islets generated by various single cell technologies[590–592], and all showed trends consistent with the current study. Finally, taking advantage of the unique Patch-seq approach from our previous study, we were able to validate increased cellular function reflected by electrophysiological parameters (**Figure 64**). Together, these data indicate that our observations are not technical in nature and instead represent important aspects of human islet biology.

Given the potential inconsistencies between transcript and protein-level expression in human islets[797], we pursued identification of heterogeneous TF protein expression in human pancreatic

tissue. Though there were discrepancies in subpopulation distribution estimated by transcript versus by immunodetection, the presence of all TF combinations in tissue suggests this heterogeneity is not limited to one experimental approach. Differences may also arise from post-transcriptional control of protein levels that would not be apparent at the transcript level. Novel, single cell multi-omic techniques will be required to define the precise correlation between TF mRNA and protein abundance, and these techniques may also help define how the described heterogeneity relates to other forms of β cell heterogeneity that have been previously reported or hypothesized[592,778–781]. Heterogeneity within α cell populations has been less studied but our data indicate it may have an unappreciated role within the islet as well.

There are limitations to the current study that suggest opportunities for future work. Importantly, the nature of scRNA-seq means we cannot discern whether the heterogeneity described here is stable or a snapshot of a dynamic cell state. How the α and β cell subpopulations defined in this study function in the islet context is presently unknown – while having all highly functional cells would seem beneficial, some data has suggested that both mature and immature cells are required within an islet for optimal function[800]. Finally, the dispersion of islet cells required for scRNA-seq disrupts the microenvironment, which is known to be crucial for coordinated islet function[168,281].

To directly evaluate the role of TFs in an intact islet, shRNA-mediated knockdown in pseudoislets is an alternative to scRNA-seq. We pursued this approach with RFX6, an islet-enriched TF that we have shown is reduced in short-duration T2D β cells (Chapter V). While we did not observe differences in β cell composition with RFX6 reduction, we did observe reduced stimulated insulin secretion. Further, we noted a similarity in insulin secretory profiles in RFX6 shRNA treated pseudoislets compared to scramble shRNA treated pseudoislets and T2D islets compared to ND islets, highlighting that RFX6 reduction contributes to the β cell dysfunction seen in short-duration T2D islets. Future work investigating how reduced RFX6 expression alters the β cell transcriptional landscape will be important to define how RFX6 controls stimulated insulin secretion and how it relates to broader changes described in T2D datasets. Further, we studied RFX6^{down} pseudoislets in vitro after ~6 days; whether the defects described here are stable or would change with prolonged knockdown is particularly relevant and could be addressed by transplanting these pseudoislets into immune-deficient mice.

In sum, we highlight the utility of a large, scRNA-seq dataset by uncovering previously unappreciated heterogeneity in combined key islet-enriched TF expression and demonstrate that it has implications for human β cell function. We also highlight how complementary experimental approaches in pseudoislets can be used to directly evaluate the role of TFs in human islet function. Ultimately, defining the key characteristics of highly functional human α and β cells will allow not only a greater understanding of pathways governing coordinated hormone secretion but also inform the engineering of cells closely resembling native α or β cell function for cell replacement therapy to treat diabetes.

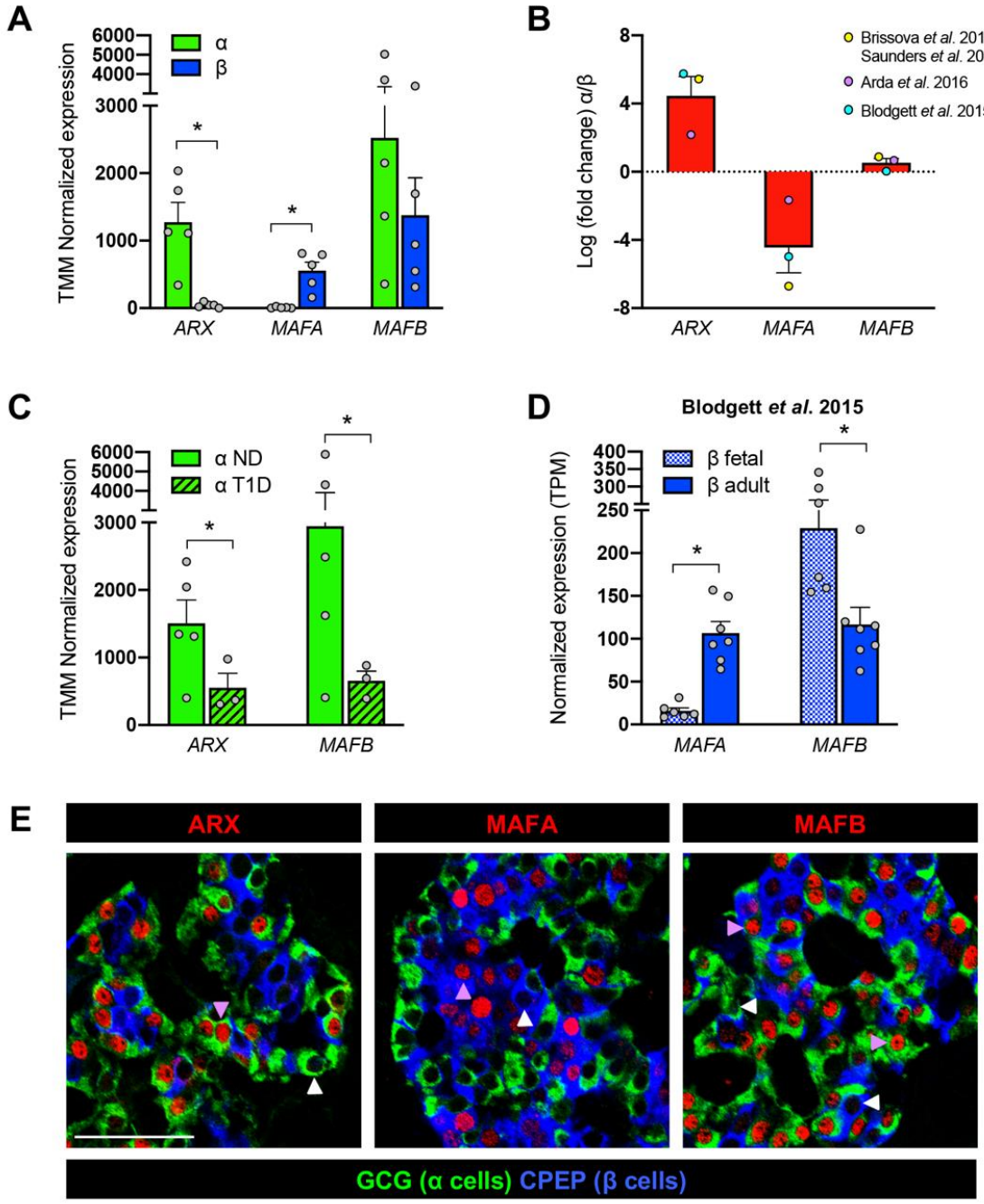

Figure 54. Bulk RNA-sequencing and immunohistochemistry data highlight unique expression patterns of transcription factors ARX, MAFA, and MAFB in human α and β cells.

(A–D) Normalized expression values (**A, C-D**) and fold change (**B**) of *ARX*, *MAFA*, and *MAFB* in previously published bulk RNA-sequencing (RNA-seq) datasets from α cells (green) and β cells (blue). Data in **A** is from Brissova *et al*. 2018[777] and Saunders *et al*. 2019[783] (n=5 donors); additional datasets Arda *et al*. 2016[770] (n=5 donors) and Blodgett *et al*. 2015[782] (n=7 donors) are included in panel **B**. See also **Figure 55A-55B**. **(C)** Expression of *ARX* and *MAFB* is decreased (*ARX* fold change: -2.7; *MAFB*: -3.4) in α cells from donors with type 1 diabetes (T1D) compared

to nondiabetic (ND) donors[777]. **(D)** Expression of *MAFA* is increased (fold change: 7.1) in adult β cells compared to fetal β cells, while *MAFB* is decreased (fold change: -2.0)[782]. All bar graphs show mean + SEM; symbols represent individual donors (panels **A**, **C-D**) or average value per dataset (**B**). Asterisks indicate significant (adjusted p-value <0.05) fold change of α vs. β in panels **A** and **B**, T1D vs. ND in **C**, and adult vs. fetal in **D**. **(E)** Immunohistochemical staining of pancreatic sections from a nondiabetic adult (55 years, **Table S4**), showing specificity of ARX, MAFA, and MAFB (red) in α cells (GCG; green) and β cells (CPEP; blue). Arrowheads indicate cells negative (white) or positive (purple) for transcription factors; scale bar, 50 μm. See also **Figure 55C-D**. Figure adapted from Shrestha, Saunders, Walker, et al.[561].

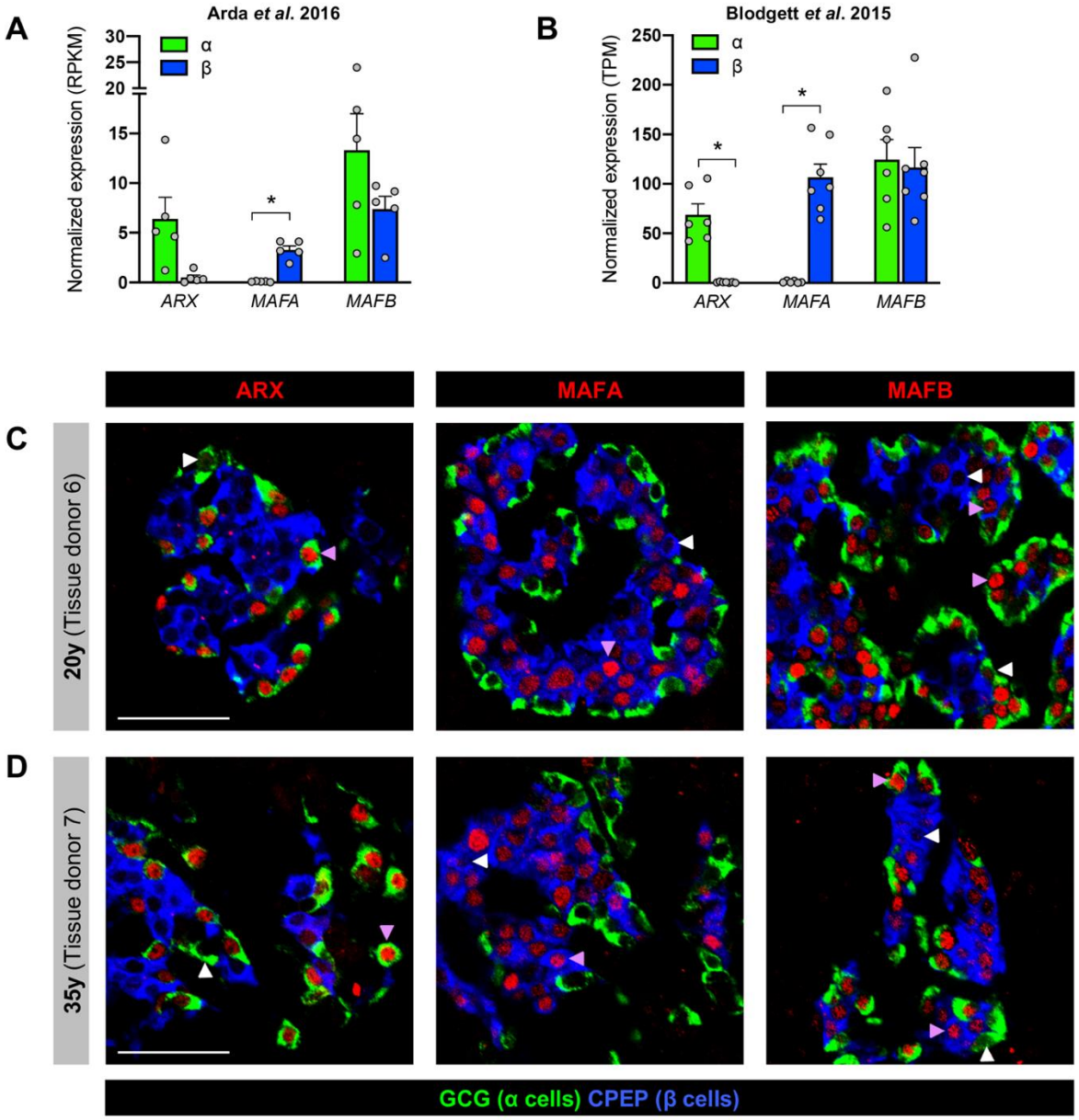

Figure 55. Related to Figure 54. ARX is expressed specifically in human α cells and MAFA in β cells, while MAFB is expressed in both α and β cells.

(A–B) Normalized expression of *ARX*, *MAFA*, and *MAFB* in previously published bulk RNA-sequencing (RNA-seq) datasets Arda *et al*. 2016[770] (**A**) and Blodgett *et al*. 2015[782] (**B**) from α cells (green) and β cells (blue). Bars in both panels show mean + SEM; symbols represent individual donors. Asterisks indicate significantly different (adjusted p-value <0.05) fold change (α vs. β). See also **Figure 54B**. **(C–D)** Immunohistochemical staining of pancreatic sections from nondiabetic adults (**Table 4**), showing specificity of ARX, MAFA, and MAFB (red) in α cells (GCG; green) and β cells (CPEP; blue). Arrowheads indicate cells negative (white) or positive (purple) for transcription factors; scale bars, 50 μm. See also **Figure 54C**. Figure adapted from Shrestha, Saunders, Walker, et al.[561].

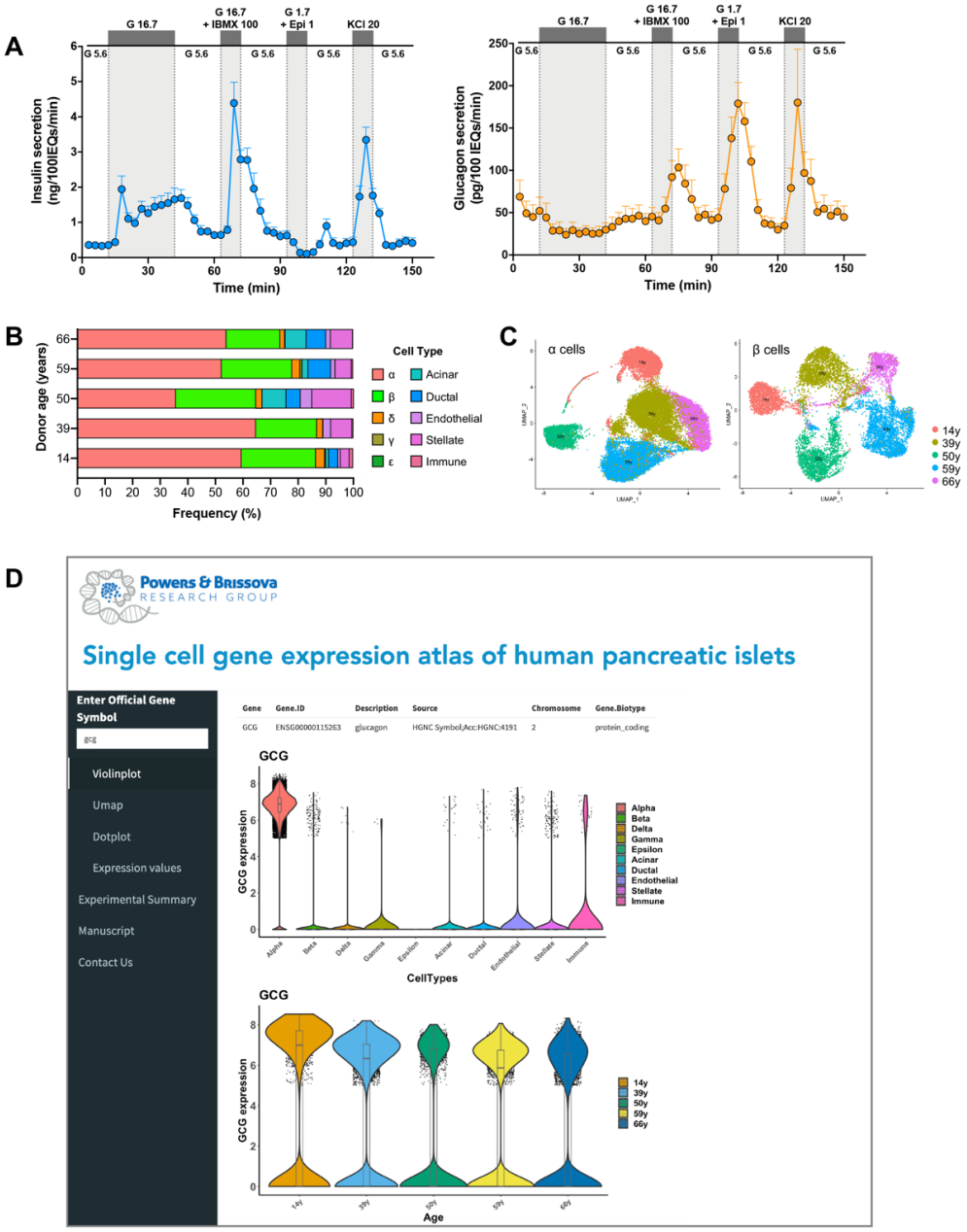

Figure 56. Detailed characterization of endocrine cells from five nondiabetic human islet donors.

(A) Insulin and glucagon secretion were assessed in islets isolated from n=5 donors (age range 14–66 years) stimulated with 5.6 mM glucose (G 5.6), 16.7 mM glucose (G 16.7), 16.7 mM glucose + 100 mM isobutylmethylxanthine (IBMX) (G 16.7 + IBMX 100), 1.7 mM glucose + 1 mM epinephrine (G 1.7 + Epi 1), and 20 mM potassium chloride (KCl 20). Insulin and glucagon secretion is normalized to overall islet cell volume (expressed as islet equivalents; IEQs). **(B)** Bar graph illustrating cell type distribution within each islet preparation as per cell types annotated in **Figure 57A**. **(C)** UMAP of only α or β cells, showing clustering by islet preparation. **(D)** User-friendly web portal application for searching and viewing pancreatic cell types and their gene expression. Figure adapted from Shrestha, Saunders, Walker, et al.[561].

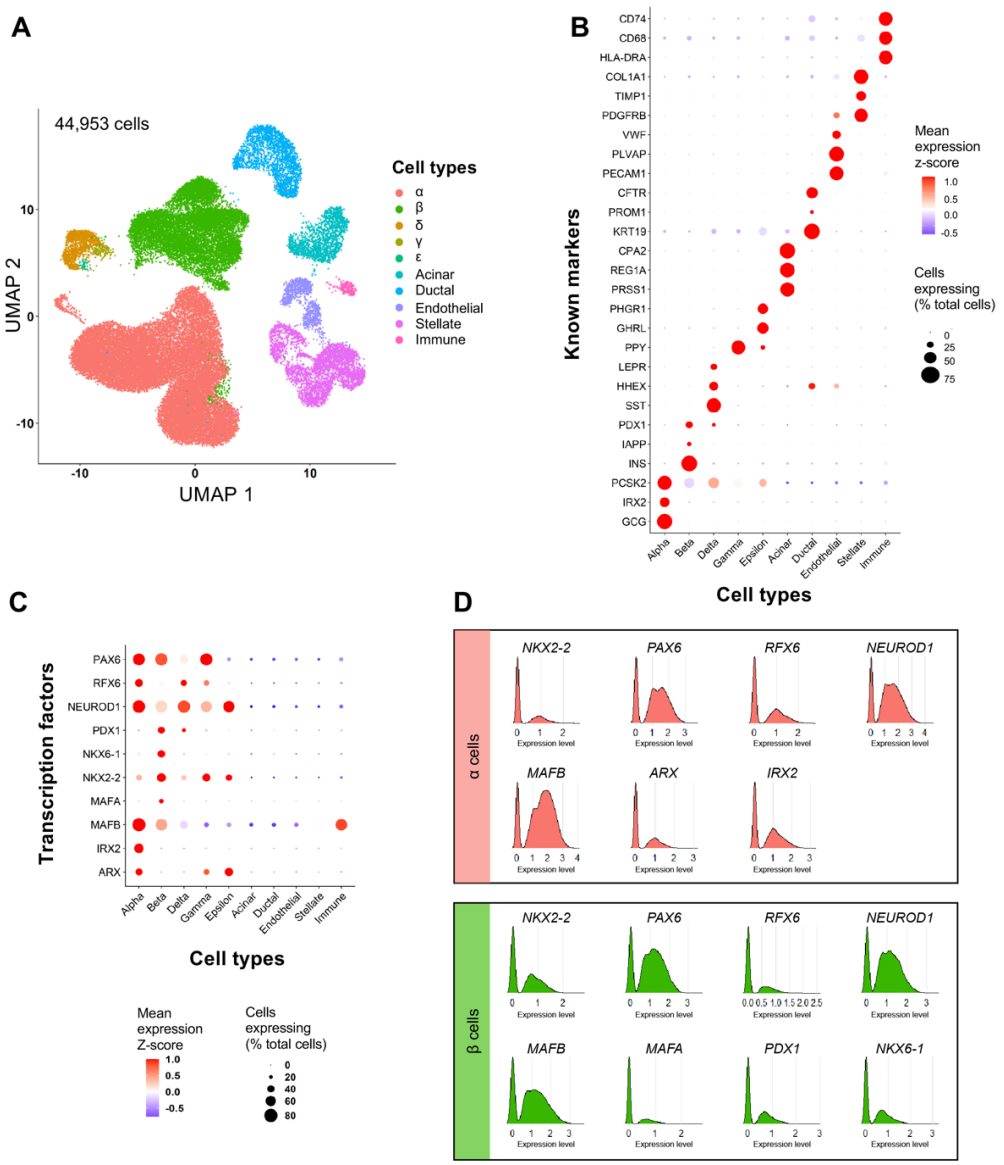

Figure 57. Transcription factor expression in human pancreatic islets by scRNA-seq. **(A)** UMAP visualization of 44,953 pancreatic islet cells from n=5 islet preparations, identified by unsupervised clustering; cell populations include β (24%), α (54%), δ (2.5%), ε (0.08%), acinar (3.3%), ductal (4.7%), endothelial (2.2%), stellate (7.7%), and immune cells (0.5%). Cell clusters were annotated using known gene markers (**Table 11**). γ and ε cells could not be resolved from the δ cell cluster; thus, these populations were manually selected using the "CellSelector" function to identify cells positive for *PPY* and *GHRL*, respectively. Libraries were sequenced at ~80,000 reads/cell yielding a median of 2,365 genes per cell. **(B)** Dot plot showing relative expression of cell type markers to validate cell type annotation post-unsupervised clustering. **(C)** Dot plot showing relative expression of transcription factors across all cell types. In panels **B**-**C**, dot size indicates the percentage of cells with detectable transcripts; color indicates gene's mean expression z-score. **(D)** Natural log expression level of common transcription factors expressed in α and β cells. Figure adapted from Shrestha, Saunders, Walker, et al.[561].

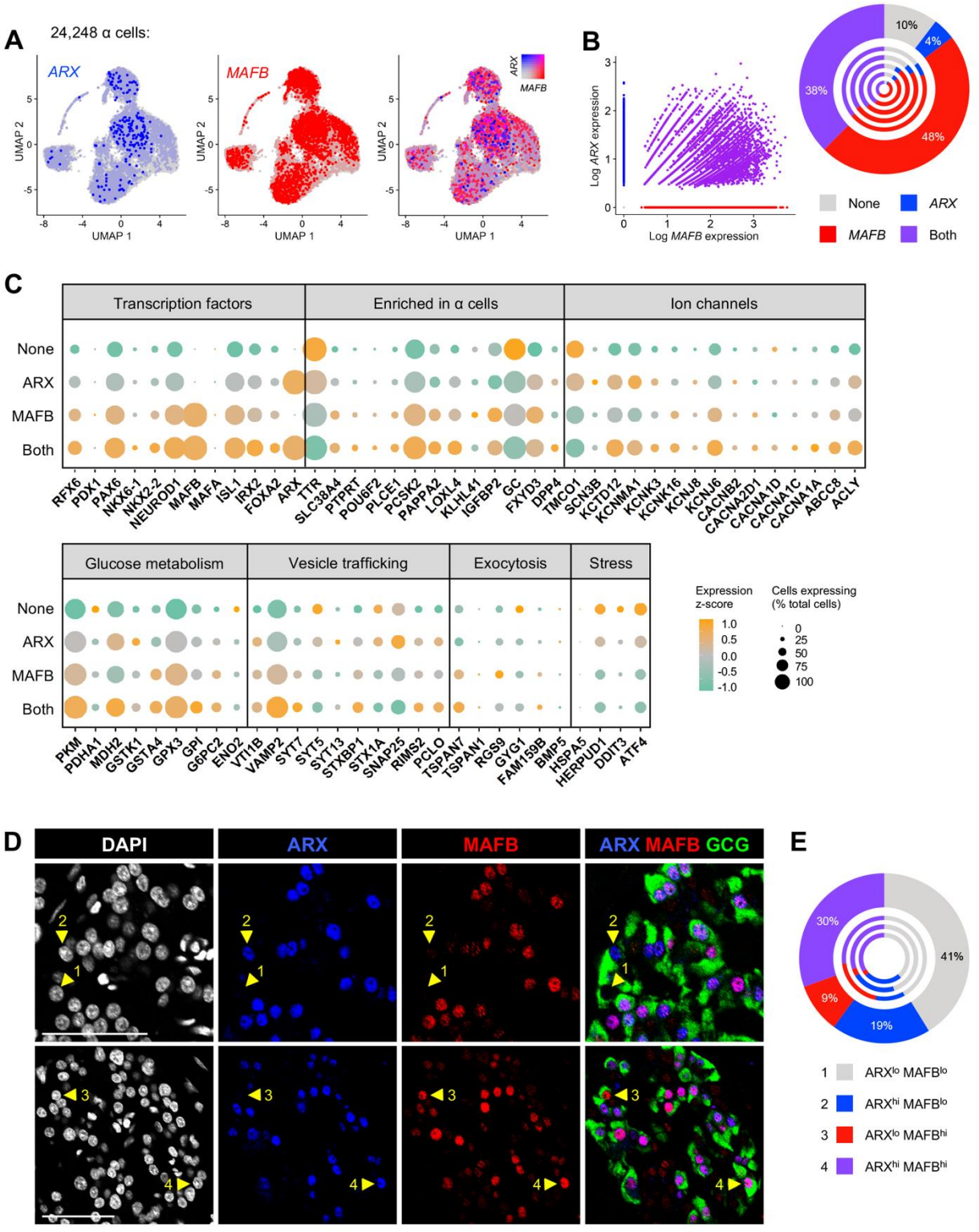

Figure 58. Heterogeneity of *ARX* and *MAFB* expression in α cells by scRNA-seq correlates with expression of key functional genes.

(A) UMAP visualization of 24,248 α cells (n=5 donors) pseudocolored to show, from left to right, expression of *ARX* (blue); *MAFB* (red); and both *ARX* and *MAFB* with 0.5 color threshold scale.

(B) Scatterplot on the left is depicting four distinct α cell populations based on *ARX* and *MAFB* expression: those expressing neither factor (10%), those expressing only *ARX* (4%) or only *MAFB* (48%), and those co-expressing *ARX* and *MAFB* (38%). Chart on the right shows cell populations by donor, with the outermost circle reflecting totals. **(C)** Dot plot showing the relative expression of selected genes related to α cell identity, ion flux, glucose metabolism, vesicle trafficking, exocytotic machinery, and cellular stress of the four α cell populations in panel **B**. Dot size indicates the percentage of α cells with detectable transcripts; color indicates the gene's mean expression z-score. See **Figure 60A** for comparison to other single cell studies. **(D)** Immunohistochemical staining of ARX (blue) and MAFB (red) in glucagon (GCG)-expressing α cells (green) of a nondiabetic adult (55 years, **Table 4**). Numbered arrowheads indicate the presence of 4 α populations: 1, ARX^{lo} $MAFB^{lo}$; 2, ARX^{hi} $MAFB^{lo}$; 3, ARX^{lo} $MAFB^{hi}$; 4, ARX^{hi} $MAFB^{hi}$. **(E)** Quantification of α cell populations shown in panel **D** (n= 2,369 α cells). Outermost circle represents composite count and inner circles represent α cells from each of n=3 donors (see also **Figure 60B**). Figure adapted from Shrestha, Saunders, Walker, et al.[561].

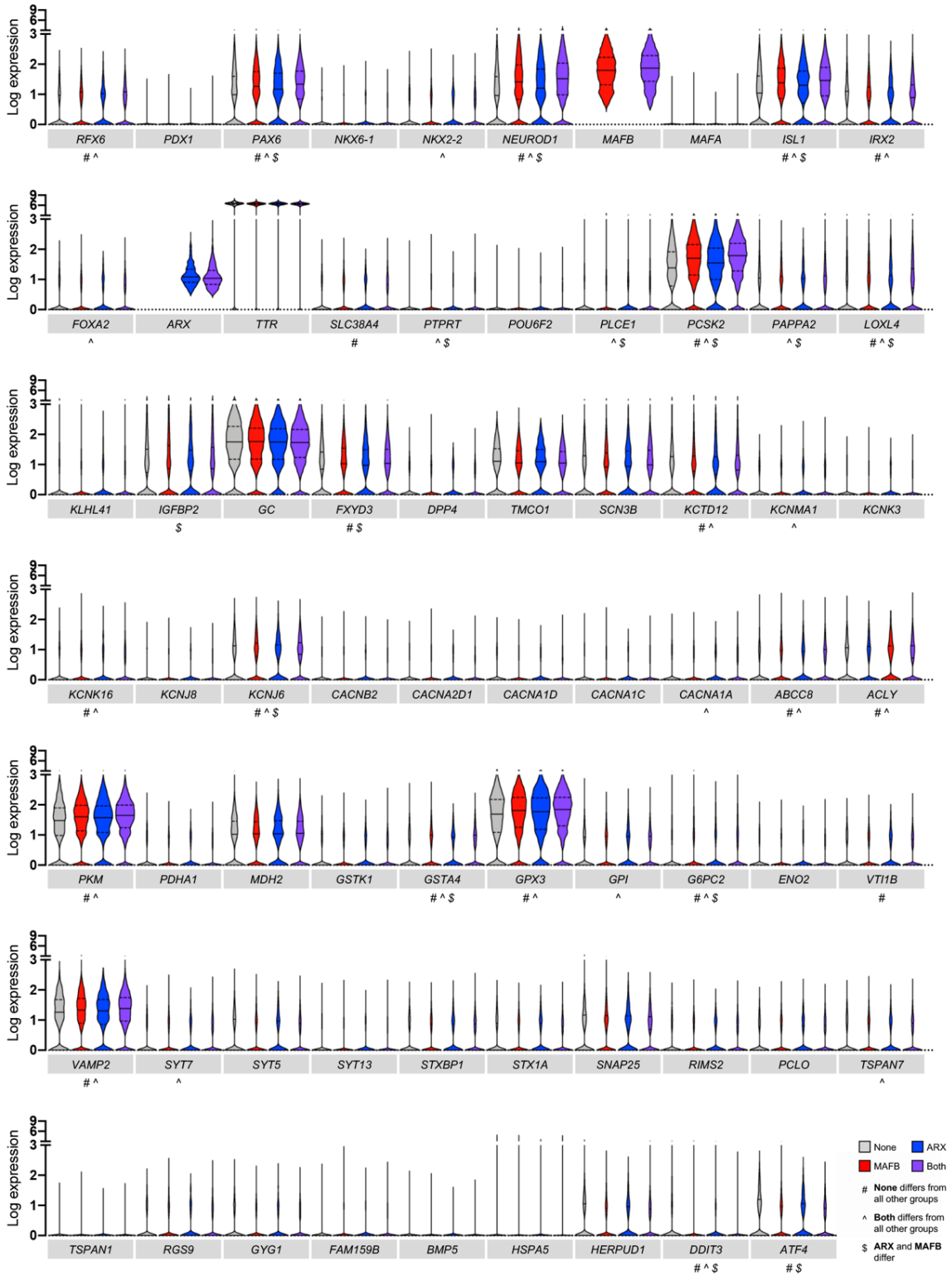

Figure 59. Related to Figure 58. Raw expression values for transcription factor, α cell-enriched, ion channel, glucose metabolism, vesicle trafficking, exocytosis, and stress genes in *ARX*/*MAFB* populations.

Violin plots depict gene expression in α cell populations lacking *ARX* and *MAFB* (grey) and those expressing *MAFB* only (red), *ARX* only (blue), or co-expressing *both MAFB* and *ARX* (purple); n=24,248 total α cells. Data corresponds to dot plot in **Figure 58C**. Symbols underneath gene names indicate significance ($p<0.05$) from Tukey's multiple comparisons test following 2-way ANOVA. Figure adapted from Shrestha, Saunders, Walker, et al.[561].

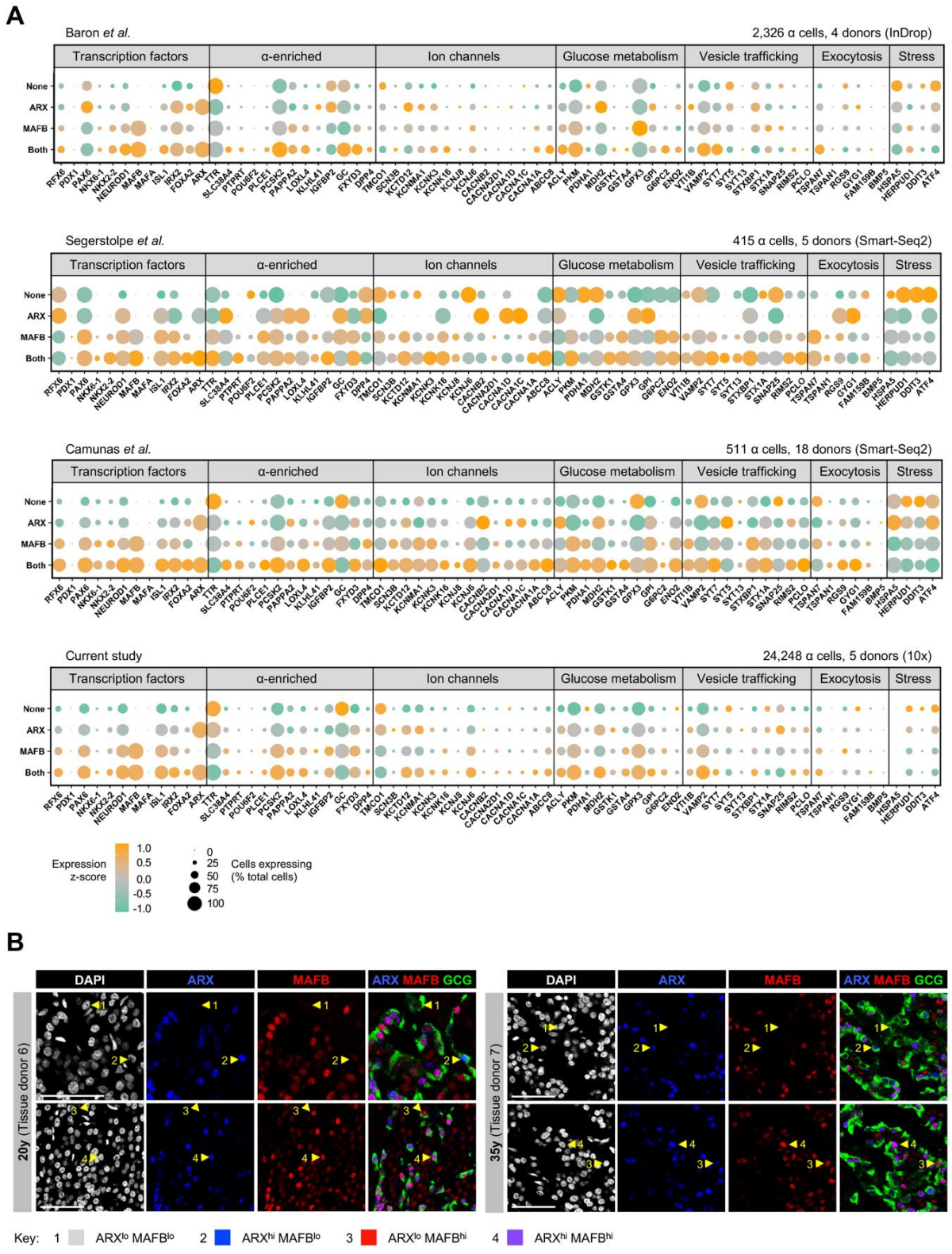

Figure 60. Related to Figure 58. Validation of α cell populations based on *ARX* and *MAFB* expression, as determined by previous scRNA-seq studies.

(A) Dot plots showing the expression patterns of selected genes related to cell identify, ion flux, glucose metabolism, vesicle trafficking, and exocytotic machinery. α cell populations (rows) are identified by expression of neither *ARX* nor *MAFB* (None), *ARX* only (ARX), *MAFB* only (MAFB), and co-expression of *ARX* and *MAFB* (Both). Dot size indicates the percentage of cells with detectable transcripts; color indicates gene's average scaled expression. Headers list study details from previously published datasets (Segerstolpe *et al.*, 2016[21]; Baron *et al.*, 2016[20]; Camunas-Soler *et al.*, 2020[15]) and final dot plot is as shown in **Figure 58C** for comparison. **(B)** Immunohistochemical staining of ARX (blue) and MAFB (red) in glucagon (GCG)-expressing α cells (green) of two nondiabetic adults (**Table 4**). Numbered arrowheads indicate the presence of α cell populations: 1, ARX^{lo} $MAFB^{lo}$; 2, ARX^{hi} $MAFB^{lo}$; 3, ARX^{lo} $MAFB^{hi}$; 4, ARX^{hi} $MAFB^{hi}$. See also **Figure 58E**. Figure adapted from Shrestha, Saunders, Walker, et al.[561].

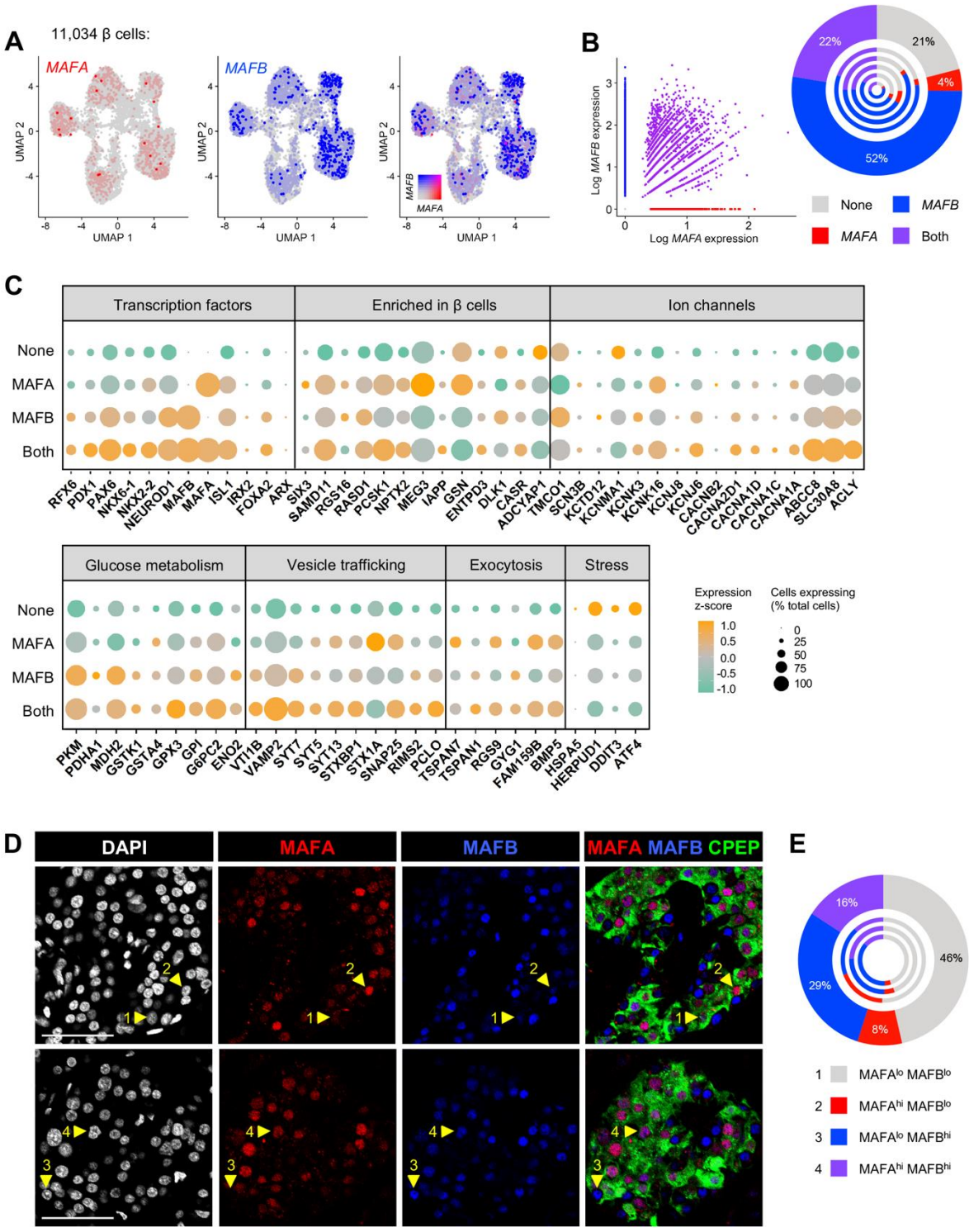

Figure 61. Heterogeneity of MAFA and MAFB expression in β cells by single cell RNA-seq correlates with expression of key genes involved in β cell function.

(A) UMAP visualization of 11,034 β cells (n=5 donors), pseudocolored to show, from left to right, expression of *MAFA* (red); *MAFB* (blue); and both *MAFA* and *MAFB* with 0.5 color threshold scale. **(B)** Scatterplot on the left depicts four distinct β cell populations based on *MAFA* and

MAFB expression: those expressing neither factor (22%), those expressing only *MAFA* (4%) or only *MAFB* (52%), and those co-expressing *MAFA* and *MAFB* (22%). Chart on the right shows cell populations by donor, with the outermost circle reflecting totals. **(C)** Dot plot showing the relative expression of selected genes related to β cell identity, ion flux, glucose metabolism, vesicle trafficking, exocytotic machinery, and cellular stress of the four β cell populations in panel **B**. Dot size indicates the percentage of β cells with detectable transcripts; color indicates the gene's mean expression z-score. See **Figure 63A** for comparison to other single cell studies. **(D)** Immunohistochemical staining of MAFA (red) and MAFB (blue) in C-peptide (CPEP)-expressing β cells (green) of a nondiabetic adult (55 years, **Table 4**). Numbered arrowheads indicate the presence of 4 populations: 1, $MAFA^{lo}$ $MAFB^{lo}$; 2, $MAFA^{hi}$ $MAFB^{lo}$; 3, $MAFA^{lo}$ $MAFB^{hi}$; 4, $MAFA^{hi}$ $MAFB^{hi}$. **(E)** Quantification of β cell populations shown in **D** (n= 2,566 β cells). Outermost circle represents composite count and inner circles represent β cells from each of n=3 donors (see also **Figure 63B**). Figure adapted from Shrestha, Saunders, Walker, et al.[561].

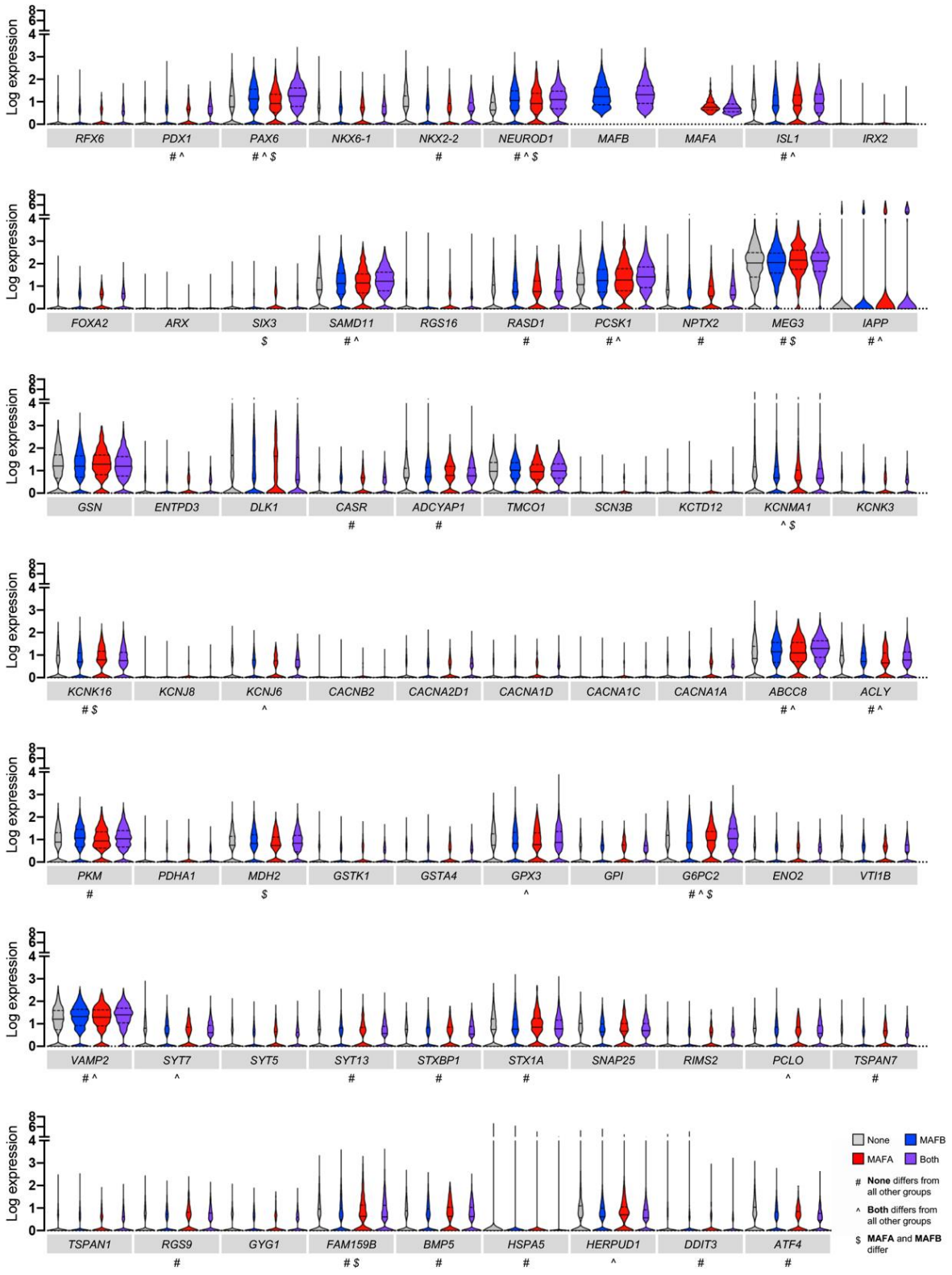

Figure 62. Related to Figure 61. Raw expression values for transcription factor, β-enriched, ion channel, glucose metabolism, vesicle trafficking, exocytosis, and stress genes in *MAFA*/*MAFB* populations.

Violin plots depict gene expression in β cell populations (n=11,034 total β cells) lacking *MAFA* and *MAFB* (grey) and those expressing *MAFA* only (red), *MAFB only* (blue), or co-expressing *both MAFA* and *MAFB* (purple); n=11,034 total β cells. Data corresponds to dot plot in **Figure 61C**. Symbols underneath gene names indicate significance ($p<0.05$) from Tukey's multiple comparisons test following 2-way ANOVA. Figure adapted from Shrestha, Saunders, Walker, et al.[561].

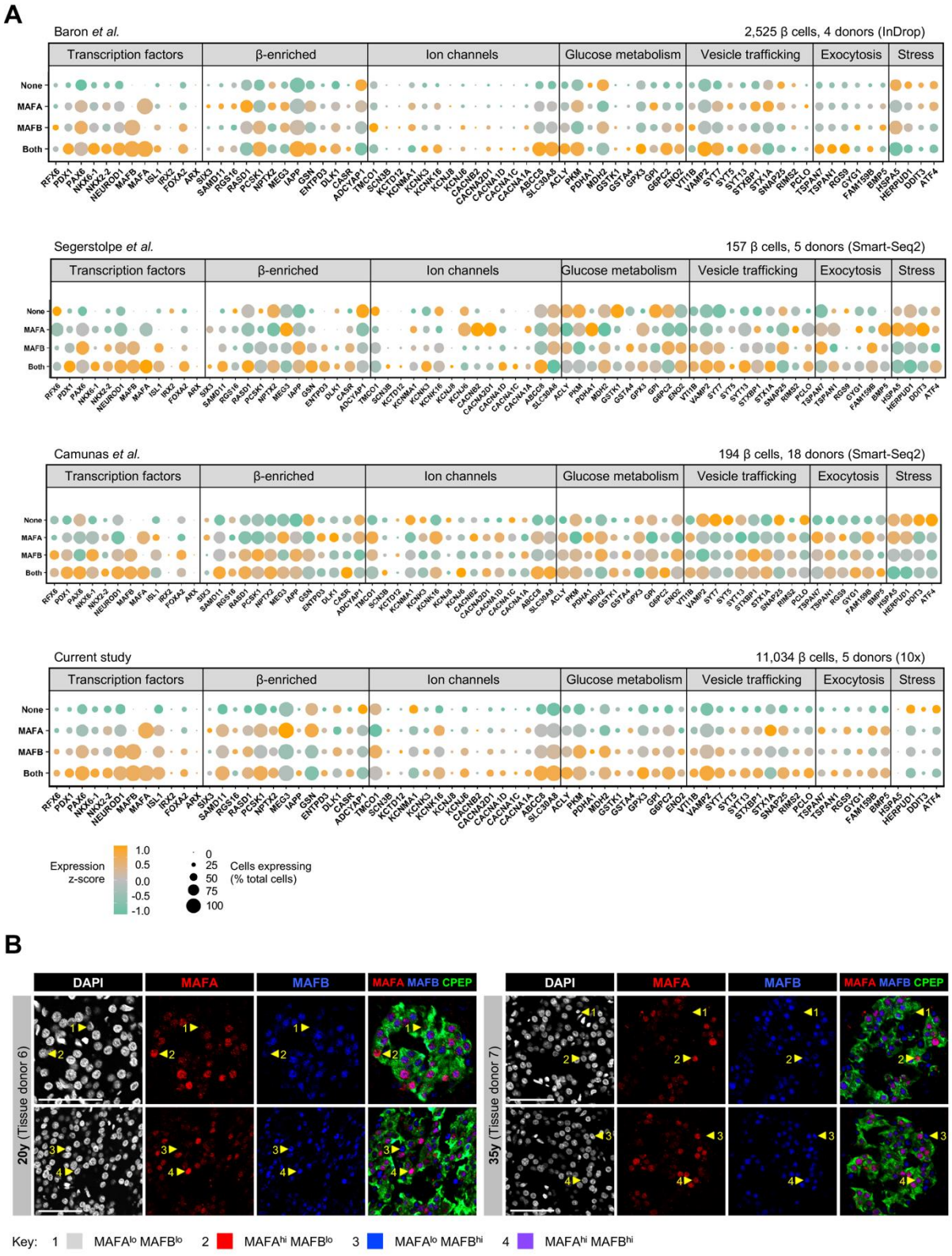

Figure 63. Related to Figure 61. Validation of β cell populations based on *MAFA* and *MAFB* expression, as determined by previous scRNA-seq studies.

(A) Dot plots showing the expression patterns of selected genes related to cell identify, ion flux, glucose metabolism, vesicle trafficking, and exocytotic machinery. β cell populations (rows) are identified by expression of neither *MAFA* nor *MAFB* (None), *MAFA* only (MAFA), *MAFB* only (MAFB), and co-expression of *MAFA* and *MAFB* (Both). Dot size indicates the percentage of cells with detectable transcripts; color indicates gene's average scaled expression. Headers list study details from previously published datasets (Segerstolpe *et al.*, 2016[21]; Baron *et al.*, 2016[20]; Camunas-Soler *et al.*, 2020[15]) and final dot plot is as shown in **Figure 61C** for comparison. **(B)** Immunohistochemical staining of MAFA (red) and MAFB (blue) in C-peptide (CPEP)-expressing β cells (green) of two nondiabetic adults (**Table 4**). Numbered arrowheads indicate the presence of β cell populations: 1, $MAFA^{lo}$ $MAFB^{lo}$; 2, $MAFA^{hi}$ $MAFB^{lo}$; 3, $MAFA^{lo}$ $MAFB^{hi}$; 4, $MAFA^{hi}$ $MAFB^{hi}$. See also **Figure 61E**. Figure adapted from Shrestha, Saunders, Walker, et al.[561].

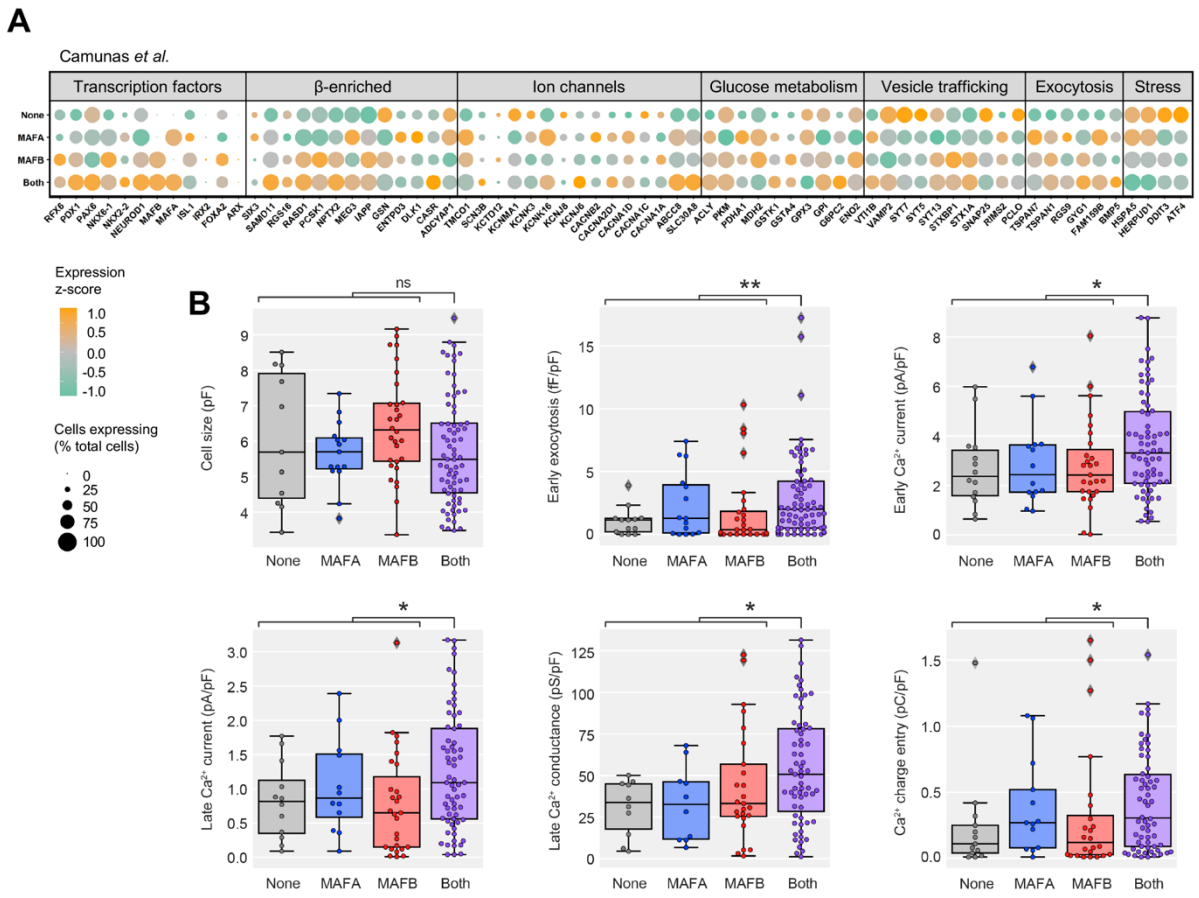

Figure 64. Beta cells co-expressing *MAFA* and *MAFB* have enhanced electrophysiolgic activity compared to β cells expressing one or neither factor.

(A) Dot plot showing the relative expression of selected genes in β cells expressing neither *MAFA* nor *MAFB*, those expressing only *MAFA* or only *MAFB*, and those co-expressing *MAFA* and *MAFB*, based on data from Camunas *et al.* 2020[592]. Dot size indicates the percentage of cells with detectable transcripts; color indicates gene's mean expression z-score. **(B)** Electrophysiological function in *MAFA*- and *MAFB*-expressing β cell subpopulations. Significantly higher Ca^{2+} currents and exocytosis are observed for β cells expressing both *MAFA* and *MAFB* with similar cell size across all subpopulations. Mann-Whitney test adjusted for multiple hypothesis testing with Benjamini-Hochberg (BH) procedure; *, $p < 0.05$; **, $p < 0.01$. Figure adapted from Shrestha, Saunders, Walker, et al.[561].

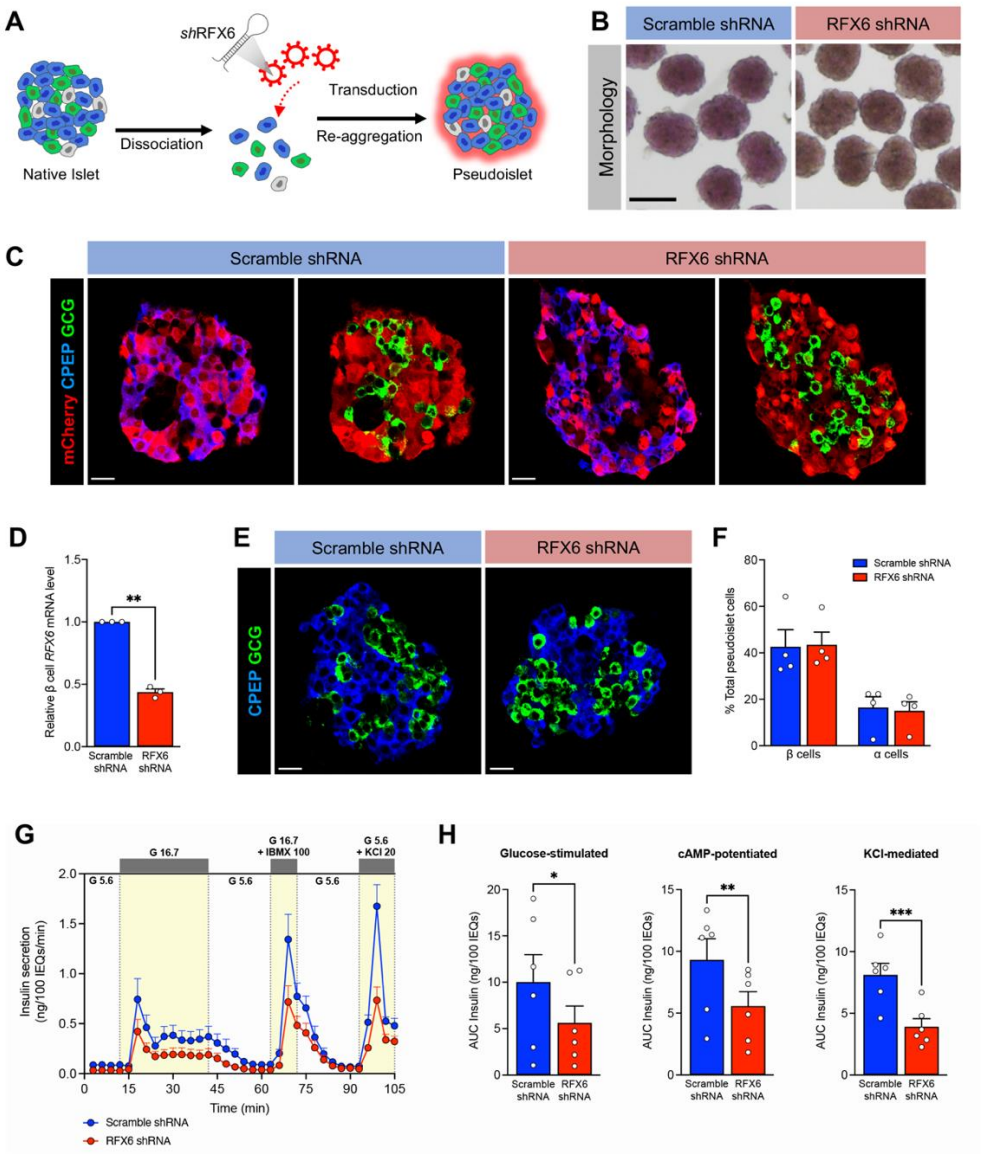

Figure 65. RFX6 controls stimulated insulin secretion in human β cells.
(A) Schematic of adenoviral delivery of shRNA to pseudoislets. **(B)** Bright-field images showing the morphology of scramble shRNA- or RFX6 shRNA-treated pseudoislets. Scale bar is 200 μm. **(C)** Immunofluorescent images of pseudoislets embedded in type I collagen showing mCherry (red) marking transduced cells, CPEP (blue) marking β cells, and GCG (green) marking α cells. **(D)** Relative *RFX6* mRNA expression in β cells treated with scramble or RFX6 shRNA. **(E-F)** Immunofluorescent images of pseudoislets showing β cells (CPEP, blue) and α cells (GCG, green) with quantification of % cells in pseudoislet expressing each marker. **(G)** Dynamic insulin secretion assessed by macroperifusion in basal glucose (G 5.6 – 5.6 mM glucose; white) with stimulations (yellow) of high glucose (G 16.7 – 16.7 mM glucose), cAMP-potentiation (G 16.7 + IBMX 100 – 16.7 mM glucose + 100 μM isobutylmethylxanthine (IBMX)), and KCl-mediated depolarization (KCl 20 – 20 mM potassium chloride); n=6 matched donors in each trace. **(H)** Insulin secretion was integrated by calculating the area under the curve (AUC) for response to each of the stimuli.

CHAPTER VII:
SIGNIFICANCE AND FUTURE DIRECTIONS

Summary

The primary goal of my research was to discover information that would advance our understanding of molecular mechanisms of human islet dysfunction in diabetes. To accomplish this, I took a multi-pronged approach that applied existing scientific tools to new scientific questions as well as developed new techniques to allow studies that were previously unachievable.

First, we sought to understand how commonly used therapeutics affect human islets in an *in vivo* environment and how these effects relate to the pathophysiology of diabetes. Prolonged exposure to clinically relevant levels of the immunosuppressive agents tacrolimus and sirolimus lead to impaired insulin secretion that was not caused by β cell loss. Instead, islet dysfunction was characterized by disruptions to β cell granules, increased amyloid deposition, and transcriptional dysregulation of genes related to ion flux and peptide processing. Insulin secretion and molecular markers of islet dysfunction normalized after withdrawal of treatment, and dysfunction was prevented by co-treatment with a GLP-1 receptor agonist. In addition, we studied the effects of dapagliflozin, a SGLT2 inhibitor, and demonstrated that the human islet is not a principal target of this therapeutic and instead, islet effects are mediated through changes in blood glucose. These findings open exciting translational opportunities as discussed below.

To facilitate investigation of new mechanistic questions in the field of human islet biology, we developed a culture system that involves dispersing islets into a single cell state and then allowing them to reaggregate to form pseudoislets. These pseudoislets resemble native human islets in morphology, function, composition, and cellular identity, thus enabling targeted genetic and cellular manipulation of primary human islet cells in an islet-like context. We used this system to 1) describe cell type-specific effects of GPCR signaling, 2) study calcium signaling and hormone secretion from α cell-only, “T1D-like” pseudoislets and 3) investigate how islet cells physically interact with one another to form pseudoislet clusters. The establishment of this system and applications explored here have the potential to develop in many different directions as described below.

Complexities in disease processes underscore the need to perform integrated analyses on pancreatic tissue and isolated islets to appreciate interacting disease processes. We describe a large-scale analysis of islet function, microenvironment, and transcriptome from a large cohort of short-duration T2D donors. Integration of these studies revealed that a defect in stimulated insulin secretion is prominent in short-duration T2D. Moreover, this effect is not explained by reductions in β cell mass and is not reversed by transplantation into a normoglycemic, non-insulin resistant environment. Assessment of the T2D islet microenvironment by traditional and multiplexed immunohistochemistry uncovered changes in cell abundance and phenotype, especially in the context of amyloid deposition. Finally, integrative transcriptional analysis revealed numerous molecular changes to T2D β cells, including that the transcription factor

RFX6 is a highly connected β cell hub gene and is reduced in T2D β cells. In parallel to our in-depth study of short-duration T2D, we describe how such an integrative approach can be applied to investigate atypical pathobiological findings in a single T1D donor, expanding the field's understanding of human T1D heterogeneity. Collectively, these results open up numerous future directions discussed below.

Transcription factors play a crucial role in the islet physiology and pathophysiology of diabetes. To define the specific role that several transcription factors play in adult human islet cells, we investigated heterogeneous cell states in single cell RNA-seq data and also directly manipulated transcription factors in our pseudoislet system. We demonstrated how combinatorial expression of *ARX* and *MAFB* in α cells and *MAFA* and *MAFB* in β cells define mature and highly functional subpopulations of each cell type, based on expression of genes related to hormone secretion as well as electrophysiological features of β cells. We also assessed the transcription factor RFX6 by using shRNA knockdown in pseudoislets, demonstrating a role for RFX6 in controlling insulin secretion from human β cells. These findings have important implications for how islet cells become dysfunctional in disease and suggest exciting experimental opportunities discussed below.

Implications and Future Directions

New treatment paradigms for PTDM

Our findings about the mechanisms of β cell dysfunction with TAC and SIR provide an opportunity for developing new therapeutic approaches to reduce the incidence of PTDM. While immunosuppressive agents are not the sole cause of PTDM, their strong association indicates that alleviating this aspect of PTDM would have a significant impact on incidence[607–610]. While withdrawal of TAC or SIR is usually not clinically feasible, the fact that β cells showed strong capacity for recovery indicates that transitioning to a different immunosuppressive regimen with fewer off target effects on β cells could be considered upon signs of dysregulated glucose. For example, building off of our work, other groups have since shown that voclosporin, a next-generation calcineurin inhibitor, does not have the same detrimental effects on β cells that TAC does[801]. Thus, with continued development of new agents and new generations of immunosuppressive therapeutics, one could envision individually selecting therapeutic agents and doses during the period when β cell dysfunction is still reversible, so as to find optimal balance of glucose homeostasis and adequate transplant tolerance for each individual. Given the significance and consequence of PTDM, future work should focus on establishing a β cell dysfunction profile for an array of these medications, both alone and in combination, to allow for informed selection of treatment.

Of particular interest are our findings that GLP-1 receptor agonist treatment was able to fully prevent β cell dysfunction with TAC treatment and partially prevent it with SIR treatment. This data provides strong rationale for a clinical trial to evaluate whether incidence and severity of PTDM could be reduced with initiation of GLP-1 receptor agonist-based treatment, which has an excellent safety profile, soon after transplantation for patients who will be treated with TAC. Future preclinical work in this arena might seek to evaluate whether initiating GLP-1 receptor

agonist treatment after β cell dysfunction is observed is as effective as using it for primary prevention in order to guide clinical care most effectively.

We noted that one of the pathways activated by GLP-1 in β cells is the calcineurin/NFAT pathway, the same pathway targeted by TAC. Thus, one possible explanation for why GLP-1R agonists were more beneficial in the TAC-treated group is that in the case of TAC, there was β cell-specific targeting and activation of the key pathway that had been inhibited, while in SIR there was activation of a beneficial pathway (calcineurin/NFAT), but not the one that had been inhibited (mTOR). Studies that genetically manipulate either the calcineurin/NFAT or mTOR pathways in human islets during the dysfunction induced by TAC or SIR, respectively, as well as the reversal with GLP-1R agonists, would be particularly enlightening and may reveal a general approach to countering side effects in islets from off target effects.

Opportunities for in vivo study of human islets

Collectively, our results highlight the importance of considering *in vivo* studies of human islets in addition to those conducted *in vitro*. Islets are complicated mini-organs whose primary role is to dynamically sense nutrients and hormonal signals and respond in a coordinated manner; however, there are numerous situations where the islet's response *in vitro* is substantially different from its response *in vivo*[569,631–635]. While *in vitro* studies have benefits, transplantation and subsequent evaluation of islets *in vivo* provide a more nuanced picture of physiology in the context of the entire organism. This context was particularly important for the three therapeutics discussed, whose primary cellular targets were not the islet but rather immune cells (TAC and SIR) or kidney (DAPA). Furthermore, the *in vivo* approach allows for longer-term study, which can be quite significant as highlighted by the disparity between acute versus chronic effects of DAPA on *in vivo* glucagon secretion. While such approaches are technically complex, the results of this chapter underscore how they bridge an important gap by providing more detailed molecular information than can be obtained about islets through clinical research and thus should be considered when working with human islets.

There has been a debate as to whether the transient rise in glucagon secretion seen with initiation of SGLT2 inhibitor treatment, which might exacerbate hypergylcemia, occurs via direct effects on the α cells or whether the effects are indirect[802]. Our data provides strong *in vivo* evidence that this effect is indirect and likely mediated through acute changes in glucose. Interestingly, recent work has highlighted the hypothesis that the glycemic set point of an organism is set primarily by α cell input to β cells[26]. Our work confirmed clinical findings which saw acute (~1 week) changes to glucagon secretion after initiation of treatment that eventually normalized (~4 weeks)[637,638]. Taken together, these results imply that the α cell acutely responds in an effort to maintain a consistent glucose level, but over time it adapts to the lower glucose level and glucagon secretion normalizes as a result. This raises interesting questions about how the α cell senses acute changes in glucose and what conditions lead the cell to accommodate a new baseline. Whether these sensing mechanisms become disrupted in either type 1 or type 2 diabetes, both of which can have α cell dysfunction[357,594], would be of particular interest. Such *in vivo* human α cell physiology has long been difficult to investigate in transplant models due to 100% sequence homology of human and mouse glucagon. However, the recent

development of a *Gcg* knockout mouse on the NSG background provides a new tool to address these questions[803]. Combining biosensor labeling of human pseudoislets with transplantation into the anterior chamber of the eye[804,805] of *Gcg* KO mice would allow for specific assessment of both glucagon secretion and biosensor dynamics as α cells respond to short-, medium-, and long-term changes in glucose.

Deciphering the islet microenvironment

A common theme across all the studies in this Dissertation is the critical role of the microenvironment in coordinated islet function. Whether defining how the islet microenvironment changes in models of PTDM and human samples of T1D or T2D or recreating the islet microenvironment in our pseudoislet system, the context in which endocrine cells find themselves has proven to be paramount to understanding islet physiology and pathophysiology. With the aid of the pseudoislet system, we are now in a position to investigate this is with greater detail than was possible before. Some important questions to tackle include:

- What are the processes and mechanisms responsible for the arrangement of islet endocrine and non-endocrine cells? Are these processes dependent on donor age or disease status?
- What role do endothelial cells, pericytes, macrophages, and other non-endocrine cells within the human islet mini-organ play in nutrient sensing, hormone secretion, and the islet response to stressors?
- What is the role of electrical coupling and stimuli between human islet cells?
- What is the full array of secreted factors from endocrine and non-endocrine cells how do these signal to nearby cells within the human islet? Are these altered in pathophysiologic conditions?

Disease processes in the T2D islet

To identify early, disease-driving mechanisms of T2D, we focused on collection and analysis of donors with short-duration T2D. This focused collection likely explains some differences in findings of our study compared to others, such as the lack of reduction in β cell mass[720,721] or confirming a reduction in *MAFA* but not observing changes in *NKX6*.1, *PDX1*, and *MAFB*[806]. While we have taken great care to focus our organ collection efforts, the natural history of T2D makes precise determination of disease onset difficult. Thus, ultimately relating our transcriptional findings to GWAS loci should help define which processes are heavily influenced by underlying genetic risk and presumably are more likely to be causal. Further, to add specificity to our findings, future work that includes analogous studies on long-duration T2D would allow for categorization of processes that are stable during disease progression as opposed to those that are unique to either early or later stages. This classification would greatly aid in identifying central processes to target in a complex metabolic disease. Further questions in this area that will be key to address:

- What are the electrophysiologic, proteomic, or metabolomic changes in short-duration T2D islets and how do these relate to our findings?
- What human islet adaptations allow some obese individuals to maintain glucose homeostasis while others progress to diabetes?

- What are the epigenetic changes (intrinsic or environmentally induced) in human islets with age or disease and how do they impact islet cell function, survival, and adaptation?
- How do these processes differ depending on ethnicity and age of onset of T2D?
- How do current therapies (medication, bariatric surgery, weight loss, etc.) alter islet cell function and mass and the progression of T2D?

Mechanistic investigation of T2D islet pathophysiology

To translate the findings of our study on T2D into the preclinical realm, detailed mechanistic studies, ideally with human islets, will be essential. Our results point to many interesting targets that will be worthwhile to pursue; one of these, RFX6, is included in Chapter VI of this Dissertation. In Chapter V, we show that RFX6 is a central regulator of β gene expression and is specifically reduced in the T2D β cell, and in Chapter VI, we use this finding to design experiments ultimately demonstrating that RFX6 has a role in controlling stimulated insulin secretion. Additional questions that are raised from our studies include:

- What is the contribution of other genes that are disrupted in T2D to β cell dysfunction?
- How do the non-endocrine cells that are changed in T2D, specifically endothelial cells and T cells, interact in the human islet microenvironment to impact insulin secretion?
- What are the functional consequences of increased or decreased amyloid deposition within an islet?
- Are increased cilia in T2D a compensatory response to β cell dysfunction or a pathophysiologic mechanism?

Lessons from T1D heterogeneity

T1D is classically defined by autoimmune destruction of pancreatic β cells resulting in absolute insulin deficiency. However, there is increasing awareness that within this single disease, there is considerable heterogeneity, especially in age of disease onset, genetic susceptibility, rates of progression, and residual insulin secretory capacity[751,807]. This has led the field to propose an "endotype" concept where multiple, distinct biological mechanisms may produce T1D as we currently define it. Therefore, atypical cases of T1D, such as the one described in Chapter V of this Dissertation, are critical to define heterogeneity at the level of the pancreas and islet. In this case, we describe dynamic insulin secretion resembling that of non-diabetic donor islets, and we detect substantial remaining β cell mass after 8 years of T1D, though the high correlation of these β cells with $CD45^+$ immune cells suggests possible autoimmunity. Despite this, the donor HbA1C (11.9%) insinuates severe loss of insulin, raising several interesting questions.

- Were the β cells that were functional *ex vivo* able to secrete insulin *in vivo*, and if not, what component of the pancreatic environment prevented this?
- What is the natural history of β cell loss in T1D?
- Do remaining β cells represent a subset that is more resistant to autoimmunity, or are they the result of a regenerative response through progenitor differentiation, transdifferentiation, or β cell replication?
- Does β cell loss contribute to the α cell dysfunction seen? What degree of β cell loss is required?

Efforts from consortia such as HPAP and nPOD to obtain and study T1D pancreata, as well as to define the full range of phenotypic and molecular features, will be critical for us to understand

the different disease mechanisms at play in T1D and how we can precisely target these in individuals.

Combinational TF expression and islet cell heterogeneity

Studies in Chapter VI of this Dissertation utilize scRNA-seq to demonstrate that combinatorial expression of *ARX* and *MAFB* in α cells and *MAFA* and *MAFB* in β cells predicts highly functional and mature islet cell subpopulations. While we focused on these specific TFs, we noted that numerous islet-enriched TFs showed a similar bimodal distribution of expression. Further, other islet-enriched TFs were consistently elevated in *ARX*/*MAFB* co-expressing α cells and *MAFA*/*MAFB* co-expressing β cells, supporting the concept of islet-enriched TFs acting in self-regulating networks. Moving forward, systems-based analyses of these binary states across a broad range of islet-enriched TFs may reveal a hierarchal relationship among these TFs in the adult human islet β and α cells.

A critical component of identifying heterogeneity in β or α cells is further demonstrating the implications of such heterogeneity. We show selected genes related to key steps in the hormone secretory pathway, but future studies should identify genes regulated by these TFs in an unbiased manner. Defining these genes, particularly those that are regulated by combinations of TFs that we have defined as important, and the transcriptional state that they represent is crucial to understand how α and β cell heterogeneity contribute to islet physiology and pathophysiology. With large scRNA-seq datasets, novel computational approaches such as SCENIC[808,809] can be used to identify gene regulatory networks based on co-expression and TF binding motifs, known as regulons. Analysis of these regulons can then help reveal cellular programs controlled by the TF of interest. Thus, applying tools like SCENIC could provide complementary information defining cellular states that are indicative of highly functional α and β cells. Further questions to address with regard to islet cell heterogeneity include:

- What processes are responsible for establishing islet cell heterogeneity (intrinsic or extrinsic)?
- Are these cell populations stable or do they dynamically switch between cell states?
- Do these islet cell subsets play a role in islet adaptation or in diabetes?

Investigating how RFX6 controls β cell function

Building off results shown in Chapter V, we used shRNA knockdown in our pseudoislet system to investigate the role of RFX6 in insulin secretion in adult human β cells, showing that it has a critical role in stimulated insulin secretion. Given RFX6's role as a TF, we would hypothesize that this is driven through transcriptional dysregulation, likely through many of the same pathways identified in β cells from short-duration T2D donors in Chapter V. Thus, future work should focus on evaluating these processes in RFX6^{down} pseudoislets. Combined approaches that assess both single nuclear RNA and Assay for Transposase-Accessible Chromatin (ATAC) on the same cell would be ideally positioned to evaluate changes to the transcriptional and chromatin landscapes. Chromatin changes would be particularly interesting to explore in RFX6^{down} cells given the enrichment of T2D GWAS loci in β cell-specific chromatin regions[810] and the enrichment of RFX6 motifs in these same regions[746]. Finally, it will be critical to define

what processes govern RFX6 expression and how these become dysregulated to lead to RFX6 reduction.

Closing Remarks

This Dissertation provides new insights into the molecular mechanisms of islet dysfunction in human diabetes. Through a combination of molecular analyses on clinically relevant samples and the development of improved models to study human islets, my work provides a framework for integrating knowledge to deliver impactful discoveries about human islet physiology and pathophysiology. The results described here provide a new appreciation for nuances in β and α cell biology, both in their GPCR signaling pathways and in the heterogeneous expression of transcription factors. Further, this work provides new mechanistic insight into β cell dysfunction in PTDM, highlights pathobiological heterogeneity in T1D, and describes disease-driving mechanisms of β cell dysfunction in T2D. Overall, the improved understanding of these pathways paves the way to develop more effective and precise treatments for individuals with diabetes.

REFERENCES

1. Walker, J. T., Saunders, D. C., Brissova, M. & Powers, A. C. The Human Islet: Mini-organ with Mega-impact. *Endocr Rev* bnab010- (2021) doi:10.1210/endrev/bnab010.

2. Moore, K. L., Agur, A. M. R. & Dalley, A. F. *Essential Clinical Anatomy*. (Lippincott Williams & Wilkins, 2010).

3. Pandiri, A. R. Overview of Exocrine Pancreatic Pathobiology. *Toxicol Pathol* **42**, 207–216 (2014).

4. Lang, D. A., Matthews, D. R., Peto, J. & Turner, R. C. Cyclic Oscillations of Basal Plasma Glucose and Insulin Concentrations in Human Beings. *New Engl J Medicine* **301**, 1023–1027 (1979).

5. Satin, L. S., Butler, P. C., Ha, J. & Sherman, A. S. Pulsatile insulin secretion, impaired glucose tolerance and type 2 diabetes. *Mol Aspects Med* **42**, 61–77 (2015).

6. Porte, D. & Pupo, A. A. Insulin responses to glucose: evidence for a two pool system in man. *J Clin Invest* **48**, 2309–2319 (1969).

7. Dimitriadis, G., Mitrou, P., Lambadiari, V., Maratou, E. & Raptis, S. A. Insulin effects in muscle and adipose tissue. *Diabetes Res Clin Pr* **93**, S52–S59 (2011).

8. Saltiel, A. R. & Kahn, C. R. Insulin signalling and the regulation of glucose and lipid metabolism. *Nature* **414**, 799–806 (2001).

9. Bonadonna, R. C., Saccomani, M. P., Cobelli, C. & DeFronzo, R. A. Effect of insulin on system A amino acid transport in human skeletal muscle. *J Clin Invest* **91**, 514–521 (1993).

10. Galsgaard, K. D., Pedersen, J., Knop, F. K., Holst, J. J. & Albrechtsen, N. J. W. Glucagon Receptor Signaling and Lipid Metabolism. *Front Physiol* **10**, 413 (2019).

11. Boden, G., Rezvani, I. & Owen, O. E. Effects of glucagon on plasma amino acids. *J Clin Invest* **73**, 785–793 (1984).

12. Albrechtsen, N. J. W., Kuhre, R. E., Pedersen, J., Knop, F. K. & Holst, J. J. The biology of glucagon and the consequences of hyperglucagonemia. *Biomark Med* **10**, 1141–1151 (2016).

13. Albrechtsen, N. J. W. *et al.* Evidence of a liver-alpha cell axis in humans: hepatic insulin resistance attenuates relationship between fasting plasma glucagon and glucagonotropic amino acids. *Diabetologia* **61**, 671–680 (2018).

14. Galsgaard, K. D. *et al.* Disruption of glucagon receptor signaling causes hyperaminoacidemia exposing a possible liver-alpha-cell axis. *Am J Physiol-endoc M* **314**, E93–E103 (2018).

15. Kim, J. *et al.* Amino Acid Transporter Slc38a5 Controls Glucagon Receptor Inhibition-Induced Pancreatic α Cell Hyperplasia in Mice. *Cell Metab* **25**, 1348-1361.e8 (2017).

16. Dean, E. D. *et al.* Interrupted Glucagon Signaling Reveals Hepatic α Cell Axis and Role for L-Glutamine in α Cell Proliferation. *Cell Metab* **25**, 1362-1373.e5 (2017).

17. Solloway, M. J. *et al.* Glucagon Couples Hepatic Amino Acid Catabolism to mTOR-Dependent Regulation of α-Cell Mass. *Cell Reports* **12**, 495–510 (2015).

18. Warren, H. S. *et al.* Mice are not men. *Proc National Acad Sci* **112**, E345–E345 (2015).

19. Seok, J. *et al.* Genomic responses in mouse models poorly mimic human inflammatory diseases. *Proc National Acad Sci* **110**, 3507–3512 (2013).

20. Mak, I. W., Evaniew, N. & Ghert, M. Lost in translation: animal models and clinical trials in cancer treatment. *Am J Transl Res* **6**, 114–8 (2014).

21. Hart, N. J. & Powers, A. C. Use of human islets to understand islet biology and diabetes: progress, challenges and suggestions. *Diabetologia* **301**, 1580 11 (2018).

22. Brissova, M. *et al.* Assessment of human pancreatic islet architecture and composition by laser scanning confocal microscopy. *J Histochem Cytochem* **53**, 1087 1097 (2005).

23. Brissova, M. *et al.* Human Islets Have Fewer Blood Vessels than Mouse Islets and the Density of Islet Vascular Structures Is Increased in Type 2 Diabetes. *J Histochem Cytochem* **63**, 637 645 (2015).

24. Dai, C. *et al.* Islet-enriched gene expression and glucose-induced insulin secretion in human and mouse islets. *Diabetologia* **55**, 707 718 (2012).

25. Cabrera, O. *et al.* The unique cytoarchitecture of human pancreatic islets has implications for islet cell function. *P Natl Acad Sci Usa* **103**, 2334 2339 (2006).

26. Rodriguez-Diaz, R. *et al.* Paracrine Interactions within the Pancreatic Islet Determine the Glycemic Set Point. *Cell Metab* **27**, 549-558.e4 (2018).

27. Brissova, M. *et al.* Assessment of Human Pancreatic Islet Architecture and Composition by Laser Scanning Confocal Microscopy. *J Histochem Cytochem* **53**, 1087–1097 (2005).

28. Drigo, R. A. e *et al.* New insights into the architecture of the islet of Langerhans: a focused cross-species assessment. *Diabetologia* **58**, 2218–2228 (2015).

29. Bonner-Weir, S., Sullivan, B. A. & Weir, G. C. Human Islet Morphology Revisited. *J Histochem Cytochem* **63**, 604–612 (2015).

30. Cabrera, O. *et al.* The unique cytoarchitecture of human pancreatic islets has implications for islet cell function. *P Natl Acad Sci Usa* **103**, 2334–2339 (2006).

31. Bosco, D. *et al.* Unique Arrangement of α- and β-Cells in Human Islets of Langerhans. *Diabetes* **59**, 1202 1210 (2010).

32. Pisania, A. *et al.* Quantitative analysis of cell composition and purity of human pancreatic islet preparations. *Lab Invest* **90**, 1661–1675 (2010).

33. Olehnik, S. K., Fowler, J. L., Avramovich, G. & Hara, M. Quantitative analysis of intra- and inter-individual variability of human beta-cell mass. *Sci Rep-uk* **7**, 16398 (2017).

34. Dybala, M. P. & Hara, M. Heterogeneity of the Human Pancreatic Islet. *Diabetes* **68**, 1230–1239 (2019).

35. Poudel, A., Fowler, J. L., Zielinski, M. C., Kilimnik, G. & Hara, M. Stereological analyses of the whole human pancreas. *Sci Rep-uk* **6**, 34049 (2016).

36. Orci, L., Malaisse-Lagae, F., Baetens, D. & Perrelet, A. Pancreatic-Polypeptide-Rich Regions in Human Pancreas. *Lancet* **312**, 1200–1201 (1978).

37. Malaisse-Lagae, F., Stefan, Y., Cox, J., Perrelet, A. & Orci, L. Identification of a lobe in the adult human pancreas rich in pancreatic polypeptide. *Diabetologia* **17**, 361–365 (1979).

38. Stefan, Y. *et al.* Quantitation of Endocrine Cell Content in the Pancreas of Nondiabetic and Diabetic Humans. *Diabetes* **31**, 694–700 (1982).

39. Wang, X. *et al.* Quantitative Analysis of Pancreatic Polypeptide Cell Distribution in the Human Pancreas. *Plos One* **8**, e55501 (2013).

40. Damond, N. *et al.* A Map of Human Type 1 Diabetes Progression by Imaging Mass Cytometry. *Cell Metab* **29**, 755-768.e5 (2019).

41. Grube, D. & Bohn, R. The Microanatomy of Human Islets of Langerhans, with Special Reference to Somatostatin (D-) Cells. *Arch Histol Cytol* **46**, 327–353 (1983).

42. Drigo, R. A. e *et al.* Structural basis for delta cell paracrine regulation in pancreatic islets. *Nat Commun* **10**, 3700 (2019).

43. Huising, M. O. Paracrine regulation of insulin secretion. *Diabetologia* **63**, 2057–2063 (2020).

44. Almaça, J., Caicedo, A. & Landsman, L. Beta cell dysfunction in diabetes: the islet microenvironment as an unusual suspect. *Diabetologia* **63**, 2076–2085 (2020).

45. Vetterlein, F., Pethö, A. & Schmidt, G. Morphometric investigation of the microvascular system of pancreatic exocrine and endocrine tissue in the rat. *Microvascular research* **34**, 231 238 (1987).

46. Murakami, T., Fujita, T., Taguchi, T., Nonaka, Y. & Deparita, K. The Blood Vascular Bed of the Human Pancreas, with Special Reference to the Insulo-Acinar Portal System. Scanning Electron Microscopy of Corrosion Casts. *Arch Histol Cytol* **55**, 381–395 (1992).

47. Murakami, T. *et al.* Blood flow patterns in the rat pancreas: a simulative demonstration by injection replication and scanning electron microscopy. *Microsc Res Techniq* **37**, 497 508 (1997).

48. Brissova, M. *et al.* Pancreatic Islet Production of Vascular Endothelial Growth Factor-A Is Essential for Islet Vascularization, Revascularization, and Function. *Diabetes* **55**, 2974–2985 (2006).

49. Brissova, M. *et al.* Human Islets Have Fewer Blood Vessels than Mouse Islets and the Density of Islet Vascular Structures Is Increased in Type 2 Diabetes. *J Histochem Cytochem* **63**, 637 645 (2015).

50. Cohrs, C. M. *et al.* Vessel network architecture of adult human islets promotes distinct cell-cell interactions in situ and is altered after transplantation. *Endocrinology* **158**, 1373–1385 (2017).

51. Almaça, J. & Caicedo, A. Blood Flow in the Pancreatic Islet: Not so Isolated Anymore. *Diabetes* **69**, 1336–1338 (2020).

52. Dybala, M. P. *et al.* Integrated Pancreatic Blood Flow: Bi-Directional Microcirculation Between Endocrine and Exocrine Pancreas. *Diabetes* **69**, db191034 (2020).

53. Klein, T. *et al.* Nestin Is Expressed in Vascular Endothelial Cells in the Adult Human Pancreas. *J Histochem Cytochem* **51**, 697–706 (2003).

54. Virtanen, I. *et al.* Blood vessels of human islets of Langerhans are surrounded by a double basement membrane. *Diabetologia* **51**, 1181 1191 (2008).

55. Sordi, V. *et al.* Establishment, characterization and long-term culture of human endocrine pancreas-derived microvascular endothelial cells. *Cytotherapy* **19**, 141–152 (2017).

56. Almaça, J., Weitz, J., Rodriguez-Diaz, R., Pereira, E. & Caicedo, A. The Pericyte of the Pancreatic Islet Regulates Capillary Diameter and Local Blood Flow. *Cell Metab* **27**, 630-644.e4 (2018).

57. Gregersen, S., Thomsen, J. L., Brock, B. & Hermansen, K. Endothelin-1 stimulates insulin secretion by direct action on the islets of Langerhans in mice. *Diabetologia* **39**, 1030 1035 (1996).

58. Carlo, E. D. *et al.* Endothelin-1 and endothelin-3 stimulate insulin release by isolated rat pancreatic islets. *J Endocrinol Invest* **23**, 240 245 (2000).

59. Huang, G. & Greenspan, D. S. ECM roles in the function of metabolic tissues. *Trends Endocrinol Metabolism* **23**, 16 22 (2012).

60. Hogan, M. F. & Hull, R. L. The islet endothelial cell: a novel contributor to beta cell secretory dysfunction in diabetes. *Diabetologia* **60**, 1 8 (2017).

61. Li, W., Yu, G., Liu, Y. & Sha, L. Intrapancreatic Ganglia and Neural Regulation of Pancreatic Endocrine Secretion. *Front Neurosci-switz* **13**, 21 (2019).

62. Faber, C. L., Deem, J. D., Campos, C. A., Taborsky, G. J. & Morton, G. J. CNS control of the endocrine pancreas. *Diabetologia* **63**, 2086–2094 (2020).

63. Reinert, R. B. *et al.* Vascular endothelial growth factor coordinates islet innervation via vascular scaffolding. *Development* **141**, 1480–1491 (2014).

64. Rodriguez-Diaz, R. *et al.* Innervation Patterns of Autonomic Axons in the Human Endocrine Pancreas. *Cell Metab* **14**, 45–54 (2011).

65. Rodriguez-Diaz, R. & Caicedo, A. Neural control of the endocrine pancreas. *Best Pract Res Clin Endocrinol Metabolism* **28**, 745–56 (2014).

66. Ehses, J. A. *et al.* Increased Number of Islet-Associated Macrophages in Type 2 Diabetes. *Diabetes* **56**, 2356–2370 (2007).

67. Butcher, M. J. *et al.* Association of proinflammatory cytokines and islet resident leucocytes with islet dysfunction in type 2 diabetes. *Diabetologia* **57**, 491–501 (2014).

68. Wiberg, A. *et al.* Characterization of human organ donors testing positive for type 1 diabetes-associated autoantibodies. *Clin Exp Immunol* **182**, 278–288 (2015).

69. Radenkovic, M. *et al.* Characterization of resident lymphocytes in human pancreatic islets. *Clin Exp Immunol* **187**, 418–427 (2016).

70. Gassen, N. V. *et al.* Concise Review: Macrophages: Versatile Gatekeepers During Pancreatic β-Cell Development, Injury, and Regeneration. *Stem Cell Transl Med* **4**, 555 563 (2015).

71. Morris, D. L. Minireview: Emerging Concepts in Islet Macrophage Biology in Type 2 Diabetes. *Mol Endocrinol* **29**, 946–962 (2015).

72. Lytrivi, M., Igoillo-Esteve, M. & Cnop, M. Inflammatory stress in islet β-cells: therapeutic implications for type 2 diabetes? *Curr Opin Pharmacol* **43**, 40–45 (2018).

73. Otonkoski, T., Banerjee, M., Korsgren, O., Thornell, L. -E. & Virtanen, I. Unique basement membrane structure of human pancreatic islets: implications for β-cell growth and differentiation. *Diabetes Obes Metabolism* **10**, 119–127 (2008).

74. Lin, H.-Y. *et al.* Fibronectin and laminin promote differentiation of human mesenchymal stem cells into insulin producing cells through activating Akt and ERK. *J Biomed Sci* **17**, 56 (2010).

75. Banerjee, M., Virtanen, I., Palgi, J., Korsgren, O. & Otonkoski, T. Proliferation and plasticity of human beta cells on physiologically occurring laminin isoforms. *Mol Cell Endocrinol* **355**, 78 86 (2012).

76. Korpos, E. *et al.* The Peri-islet Basement Membrane, a Barrier to Infiltrating Leukocytes in Type 1 Diabetes in Mouse and Human. *Diabetes* **62**, 531–542 (2012).

77. Weber, L. M., Hayda, K. N. & Anseth, K. S. Cell–Matrix Interactions Improve β-Cell Survival and Insulin Secretion in Three-Dimensional Culture. *Tissue Eng Pt A* **14**, 1959–1968 (2008).

78. Hynes, R. O. The Extracellular Matrix: Not Just Pretty Fibrils. *Science* **326**, 1216–1219 (2009).

79. Sorokin, L. The impact of the extracellular matrix on inflammation. *Nat Rev Immunol* **10**, 712 723 (2010).

80. Bogdani, M. *et al.* Hyaluronan and hyaluronan-binding proteins accumulate in both human type 1 diabetic islets and lymphoid tissues and associate with inflammatory cells in insulitis. *Diabetes* **63**, 2727 2743 (2014).

81. Nikolova, G. *et al.* The vascular basement membrane: a niche for insulin gene expression and Beta cell proliferation. *Dev Cell* **10**, 397 405 (2006).

82. Gan, W. J. *et al.* Cell polarity defines three distinct domains in pancreatic β-cells. *J Cell Sci* **130**, 143 151 (2017).

83. Deconinck, J. F., Potvliege, P. R. & Gepts, W. The ultrastructure of the human pancreatic islets. *Diabetologia* **7**, 266–282 (1971).

84. Orci, L. A portrait of the pancreatic B-Cell: The Minkowski award lecture delivered on July 19, 1973, during the VIIIth congress of the international diabetes Federation, held in Brussels, Belgium. *Diabetologia* **10**, 163–187 (1974).

85. Pelletier, G. Identification of Four Cell Types in the Human Endocrine Pancreas By Immunoelectron Microscopy. *Diabetes* **26**, 749–756 (1977).

86. Vasiljević, J., Torkko, J. M., Knoch, K.-P. & Solimena, M. The making of insulin in health and disease. *Diabetologia* **63**, 1981–1989 (2020).

87. Steiner, D. F. Insulin Today. *Diabetes* **26**, 322–340 (1977).

88. Lukinius, A., Stridsberg, M. & Wilander, E. Cellular Expression and Specific Intragranular Localization of Chromogranin A, Chromogranin B, and Synaptophysin During Ontogeny of Pancreatic Islet Cells: An Ultrastructural Study. *Pancreas* **27**, 38–46 (2003).

89. Brereton, M. F., Vergari, E., Zhang, Q. & Clark, A. Alpha-, Delta- and PP-cells: Are They the Architectural Cornerstones of Islet Structure and Co-ordination? *J Histochem Cytochem Official J Histochem Soc* **63**, 575–91 (2015).

90. Deconinck, J. F., Potvliege, P. R. & Gepts, W. The ultrastructure of the human pancreatic islets. *Diabetologia* **7**, 266–282 (1971).

91. Melloul, D., Marshak, S. & Cerasi, E. Regulation of insulin gene transcription. *Diabetologia* **45**, 309–326 (2002).

92. Artner, I. & Stein, R. Pancreatic Beta Cell in Health and Disease. 13–30 (2008) doi:10.1007/978-4-431-75452-7_2.

93. Stein, R. Regulation of insulin gene transcription. *Trends Endocrinol Metabolism* **4**, 96–101 (1993).

94. Tokarz, V. L., MacDonald, P. E. & Klip, A. The cell biology of systemic insulin function. *J Cell Biol* **217**, jcb.201802095 (2018).

95. Steiner, D. F. *et al.* The role of prohormone convertases in insulin biosynthesis: evidence for inherited defects in their action in man and experimental animals. *Diabetes Metab* **22**, 94–104 (1996).

96. Ji, L., Wu, H.-T., Qin, X.-Y. & Lan, R. Dissecting carboxypeptidase E: properties, functions and pathophysiological roles in disease. *Endocr Connect* **6**, R18–R38 (2017).

97. Suckale, J. & Solimena, M. The insulin secretory granule as a signaling hub. *Trends Endocrinol Metabolism* **21**, 599 609 (2010).

98. Daniel, S., Noda, M., Straub, S. G. & Sharp, G. W. Identification of the docked granule pool responsible for the first phase of glucose-stimulated insulin secretion. *Diabetes* **48**, 1686–1690 (1999).

99. Bramswig, N. C. & Kaestner, K. H. Transcriptional regulation of α-cell differentiation. *Diabetes Obes Metabolism* **13**, 13–20 (2011).

100. Gromada, J., Franklin, I. & Wollheim, C. B. α-Cells of the Endocrine Pancreas: 35 Years of Research but the Enigma Remains. *Endocr Rev* **28**, 84–116 (2007).

101. Holst, J. J. *et al.* Proglucagon processing in porcine and human pancreas. *J Biological Chem* **269**, 18827–33 (1994).

102. Bell, G. I., Sanchez-Pescador, R., Laybourn, P. J. & Najarian, R. C. Exon duplication and divergence in the human preproglucagon gene. *Nature* **304**, 368–371 (1983).

103. Ahrén, B. Glucagon--Early breakthroughs and recent discoveries. *Peptides* **67**, 74–81 (2015).

104. Chen, Y.-C., Taylor, A. J. & Verchere, C. B. Islet prohormone processing in health and disease. *Diabetes Obes Metabolism* **20 Suppl 2**, 64–76 (2018).

105. Müller, T. D. *et al.* Glucagon-like peptide 1 (GLP-1). *Mol Metab* **30**, 72–130 (2019).

106. Campbell, J. E. & Drucker, D. J. Islet α cells and glucagon—critical regulators of energy homeostasis. *Nat Rev Endocrinol* **11**, 329–338 (2015).

107. Rodriguez-Diaz, R. *et al.* Alpha cells secrete acetylcholine as a non-neuronal paracrine signal priming beta cell function in humans. *Nat Med* **17**, 888–92 (2011).

108. Lyttle, B. M. *et al.* Transcription factor expression in the developing human fetal endocrine pancreas. *Diabetologia* **51**, 1169 1180 (2008).

109. Meulen, T. van der & Huising, M. O. Role of transcription factors in the transdifferentiation of pancreatic islet cells. *J Mol Endocrinol* **54**, R103-17 (2015).

110. Zhu, Z. *et al.* Genome Editing of Lineage Determinants in Human Pluripotent Stem Cells Reveals Mechanisms of Pancreatic Development and Diabetes. *Cell Stem Cell* **18**, 755–68 (2016).

111. Cyphert, H. A. *et al.* Examining How the MAFB Transcription Factor Affects Islet β Cell Function Postnatally. *Diabetes* **68**, db180903 (2018).

112. Russell, R. *et al.* Loss of the transcription factor MAFB limits β-cell derivation from human PSCs. *Nat Commun* **11**, 2742 (2020).

113. Benninger, R. K. P. & Hodson, D. J. New Understanding of β-Cell Heterogeneity and In Situ Islet Function. *Diabetes* **67**, 537–547 (2018).

114. Dorrell, C. *et al.* Human islets contain four distinct subtypes of β cells. *Nat Commun* **7**, 11756 (2016).

115. Drigo, R. A. e, Roy, B. & MacDonald, P. E. Molecular and functional profiling of human islets: from heterogeneity to human phenotypes. *Diabetologia* **63**, 2095–2101 (2020).

116. Jennings, R. E., Scharfmann, R. & Staels, W. Transcription factors that shape the mammalian pancreas. *Diabetologia* **63**, 1974–1980 (2020).

117. Zhang, J., McKenna, L. B., Bogue, C. W. & Kaestner, K. H. The diabetes gene Hhex maintains δ-cell differentiation and islet function. *Gene Dev* **28**, 829–834 (2014).

118. Gage, B. K. *et al.* The Role of ARX in Human Pancreatic Endocrine Specification. *Plos One* **10**, e0144100 (2015).

119. Andralojc, K. M. *et al.* Ghrelin-producing epsilon cells in the developing and adult human pancreas. *Diabetologia* **52**, 486–493 (2008).

120. Sousa, M. & Bruges-Armas, J. Monogenic Diabetes: Genetics and Relevance on Diabetes Mellitus Personalized Medicine. *Curr Diabetes Rev* **16**, 807–819 (2020).

121. Staffers, D. A., Ferrer, J., Clarke, W. L. & Habener, J. F. Early-onset type-ll diabetes mellitus (MODY4) linked to IPF1. *Nat Genet* **17**, 138–139 (1997).

122. Clocquet, A. R. *et al.* Impaired insulin secretion and increased insulin sensitivity in familial maturity-onset diabetes of the young 4 (insulin promoter factor 1 gene). *Diabetes* **49**, 1856–1864 (2000).

123. Brissova, M. *et al.* Reduction in Pancreatic Transcription Factor PDX-1 Impairs Glucose-stimulated Insulin Secretion. *J Biol Chem* **277**, 11225–11232 (2002).

124. Johnson, J. D. *et al.* Increased islet apoptosis in Pdx1+/– mice. *J Clin Invest* **111**, 1147–1160 (2003).

125. Pontoglio, M. *et al.* Defective insulin secretion in hepatocyte nuclear factor 1alpha-deficient mice. *J Clin Invest* **101**, 2215–2222 (1998).

126. Gupta, R. K. *et al.* The MODY1 gene HNF-4α regulates selected genes involved in insulin secretion. *J Clin Invest* **115**, 1006–1015 (2005).

127. Vaxillaire, M. & Froguel, P. Monogenic Diabetes in the Young, Pharmacogenetics and Relevance to Multifactorial Forms of Type 2 Diabetes. *Endocr Rev* **29**, 254–264 (2008).

128. Wang, J. *et al.* Mutant Neurogenin-3 in Congenital Malabsorptive Diarrhea. *New Engl J Medicine* **355**, 270–280 (2006).

129. Rubio-Cabezas, O. *et al.* Permanent Neonatal Diabetes and Enteric Anendocrinosis Associated With Biallelic Mutations in NEUROG3. *Diabetes* **60**, 1349–1353 (2011).

130. Rorsman, P. & Braun, M. Regulation of insulin secretion in human pancreatic islets. *Annu Rev Physiol* **75**, 155–79 (2012).

131. Noguchi, G. M. & Huising, M. O. Integrating the inputs that shape pancreatic islet hormone release. *Nat Metabolism* **1**, 1189–1201 (2019).

132. Rorsman, P. & Huising, M. O. The somatostatin-secreting pancreatic δ-cell in health and disease. *Nat Rev Endocrinol* **14**, 404–414 (2018).

133. Rutter, G. A., Georgiadou, E., Martinez-Sanchez, A. & Pullen, T. J. Metabolic and functional specialisations of the pancreatic beta cell: gene disallowance, mitochondrial metabolism and intercellular connectivity. *Diabetologia* **63**, 1990–1998 (2020).

134. Caicedo, A. Paracrine and autocrine interactions in the human islet: more than meets the eye. *Semin Cell Dev Biol* **24**, 11–21 (2012).

135. Rodriguez-Diaz, R., Tamayo, A., Hara, M. & Caicedo, A. The Local Paracrine Actions of the Pancreatic α-Cell. *Diabetes* **69**, 550–558 (2019).

136. Watts, M., Ha, J., Kimchi, O. & Sherman, A. Paracrine Regulation of Glucagon Secretion: The β-α-δ Model. *Am J Physiology Endocrinol Metabolism* **310**, ajpendo.00415.2015 (2016).

137. Dai, C. *et al.* Islet-enriched gene expression and glucose-induced insulin secretion in human and mouse islets. *Diabetologia* **55**, 707 718 (2012).

138. Ferrer, J., Benito, C. & Gomis, R. Pancreatic Islet GLUT2 Glucose Transporter mRNA and Protein Expression in Humans With and Without NIDDM. *Diabetes* **44**, 1369–1374 (1995).

139. Vos, A. D. *et al.* Human and rat beta cells differ in glucose transporter but not in glucokinase gene expression. *J Clin Invest* **96**, 2489–2495 (1995).

140. Thorens, B. & Mueckler, M. Glucose transporters in the 21st Century. *Am J Physiol-endoc M* **298**, E141–E145 (2010).

141. Braun, M. *et al.* Voltage-Gated Ion Channels in Human Pancreatic -Cells: Electrophysiological Characterization and Role in Insulin Secretion. *Diabetes* **57**, 1618–1628 (2008).

142. Zhang, I. X., Raghavan, M. & Satin, L. S. The Endoplasmic Reticulum and Calcium Homeostasis in Pancreatic Beta Cells. *Endocrinology* **161**, (2019).

143. Gilon, P., Shepherd, R. M. & Henquin, J. C. Oscillations of secretion driven by oscillations of cytoplasmic Ca2+ as evidences in single pancreatic islets. *J Biological Chem* **268**, 22265–8 (1993).

144. Halban, P. A. *et al.* The Possible Importance of Contact between Pancreatic Islet Cells for the Control of Insulin Release*. *Endocrinology* **111**, 86–94 (1982).

145. Ravier, M. A. *et al.* Loss of Connexin36 Channels Alters -Cell Coupling, Islet Synchronization of Glucose-Induced Ca2+ and Insulin Oscillations, and Basal Insulin Release. *Diabetes* **54**, 1798–1807 (2005).

146. Henquin, J.-C., Dufrane, D. & Nenquin, M. Nutrient control of insulin secretion in isolated normal human islets. *Diabetes* **55**, 3470 3477 (2006).

147. Henquin, J. C. Regulation of insulin secretion: a matter of phase control and amplitude modulation. *Diabetologia* **52**, 739–751 (2009).

148. Henquin, J. C. Triggering and amplifying pathways of regulation of insulin secretion by glucose. *Diabetes* **49**, 1751–1760 (2000).

149. Campbell, J. E. & Newgard, C. B. Mechanisms controlling pancreatic islet cell function in insulin secretion. *Nat Rev Mol Cell Bio* 1–17 (2021) doi:10.1038/s41580-020-00317-7.

150. Kibbey, R. G. *et al.* Mitochondrial GTP Regulates Glucose-Stimulated Insulin Secretion. *Cell Metab* **5**, 253–264 (2007).

151. Jesinkey, S. R. *et al.* Mitochondrial GTP Links Nutrient Sensing to β Cell Health, Mitochondrial Morphology, and Insulin Secretion Independent of OxPhos. *Cell Reports* **28**, 759-772.e10 (2019).

152. Ronnebaum, S. M. *et al.* A Pyruvate Cycling Pathway Involving Cytosolic NADP-dependent Isocitrate Dehydrogenase Regulates Glucose-stimulated Insulin Secretion. *J Biol Chem* **281**, 30593–30602 (2006).

153. Ivarsson, R. *et al.* Redox Control of Exocytosis: Regulatory Role of NADPH, Thioredoxin, and Glutaredoxin. *Diabetes* **54**, 2132–2142 (2005).

154. Ferdaoussi, M. *et al.* Isocitrate-to-SENP1 signaling amplifies insulin secretion and rescues dysfunctional β cells. *J Clin Investigation* **125**, 3847–60 (2015).

155. Jitrapakdee, S., Wutthisathapornchai, A., Wallace, J. C. & MacDonald, M. J. Regulation of insulin secretion: role of mitochondrial signalling. *Diabetologia* **53**, 1019–1032 (2010).

156. Nicholls, D. G. The Pancreatic β-Cell: A Bioenergetic Perspective. *Physiol Rev* **96**, 1385–1447 (2016).

157. Maechler, P. Mitochondrial function and insulin secretion. *Mol Cell Endocrinol* **379**, 12–8 (2013).

158. Maechler, P. *et al.* Role of Mitochondria in β-cell Function and Dysfunction. in vol. 654 193 216 (Springer International Publishing, 2010).

159. Malaisse, W. J., Hutton, J. C., Carpinelli, A. R., Herchuelz, A. & Sener, A. The Stimulus-secretion Coupling of Amino Acid-induced Insulin Release: Metabolism and Cationic Effects of Leucine. *Diabetes* **29**, 431–437 (1980).

160. Newsholme, P., Brennan, L. & Bender, K. Amino Acid Metabolism, -Cell Function, and Diabetes. *Diabetes* **55**, S39–S47 (2006).

161. Sener, A. & Malaisse, W. J. The stimulus–secretion coupling of amino acid-induced insulin release. Insulinotropic action of ?-alanine. *Biochimica Et Biophysica Acta Bba - Gen Subj* **1573**, 100–104 (2002).

162. Yan-Do, R. *et al.* A Glycine-Insulin Autocrine Feedback Loop Enhances Insulin Secretion From Human β-Cells and Is Impaired in Type 2 Diabetes. *Diabetes* **65**, 2311–2321 (2016).

163. Feldmann, N. *et al.* Reduction of plasma membrane glutamate transport potentiates insulin but not glucagon secretion in pancreatic islet cells. *Mol Cell Endocrinol* **338**, 46–57 (2011).

164. Newsholme, P., Cruzat, V., Arfuso, F. & Keane, K. Nutrient regulation of insulin secretion and action. *J Endocrinol* **221**, R105–R120 (2014).

165. Thams, P. & Capito, K. L-arginine stimulation of glucose-induced insulin secretion through membrane depolarization and independent of nitric oxide. *Eur J Endocrinol* **140**, 87–93 (1999).

166. Wu, Z.-Y. *et al.* AMPA receptors regulate exocytosis and insulin release in pancreatic β cells. *Traffic Cph Den* **13**, 1124–39 (2012).

167. Marquard, J. *et al.* Characterization of pancreatic NMDA receptors as possible drug targets for diabetes treatment. *Nat Med* **21**, 363–72 (2015).

168. Capozzi, M. E. *et al.* β-Cell tone is defined by proglucagon peptides through cyclic AMP signaling. *Jci Insight* **4**, e126742 (2019).

169. Briscoe, C. P. *et al.* The Orphan G Protein-coupled Receptor GPR40 Is Activated by Medium and Long Chain Fatty Acids. *J Biol Chem* **278**, 11303–11311 (2003).

170. Itoh, Y. *et al.* Free fatty acids regulate insulin secretion from pancreatic β cells through GPR40. *Nature* **422**, 173–176 (2003).

171. Tomita, T. *et al.* Expression of the gene for a membrane-bound fatty acid receptor in the pancreas and islet cell tumours in humans: evidence for GPR40 expression in pancreatic beta cells and implications for insulin secretion. *Diabetologia* **49**, 962–968 (2006).

172. Kristinsson, H., Smith, D. M., Bergsten, P. & Sargsyan, E. FFAR1 Is Involved in Both the Acute and Chronic Effects of Palmitate on Insulin Secretion. *Endocrinology* **154**, 4078–4088 (2013).

173. Mcintyre, N., Holdsworth, C. D. & Turner, D. S. NEW INTERPRETATION OF ORAL GLUCOSE TOLERANCE. *Lancet* **284**, 20–21 (1964).

174. ELRICK, H., STIMMLER, L., HLAD, C. J. & ARAI, Y. Plasma Insulin Response to Oral and Intravenous Glucose Administration1. *J Clin Endocrinol Metabolism* **24**, 1076–1082 (1964).

175. Brubaker, P. L. & Drucker, D. J. Structure-function of the glucagon receptor family of G protein-coupled receptors: the glucagon, GIP, GLP-1, and GLP-2 receptors. *Receptor Channel* **8**, 179–88 (2002).

176. Mojsov, S., Weir, G. C. & Habener, J. F. Insulinotropin: glucagon-like peptide I (7-37) co-encoded in the glucagon gene is a potent stimulator of insulin release in the perfused rat pancreas. *J Clin Invest* **79**, 616–619 (1987).

177. Kieffer, T. J. & Habener, J. F. The Glucagon-Like Peptides. *Endocr Rev* **20**, 876–913 (1999).

178. Mojsov, S. *et al.* Preproglucagon gene expression in pancreas and intestine diversifies at the level of post-translational processing. *J Biological Chem* **261**, 11880–9 (1986).

179. Drucker, D. J., Habener, J. F. & Holst, J. J. Discovery, characterization, and clinical development of the glucagon-like peptides. *J Clin Investigation* **127**, 4217–4227 (2017).

180. Lauritsen, K. B., Moody, A. J., Christensen, K. C. & Jensen, S. L. Gastric Inhibitory Polypeptide (GIP) and Insulin Release after Small-Bowel Resection in Man. *Scand J Gastroentero* **15**, 833–840 (1980).

181. BROWN, J. C., DRYBURGH, J. R., ROSS, S. A. & DUPRÉ, J. Proceedings of the 1974 Laurentian Hormone Conference. *Recent Prog Horm Res* **31**, 487–532 (1975).

182. Kolic, J. & MacDonald, P. E. cAMP-independent effects of GLP-1 on β cells. *J Clin Invest* **125**, 4327–4330 (2015).

183. Shigeto, M. *et al.* GLP-1 stimulates insulin secretion by PKC-dependent TRPM4 and TRPM5 activation. *J Clin Investigation* **125**, 4714–28 (2015).

184. Kim, S.-J. *et al.* A Novel Mechanism for the Suppression of a Voltage-gated Potassium Channel by Glucose-dependent Insulinotropic Polypeptide: PROTEIN KINASE A-DEPENDENT ENDOCYTOSIS. *J Biol Chem* **280**, 28692–28700 (2005).

185. Ehses, J. A., Pelech, S. L., Pederson, R. A. & McIntosh, C. H. S. Glucose-dependent Insulinotropic Polypeptide Activates the Raf-Mek1/2-ERK1/2 Module via a Cyclic AMP/cAMP-dependent Protein Kinase/Rap1-mediated Pathway. *J Biol Chem* **277**, 37088–37097 (2002).

186. MacDonald, P. E. *et al.* The Multiple Actions of GLP-1 on the Process of Glucose-Stimulated Insulin Secretion. *Diabetes* **51**, S434–S442 (2002).

187. Gromada, J. *et al.* Glucagon-Like Peptide 1(7-36) Amide Stimulates Exocytosis in Human Pancreatic -Cells by Both Proximal and Distal Regulatory Steps in Stimulus-Secretion Coupling. *Diabetes* **47**, 57–65 (1998).

188. Baggio, L. L. & Drucker, D. J. Biology of Incretins: GLP-1 and GIP. *Gastroenterology* **132**, 2131–2157 (2007).

189. Straub, S. G. & Sharp, G. W. G. Evolving insights regarding mechanisms for the inhibition of insulin release by norepinephrine and heterotrimeric G proteins. *Am J Physiol-cell Ph* **302**, C1687–C1698 (2012).

190. Renström, E., Ding, W.-G., Bokvist, K. & Rorsman, P. Neurotransmitter-Induced Inhibition of Exocytosis in Insulin-Secreting β Cells by Activation of Calcineurin. *Neuron* **17**, 513–522 (1996).

191. Ahrén, B. Autonomic regulation of islet hormone secretion - Implications for health and disease. *Diabetologia* **43**, 393–410 (2000).

192. Salem, V. *et al.* Leader β-cells coordinate Ca2+ dynamics across pancreatic islets in vivo. *Nat Metabolism* **1**, 615–629 (2019).

193. Johnston, N. R. *et al.* Beta Cell Hubs Dictate Pancreatic Islet Responses to Glucose. *Cell Metab* **24**, 389 401 (2016).

194. Westacott, M. J. *et al.* Age-Dependent Decline in the Coordinated [Ca(2+)] and Insulin Secretory Dynamics in Human Pancreatic Islets. *Diabetes* **66**, 2436–2445 (2017).

195. Rutter, G. A., Ninov, N., Salem, V. & Hodson, D. J. Comment on Satin et al. "Take Me To Your Leader": An Electrophysiological Appraisal of the Role of Hub Cells in Pancreatic Islets. Diabetes 2020;69:830–836. *Diabetes* **69**, e10–e11 (2020).

196. Satin, L. S., Zhang, Q. & Rorsman, P. "Take Me To Your Leader": An Electrophysiological Appraisal of the Role of Hub Cells in Pancreatic Islets. *Diabetes* **69**, 830–836 (2020).

197. Satin, L. S. & Rorsman, P. Response to Comment on Satin et al. "Take Me To Your Leader": An Electrophysiological Appraisal of the Role of Hub Cells in Pancreatic Islets. Diabetes 2020;69:830–836. *Diabetes* **69**, e12–e13 (2020).

198. Samols, E., Marri, G. & Marks, V. PROMOTION OF INSULIN SECRETION BY GLUCAGON. *Lancet* **286**, 415–416 (1965).

199. Huypens, P., Ling, Z., Pipeleers, D. & Schuit, F. Glucagon receptors on human islet cells contribute to glucose competence of insulin release. *Diabetologia* **43**, 1012–1019 (2000).

200. Zhu, L. *et al.* Intra-islet glucagon signaling is critical for maintaining glucose homeostasis. *Jci Insight* **5**, e127994 (2019).

201. Svendsen, B. *et al.* Insulin Secretion Depends on Intra-islet Glucagon Signaling. *Cell Reports* **25**, 1127-1134.e2 (2018).

202. Souza, A. H. de *et al.* Intra-islet GLP-1, but not CCK, is necessary for β-cell function in mouse and human islets. *Sci Rep-uk* **10**, 2823 (2020).

203. Moede, T., Leibiger, I. B. & Berggren, P.-O. Alpha cell regulation of beta cell function. *Diabetologia* **63**, 2064–2075 (2020).

204. Ampofo, E., Nalbach, L., Menger, M. D. & Laschke, M. W. Regulatory Mechanisms of Somatostatin Expression. *Int J Mol Sci* **21**, 4170 (2020).

205. Zhang, Q. *et al.* R-type Ca2+-channel-evoked CICR regulates glucose-induced somatostatin secretion. *Nat Cell Biol* **9**, 453–460 (2007).

206. Meulen, T. van der *et al.* Urocortin3 mediates somatostatin-dependent negative feedback control of insulin secretion. *Nat Med* **21**, 769–776 (2015).

207. DiGruccio, M. R. *et al.* Comprehensive alpha, beta and delta cell transcriptomes reveal that ghrelin selectively activates delta cells and promotes somatostatin release from pancreatic islets. *Mol Metab* **5**, 449–58 (2016).

208. Kailey, B. *et al.* SSTR2 is the functionally dominant somatostatin receptor in human pancreatic β- and α-cells. *Am J Physiology Endocrinol Metabolism* **303**, E1107-16 (2012).

209. Singh, V. *et al.* Characterization of Somatostatin Receptor Subtype-Specific Regulation of Insulin and Glucagon Secretion: An in Vitro Study on Isolated Human Pancreatic Islets. *J Clin Endocrinol Metabolism* **92**, 673–680 (2006).

210. Hauge-Evans, A. C. *et al.* Somatostatin secreted by islet delta-cells fulfills multiple roles as a paracrine regulator of islet function. *Diabetes* **58**, 403–11 (2008).

211. Yada, T. *et al.* Ghrelin signalling in β-cells regulates insulin secretion and blood glucose. *Diabetes Obes Metabolism* **16**, 111–117 (2014).

212. Dezaki, K., Kakei, M. & Yada, T. Ghrelin Uses G i2 and Activates Voltage-Dependent K+ Channels to Attenuate Glucose-Induced Ca2+ Signaling and Insulin Release in Islet -Cells: Novel Signal Transduction of Ghrelin. *Diabetes* **56**, 2319–2327 (2007).

213. Broglio, F. *et al.* Ghrelin, a Natural GH Secretagogue Produced by the Stomach, Induces Hyperglycemia and Reduces Insulin Secretion in Humans. *J Clin Endocrinol Metabolism* **86**, 5083–5083 (2001).

214. Broglio, F. *et al.* The Endocrine Response to Ghrelin as a Function of Gender in Humans in Young and Elderly Subjects. *J Clin Endocrinol Metabolism* **88**, 1537–1542 (2003).

215. Alamri, B. N., Shin, K., Chappe, V. & Anini, Y. The role of ghrelin in the regulation of glucose homeostasis. *Hormone Mol Biology Clin Investigation* **26**, 3–11 (2016).

216. Hanna, S. T. *et al.* Kiss-and-run exocytosis and fusion pores of secretory vesicles in human beta-cells. *Pflügers Archiv European J Physiology* **457**, 1343–50 (2008).

217. MacDonald, P. E., Braun, M., Galvanovskis, J. & Rorsman, P. Release of small transmitters through kiss-and-run fusion pores in rat pancreatic β cells. *Cell Metab* **4**, 283–290 (2006).

218. Fernandez-Alvarez, J., Hillaire-Buys, D., Loubatières-Mariani, M.-M., Gomis, R. & Petit, P. P2 Receptor Agonists Stimulate Insulin Release from Human Pancreatic Islets. *Pancreas* **22**, 69–71 (2001).

219. Silva, A. M. *et al.* Electrophysiological and immunocytochemical evidence for P2X purinergic receptors in pancreatic beta cells. *Pancreas* **36**, 279–83 (2008).

220. Saunders, D. C. *et al.* Ectonucleoside Triphosphate Diphosphohydrolase-3 Antibody Targets Adult Human Pancreatic β Cells for In Vitro and In Vivo Analysis. *Cell Metab* **29**, 745-754.e4 (2019).

221. Almaça, J. *et al.* Human Beta Cells Produce and Release Serotonin to Inhibit Glucagon Secretion from Alpha Cells. *Cell Reports* **17**, 3281–3291 (2016).

222. Kim, H. *et al.* Serotonin regulates pancreatic beta cell mass during pregnancy. *Nat Med* **16**, 804–808 (2010).

223. Moon, J. H. *et al.* Serotonin Regulates Adult β-Cell Mass by Stimulating Perinatal β-Cell Proliferation. *Diabetes* **69**, 205–214 (2019).

224. Kim, K. *et al.* Functional Role of Serotonin in Insulin Secretion in a Diet-Induced Insulin-Resistant State. *Endocrinology* **156**, 444–452 (2015).

225. Ohara-Imaizumi, M. *et al.* Serotonin regulates glucose-stimulated insulin secretion from pancreatic β cells during pregnancy. *Proc National Acad Sci* **110**, 19420–19425 (2013).

226. Wang, C., Ling, Z. & Pipeleers, D. Comparison of cellular and medium insulin and GABA content as markers for living β-cells. *Am J Physiol-endoc M* **288**, E307–E313 (2005).

227. Menegaz, D. *et al.* Mechanism and effects of pulsatile GABA secretion from cytosolic pools in the human beta cell. *Nat Metabolism* **1**, 1110–1126 (2019).

228. Braun, M. *et al.* Gamma-aminobutyric acid (GABA) is an autocrine excitatory transmitter in human pancreatic beta-cells. *Diabetes* **59**, 1694–701 (2010).

229. Rodriguez-Diaz, R. *et al.* Alpha cells secrete acetylcholine as a non-neuronal paracrine signal priming beta cell function in humans. *Nat Med* **17**, 888–92 (2011).

230. Molina, J. *et al.* Control of insulin secretion by cholinergic signaling in the human pancreatic islet. *Diabetes* **63**, 2714–26 (2014).

231. Molina, J. *et al.* Control of insulin secretion by cholinergic signaling in the human pancreatic islet. *Diabetes* **63**, 2714–26 (2014).

232. Gilon, P., Nenquin, M. & Henquin, J. C. Muscarinic stimulation exerts both stimulatory and inhibitory effects on the concentration of cytoplasmic Ca2+ in the electrically excitable pancreatic B-cell. *Biochem J* **311**, 259–267 (1995).

233. Gylfe, E. Glucose control of glucagon secretion—'There's a brand-new gimmick every year.' *Upsala J Med Sci* **121**, 120–132 (2016).

234. Gylfe, E. & Gilon, P. Glucose regulation of glucagon secretion. *Diabetes Res Clin Pr* **103**, 1–10 (2014).

235. Briant, L., Salehi, A., Vergari, E., Zhang, Q. & Rorsman, P. Glucagon secretion from pancreatic α-cells. *Upsala J Med Sci* **121**, 113–9 (2016).

236. Gromada, J., Chabosseau, P. & Rutter, G. A. The α-cell in diabetes mellitus. *Nat Rev Endocrinol* **14**, 694–704 (2018).

237. Walker, J. N. *et al.* Regulation of glucagon secretion by glucose: paracrine, intrinsic or both? *Diabetes Obes Metabolism* **13 Suppl 1**, 95–105 (2011).

238. Blodgett, D. M. *et al.* Novel Observations From Next-Generation RNA Sequencing of Highly Purified Human Adult and Fetal Islet Cell Subsets. *Diabetes* **64**, 3172 3181 (2015).

239. Basco, D. *et al.* α-cell glucokinase suppresses glucose-regulated glucagon secretion. *Nat Commun* **9**, 546 (2018).

240. Briant, L. J. B. *et al.* Functional identification of islet cell types by electrophysiological fingerprinting. *J Roy Soc Interface* **14**, 20160999 (2017).

241. Barg, S., Galvanovskis, J., Gopel, S. O., Rorsman, P. & Eliasson, L. Tight coupling between electrical activity and exocytosis in mouse glucagon-secreting alpha-cells. *Diabetes* **49**, 1500–1510 (2000).

242. Zhang, Q. *et al.* Role of KATP channels in glucose-regulated glucagon secretion and impaired counterregulation in type 2 diabetes. *Cell Metab* **18**, 871–82 (2013).

243. MacDonald, P. E. *et al.* A K ATP channel-dependent pathway within alpha cells regulates glucagon release from both rodent and human islets of Langerhans. *Plos Biol* **5**, e143 (2007).

244. Gromada, J. *et al.* ATP-Sensitive K+ Channel-Dependent Regulation of Glucagon Release and Electrical Activity by Glucose in Wild-Type and SUR1-/- Mouse -Cells. *Diabetes* **53**, S181–S189 (2004).

245. Quoix, N. *et al.* Glucose and pharmacological modulators of ATP-sensitive K+ channels control [Ca2+]c by different mechanisms in isolated mouse alpha-cells. *Diabetes* **58**, 412–21 (2008).

246. Liu, Y.-J., Vieira, E. & Gylfe, E. A store-operated mechanism determines the activity of the electrically excitable glucagon-secreting pancreatic α-cell. *Cell Calcium* **35**, 357–365 (2004).

247. Vieira, E., Salehi, A. & Gylfe, E. Glucose inhibits glucagon secretion by a direct effect on mouse pancreatic alpha cells. *Diabetologia* **50**, 370–379 (2006).

248. Tian, G., Tepikin, A. V., Tengholm, A. & Gylfe, E. cAMP Induces Stromal Interaction Molecule 1 (STIM1) Puncta but neither Orai1 Protein Clustering nor Store-operated Ca 2+ Entry (SOCE) in Islet Cells. *J Biol Chem* **287**, 9862–9872 (2012).

249. Hughes, J. W., Ustione, A., Lavagnino, Z. & Piston, D. W. Regulation of islet glucagon secretion: Beyond calcium. *Diabetes Obes Metabolism* **20**, 127–136 (2018).

250. Marchand, S. J. L. & Piston, D. W. Glucose decouples intracellular Ca2+ activity from glucagon secretion in mouse pancreatic islet alpha-cells. *Plos One* **7**, e47084 (2012).

251. Marchand, S. J. L. & Piston, D. W. Glucose Suppression of Glucagon Secretion: METABOLIC AND CALCIUM RESPONSES FROM α-CELLS IN INTACT MOUSE PANCREATIC ISLETS. *J Biol Chem* **285**, 14389–14398 (2010).

252. Johansson, H., Gylfe, E. & Hellman, B. Cyclic AMP raises cytoplasmic calcium in pancreatic α2-cells by mobilizing calcium incorporated in response to glucose. *Cell Calcium* **10**, 205–211 (1989).

253. Yu, Q., Shuai, H., Ahooghalandari, P., Gylfe, E. & Tengholm, A. Glucose controls glucagon secretion by directly modulating cAMP in alpha cells. *Diabetologia* **62**, 1212–1224 (2019).

254. Zhou, C., Dhall, D., Nissen, N. N., Chen, C.-R. & Yu, R. Homozygous P86S Mutation of the Human Glucagon Receptor Is Associated With Hyperglucagonemia, &agr; Cell Hyperplasia, and Islet Cell Tumor. *Pancreas* **38**, 941–946 (2009).

255. Dean, E. D. *et al.* Interrupted Glucagon Signaling Reveals Hepatic α Cell Axis and Role for L-Glutamine in α Cell Proliferation. *Cell Metab* **25**, 1362-1373.e5 (2017).

256. Galsgaard, K. D. *et al.* Disruption of glucagon receptor signaling causes hyperaminoacidemia exposing a possible liver-alpha-cell axis. *Am J Physiol-endoc M* **314**, E93–E103 (2018).

257. Albrechtsen, N. J. W. *et al.* Evidence of a liver-alpha cell axis in humans: hepatic insulin resistance attenuates relationship between fasting plasma glucagon and glucagonotropic amino acids. *Diabetologia* **61**, 671–680 (2018).

258. Solloway, M. J. *et al.* Glucagon Couples Hepatic Amino Acid Catabolism to mTOR-Dependent Regulation of α-Cell Mass. *Cell Reports* **12**, 495–510 (2015).

259. Kim, J. *et al.* Amino Acid Transporter Slc38a5 Controls Glucagon Receptor Inhibition-Induced Pancreatic α Cell Hyperplasia in Mice. *Cell Metab* **25**, 1348-1361.e8 (2017).

260. Ohneda, A., Parada, E., Eisentraut, A. M. & Unger, R. H. Characterization of response of circulating glucagon to intraduodenal and intravenous administration of amino acids. *J Clin Invest* **47**, 2305–2322 (1968).

261. Müller, W. A., Faloona, G. R. & Unger, R. H. The effect of alanine on glucagon secretion. *J Clin Invest* **50**, 2215–2218 (1971).

262. Ang, T., Bruce, C. R. & Kowalski, G. M. Postprandial Aminogenic Insulin and Glucagon Secretion Can Stimulate Glucose Flux in Humans. *Diabetes* **68**, 939–946 (2019).

263. Marroquí, L. *et al.* Nutrient regulation of glucagon secretion: involvement in metabolism and diabetes. *Nutr Res Rev* **27**, 48–62 (2014).

264. Hayashi, M. *et al.* Secretory Granule-mediated Co-secretion ofl-Glutamate and Glucagon Triggers Glutamatergic Signal Transmission in Islets of Langerhans. *J Biol Chem* **278**, 1966–1974 (2002).

265. Li, C. *et al.* Regulation of glucagon secretion in normal and diabetic human islets by γ-hydroxybutyrate and glycine. *J Biological Chem* **288**, 3938–51 (2012).

266. Gannon, M. C., Nuttall, J. A. & Nuttall, F. Q. The metabolic response to ingested glycine. *Am J Clin Nutrition* **76**, 1302–1307 (2002).

267. Dean, E. D. A Primary Role for α-Cells as Amino Acid Sensors. *Diabetes* **69**, 542–549 (2020).

268. Radulescu, A., Gannon, M. C. & Nuttall, F. Q. The Effect on Glucagon, Glucagon-Like Peptide-1, Total and Acyl-Ghrelin of Dietary Fats Ingested with and without Potato. *J Clin Endocrinol Metabolism* **95**, 3385–3391 (2010).

269. Raben, A., Holst, J. J., Madsen, J. & Astrup, A. Diurnal metabolic profiles after 14 d of an ad libitum high-starch, high-sucrose, or high-fat diet in normal-weight never-obese and postobese women. *Am J Clin Nutrition* **73**, 177–189 (2001).

270. Kristinsson, H. *et al.* Basal hypersecretion of glucagon and insulin from palmitate-exposed human islets depends on FFAR1 but not decreased somatostatin secretion. *Sci Rep-uk* **7**, 4657 (2017).

271. Olofsson, C. S., Salehi, A., Gopel, S. O., Holm, C. & Rorsman, P. Palmitate Stimulation of Glucagon Secretion in Mouse Pancreatic -Cells Results From Activation of L-Type Calcium Channels and Elevation of Cytoplasmic Calcium. *Diabetes* **53**, 2836–2843 (2004).

272. Vieira, E., Liu, Y.-J. & Gylfe, E. Involvement of alpha1 and beta-adrenoceptors in adrenaline stimulation of the glucagon-secreting mouse alpha-cell. *Naunyn-schmiedeberg's Archives Pharmacol* **369**, 179–183 (2004).

273. Dai, X.-Q. *et al.* SUMO1 enhances cAMP-dependent exocytosis and glucagon secretion from pancreatic α-cells: SUMO1 enhances α-cell exocytosis and glucagon secretion. *J Physiology* **592**, 3715–3726 (2014).

274. Hamilton, A. *et al.* Adrenaline Stimulates Glucagon Secretion by Tpc2-Dependent Ca2+ Mobilization From Acidic Stores in Pancreatic α-Cells. *Diabetes* **67**, 1128–1139 (2018).

275. Gromada, J. *et al.* Adrenaline Stimulates Glucagon Secretion in Pancreatic A-Cells by Increasing the Ca2+ Current and the Number of Granules Close to the L-Type Ca2+ Channels. *J Gen Physiology* **110**, 217–228 (1997).

276. Unger, R. H. & Orci, L. Paracrinology of islets and the paracrinopathy of diabetes. *Proc National Acad Sci* **107**, 16009–16012 (2010).

277. Olsen, H. L. *et al.* Glucose Stimulates Glucagon Release in Single Rat α-Cells by Mechanisms that Mirror the Stimulus-Secretion Coupling in β-Cells. *Endocrinology* **146**, 4861–4870 (2005).

278. Salehi, A., Vieira, E. & Gylfe, E. Paradoxical Stimulation of Glucagon Secretion by High Glucose Concentrations. *Diabetes* **55**, 2318–2323 (2006).

279. Ishihara, H., Maechler, P., Gjinovci, A., Herrera, P.-L. & Wollheim, C. B. Islet β-cell secretion determines glucagon release from neighbouring α-cells. *Nat Cell Biol* **5**, 330–335 (2003).

280. Franklin, I., Gromada, J., Gjinovci, A., Theander, S. & Wollheim, C. B. -Cell Secretory Products Activate -Cell ATP-Dependent Potassium Channels to Inhibit Glucagon Release. *Diabetes* **54**, 1808–1815 (2005).

281. Elliott, A. D., Ustione, A. & Piston, D. W. Somatostatin and insulin mediate glucose-inhibited glucagon secretion in the pancreatic α-cell by lowering cAMP. *Am J Physiology Endocrinol Metabolism* **308**, E130-43 (2014).

282. Xu, E. *et al.* Intra-islet insulin suppresses glucagon release via GABA-GABAA receptor system. *Cell Metab* **3**, 47–58 (2006).

283. Jin, Y., Korol, S. V., Jin, Z., Barg, S. & Birnir, B. In intact islets interstitial GABA activates GABA(A) receptors that generate tonic currents in α-cells. *Plos One* **8**, e67228 (2013).

284. Rorsman, P. *et al.* Glucose-inhibition of glucagon secretion involves activation of GABAA-receptor chloride channels. *Nature* **341**, 233–236 (1989).

285. Grapengiesser, E., Salehi, A., Qader, S. S. & Hellman, B. Glucose Induces Glucagon Release Pulses Antisynchronous with Insulin and Sensitive to Purinoceptor Inhibition. *Endocrinology* **147**, 3472–3477 (2006).

286. Gylfe, E., Grapengiesser, E., Dansk, H. & Hellman, B. The neurotransmitter ATP triggers Ca2+ responses promoting coordination of pancreatic islet oscillations. *Pancreas* **41**, 258–63 (2012).

287. Hutchens, T. & Piston, D. W. EphA4 Receptor Forward Signaling Inhibits Glucagon Secretion From α-Cells. *Diabetes* **64**, 3839–3851 (2015).

288. Klaff, L. J. & Taborsky, G. J. Pancreatic Somatostatin is a Mediator of Glucagon Inhibition by Hyperglycemia. *Diabetes* **36**, 592–596 (1987).

289. Lai, B.-K. *et al.* Somatostatin Is Only Partly Required for the Glucagonostatic Effect of Glucose but Is Necessary for the Glucagonostatic Effect of K ATP Channel Blockers. *Diabetes* **67**, 2239–2253 (2018).

290. Otter, S. & Lammert, E. Exciting Times for Pancreatic Islets: Glutamate Signaling in Endocrine Cells. *Trends Endocrinol Metabolism Tem* **27**, 177–88 (2015).

291. Cabrera, O. *et al.* Glutamate Is a Positive Autocrine Signal for Glucagon Release. *Cell Metab* **7**, 545–554 (2008).

292. Ma, X. *et al.* Glucagon Stimulates Exocytosis in Mouse and Rat Pancreatic α-Cells by Binding to Glucagon Receptors. *Mol Endocrinol* **19**, 198–212 (2005).

293. (CDC), C. for D. C. and P. National Diabetes Statistics Report. (2020).

294. Redondo, M. J. *et al.* The clinical consequences of heterogeneity within and between different diabetes types. *Diabetologia* **63**, 2040–2048 (2020).

295. Ashcroft, F. M. & Rorsman, P. Diabetes Mellitus and the β Cell: The Last Ten Years. *Cell* **148**, 1160–1171 (2012).

296. Insel, R. A. *et al.* Staging Presymptomatic Type 1 Diabetes: A Scientific Statement of JDRF, the Endocrine Society, and the American Diabetes Association. *Diabetes Care* **38**, 1964–1974 (2015).

297. Atkinson, M. A., Eisenbarth, G. S. & Michels, A. W. Type 1 diabetes. *Lancet* **383**, 69–82 (2014).

298. Sherry, N. A., Tsai, E. B. & Herold, K. C. Natural History of -Cell Function in Type 1 Diabetes. *Diabetes* **54**, S32–S39 (2005).

299. Peters, L., Posgai, A. & Brusko, T. M. Islet–immune interactions in type 1 diabetes: the nexus of beta cell destruction. *Clin Exp Immunol* **198**, 326–340 (2019).

300. Thomas, N. J. *et al.* Frequency and phenotype of type 1 diabetes in the first six decades of life: a cross-sectional, genetically stratified survival analysis from UK Biobank. *Lancet Diabetes Endocrinol* **6**, 122–129 (2018).

301. Consortium, E.-T. *et al.* Type 1 diabetes can present before the age of 6 months and is characterised by autoimmunity and rapid loss of beta cells. *Diabetologia* 1–11 (2020) doi:10.1007/s00125-020-05276-4.

302. Leete, P. *et al.* Studies of insulin and proinsulin in pancreas and serum support the existence of aetiopathological endotypes of type 1 diabetes associated with age at diagnosis. *Diabetologia* **63**, 1258–1267 (2020).

303. Battaglia, M. *et al.* Introducing the Endotype Concept to Address the Challenge of Disease Heterogeneity in Type 1 Diabetes. *Diabetes Care* **43**, 5–12 (2019).

304. Campbell-Thompson, M. *et al.* Insulitis and β-Cell Mass in the Natural History of Type 1 Diabetes. *Diabetes* **65**, 719–31 (2015).

305. Campbell-Thompson, M. L. *et al.* The diagnosis of insulitis in human type 1 diabetes. *Diabetologia* **56**, 2541–3 (2013).

306. Coppieters, K. T. *et al.* Demonstration of islet-autoreactive CD8 T cells in insulitic lesions from recent onset and long-term type 1 diabetes patients. *J Exp Medicine* **209**, 51–60 (2012).

307. Delong, T. *et al.* Pathogenic CD4 T cells in type 1 diabetes recognize epitopes formed by peptide fusion. *Science* **351**, 711–714 (2016).

308. Babon, J. A. B. *et al.* Analysis of self-antigen specificity of islet-infiltrating T cells from human donors with type 1 diabetes. *Nat Med* **22**, 1482–1487 (2016).

309. Richardson, S. J. *et al.* Islet cell hyperexpression of HLA class I antigens: a defining feature in type 1 diabetes. *Diabetologia* **59**, 2448–58 (2016).

310. Russell, M. A. *et al.* HLA Class II Antigen Processing and Presentation Pathway Components Demonstrated by Transcriptome and Protein Analyses of Islet β-Cells From Donors With Type 1 Diabetes. *Diabetes* **68**, 988–1001 (2019).

311. Mallone, R. & Eizirik, D. L. Presumption of innocence for beta cells: why are they vulnerable autoimmune targets in type 1 diabetes? *Diabetologia* **63**, 1999–2006 (2020).

312. Wang, Y. J. *et al.* Multiplexed In Situ Imaging Mass Cytometry Analysis of the Human Endocrine Pancreas and Immune System in Type 1 Diabetes. *Cell Metab* **29**, 769-783.e4 (2019).

313. Brissova, M. *et al.* α Cell Function and Gene Expression Are Compromised in Type 1 Diabetes. *Cell Reports* **22**, 2667 2676 (2018).

314. Sherr, J. *et al.* Evolution of abnormal plasma glucagon responses to mixed-meal feedings in youth with type 1 diabetes during the first 2 years after diagnosis. *Diabetes Care* **37**, 1741–4 (2014).

315. Gerich, J. E., Langlois, M., Noacco, C., Karam, J. H. & Forsham, P. H. Lack of Glucagon Response to Hypoglycemia in Diabetes: Evidence for an Intrinsic Pancreatic Alpha Cell Defect. *Science* **182**, 171–173 (1973).

316. Bolli, G. *et al.* Abnormal Glucose Counterregulation in Insulin-dependent Diabetes Mellitus: Interaction of Anti-Insulin Antibodies and Impaired Glucagon and Epinephrine Secretion. *Diabetes* **32**, 134–141 (1983).

317. Virostko, J. *et al.* Pancreas Volume Declines During the First Year After Diagnosis of Type 1 Diabetes and Exhibits Altered Diffusion at Disease Onset. *Diabetes Care* **42**, 248–257 (2018).

318. Wright, J. J. *et al.* Decreased pancreatic acinar cell number in type 1 diabetes. *Diabetologia* 1–6 (2020) doi:10.1007/s00125-020-05155-y.

319. Campbell-Thompson, M. L. *et al.* Relative Pancreas Volume Is Reduced in First-Degree Relatives of Patients With Type 1 Diabetes. *Diabetes Care* **42**, dc181512 (2018).

320. Campbell-Thompson, M. L. *et al.* The influence of type 1 diabetes on pancreatic weight. *Diabetologia* **59**, 217–221 (2015).

321. Halban, P. A. *et al.* β-Cell Failure in Type 2 Diabetes: Postulated Mechanisms and Prospects for Prevention and Treatment. *Diabetes Care* **37**, 1751 1758 (2014).

322. Kahn, S. E., Hull, R. L. & Utzschneider, K. M. Mechanisms linking obesity to insulin resistance and type 2 diabetes. *Nature* **444**, 840–846 (2006).

323. Kahn, S. E., Cooper, M. E. & Prato, S. D. Pathophysiology and treatment of type 2 diabetes: perspectives on the past, present, and future. *Lancet* **383**, 1068 1083 (2014).

324. Esser, N., Utzschneider, K. M. & Kahn, S. E. Early beta cell dysfunction vs insulin hypersecretion as the primary event in the pathogenesis of dysglycaemia. *Diabetologia* **63**, 2007–2021 (2020).

325. Rahier, J., Guiot, Y., Goebbels, R. M., Sempoux, C. & Henquin, J. C. Pancreatic beta-cell mass in European subjects with type 2 diabetes. *Diabetes Obes Metabolism* **10 Suppl 4**, 32–42 (2008).

326. Henquin, J. C. & Rahier, J. Pancreatic alpha cell mass in European subjects with type 2 diabetes. *Diabetologia* **54**, 1720–1725 (2011).

327. Butler, A. E. *et al.* β-Cell Deficit and Increased β-Cell Apoptosis in Humans With Type 2 Diabetes. *Diabetes* **52**, 102–110 (2003).

328. Bonner-Weir, S. & O'Brien, T. D. Islets in Type 2 Diabetes: In Honor of Dr. Robert C. Turner. *Diabetes* **57**, 2899–2904 (2008).

329. Yoon, K. H. *et al.* Selective β-Cell Loss and α-Cell Expansion in Patients with Type 2 Diabetes Mellitus in Korea. *J Clin Endocrinol Metabolism* **88**, 2300–2308 (2003).

330. Mezza, T. *et al.* Insulin resistance alters islet morphology in nondiabetic humans. *Diabetes* **63**, 994–1007 (2013).

331. Fuchsberger, C. *et al.* The genetic architecture of type 2 diabetes. *Nature* **536**, 41–47 (2016).

332. Barroso, I. & McCarthy, M. I. The Genetic Basis of Metabolic Disease. *Cell* **177**, 146 161 (2019).

333. Thomsen, S. K. *et al.* Type 2 diabetes risk alleles in PAM impact insulin release from human pancreatic β-cells. *Nat Genet* **50**, 1122–1131 (2018).

334. investigators, T. M. *et al.* Twelve type 2 diabetes susceptibility loci identified through large-scale association analysis. *Nat Genet* **42**, 579–589 (2010).

335. Rosengren, A. H. *et al.* Reduced Insulin Exocytosis in Human Pancreatic -Cells With Gene Variants Linked to Type 2 Diabetes. *Diabetes* **61**, 1726–1733 (2012).

336. Manolio, T. A. *et al.* Finding the missing heritability of complex diseases. *Nature* **461**, 747–753 (2009).

337. Pasquali, L. *et al.* Pancreatic islet enhancer clusters enriched in type 2 diabetes risk-associated variants. *Nat Genet* **46**, 136–43 (2014).

338. Mahajan, A. *et al.* Fine-mapping type 2 diabetes loci to single-variant resolution using high-density imputation and islet-specific epigenome maps. *Nat Genet* **50**, 1505–1513 (2018).

339. Cohrs, C. M. *et al.* Dysfunction of Persisting β Cells Is a Key Feature of Early Type 2 Diabetes Pathogenesis. *Cell Reports* **31**, 107469 (2020).

340. Fu, J. *et al.* A glucose-dependent spatial patterning of exocytosis in human β cells is disrupted in type 2 diabetes. *JCI Insight* **4**, e127896 (2019).

341. Camunas-Soler, J. *et al.* Patch-Seq Links Single-Cell Transcriptomes to Human Islet Dysfunction in Diabetes. *Cell Metab* **31**, 1017-1031.e4 (2020).

342. Ly, L. D. *et al.* Oxidative stress and calcium dysregulation by palmitate in type 2 diabetes. *Exp Mol Medicine* **49**, e291–e291 (2017).

343. Dai, C. *et al.* Stress-impaired transcription factor expression and insulin secretion in transplanted human islets. *J Clin Invest* **126**, 1857 1870 (2016).

344. Sidarala, V. *et al.* Mitophagy protects beta cells from inflammatory damage in diabetes. *JCI Insight* **5**, e141138 (2020).

345. Gerber, P. A. & Rutter, G. A. The Role of Oxidative Stress and Hypoxia in Pancreatic Beta-Cell Dysfunction in Diabetes Mellitus. *Antioxid Redox Sign* **26**, 501–518 (2017).

346. Wang, J., Yang, X. & Zhang, J. Bridges between mitochondrial oxidative stress, ER stress and mTOR signaling in pancreatic β cells. *Cell Signal* **28**, 1099–1104 (2016).

347. Westermark, P., Andersson, A. & Westermark, G. T. Islet Amyloid Polypeptide, Islet Amyloid, and Diabetes Mellitus. *Physiol Rev* **91**, 795 826 (2011).

348. Cooper, G. J. *et al.* Purification and characterization of a peptide from amyloid-rich pancreases of type 2 diabetic patients. *Proc National Acad Sci* **84**, 8628–8632 (1987).

349. Rivera, J. F., Costes, S., Gurlo, T., Glabe, C. G. & Butler, P. C. Autophagy defends pancreatic β cells from human islet amyloid polypeptide-induced toxicity. *J Clin Invest* **124**, 3489 3500 (2014).

350. Montemurro, C. *et al.* IAPP toxicity activates HIF1α/PFKFB3 signaling delaying β-cell loss at the expense of β-cell function. *Nat Commun* **10**, 2679 (2019).

351. Janson, J., Ashley, R. H., Harrison, D., McIntyre, S. & Butler, P. C. The mechanism of islet amyloid polypeptide toxicity is membrane disruption by intermediate-sized toxic amyloid particles. *Diabetes* **48**, 491–498 (1999).

352. Paulsson, J. F. & Westermark, G. T. Aberrant processing of human proislet amyloid polypeptide results in increased amyloid formation. *Diabetes* **54**, 2117 2125 (2005).

353. Shigihara, N. *et al.* Human IAPP–induced pancreatic β cell toxicity and its regulation by autophagy. *J Clin Invest* **124**, 3634 3644 (2014).

354. Montane, J., Klimek-Abercrombie, A., Potter, K. J., Westwell-Roper, C. & Verchere, C. B. Metabolic stress, IAPP and islet amyloid. *Diabetes Obes Metabolism* **14**, 68–77 (2012).

355. Gloyn, A. L. & Drucker, D. J. Precision medicine in the management of type 2 diabetes. *Lancet Diabetes Endocrinol* **6**, 891–900 (2018).

356. Consortium, R. & Investigators, R. C. Effects of Treatment of Impaired Glucose Tolerance or Recently Diagnosed Type 2 Diabetes With Metformin Alone or in Combination With Insulin Glargine on β-Cell Function: Comparison of Responses In Youth And Adults. *Diabetes* **68**, db190299 (2019).

357. Unger, R. H. & Cherrington, A. D. Glucagonocentric restructuring of diabetes: a pathophysiologic and therapeutic makeover. *J Clin Invest* **122**, 4 12 (2012).

358. Albrechtsen, N. J. W. *et al.* The Liver–α-Cell Axis and Type 2 Diabetes. *Endocr Rev* **40**, 1353–1366 (2019).

359. Kraakman, M. J., Murphy, A. J., Jandeleit-Dahm, K. & Kammoun, H. L. Macrophage polarization in obesity and type 2 diabetes: weighing down our understanding of macrophage function? *Front Immunol* **5**, 470 (2014).

360. Eguchi, K. & Nagai, R. Islet inflammation in type 2 diabetes and physiology. *J Clin Invest* **127**, 14 23 (2017).

361. Masters, S. L. *et al.* Activation of the NLRP3 inflammasome by islet amyloid polypeptide provides a mechanism for enhanced IL-1β in type 2 diabetes. *Nat Immunol* **11**, 897 904 (2010).

362. Westwell-Roper, C. Y., Ehses, J. A. & Verchere, C. B. Resident macrophages mediate islet amyloid polypeptide-induced islet IL-1β production and β-cell dysfunction. *Diabetes* **63**, 1698 1711 (2014).

363. Lekva, T., Norwitz, E. R., Aukrust, P. & Ueland, T. Impact of Systemic Inflammation on the Progression of Gestational Diabetes Mellitus. *Curr Diabetes Rep* **16**, 26 (2016).

364. Kenna, L. A., Olsen, J. A., Spelios, M. G., Radin, M. S. & Akirav, E. M. β-Cell death is decreased in women with gestational diabetes mellitus. *Diabetol Metab Syndr* **8**, 60 (2016).

365. Kelly, R. W. Pregnancy Maintenance and Parturition: The Role of Prostaglandin in Manipulating the Immune and Inflammatory Response. *Endocr Rev* **15**, 684–706 (1994).

366. Rosik, J., Szostak, B., Machaj, F. & Pawlik, A. The role of genetics and epigenetics in the pathogenesis of gestational diabetes mellitus. *Ann Hum Genet* **84**, 114–124 (2019).

367. Bellamy, L., Casas, J.-P., Hingorani, A. D. & Williams, D. Type 2 diabetes mellitus after gestational diabetes: a systematic review and meta-analysis. *Lancet* **373**, 1773–1779 (2009).

368. Urakami, T. Maturity-onset diabetes of the young (MODY): current perspectives on diagnosis and treatment. *Diabetes Metabolic Syndrome Obes Targets Ther* **Volume 12**, 1047–1056 (2019).

369. Nkonge, K. M., Nkonge, D. K. & Nkonge, T. N. The epidemiology, molecular pathogenesis, diagnosis, and treatment of maturity-onset diabetes of the young (MODY). *Clin Diabetes Endocrinol* **6**, 20 (2020).

370. Molven, A. *et al.* Mutations in the Insulin Gene Can Cause MODY and Autoantibody-Negative Type 1 Diabetes. *Diabetes* **57**, 1131–1135 (2008).

371. Prudente, S. *et al.* Loss-of-Function Mutations in APPL1 in Familial Diabetes Mellitus. *Am J Hum Genetics* **97**, 177–185 (2015).

372. Cardenas-Diaz, F. L. *et al.* Modeling Monogenic Diabetes using Human ESCs Reveals Developmental and Metabolic Deficiencies Caused by Mutations in HNF1A. *Cell Stem Cell* **25**, 273-289.e5 (2019).

373. Haliyur, R. *et al.* Human islets expressing HNF1A variant have defective β cell transcriptional regulatory networks. *J Clin Invest* **129**, 246–251 (2018).

374. Naylor, R. N., Greeley, S. A. W., Bell, G. I. & Philipson, L. H. Genetics and pathophysiology of neonatal diabetes mellitus. *J Diabetes Invest* **2**, 158–169 (2011).

375. Aguilar-Bryan, L. & Bryan, J. Neonatal diabetes mellitus. *Endocr Rev* **29**, 265–91 (2008).

376. Pipatpolkai, T., Usher, S., Stansfeld, P. J. & Ashcroft, F. M. New insights into KATP channel gene mutations and neonatal diabetes mellitus. *Nat Rev Endocrinol* **16**, 378–393 (2020).

377. Gloyn, A. L. *et al.* Activating Mutations in the Gene Encoding the ATP-Sensitive Potassium-Channel Subunit Kir6.2 and Permanent Neonatal Diabetes. *New Engl J Medicine* **350**, 1838–1849 (2004).

378. Babenko, A. P. *et al.* Activating Mutations in theABCC8Gene in Neonatal Diabetes Mellitus. *New Engl J Med* **355**, 456–466 (2006).

379. León, D. D. D. & Stanley, C. A. Mechanisms of Disease: advances in diagnosis and treatment of hyperinsulinism in neonates. *Nat Clin Pract Endoc* **3**, 57–68 (2007).

380. Li, C. *et al.* Functional and Metabolomic Consequences of KATP Channel Inactivation in Human Islets. *Diabetes* **66**, 1901–1913 (2017).

381. Rosenfeld, E., Ganguly, A. & Leon, D. D. D. Congenital hyperinsulinism disorders: Genetic and clinical characteristics. *Am J Medical Genetics Part C Seminars Medical Genetics* **181**, 682–692 (2019).

382. Rickels, M. R., Norris, A. W. & Hull, R. L. A tale of two pancreases: exocrine pathology and endocrine dysfunction. *Diabetologia* **63**, 2030–2039 (2020).

383. Norris, A. W. *et al.* Survival in a bad neighborhood: pancreatic islets in cystic fibrosis. *J Endocrinol* **241**, R35–R50 (2019).

384. Hart, N. J. *et al.* Cystic fibrosis–related diabetes is caused by islet loss and inflammation. *Jci Insight* **3**, e98240 (2018).

385. Pham, P.-T. T., Pham, P.-M. T., Pham, S. V., Pham, P.-A. T. & Pham, P.-C. T. New onset diabetes after transplantation (NODAT): an overview. *Diabetes Metabolic Syndrome Obes Targets Ther* **4**, 175 186 (2011).

386. Shivaswamy, V., Boerner, B. & Larsen, J. Post-Transplant Diabetes Mellitus: Causes, Treatment, and Impact on Outcomes. *Endocr Rev* **37**, 37 61 (2016).

387. Dai, C. *et al.* Tacrolimus- and sirolimus-induced human β cell dysfunction is reversible and preventable. *Jci Insight* **5**, e130770 (2020).

388. Johnson, J. D. *et al.* Different effects of FK506, rapamycin, and mycophenolate mofetil on glucose-stimulated insulin release and apoptosis in human islets. *Cell Transplant* **18**, 833 845 (2009).

389. Kolic, J. *et al.* Differential effects of voclosporin and tacrolimus on insulin secretion from human islets. *Endocrinology* **161**, bqaa162- (2020).

390. Bellin, M. D. & Dunn, T. B. Transplant strategies for type 1 diabetes: whole pancreas, islet and porcine beta cell therapies. *Diabetologia* **63**, 2049–2056 (2020).

391. Shapiro, A. M. *et al.* Islet transplantation in seven patients with type 1 diabetes mellitus using a glucocorticoid-free immunosuppressive regimen. *New Engl J Medicine* **343**, 230 238 (2000).

392. Chang, C. A., Lawrence, M. C. & Naziruddin, B. Current issues in allogeneic islet transplantation. *Curr Opin Organ Tran* **22**, 437–443 (2017).

393. Ricordi, C. *et al.* National Institutes of Health–Sponsored Clinical Islet Transplantation Consortium Phase 3 Trial: Manufacture of a Complex Cellular Product at Eight Processing Facilities. *Diabetes* **65**, 3418–3428 (2016).

394. Rickels, M. R. & Robertson, R. P. Pancreatic Islet Transplantation in Humans: Recent Progress and Future Directions. *Endocr Rev* **40**, 631–668 (2018).

395. Markmann, J. F. *et al.* Phase 3 trial of human islet-after-kidney transplantation in type 1 diabetes. *Am J Transplant* 1–16 (2020) doi:10.1111/ajt.16174.

396. Gamble, A., Pepper, A. R., Bruni, A. & Shapiro, A. M. J. The Journey of Islet Cell Transplantation and Future Development. *Islets* **10**, 0 (2018).

397. Harlan, D. M. Islet Transplantation for Hypoglycemia Unawareness/Severe Hypoglycemia: Caveat Emptor. *Diabetes Care* **39**, 1072–1074 (2016).

398. Pagliuca, F. W. *et al.* Generation of functional human pancreatic β cells in vitro. *Cell* **159**, 428 439 (2014).

399. Rezania, A. *et al.* Reversal of diabetes with insulin-producing cells derived in vitro from human pluripotent stem cells. *Nat Biotechnol* **32**, 1121 1133 (2014).

400. Szot, G. L. *et al.* Tolerance Induction and Reversal of Diabetes in Mice Transplanted with Human Embryonic Stem Cell-Derived Pancreatic Endoderm. *Cell Stem Cell* **16**, 148–157 (2015).

401. Russ, H. A. *et al.* Controlled induction of human pancreatic progenitors produces functional beta-like cells in vitro. *Embo J* **34**, 1759–72 (2015).

402. Millman, J. R. *et al.* Generation of stem cell-derived β-cells from patients with type 1 diabetes. *Nat Commun* **7**, 11463 (2016).

403. Yoshihara, E. *et al.* Immune-evasive human islet-like organoids ameliorate diabetes. *Nature* **586**, 606–611 (2020).

404. Nair, G. G. *et al.* Recapitulating endocrine cell clustering in culture promotes maturation of human stem-cell-derived β cells. *Nat Cell Biol* **21**, 263 274 (2019).

405. Alvarez-Dominguez, J. R. *et al.* Circadian Entrainment Triggers Maturation of Human In Vitro Islets. *Cell Stem Cell* 108-122.e10 (2019) doi:10.1016/j.stem.2019.11.011.

406. Yoshihara, E. *et al.* ERRγ Is Required for the Metabolic Maturation of Therapeutically Functional Glucose-Responsive β Cells. *Cell Metab* **23**, 622–634 (2016).

407. Velazco-Cruz, L. *et al.* Acquisition of Dynamic Function in Human Stem Cell-Derived β Cells. *Stem Cell Rep* **12**, 351–365 (2019).

408. Peterson, Q. P. *et al.* A method for the generation of human stem cell-derived alpha cells. *Nat Commun* **11**, 2241 (2020).

409. Kahn, S. E. *et al.* Glycemic Durability of Rosiglitazone, Metformin, or Glyburide Monotherapy. *New Engl J Medicine* **355**, 2427–2443 (2006).

410. Frias, J. P. *et al.* Efficacy and safety of LY3298176, a novel dual GIP and GLP-1 receptor agonist, in patients with type 2 diabetes: a randomised, placebo-controlled and active comparator-controlled phase 2 trial. *Lancet* **392**, 2180–2193 (2018).

411. Willard, F. S. *et al.* Tirzepatide is an imbalanced and biased dual GIP and GLP-1 receptor agonist. *JCI Insight* **5**, e140532 (2020).

412. Schauer, P. R. *et al.* Bariatric Surgery versus Intensive Medical Therapy for Diabetes — 3-Year Outcomes. *New Engl J Medicine* **370**, 2002–2013 (2014).

413. Douros, J. D. *et al.* Sleeve gastrectomy rapidly enhances islet function independently of body weight. *Jci Insight* **4**, e126688 (2019).

414. Nannipieri, M. *et al.* Roux-en-Y gastric bypass and sleeve gastrectomy: mechanisms of diabetes remission and role of gut hormones. *J Clin Endocrinol Metabolism* **98**, 4391–9 (2013).

415. Douros, J. D. *et al.* Temporal plasticity of insulin and incretin secretion and insulin sensitivity following sleeve gastrectomy contribute to sustained improvements in glucose control. *Mol Metab* **28**, 144–150 (2019).

416. Douros, J. D., Tong, J. & D'Alessio, D. A. The Effects of Bariatric Surgery on Islet Function, Insulin Secretion, and Glucose Control. *Endocr Rev* **40**, 1394–1423 (2019).

417. White, M. G., Shaw, J. A. M. & Taylor, R. Type 2 Diabetes: The Pathologic Basis of Reversible β-Cell Dysfunction. *Diabetes Care* **39**, 2080 2088 (2016).

418. Steven, S. *et al.* Very Low-Calorie Diet and 6 Months of Weight Stability in Type 2 Diabetes: Pathophysiological Changes in Responders and Nonresponders. *Diabetes Care* **39**, 808–15 (2016).

419. Lean, M. E. *et al.* Primary care-led weight management for remission of type 2 diabetes (DiRECT): an open-label, cluster-randomised trial. *Lancet Lond Engl* **391**, 541–551 (2017).

420. Taylor, R., Al-Mrabeh, A. & Sattar, N. Understanding the mechanisms of reversal of type 2 diabetes. *Lancet Diabetes Endocrinol* **7**, 726–736 (2019).

421. Taylor, R. *et al.* Remission of Human Type 2 Diabetes Requires Decrease in Liver and Pancreas Fat Content but Is Dependent upon Capacity for β Cell Recovery. *Cell Metab* **28**, 547-556.e3 (2018).

422. Dayan, C. M., Korah, M., Tatovic, D., Bundy, B. N. & Herold, K. C. Changing the landscape for type 1 diabetes: the first step to prevention. *Lancet* **394**, 1286–1296 (2019).

423. Coppieters, K. & Herrath, M. von. The Development of Immunotherapy Strategies for the Treatment of Type 1 Diabetes. *Frontiers Medicine* **5**, 283 (2018).

424. Warshauer, J. T., Bluestone, J. A. & Anderson, M. S. New Frontiers in the Treatment of Type 1 Diabetes. *Cell Metab* **31**, 46–61 (2019).

425. Herold, K. C. *et al.* An Anti-CD3 Antibody, Teplizumab, in Relatives at Risk for Type 1 Diabetes. *New Engl J Medicine* **381**, 603–613 (2019).

426. Quattrin, T. *et al.* Golimumab and Beta-Cell Function in Youth with New-Onset Type 1 Diabetes. *New Engl J Med* **383**, 2007–2017 (2020).

427. Xu, G., Chen, J., Jing, G. & Shalev, A. Preventing β-Cell Loss and Diabetes With Calcium Channel Blockers. *Diabetes* **61**, 848–856 (2012).

428. Ovalle, F. *et al.* Verapamil and beta cell function in adults with recent-onset type 1 diabetes. *Nat Med* **24**, 1108–1112 (2018).

429. Wei, Z. *et al.* Vitamin D Switches BAF Complexes to Protect β Cells. *Cell* **173**, 1135-1149.e15 (2018).

430. Carboneau, B. A. *et al.* Opposing effects of prostaglandin E2 receptors EP3 and EP4 on mouse and human β-cell survival and proliferation. *Mol Metab* **6**, 548–559 (2017).

431. Carboneau, B. A., Breyer, R. M. & Gannon, M. Regulation of pancreatic β-cell function and mass dynamics by prostaglandin signaling. *J Cell Commun Signal* **11**, 105–116 (2017).

432. Chou, D. H.-C. *et al.* Inhibition of histone deacetylase 3 protects beta cells from cytokine-induced apoptosis. *Chem Biol* **19**, 669–73 (2012).

433. Christensen, D. P. *et al.* Histone Deacetylase (HDAC) Inhibition as a Novel Treatment for Diabetes Mellitus. *Mol Med* **17**, 378–390 (2011).

434. Syed, I. *et al.* PAHSAs attenuate immune responses and promote β cell survival in autoimmune diabetic mice. *J Clin Invest* **129**, 3717–3731 (2019).

435. Farilla, L. *et al.* Glucagon-Like Peptide 1 Inhibits Cell Apoptosis and Improves Glucose Responsiveness of Freshly Isolated Human Islets. *Endocrinology* **144**, 5149–5158 (2003).

436. Yusta, B. *et al.* GLP-1 receptor activation improves β cell function and survival following induction of endoplasmic reticulum stress. *Cell Metab* **4**, 391–406 (2006).

437. Stewart, A. F. *et al.* Human β-cell proliferation and intracellular signaling: part 3. *Diabetes* **64**, 1872–85 (2015).

438. Bernal-Mizrachi, E. *et al.* Human β-cell proliferation and intracellular signaling part 2: still driving in the dark without a road map. *Diabetes* **63**, 819–31 (2014).

439. Kulkarni, R. N., Mizrachi, E.-B., Ocana, A. G. & Stewart, A. F. Human β-Cell Proliferation and Intracellular Signaling: Driving in the Dark Without a Road Map. *Diabetes* **61**, 2205–2213 (2012).

440. Heit, J. J. *et al.* Calcineurin/NFAT signalling regulates pancreatic beta-cell growth and function. *Nature* **443**, 345 349 (2006).

441. Dai, C. *et al.* Age-dependent human β cell proliferation induced by glucagon-like peptide 1 and calcineurin signaling. *J Clin Invest* **127**, 3835 3844 (2017).

442. Wang, P. *et al.* Diabetes mellitus--advances and challenges in human β-cell proliferation. *Nat Rev Endocrinol* **11**, 201 212 (2015).

443. Fiaschi-Taesch, N. M. *et al.* Cytoplasmic-nuclear trafficking of G1/S cell cycle molecules and adult human β-cell replication: a revised model of human β-cell G1/S control. *Diabetes* **62**, 2460–70 (2013).

444. Fiaschi-Taesch, N. M. *et al.* Human Pancreatic -Cell G1/S Molecule Cell Cycle Atlas. *Diabetes* **62**, 2450–2459 (2013).

445. Cozar-Castellano, I. *et al.* Molecular Control of Cell Cycle Progression in the Pancreatic β-Cell. *Endocr Rev* **27**, 356–370 (2006).

446. Tiwari, S. *et al.* Early and Late G1/S Cyclins and Cdks Act Complementarily to Enhance Authentic Human β-Cell Proliferation and Expansion. *Diabetes* **64**, 3485–98 (2015).

447. Fiaschi-Taesch, N. M. *et al.* Induction of human beta-cell proliferation and engraftment using a single G1/S regulatory molecule, cdk6. *Diabetes* **59**, 1926–36 (2010).

448. Dirice, E. *et al.* Inhibition of DYRK1A Stimulates Human β-Cell Proliferation. *Diabetes* **65**, 1660–71 (2016).

449. Wang, P. *et al.* A high-throughput chemical screen reveals that harmine-mediated inhibition of DYRK1A increases human pancreatic beta cell replication. *Nat Med* **21**, 383 388 (2015).

450. Wang, P. *et al.* Combined Inhibition of DYRK1A, SMAD, and Trithorax Pathways Synergizes to Induce Robust Replication in Adult Human Beta Cells. *Cell Metab* **29**, 638 652.e5 (2019).

451. Ackeifi, C. *et al.* GLP-1 receptor agonists synergize with DYRK1A inhibitors to potentiate functional human β cell regeneration. *Sci Transl Med* **12**, eaaw9996 (2020).

452. Rosselot, C. *et al.* The Harmine and Exendin-4 Combination Markedly Expands Human Beta Cell Mass In Vivo: Quantification and Visualization By iDISCO+ 3D Imaging. *Biorxiv* 2020.07.24.220244 (2020) doi:10.1101/2020.07.24.220244.

453. Arbones, M. L., Thomazeau, A., Nakano-Kobayashi, A., Hagiwara, M. & Delabar, J. M. DYRK1A and cognition: A lifelong relationship. *Pharmacol Therapeut* **194**, 199–221 (2019).

454. Qadir, M. M. F. *et al.* Long-term culture of human pancreatic slices as a model to study real-time islet regeneration. *Nat Commun* **11**, 3265 (2020).

455. Aguayo-Mazzucato, C. & Bonner-Weir, S. Pancreatic β Cell Regeneration as a Possible Therapy for Diabetes. *Cell Metab* **27**, 57–67 (2017).

456. Thorel, F. *et al.* Conversion of adult pancreatic α-cells to β-cells after extreme β-cell loss. *Nature* **464**, 1149 1154 (2010).

457. Chera, S. *et al.* Diabetes recovery by age-dependent conversion of pancreatic δ-cells into insulin producers. *Nature* **514**, 503–7 (2014).

458. Courtney, M. *et al.* The inactivation of Arx in pancreatic α-cells triggers their neogenesis and conversion into functional β-like cells. *Plos Genet* **9**, e1003934 (2013).

459. Collombat, P. *et al.* The ectopic expression of Pax4 in the mouse pancreas converts progenitor cells into alpha and subsequently beta cells. *Cell* **138**, 449–62 (2009).

460. Zhang, Y. *et al.* PAX4 Gene Transfer Induces α-to-β Cell Phenotypic Conversion and Confers Therapeutic Benefits for Diabetes Treatment. *Mol Ther J Am Soc Gene Ther* **24**, 251–60 (2015).

461. Talchai, C., Xuan, S., Kitamura, T., DePinho, R. A. & Accili, D. Generation of functional insulin-producing cells in the gut by Foxo1 ablation. *Nat Genet* **44**, 406–12, S1 (2012).

462. Bouchi, R. *et al.* FOXO1 inhibition yields functional insulin-producing cells in human gut organoid cultures. *Nat Commun* **5**, 4242 (2014).

463. Xiao, X. *et al.* Endogenous Reprogramming of Alpha Cells into Beta Cells, Induced by Viral Gene Therapy, Reverses Autoimmune Diabetes. *Cell Stem Cell* **22**, 78-90.e4 (2018).

464. Zhou, Q., Brown, J., Kanarek, A., Rajagopal, J. & Melton, D. A. In vivo reprogramming of adult pancreatic exocrine cells to beta-cells. *Nature* **455**, 627–32 (2008).

465. Furuyama, K. *et al.* Diabetes relief in mice by glucose-sensing insulin-secreting human α-cells. *Nature* **567**, 43–48 (2019).

466. Saunders, D. C. *et al.* Ectonucleoside Triphosphate Diphosphohydrolase-3 Antibody Targets Adult Human Pancreatic β Cells for In Vitro and In Vivo Analysis. *Cell Metab* **29**, 745-754.e4 (2019).

467. Dorrell, C. *et al.* Transcriptomes of the major human pancreatic cell types. *Diabetologia* **54**, 2832 2844 (2011).

468. Dorrell, C. *et al.* Isolation of major pancreatic cell types and long-term culture-initiating cells using novel human surface markers. *Stem Cell Res* **1**, 183 194 (2008).

469. Vetere, A., Choudhary, A., Burns, S. M. & Wagner, B. K. Targeting the pancreatic β-cell to treat diabetes. *Nat Rev Drug Discov* **13**, 278–289 (2014).

470. Pekrun, K. *et al.* Using a barcoded AAV capsid library to select for clinically relevant gene therapy vectors. *Jci Insight* **4**, e131610 (2019).

471. Wang, H. *et al.* Insights into beta cell regeneration for diabetes via integration of molecular landscapes in human insulinomas. *Nat Commun* **8**, 767 (2017).

472. Pauerstein, P. T., Park, K. M., Peiris, H. S., Wang, J. & Kim, S. K. Research Resource: Genetic Labeling of Human Islet Alpha Cells. *Mol Endocrinol* **30**, 248–253 (2016).

473. Shuai, H., Xu, Y., Yu, Q., Gylfe, E. & Tengholm, A. Fluorescent protein vectors for pancreatic islet cell identification in live-cell imaging. *Pflugers Archiv European J Physiology* **468**, 1765–77 (2016).

474. Pierini, A. *et al.* T cells expressing chimeric antigen receptor promote immune tolerance. *Jci Insight* **2**, e92865 (2017).

475. Hull, C. M. *et al.* Generation of human islet-specific regulatory T cells by TCR gene transfer. *J Autoimmun* **79**, 63–73 (2017).

476. Fava, G. E., Dong, E. W. & Wu, H. Intra-islet glucagon-like peptide 1. *J Diabetes Complicat* **30**, 1651–1658 (2016).

477. Marciniak, A. *et al.* Using pancreas tissue slices for in situ studies of islet of Langerhans and acinar cell biology. *Nat Protoc* **9**, 2809–22 (2014).

478. Panzer, J. K. *et al.* Pancreas tissue slices from organ donors enable in situ analysis of type 1 diabetes pathogenesis. *Jci Insight* **5**, e134525 (2020).

479. Kayton, N. S. *et al.* Human islet preparations distributed for research exhibit a variety of insulin-secretory profiles. *Am J Physiol-endoc M* **308**, E592–E602 (2015).

480. Brissova, M. *et al.* The Integrated Islet Distribution Program Answers the Call for Improved Human Islet Phenotyping and Reporting of Human Islet Characteristics in Research Articles. *Diabetes* **68**, dbi190019 (2019).

481. Hart, N. J. & Powers, A. C. Use of human islets to understand islet biology and diabetes: progress, challenges and suggestions. *Diabetologia* **62**, 212–222 (2019).

482. Les, E. E., Téllez, N., Nacher, M. & Montanya, E. A model for human islet transplantation to immunodeficient streptozotocin-induced diabetic mice. *Cell Transplant* **27**, 963689718801006 (2018).

483. Stokes, R. A. *et al.* Transplantation sites for human and murine islets. *Diabetologia* **60**, 1961–1971 (2017).

484. Speier, S. *et al.* Noninvasive in vivo imaging of pancreatic islet cell biology. *Nat Med* **14**, 574 578 (2008).

485. Abdulreda, M. H., Caicedo, A. & Berggren, P.-O. Transplantation into the anterior chamber of the eye for longitudinal, non-invasive in vivo imaging with single-cell resolution in real-time. *J Vis Exp* e50466 (2013) doi:10.3791/50466.

486. Nilsson, J., Holmberg, D. & Schmidt-Christensen, A. Longitudinal In Vivo Imaging and Quantification of Human Pancreatic Islet Grafting and Contributing Host Cells in the Anterior Eye Chamber. *J Vis Exp Jove* e61234 (2020) doi:10.3791/61234.

487. Shultz, L. D., Ishikawa, F. & Greiner, D. L. Humanized mice in translational biomedical research. *Nat Rev Immunol* **7**, 118 130 (2007).

488. Cantarelli, E. *et al.* Murine animal models for preclinical islet transplantation: No model fits all (research purposes). *Islets* **5**, 79–86 (2013).

489. Halban, P. A., Powers, S. L., George, K. L. & Bonner-Weir, S. Spontaneous Reassociation of Dispersed Adult Rat Pancreatic Islet Cells Into Aggregates With Three-Dimensional Architecture Typical of Native Islets. *Diabetes* **36**, 783–790 (1987).

490. Foty, R. A Simple Hanging Drop Cell Culture Protocol for Generation of 3D Spheroids. *J Vis Exp* 1 4 (2011) doi:10.3791/2720.

491. Yu, Y. *et al.* Bioengineered human pseudoislets form efficiently from donated tissue, compare favourably with native islets in vitro and restore normoglycaemia in mice. *Diabetologia* **61**, 2016–2029 (2018).

492. Walker, J. T. *et al.* Integrated human pseudoislet system and microfluidic platform demonstrate differences in GPCR signaling in islet cells. *JCI Insight* **5**, e137017 (2020).

493. Arda, H. E. *et al.* Age-Dependent Pancreatic Gene Regulation Reveals Mechanisms Governing Human β Cell Function. *Cell Metab* **23**, 909–920 (2016).

494. Peiris, H. *et al.* Discovering human diabetes-risk gene function with genetics and physiological assays. *Nat Commun* **9**, 3855 (2018).

495. Balak, J. R. A., Juksar, J., Carlotti, F., Nigro, A. L. & Koning, E. J. P. de. Organoids from the Human Fetal and Adult Pancreas. *Curr Diabetes Rep* **19**, 160 (2019).

496. Nair, G. & Hebrok, M. Islet formation in mice and men: lessons for the generation of functional insulin-producing β-cells from human pluripotent stem cells. *Curr Opin Genet Dev* **32**, 171–180 (2015).

497. Teo, A. K. K. *et al.* Derivation of human induced pluripotent stem cells from patients with maturity onset diabetes of the young. *J Biological Chem* **288**, 5353–6 (2013).

498. Memon, B. & Abdelalim, E. M. Stem Cell Therapy for Diabetes: Beta Cells versus Pancreatic Progenitors. *Cells* **9**, 283 (2020).

499. Nair, G. G., Tzanakakis, E. S. & Hebrok, M. Emerging routes to the generation of functional β-cells for diabetes mellitus cell therapy. *Nat Rev Endocrinol* 1–13 (2020) doi:10.1038/s41574-020-0375-3.

500. Zhou, Q. & Melton, D. A. Pancreas regeneration. *Nature* **557**, 351–358 (2018).

501. Tremmel, D. M., Mitchell, S. A., Sackett, S. D. & Odorico, J. S. Mimicking nature-made beta cells: recent advances towards stem cell-derived islets. *Curr Opin Organ Tran* **24**, 574–581 (2019).

502. Balboa, D., Saarimäki-Vire, J. & Otonkoski, T. Concise Review: Human Pluripotent Stem Cells for the Modeling of Pancreatic β-Cell Pathology. *Stem Cells Dayt Ohio* **37**, 33–41 (2018).

503. Millman, J. R. & Pagliuca, F. W. Autologous Pluripotent Stem Cell-Derived β-Like Cells for Diabetes Cellular Therapy. *Diabetes* **66**, 1111–1120 (2017).

504. Skelin, M., Rupnik, M. & Cencic, A. Pancreatic beta cell lines and their applications in diabetes mellitus research. *Altex* **27**, 105–113 (2010).

505. Ravassard, P. *et al.* A genetically engineered human pancreatic β cell line exhibiting glucose-inducible insulin secretion. *J Clin Investigation* **121**, 3589–97 (2011).

506. Scharfmann, R. *et al.* Development of a conditionally immortalized human pancreatic β cell line. *J Clin Investigation* **124**, 2087–98 (2014).

507. Canzano, J. S. *et al.* Islet Microvasculature Alterations With Loss of Beta-cells in Patients With Type 1 Diabetes. *J Histochem Cytochem* **67**, 41–52 (2018).

508. Boer, P. de *et al.* Large-scale electron microscopy database for human type 1 diabetes. *Nat Commun* **11**, 2475 (2020).

509. Wilcox, N. S., Rui, J., Hebrok, M. & Herold, K. C. Life and death of β cells in Type 1 diabetes: A comprehensive review. *J Autoimmun* **71**, 51–58 (2016).

510. Eizirik, D. L., Pasquali, L. & Cnop, M. Pancreatic β-cells in type 1 and type 2 diabetes mellitus: different pathways to failure. *Nat Rev Endocrinol* **16**, 349–362 (2020).

511. Sims, E. K., Mirmira, R. G. & Evans-Molina, C. The role of beta-cell dysfunction in early type 1 diabetes. *Curr Opin Endocrinol Diabetes Obes* **27**, 215–224 (2020).

512. Solimena, M. *et al.* Systems biology of the IMIDIA biobank from organ donors and pancreatectomised patients defines a novel transcriptomic signature of islets from individuals with type 2 diabetes. *Diabetologia* **61**, 641–657 (2017).

513. Kono, T. *et al.* Impaired Store-Operated Calcium Entry and STIM1 Loss Lead to Reduced Insulin Secretion and Increased Endoplasmic Reticulum Stress in the Diabetic β-Cell. *Diabetes* **67**, 2293–2304 (2018).

514. Cinti, F. *et al.* Evidence of β-Cell Dedifferentiation in Human Type 2 Diabetes. *J Clin Endocrinol Metabolism* **101**, 1044 1054 (2016).

515. Deng, S. *et al.* Structural and Functional Abnormalities in the Islets Isolated From Type 2 Diabetic Subjects. *Diabetes* **53**, 624–632 (2004).

516. Chabosseau, P. & Rutter, G. A. Zinc and diabetes. *Arch Biochem Biophys* **611**, 79–85 (2016).

517. Böni-Schnetzler, M. & Meier, D. T. Islet inflammation in type 2 diabetes. *Semin Immunopathol* **41**, 501–513 (2019).

518. Krentz, N. A. J. & Gloyn, A. L. Insights into pancreatic islet cell dysfunction from type 2 diabetes mellitus genetics. *Nat Rev Endocrinol* 1–11 (2020) doi:10.1038/s41574-020-0325-0.

519. Grant, S. F. A., Wells, A. D. & Rich, S. S. Next steps in the identification of gene targets for type 1 diabetes. *Diabetologia* **63**, 2260–2269 (2020).

520. Hayes, M. G. *et al.* Identification of HKDC1 and BACE2 as genes influencing glycemic traits during pregnancy through genome-wide association studies. *Diabetes* **62**, 3282–91 (2013).

521. Lorenzo, P. I., Martín-Montalvo, A., Vuilleumier, N. C. & Gauthier, B. R. Molecular Modelling of Islet β-Cell Adaptation to Inflammation in Pregnancy and Gestational Diabetes Mellitus. *Int J Mol Sci* **20**, 6171 (2019).

522. Arya, V. B. *et al.* HNF4Amutation: switch from hyperinsulinaemic hypoglycaemia to maturity-onset diabetes of the young, and incretin response. *Diabetic Med* **31**, e11–e15 (2014).

523. Braverman-Gross, C. *et al.* Derivation and molecular characterization of pancreatic differentiated MODY1-iPSCs. *Stem Cell Res* **31**, 16–26 (2018).

524. García-Herrero, C. M. *et al.* Functional analysis of human glucokinase gene mutations causing MODY2: exploring the regulatory mechanisms of glucokinase activity. *Diabetologia* **50**, 325–333 (2006).

525. Bonfig, W. *et al.* GCK-MODY (MODY 2) Caused by a Novel p.Phe330Ser Mutation. *Isrn Pediatrics* **2011**, 1–5 (2011).

526. Richter, S. *et al.* Regulation of Apolipoprotein M Gene Expression by MODY3 Gene Hepatocyte Nuclear Factor-1 : Haploinsufficiency Is Associated With Reduced Serum Apolipoprotein M Levels. *Diabetes* **52**, 2989–2995 (2003).

527. Sachdeva, M. M. *et al.* Pdx1 (MODY4) regulates pancreatic beta cell susceptibility to ER stress. *Proc National Acad Sci* **106**, 19090–19095 (2009).

528. Caetano, L. A. *et al.* PDX1 -MODY and dorsal pancreatic agenesis: New phenotype of a rare disease. *Clin Genet* **93**, 382–386 (2017).

529. Bellanné-Chantelot, C. *et al.* Clinical Spectrum Associated with Hepatocyte Nuclear Factor-1β Mutations. *Ann Intern Med* **140**, 510 (2004).

530. Teo, A. K. K. *et al.* Early Developmental Perturbations in a Human Stem Cell Model of MODY5/HNF1B Pancreatic Hypoplasia. *Stem Cell Rep* **6**, 357–367 (2016).

531. Iwasaki, N. *et al.* Pancreatic developmental defect evaluated by celiac artery angiography in a patient with MODY5. *Hum Genome Var* **3**, 16022 (2016).

532. Fajans, S. S. & Bell, G. I. Phenotypic heterogeneity between different mutations of MODY subtypes and within MODY pedigrees. *Diabetologia* **49**, 1106–1108 (2006).

533. Yamagata, K. Chapter Sixteen Roles of HNF1α and HNF4α in Pancreatic β-Cells Lessons from a Monogenic Form of Diabetes (MODY). in *The Pancreatic Beta Cell* vol. 95 407–423 (Academic Press, 2014).

534. Meur, G. *et al.* Insulin gene mutations resulting in early-onset diabetes: marked differences in clinical presentation, metabolic status, and pathogenic effect through endoplasmic reticulum retention. *Diabetes* **59**, 653–61 (2009).

535. Balboa, D. *et al.* Insulin mutations impair beta-cell development in a patient-derived iPSC model of neonatal diabetes. *Elife* **7**, e38519 (2018).

536. Mitchell, J. *et al.* Neonatal diabetes, with hypoplastic pancreas, intestinal atresia and gall bladder hypoplasia: search for the aetiology of a new autosomal recessive syndrome. *Diabetologia* **47**, 2160–2167 (2004).

537. Smith, S. B. *et al.* Rfx6 directs islet formation and insulin production in mice and humans. *Nature* **463**, 775 780 (2010).

538. Pinney, S. E. *et al.* Neonatal Diabetes and Congenital Malabsorptive Diarrhea Attributable to a Novel Mutation in the Human Neurogenin-3 Gene Coding Sequence. *J Clin Endocrinol Metabolism* **96**, 1960–1965 (2011).

539. Rubio-Cabezas, O. & Ellard, S. Diabetes mellitus in neonates and infants: genetic heterogeneity, clinical approach to diagnosis, and therapeutic options. *Hormone Res Pædiatrics* **80**, 137–46 (2013).

540. Sempoux, C. *et al.* Pancreatic B-cell proliferation in persistent hyperinsulinemic hypoglycemia of infancy: an immunohistochemical study of 18 cases. *Mod Pathology Official J United States Can Acad Pathology Inc* **11**, 444–9 (1998).

541. Kassem, S. A., Ariel, I., Thornton, P. S., Scheimberg, I. & Glaser, B. Beta-cell proliferation and apoptosis in the developing normal human pancreas and in hyperinsulinism of infancy. *Diabetes* **49**, 1325 1333 (2000).

542. Sempoux, C. *et al.* The Focal Form of Persistent Hyperinsulinemic Hypoglycemia of Infancy: Morphological and Molecular Studies Show Structural and Functional Differences With Insulinoma. *Diabetes* **52**, 784–794 (2003).

543. Lord, K., Dzata, E., Snider, K. E., Gallagher, P. R. & León, D. D. D. Clinical Presentation and Management of Children With Diffuse and Focal Hyperinsulinism: A Review of 223 Cases. *J Clin Endocrinol Metabolism* **98**, E1786–E1789 (2013).

544. Salisbury, R. J. *et al.* Altered Phenotype of β-Cells and Other Pancreatic Cell Lineages in Patients With Diffuse Congenital Hyperinsulinism in Infancy Caused by Mutations in the ATP-Sensitive K-Channel. *Diabetes* **64**, 3182–8 (2015).

545. Boodhansingh, K. E. *et al.* Novel dominant KATP channel mutations in infants with congenital hyperinsulinism: Validation by in vitro expression studies and in vivo carrier phenotyping. *Am J Medical Genetics Part* **179**, 2214–2227 (2019).

546. Goel, P. & Choudhury, S. R. Persistent hyperinsulinemic hypoglycemia of infancy: An overview of current concepts. *J Indian Assoc Pediatric Surg* **17**, 99–103 (2012).

547. Lord, K. & León, D. D. D. Monogenic hyperinsulinemic hypoglycemia: current insights into the pathogenesis and management. *Int J Pediatric Endocrinol* **2013**, 3 (2013).

548. Cory, M. *et al.* An Increase in Chromogranin A-Positive, Hormone-Negative Endocrine Cells in Pancreas in Cystic Fibrosis. *J Endocr Soc* **2**, 1058–1066 (2018).

549. Hull, R. L. *et al.* Islet Interleukin-1β Immunoreactivity Is an Early Feature of Cystic Fibrosis That May Contribute to β-Cell Failure. *Diabetes Care* **41**, 823–830 (2018).

550. Elborn, J. S. Cystic fibrosis. *Lancet* **388**, 2519–2531 (2016).

551. Marunaka, Y. The Mechanistic Links between Insulin and Cystic Fibrosis Transmembrane Conductance Regulator (CFTR) Cl− Channel. *Int J Mol Sci* **18**, 1767 (2017).

552. Kelsey, R., Koivula, F. N. M., McClenaghan, N. H. & Kelly, C. Cystic Fibrosis–Related Diabetes: Pathophysiology and Therapeutic Challenges. *Clin Medicine Insights Endocrinol Diabetes* **12**, 117955141985177 (2019).

553. Kim, Y. G. *et al.* Association of Genetic Polymorphisms of Interleukins With New-Onset Diabetes After Transplantation in Renal Transplantation. *Transplant J* **93**, 900–907 (2012).

554. Yang, J., Hutchinson, I. I., Shah, T. & Min, D. I. Genetic and clinical risk factors of new-onset diabetes after transplantation in Hispanic kidney transplant recipients. *Transplantation* **91**, 1114–9 (2011).

555. Kurzawski, M., Dziewanowski, K., Łapczuk, J., Wajda, A. & Droździk, M. Analysis of common type 2 diabetes mellitus genetic risk factors in new-onset diabetes after transplantation in kidney transplant patients medicated with tacrolimus. *Eur J Clin Pharmacol* **68**, 1587–1594 (2012).

556. Drachenberg, C. B. *et al.* Islet Cell Damage Associated with Tacrolimus and Cyclosporine: Morphological Features in Pancreas Allograft Biopsies and Clinical Correlation. *Transplantation* **68**, 396–402 (1999).

557. Sharif, A. *et al.* Proceedings from an international consensus meeting on posttransplantation diabetes mellitus: recommendations and future directions. in vol. 14 1992 2000 (2014).

558. Dai, C. *et al.* Tacrolimus- and sirolimus-induced human β cell dysfunction is reversible and preventable. *Jci Insight* **5**, e130770 (2020).

559. Dai, C. *et al.* Dapagliflozin does not directly affect human α or β cells. *Endocrinology* (2020) doi:10.1210/endocr/bqaa080.

560. Walker, J. T. *et al.* Integrated human pseudoislet system and microfluidic platform demonstrate differences in GPCR signaling in islet cells. *JCI Insight* **5**, e137017 (2020).

561. Shrestha, S. *et al.* Combinatorial transcription factor profiles predict mature and functional human islet α and β cells. *Biorxiv* 2021.02.23.432522 (2021) doi:10.1101/2021.02.23.432522.

562. Brissova, M. *et al.* Islet microenvironment, modulated by vascular endothelial growth factor-A signaling, promotes β cell regeneration. *Cell Metab* **19**, 498 511 (2014).

563. Brissova, M. *et al.* α Cell Function and Gene Expression Are Compromised in Type 1 Diabetes. *Cell Reports* **22**, 2667 2676 (2018).

564. Aamodt, K. I. *et al.* Development of a reliable automated screening system to identify small molecules and biologics that promote human β-cell regeneration. *Am J Physiol-endoc M* **311**, E859 E868 (2016).

565. Dorrell, C. *et al.* Transcriptomes of the major human pancreatic cell types. *Diabetologia* **54**, 2832 2844 (2011).

566. Blodgett, D. M. *et al.* Novel Observations From Next-Generation RNA Sequencing of Highly Purified Human Adult and Fetal Islet Cell Subsets. *Diabetes* **64**, 3172–3181 (2015).

567. Babon, J. A. B. *et al.* Analysis of self-antigen specificity of islet-infiltrating T cells from human donors with type 1 diabetes. *Nat Med* **22**, 1482–1487 (2016).

568. Dai, C. *et al.* Age-dependent human β cell proliferation induced by glucagon-like peptide 1 and calcineurin signaling. *J Clin Invest* **127**, 3835 3844 (2017).

569. Dai, C. *et al.* Stress-impaired transcription factor expression and insulin secretion in transplanted human islets. *J Clin Invest* **126**, 1857 1870 (2016).

570. Kayton, N. S. *et al.* Human islet preparations distributed for research exhibit a variety of insulin-secretory profiles. *Am J Physiol-endoc M* **308**, E592 E602 (2015).

571. Lenguito, G. *et al.* Resealable, optically accessible, PDMS-free fluidic platform for ex vivo interrogation of pancreatic islets. *Lab Chip* **17**, 772–781 (2017).

572. Buchwald, P. A local glucose-and oxygen concentration-based insulin secretion model for pancreatic islets. *Theor Biol Med Model* **8**, 20 (2011).

573. Buchwald, P., Tamayo-Garcia, A., Manzoli, V., Tomei, A. A. & Stabler, C. L. Glucose-stimulated insulin release: Parallel perifusion studies of free and hydrogel encapsulated human pancreatic islets. *Biotechnol Bioeng* **115**, 232–245 (2018).

574. Shultz, L. D. *et al.* Human Lymphoid and Myeloid Cell Development in NOD/LtSz-scid IL2R null Mice Engrafted with Mobilized Human Hemopoietic Stem Cells. *J Immunol* **174**, 6477 6489 (2005).

575. Huang, D. W., Sherman, B. T. & Lempicki, R. A. Systematic and integrative analysis of large gene lists using DAVID bioinformatics resources. *Nat Protoc* **4**, 44 57 (2009).

576. Dobin, A. *et al.* STAR: ultrafast universal RNA-seq aligner. *Bioinformatics* **29**, 15–21 (2013).

577. Liao, Y., Smyth, G. K. & Shi, W. featureCounts: an efficient general purpose program for assigning sequence reads to genomic features. *Bioinformatics* **30**, 923–930 (2014).

578. Hartley, S. W. & Mullikin, J. C. QoRTs: a comprehensive toolset for quality control and data processing of RNA-Seq experiments. *Bmc Bioinformatics* **16**, 224 (2015).

579. Wang, L. *et al.* Measure transcript integrity using RNA-seq data. *Bmc Bioinformatics* **17**, 58 (2016).

580. Love, M. I., Huber, W. & Anders, S. Moderated estimation of fold change and dispersion for RNA-seq data with DESeq2. *Genome Biol* **15**, 550 (2014).

581. Risso, D., Ngai, J., Speed, T. P. & Dudoit, S. Normalization of RNA-seq data using factor analysis of control genes or samples. *Nat Biotechnol* **32**, 896–902 (2014).

582. Lee, C., Patil, S. & Sartor, M. A. RNA-Enrich: a cut-off free functional enrichment testing method for RNA-seq with improved detection power. *Bioinformatics* **32**, 1100–1102 (2016).

583. Supek, F., Bošnjak, M., Škunca, N. & Šmuc, T. REVIGO Summarizes and Visualizes Long Lists of Gene Ontology Terms. *Plos One* **6**, e21800 (2011).

584. Shannon, P. *et al.* Cytoscape: A Software Environment for Integrated Models of Biomolecular Interaction Networks. *Genome Res* **13**, 2498–2504 (2003).

585. Zhou, Y. *et al.* Metascape provides a biologist-oriented resource for the analysis of systems-level datasets. *Nat Commun* **10**, 1523 (2019).

586. Langfelder, P. & Horvath, S. WGCNA: an R package for weighted correlation network analysis. *Bmc Bioinformatics* **9**, 559 (2008).

587. Ritchie, M. E. *et al.* limma powers differential expression analyses for RNA-sequencing and microarray studies. *Nucleic Acids Res* **43**, e47–e47 (2015).

588. Butler, A., Hoffman, P., Smibert, P., Papalexi, E. & Satija, R. Integrating single-cell transcriptomic data across different conditions, technologies, and species. *Nat Biotechnol* **36**, 411 (2018).

589. Lun, A. T. L. *et al.* EmptyDrops: distinguishing cells from empty droplets in droplet-based single-cell RNA sequencing data. *Genome Biol* **20**, 63 (2019).

590. Baron, M. *et al.* A Single-Cell Transcriptomic Map of the Human and Mouse Pancreas Reveals Inter- and Intra-cell Population Structure. *Cell Syst* **3**, 346-360.e4 (2016).

591. Segerstolpe, Å. *et al.* Single-Cell Transcriptome Profiling of Human Pancreatic Islets in Health and Type 2 Diabetes. *Cell Metab* **24**, 593–607 (2016).

592. Camunas-Soler, J. *et al.* Patch-Seq Links Single-Cell Transcriptomes to Human Islet Dysfunction in Diabetes. *Cell Metab* **31**, 1017-1031.e4 (2020).

593. Picelli, S. *et al.* Full-length RNA-seq from single cells using Smart-seq2. *Nat Protoc* **9**, 171–181 (2014).

594. Brissova, M. *et al.* α Cell Function and Gene Expression Are Compromised in Type 1 Diabetes. *Cell Reports* **22**, 2667 2676 (2018).

595. Haliyur, R. *et al.* Human islets expressing HNF1A variant have defective β cell transcriptional regulatory networks. *J Clin Invest* **129**, 246–251 (2018).

596. Alkorta-Aranburu, G. *et al.* Improved molecular diagnosis of patients with neonatal diabetes using a combined next-generation sequencing and MS-MLPA approach. *J Pediatric Endocrinol Metabolism* **29**, 523–531 (2016).

597. Oram, R. A. *et al.* A Type 1 Diabetes Genetic Risk Score Can Aid Discrimination Between Type 1 and Type 2 Diabetes in Young Adults. *Diabetes Care* **39**, 337–344 (2015).

598. Buse, J. B. *et al.* 2019 Update to: Management of Hyperglycemia in Type 2 Diabetes, 2018. A Consensus Report by the American Diabetes Association (ADA) and the European Association for the Study of Diabetes (EASD). *Diabetes Care* **43**, 487–493 (2019).

599. Davies, M. J. *et al.* Management of Hyperglycemia in Type 2 Diabetes, 2018. A Consensus Report by the American Diabetes Association (ADA) and the European Association for the Study of Diabetes (EASD). *Diabetes Care* **41**, 2669–2701 (2018).

600. Fathallah, N., Slim, R., Larif, S., Hmouda, H. & Salem, C. B. Drug-Induced Hyperglycaemia and Diabetes. *Drug Safety* **38**, 1153–1168 (2015).

601. Jain, V. *et al.* Drugs and hyperglycemia: A practical guide. *Maturitas* **104**, 80–83 (2017).

602. Sharif, A. *et al.* Proceedings from an international consensus meeting on posttransplantation diabetes mellitus: recommendations and future directions. in vol. 14 1992 2000 (2014).

603. Shivaswamy, V., Boerner, B. & Larsen, J. Post-Transplant Diabetes Mellitus: Causes, Treatment, and Impact on Outcomes. *Endocr Rev* **37**, 37 61 (2016).

604. Cosio, F. G., Pesavento, T. E., Osei, K., Henry, M. L. & Ferguson, R. M. Post-transplant diabetes mellitus: Increasing incidence in renal allograft recipients transplanted in recent years. *Kidney Int* **59**, 732 737 (2001).

605. Davidson, J. *et al.* New-onset diabetes after transplantation: 2003 International consensus guidelines. Proceedings of an international expert panel meeting. Barcelona, Spain, 19 February 2003. in vol. 75 SS3 24 (2003).

606. Pham, P.-T. T., Pham, P.-M. T., Pham, S. V., Pham, P.-A. T. & Pham, P.-C. T. New onset diabetes after transplantation (NODAT): an overview. *Diabetes Metabolic Syndrome Obes Targets Ther* **4**, 175 186 (2011).

607. Ekberg, H. *et al.* Reduced exposure to calcineurin inhibitors in renal transplantation. *New Engl J Medicine* **357**, 2562 2575 (2007).

608. Vincenti, F. *et al.* Results of an international, randomized trial comparing glucose metabolism disorders and outcome with cyclosporine versus tacrolimus. *Am J Transplant* **7**, 1506 1514 (2007).

609. Johnston, O., Rose, C. L., Webster, A. C. & Gill, J. S. Sirolimus is associated with new-onset diabetes in kidney transplant recipients. *J Am Soc Nephrol* **19**, 1411 1418 (2008).

610. Teutonico, A., Schena, P. F. & Paolo, S. D. Glucose metabolism in renal transplant recipients: effect of calcineurin inhibitor withdrawal and conversion to sirolimus. *J Am Soc Nephrol* **16**, 3128 3135 (2005).

611. Macian, F. NFAT proteins: key regulators of T-cell development and function. *Nat Rev Immunol* **5**, 472 484 (2005).

612. Heit, J. J. *et al.* Calcineurin/NFAT signalling regulates pancreatic beta-cell growth and function. *Nature* **443**, 345 349 (2006).

613. Soleimanpour, S. A. *et al.* Calcineurin signaling regulates human islet {beta}-cell survival. *J Biol Chem* **285**, 40050 40059 (2010).

614. Johnson, J. D. *et al.* Different effects of FK506, rapamycin, and mycophenolate mofetil on glucose-stimulated insulin release and apoptosis in human islets. *Cell Transplant* **18**, 833 845 (2009).

615. Li, J., Kim, S. G. & Blenis, J. Rapamycin: one drug, many effects. *Cell Metab* **19**, 373 379 (2014).

616. Thomson, A. W., Turnquist, H. R. & Raimondi, G. Immunoregulatory functions of mTOR inhibition. *Nat Rev Immunol* **9**, 324 337 (2009).

617. Lamming, D. W. *et al.* Rapamycin-induced insulin resistance is mediated by mTORC2 loss and uncoupled from longevity. *Science* **335**, 1638 1643 (2012).

618. Barlow, A. D., Nicholson, M. L. & Herbert, T. P. Evidence for rapamycin toxicity in pancreatic β-cells and a review of the underlying molecular mechanisms. *Diabetes* **62**, 2674 2682 (2013).

619. Nir, T., Melton, D. A. & Dor, Y. Recovery from diabetes in mice by beta cell regeneration. *J Clin Invest* **117**, 2553 2561 (2007).

620. Andrews, L. M. *et al.* Pharmacokinetic considerations related to therapeutic drug monitoring of tacrolimus in kidney transplant patients. *Expert Opin Drug Met* **13**, 1225 1236 (2017).

621. Mahalati, K. & Kahan, B. D. Clinical pharmacokinetics of sirolimus. *Clin Pharmacokinet* **40**, 573 585 (2001).

622. Aamodt, K. I. & Powers, A. C. Signals in the pancreatic islet microenvironment influence β-cell proliferation. *Diabetes Obes Metabolism* **19 Suppl 1**, 124 136 (2017).

623. Eguchi, K. & Nagai, R. Islet inflammation in type 2 diabetes and physiology. *J Clin Invest* **127**, 14 23 (2017).

624. Ying, W. *et al.* Expansion of Islet-Resident Macrophages Leads to Inflammation Affecting β Cell Proliferation and Function in Obesity. *Cell Metab* **29**, (2018).

625. Fric, J. *et al.* NFAT control of innate immunity. *Blood* **120**, 1380 1389 (2012).

626. Kang, Y. J. *et al.* Calcineurin negatively regulates TLR-mediated activation pathways. *The Journal of Immunology* **179**, 4598 4607 (2007).

627. Weichhart, T., Hengstschläger, M. & Linke, M. Regulation of innate immune cell function by mTOR. *Nat Rev Immunol* **15**, 599 614 (2015).

628. Mercalli, A. *et al.* Rapamycin unbalances the polarization of human macrophages to M1. *Immunology* **140**, 179 190 (2013).

629. Arunagiri, A. *et al.* Proinsulin misfolding is an early event in the progression to type 2 diabetes. *Elife* **8**, 117 (2019).

630. Drucker, D. J. Mechanisms of Action and Therapeutic Application of Glucagon-like Peptide-1. *Cell Metab* **27**, 740–756 (2018).

631. Wang, P. *et al.* A high-throughput chemical screen reveals that harmine-mediated inhibition of DYRK1A increases human pancreatic beta cell replication. *Nat Med* **21**, 383 388 (2015).

632. Wang, P. *et al.* Combined Inhibition of DYRK1A, SMAD, and Trithorax Pathways Synergizes to Induce Robust Replication in Adult Human Beta Cells. *Cell Metab* **29**, 638 652.e5 (2019).

633. Nair, G. G. *et al.* Recapitulating endocrine cell clustering in culture promotes maturation of human stem-cell-derived β cells. *Nat Cell Biol* **21**, 263 274 (2019).

634. Pagliuca, F. W. *et al.* Generation of functional human pancreatic β cells in vitro. *Cell* **159**, 428 439 (2014).

635. Rezania, A. *et al.* Reversal of diabetes with insulin-producing cells derived in vitro from human pluripotent stem cells. *Nat Biotechnol* **32**, 1121 1133 (2014).

636. Halden, T. A. S. *et al.* GLP-1 Restores Altered Insulin and Glucagon Secretion in Posttransplantation Diabetes. *Diabetes Care* **39**, 617 624 (2016).

637. Ferrannini, E. *et al.* Metabolic response to sodium-glucose cotransporter 2 inhibition in type 2 diabetic patients. *J Clin Invest* **124**, 1868–1868 (2014).

638. Merovci, A. *et al.* Dapagliflozin improves muscle insulin sensitivity but enhances endogenous glucose production. *J Clin Invest* **124**, 509–514 (2014).

639. Tang, W., Leil, T. A., Johnsson, E., Boulton, D. W. & LaCreta, F. Comparison of the pharmacokinetics and pharmacodynamics of dapagliflozin in patients with type 1 versus type 2 diabetes mellitus. *Diabetes Obes Metabolism* **18**, 236–240 (2016).

640. Chang, M. *et al.* Bioequivalence, Food Effect, and Steady-State Assessment of Dapagliflozin/Metformin Extended-release Fixed-dose Combination Tablets Relative to Single-component Dapagliflozin and Metformin Extended-release Tablets in Healthy Subjects. *Clin Ther* **37**, 1517–28 (2015).

641. Kasichayanula, S., Liu, X., LaCreta, F., Griffen, S. C. & Boulton, D. W. Clinical Pharmacokinetics and Pharmacodynamics of Dapagliflozin, a Selective Inhibitor of Sodium-Glucose Co-transporter Type 2. *Clin Pharmacokinet* **53**, 17–27 (2013).

642. Pedersen, M. G., Ahlstedt, I., Hachmane, M. F. E. & Göpel, S. O. Dapagliflozin stimulates glucagon secretion at high glucose: experiments and mathematical simulations of human A-cells. *Sci Rep-uk* **6**, 31214 (2016).

643. Bonner, C. *et al.* Inhibition of the glucose transporter SGLT2 with dapagliflozin in pancreatic alpha cells triggers glucagon secretion. *Nat Med* **21**, 512–517 (2015).

644. Saponaro, C. *et al.* Inter-Individual Heterogeneity of SGLT2 Expression and Function in Human Pancreatic Islets. *Diabetes* db190888 (2020) doi:10.2337/db19-0888.

645. Kuhre, R. E. *et al.* No direct effect of SGLT2 activity on glucagon secretion. *Diabetologia* **62**, 1011–1023 (2019).

646. Suga, T. *et al.* SGLT1 in pancreatic α cells regulates glucagon secretion in mice, possibly explaining the distinct effects of SGLT2 inhibitors on plasma glucagon levels. *Mol Metab* **19**, 1–12 (2018).

647. Lundkvist, P. *et al.* Glucagon Levels During Short-Term SGLT2 Inhibition Are Largely Regulated by Glucose Changes in Patients With Type 2 Diabetes. *J Clin Endocrinol Metabolism* **104**, 193–201 (2019).

648. Shirakawa, J. *et al.* Luseogliflozin increases beta cell proliferation through humoral factors that activate an insulin receptor- and IGF-1 receptor-independent pathway. *Diabetologia* 1–11 (2020) doi:10.1007/s00125-019-05071-w.

649. Vergari, E. *et al.* Insulin inhibits glucagon release by SGLT2-induced stimulation of somatostatin secretion. *Nat Commun* **10**, 139 (2019).

650. Chen, C., Cohrs, C. M., Stertmann, J., Bozsak, R. & Speier, S. Human beta cell mass and function in diabetes: Recent advances in knowledge and technologies to understand disease pathogenesis. *Mol Metab* **6**, 943–957 (2017).

651. Halban, P. A. *et al.* β-Cell Failure in Type 2 Diabetes: Postulated Mechanisms and Prospects for Prevention and Treatment. *Diabetes Care* **37**, 1751 1758 (2014).

652. Lu, M. & Li, C. Nutrient sensing in pancreatic islets: lessons from congenital hyperinsulinism and monogenic diabetes. *Ann Ny Acad Sci* **1411**, 65–82 (2018).

653. Naylor, R. N., Greeley, S. A. W., Bell, G. I. & Philipson, L. H. Genetics and pathophysiology of neonatal diabetes mellitus. *J Diabetes Invest* **2**, 158–169 (2011).

654. Hart, N. J. *et al.* Cystic fibrosis–related diabetes is caused by islet loss and inflammation. *Jci Insight* **3**, e98240 (2018).

655. Gloyn, A. L. *et al.* Activating Mutations in the Gene Encoding the ATP-Sensitive Potassium-Channel Subunit Kir6.2 and Permanent Neonatal Diabetes. *New Engl J Medicine* **350**, 1838–1849 (2004).

656. Talchai, C., Xuan, S., Lin, H. V., Sussel, L. & Accili, D. Pancreatic β cell dedifferentiation as a mechanism of diabetic β cell failure. *Cell* **150**, 1223 1234 (2012).

657. Cnop, M. *et al.* Mechanisms of Pancreatic β-Cell Death in Type 1 and Type 2 Diabetes Many Differences, Few Similarities. *Diabetes* **54**, S97–S107 (2005).

658. Yu, Y. *et al.* Bioengineered human pseudoislets form efficiently from donated tissue, compare favourably with native islets in vitro and restore normoglycaemia in mice. *Diabetologia* **61**, 2016–2029 (2018).

659. Hilderink, J. *et al.* Controlled aggregation of primary human pancreatic islet cells leads to glucose-responsive pseudoislets comparable to native islets. *J Cell Mol Med* **19**, 1836 1846 (2015).

660. Furuyama, K. *et al.* Diabetes relief in mice by glucose-sensing insulin-secreting human α-cells. *Nature* **567**, 43–48 (2019).

661. Zuellig, R. A. *et al.* Improved physiological properties of gravity-enforced reassembled rat and human pancreatic pseudo-islets. *J Tissue Eng Regen M* **11**, 109 120 (2014).

662. Foty, R. A Simple Hanging Drop Cell Culture Protocol for Generation of 3D Spheroids. *J Vis Exp* 1 4 (2011) doi:10.3791/2720.

663. Ahrén, B. Islet G protein-coupled receptors as potential targets for treatment of type 2 diabetes. *Nat Rev Drug Discov* **8**, 369–385 (2009).

664. Persaud, S. J. Islet G-protein coupled receptors: therapeutic potential for diabetes. *Curr Opin Pharmacol* **37**, 24–28 (2017).

665. Weis, W. I. & Kobilka, B. K. The Molecular Basis of G Protein–Coupled Receptor Activation. *Annu Rev Biochem* **87**, 897–919 (2014).

666. Foord, S. M. *et al.* International Union of Pharmacology. XLVI. G Protein-Coupled Receptor List. *Pharmacol Rev* **57**, 279–288 (2005).

667. Hauser, A. S., Attwood, M. M., Rask-Andersen, M., Schiöth, H. B. & Gloriam, D. E. Trends in GPCR drug discovery: new agents, targets and indications. *Nat Rev Drug Discov* **16**, 829–842 (2017).

668. Armbruster, B. N., Li, X., Pausch, M. H., Herlitze, S. & Roth, B. L. Evolving the lock to fit the key to create a family of G protein-coupled receptors potently activated by an inert ligand. *Proc National Acad Sci* **104**, 5163–5168 (2007).

669. Wess, J. Use of Designer G Protein-Coupled Receptors to Dissect Metabolic Pathways. *Trends Endocrinol Metabolism* **27**, 600–603 (2016).

670. Roth, B. L. DREADDs for Neuroscientists. *Neuron* **89**, 683–694 (2016).

671. Guettier, J.-M. *et al.* A chemical-genetic approach to study G protein regulation of β cell function in vivo. *Proc National Acad Sci* **106**, 19197–19202 (2009).

672. Wang, Y. *et al.* Application of microfluidic technology to pancreatic islet research: first decade of endeavor. *Bioanalysis* **2**, 1729–1744 (2010).

673. Jun, Y. *et al.* In vivo-mimicking microfluidic perfusion culture of pancreatic islet spheroids. *Sci Adv* **5**, eaax4520 (2019).

674. Dorrell, C. *et al.* Isolation of major pancreatic cell types and long-term culture-initiating cells using novel human surface markers. *Stem Cell Res* **1**, 183 194 (2008).

675. Gregg, B. E. *et al.* Formation of a Human β-Cell Population within Pancreatic Islets Is Set Early in Life. *J Clin Endocrinol Metabolism* **97**, 3197–3206 (2012).

676. Benninger, R. K. P., Head, W. S., Zhang, M., Satin, L. S. & Piston, D. W. Gap junctions and other mechanisms of cell–cell communication regulate basal insulin secretion in the pancreatic islet. *J Physiology* **589**, 5453–5466 (2011).

677. Schwetz, T. A., Ustione, A. & Piston, D. W. Neuropeptide Y and somatostatin inhibit insulin secretion through different mechanisms. *Am J Physiology Endocrinol Metabolism* **304**, E211-21 (2012).

678. Tengholm, A. & Gylfe, E. cAMP signalling in insulin and glucagon secretion. *Diabetes Obes Metabolism* **19**, 42–53 (2017).

679. Gomez, J. L. *et al.* Chemogenetics revealed: DREADD occupancy and activation via converted clozapine. *Science* **357**, 503–507 (2017).

680. Smith, K. S., Bucci, D. J., Luikart, B. W. & Mahler, S. V. DREADDS: Use and application in behavioral neuroscience. *Behav Neurosci* **130**, 137 (2016).

681. Jain, S. *et al.* Chronic activation of a designer Gq-coupled receptor improves β cell function. *J Clin Invest* **123**, 1750–1762 (2013).

682. Regard, J. B. *et al.* Probing cell type–specific functions of Gi in vivo identifies GPCR regulators of insulin secretion. *J Clin Invest* **117**, 4034–43 (2007).

683. Peterson, Q. P. *et al.* A method for the generation of human stem cell-derived alpha cells. *Nat Commun* **11**, 2241 (2020).

684. Gray, S. M. *et al.* Intraislet Ghrelin Signaling Does Not Regulate Insulin Secretion From Adult Mice. *Diabetes* **68**, 1795–1805 (2019).

685. DiGruccio, M. R. *et al.* Comprehensive alpha, beta and delta cell transcriptomes reveal that ghrelin selectively activates delta cells and promotes somatostatin release from pancreatic islets. *Mol Metab* **5**, 449–58 (2016).

686. Saeedi, P. *et al.* Global and regional diabetes prevalence estimates for 2019 and projections for 2030 and 2045: Results from the International Diabetes Federation Diabetes Atlas, 9th edition. *Diabetes Res Clin Pr* **157**, 107843 (2019).

687. DeFronzo, R. A. From the Triumvirate to the Ominous Octet: A New Paradigm for the Treatment of Type 2 Diabetes Mellitus. *Diabetes* **58**, 773–795 (2009).

688. Taylor, S. I., Yazdi, Z. S. & Beitelshees, A. L. Pharmacological treatment of hyperglycemia in type 2 diabetes. *J Clin Invest* **131**, (2021).

689. Kahn, S. E. *et al.* Glycemic Durability of Rosiglitazone, Metformin, or Glyburide Monotherapy. *New Engl J Medicine* **355**, 2427–2443 (2006).

690. Ahlqvist, E., Prasad, R. B. & Groop, L. Subtypes of Type 2 Diabetes Determined From Clinical Parameters. *Diabetes* **69**, 2086–2093 (2020).

691. Mahajan, A. *et al.* Fine-mapping type 2 diabetes loci to single-variant resolution using high-density imputation and islet-specific epigenome maps. *Nat Genet* **50**, 1505–1513 (2018).

692. Fuchsberger, C. *et al.* The genetic architecture of type 2 diabetes. *Nature* **536**, 41–47 (2016).

693. Barroso, I. & McCarthy, M. I. The Genetic Basis of Metabolic Disease. *Cell* **177**, 146 161 (2019).

694. Atkinson, M. A. Pancreatic biopsies in type 1 diabetes: revisiting the myth of Pandora's box. *Diabetologia* **57**, 656–659 (2014).

695. Rodriguez-Diaz, R. *et al.* Innervation Patterns of Autonomic Axons in the Human Endocrine Pancreas. *Cell Metab* **14**, 45–54 (2011).

696. Brissova, M. *et al.* The Integrated Islet Distribution Program Answers the Call for Improved Human Islet Phenotyping and Reporting of Human Islet Characteristics in Research Articles. *Diabetes* **68**, dbi190019 (2019).

697. Brissova, M. *et al.* The Integrated Islet Distribution Program answers the call for improved human islet phenotyping and reporting of human islet characteristics in research articles. *Diabetologia* **62**, 1312–1314 (2019).

698. Traub, S. *et al.* Pancreatic α Cell-Derived Glucagon-Related Peptides Are Required for β Cell Adaptation and Glucose Homeostasis. *Cell Reports* **18**, 3192–3203 (2017).

699. Fernandez-Zapico, M. E. *et al.* MODY7 Gene, KLF11, Is a Novel p300-dependent Regulator of Pdx-1 (MODY4) Transcription in Pancreatic Islet β Cells*. *J Biol Chem* **284**, 36482–36490 (2009).

700. Zhang, H. *et al.* Involvement of KLF11 in Hepatic Glucose Metabolism in Mice via Suppressing of PEPCK-C Expression. *Plos One* **9**, e89552 (2014).

701. Calvo, E. *et al.* Single and combinatorial chromatin coupling events underlies the function of transcript factor krüppel-like factor 11 in the regulation of gene networks. *Bmc Mol Biol* **15**, 10 (2014).

702. Kumar, U. *et al.* Subtype-selective expression of the five somatostatin receptors (hSSTR1-5) in human pancreatic islet cells: a quantitative double-label immunohistochemical analysis. *Diabetes* **48**, 77–85 (1999).

703. Martin, D., Galisteo, R. & Gutkind, J. S. CXCL8/IL8 Stimulates Vascular Endothelial Growth Factor (VEGF) Expression and the Autocrine Activation of VEGFR2 in Endothelial Cells by Activating NFκB through the CBM (Carma3/Bcl10/Malt1) Complex*. *J Biol Chem* **284**, 6038–6042 (2009).

704. Angelo, M. *et al.* Multiplexed ion beam imaging of human breast tumors. *Nat Med* **20**, 436–442 (2014).

705. Giesen, C. *et al.* Highly multiplexed imaging of tumor tissues with subcellular resolution by mass cytometry. *Nat Methods* **11**, 417–422 (2014).

706. Cinti, F. *et al.* Evidence of β-Cell Dedifferentiation in Human Type 2 Diabetes. *J Clin Endocrinol Metabolism* **101**, 1044 1054 (2016).

707. Amo-Shiinoki, K. *et al.* Islet cell dedifferentiation is a pathologic mechanism of long-standing progression of type 2 diabetes. *Jci Insight* **6**, e143791 (2021).

708. Reinert, R. B. *et al.* Vascular Endothelial Growth Factor-A and Islet Vascularization Are Necessary in Developing, but Not Adult, Pancreatic Islets. *Diabetes* **62**, 4154–4164 (2013).

709. Saunders, D. C. *et al.* Coordinated interactions between endothelial cells and macrophages in the islet microenvironment promote β cell regeneration. *Npj Regen Medicine* **6**, 22 (2021).

710. Fina, L. *et al.* Expression of the CD34 gene in vascular endothelial cells. *Blood* **75**, 2417–26 (1990).

711. Klein, T. *et al.* Nestin Is Expressed in Vascular Endothelial Cells in the Adult Human Pancreas. *J Histochem Cytochem* **51**, 697–706 (2003).

712. Morris, D. L. Minireview: Emerging Concepts in Islet Macrophage Biology in Type 2 Diabetes. *Mol Endocrinol* **29**, 946 962 (2015).

713. Gassen, N. V. *et al.* Concise Review: Macrophages: Versatile Gatekeepers During Pancreatic β-Cell Development, Injury, and Regeneration. *Stem Cell Transl Med* **4**, 555 563 (2015).

714. McInnes, L., Healy, J., Saul, N. & Großberger, L. UMAP: Uniform Manifold Approximation and Projection. *J Open Source Softw* **3**, 861 (2018).

715. Dam, T. J. P. van *et al.* CiliaCarta: An integrated and validated compendium of ciliary genes. *Plos One* **14**, e0216705 (2019).

716. Kahn, S. E., Zraika, S., Utzschneider, K. M. & Hull, R. L. The beta cell lesion in type 2 diabetes: there has to be a primary functional abnormality. *Diabetologia* **52**, 1003–1012 (2009).

717. Meier, J. J. & Bonadonna, R. C. Role of Reduced -Cell Mass Versus Impaired -Cell Function in the Pathogenesis of Type 2 Diabetes. *Diabetes Care* **36**, S113–S119 (2013).

718. Bonner-Weir, S. & O'Brien, T. D. Islets in Type 2 Diabetes: In Honor of Dr. Robert C. Turner. *Diabetes* **57**, 2899–2904 (2008).

719. Christensen, A. A. & Gannon, M. The Beta Cell in Type 2 Diabetes. *Curr Diabetes Rep* **19**, 81 (2019).

720. Butler, A. E. *et al.* β-Cell Deficit and Increased β-Cell Apoptosis in Humans With Type 2 Diabetes. *Diabetes* **52**, 102–110 (2003).

721. Yoon, K. H. *et al.* Selective β-Cell Loss and α-Cell Expansion in Patients with Type 2 Diabetes Mellitus in Korea. *J Clin Endocrinol Metabolism* **88**, 2300–2308 (2003).

722. Rahier, J., Guiot, Y., Goebbels, R. M., Sempoux, C. & Henquin, J. C. Pancreatic beta-cell mass in European subjects with type 2 diabetes. *Diabetes Obes Metabolism* **10 Suppl 4**, 32–42 (2008).

723. Mezza, T. *et al.* β-Cell Fate in Human Insulin Resistance and Type 2 Diabetes: A Perspective on Islet Plasticity. *Diabetes* **68**, 1121–1129 (2019).

724. Wu, M. *et al.* Single-cell analysis of the human pancreas in type 2 diabetes using multi-spectral imaging mass cytometry. *Biorxiv* 2021.03.29.437504 (2021) doi:10.1101/2021.03.29.437504.

725. Mizera, M. *et al.* Type 2 Diabetes Remission 5 Years After Laparoscopic Sleeve Gastrectomy: Multicenter Cohort Study. *Obes Surg* **31**, 980–986 (2021).

726. Lean, M. E. J. *et al.* Durability of a primary care-led weight-management intervention for remission of type 2 diabetes: 2-year results of the DiRECT open-label, cluster-randomised trial. *Lancet Diabetes Endocrinol* **7**, 344–355 (2019).

727. Lean, M. E. *et al.* Primary care-led weight management for remission of type 2 diabetes (DiRECT): an open-label, cluster-randomised trial. *Lancet Lond Engl* **391**, 541–551 (2017).

728. Taylor, R. *et al.* Remission of Human Type 2 Diabetes Requires Decrease in Liver and Pancreas Fat Content but Is Dependent upon Capacity for β Cell Recovery. *Cell Metab* **28**, 667 (2018).

729. Taylor, R., Al-Mrabeh, A. & Sattar, N. Understanding the mechanisms of reversal of type 2 diabetes. *Lancet Diabetes Endocrinol* **7**, 726–736 (2019).

730. Steven, S. *et al.* Very Low-Calorie Diet and 6 Months of Weight Stability in Type 2 Diabetes: Pathophysiological Changes in Responders and Nonresponders. *Diabetes Care* **39**, 808–15 (2016).

731. Hogan, M. F. & Hull, R. L. The islet endothelial cell: a novel contributor to beta cell secretory dysfunction in diabetes. *Diabetologia* **60**, 1 8 (2017).

732. Brissova, M. *et al.* Intraislet Endothelial Cells Contribute to Revascularization of Transplanted Pancreatic Islets. *Diabetes* **53**, 1318–1325 (2004).

733. Cohrs, C. M. *et al.* Vessel network architecture of adult human islets promotes distinct cell-cell interactions in situ and is altered after transplantation. *Endocrinology* **158**, 1373–1385 (2017).

734. Almaça, J. *et al.* Young capillary vessels rejuvenate aged pancreatic islets. *Proc National Acad Sci* **111**, 17612 17617 (2014).

735. Almaça, J., Weitz, J., Rodriguez-Diaz, R., Pereira, E. & Caicedo, A. The Pericyte of the Pancreatic Islet Regulates Capillary Diameter and Local Blood Flow. *Cell Metab* **27**, 630-644.e4 (2018).

736. Palikuqi, B. *et al.* Adaptable haemodynamic endothelial cells for organogenesis and tumorigenesis. *Nature* **585**, 426–432 (2020).

737. Montemurro, C. *et al.* IAPP toxicity activates HIF1α/PFKFB3 signaling delaying β-cell loss at the expense of β-cell function. *Nat Commun* **10**, 2679 (2019).

738. Ritzel, R. A., Meier, J. J., Lin, C. Y., Veldhuis, J. D. & Butler, P. C. Human Islet Amyloid Polypeptide Oligomers Disrupt Cell Coupling, Induce Apoptosis, and Impair Insulin Secretion in Isolated Human Islets. *Diabetes* **56**, 65 71 (2006).

739. Wu, C.-T. *et al.* Discovery of ciliary G protein-coupled receptors regulating pancreatic islet insulin and glucagon secretion. *Biorxiv* 2020.10.21.349423 (2020) doi:10.1101/2020.10.21.349423.

740. Hughes, J. W. *et al.* Primary cilia control glucose homeostasis via islet paracrine interactions. *Proc National Acad Sci* **117**, 8912–8923 (2020).

741. Volta, F. *et al.* Glucose homeostasis is regulated by pancreatic β-cell cilia via endosomal EphA-processing. *Nat Commun* **10**, 5686 (2019).

742. Kluth, O. *et al.* Decreased Expression of Cilia Genes in Pancreatic Islets as a Risk Factor for Type 2 Diabetes in Mice and Humans. *Cell Reports* **26**, 3027-3036.e3 (2019).

743. Smith, S. B. *et al.* Rfx6 directs islet formation and insulin production in mice and humans. *Nature* **463**, 775 780 (2010).

744. Piccand, J. *et al.* Rfx6 maintains the functional identity of adult pancreatic β cells. *Cell Reports* **9**, 2219 2232 (2014).

745. Chandra, V. *et al.* RFX6 regulates insulin secretion by modulating Ca2+ homeostasis in human β cells. *Cell Reports* **9**, 2206 2218 (2014).

746. Varshney, A. *et al.* Genetic regulatory signatures underlying islet gene expression and type 2 diabetes. *Proc National Acad Sci* **114**, 2301–2306 (2017).

747. Dabelea, D. *et al.* Etiological Approach to Characterization of Diabetes Type. *Diabetes Care* **34**, 1628–1633 (2011).

748. Consortium, E.-T. *et al.* Type 1 diabetes can present before the age of 6 months and is characterised by autoimmunity and rapid loss of beta cells. *Diabetologia* 1–11 (2020) doi:10.1007/s00125-020-05276-4.

749. Thomas, N. J. *et al.* Frequency and phenotype of type 1 diabetes in the first six decades of life: a cross-sectional, genetically stratified survival analysis from UK Biobank. *Lancet Diabetes Endocrinol* **6**, 122–129 (2018).

750. Ziegler, A. G. *et al.* Seroconversion to Multiple Islet Autoantibodies and Risk of Progression to Diabetes in Children. *Jama* **309**, 2473–2479 (2013).

751. Battaglia, M. *et al.* Introducing the Endotype Concept to Address the Challenge of Disease Heterogeneity in Type 1 Diabetes. *Diabetes Care* **43**, 5–12 (2019).

752. Carmody, D. *et al.* GCK-MODY in the US National Monogenic Diabetes Registry: frequently misdiagnosed and unnecessarily treated. *Acta Diabetol* **53**, 703–708 (2016).

753. Klip, A., McGraw, T. E. & James, D. E. Thirty sweet years of GLUT4. *J Biol Chem* **294**, 11369–11381 (2019).

754. Krogvold, L. *et al.* Insulitis and characterisation of infiltrating T cells in surgical pancreatic tail resections from patients at onset of type 1 diabetes. *Diabetologia* **59**, 492–501 (2016).

755. Camunas-Soler, J. *et al.* Patch-Seq Links Single-Cell Transcriptomes to Human Islet Dysfunction in Diabetes. *Cell Metab* **31**, 1017-1031.e4 (2020).

756. Kim, J. K. *et al.* Glucose toxicity and the development of diabetes in mice with muscle-specific inactivation of GLUT4. *J Clin Invest* **108**, 153–160 (2001).

757. Lam, C. J., Jacobson, D. R., Rankin, M. M., Cox, A. R. & Kushner, J. A. β Cells Persist in T1D Pancreata Without Evidence of Ongoing β-Cell Turnover or Neogenesis. *J Clin Endocrinol Metabolism* **102**, 2647–2659 (2017).

758. Kaestner, K. H., Powers, A. C., Naji, A., Consortium, H. & Atkinson, M. A. NIH Initiative to Improve Understanding of the Pancreas, Islet, and Autoimmunity in Type 1 Diabetes: The Human Pancreas Analysis Program (HPAP). *Diabetes* **68**, 1394–1402 (2019).

759. Carr, A. L. J. *et al.* Histological validation of a type 1 diabetes clinical diagnostic model for classification of diabetes. *Diabetic Med* **37**, 2160–2168 (2020).

760. Chaimowitz, N. S., Ebenezer, S. J., Hanson, I. C., Anderson, M. & Forbes, L. R. STAT1 Gain of Function, Type 1 Diabetes, and Reversal with JAK Inhibition. *New Engl J Med* **383**, 1494–1496 (2020).

761. Noguchi, G. M. & Huising, M. O. Integrating the inputs that shape pancreatic islet hormone release. *Nat Metabolism* **1**, 1189–1201 (2019).

762. Chen, C., Cohrs, C. M., Stertmann, J., Bozsak, R. & Speier, S. Human beta cell mass and function in diabetes: Recent advances in knowledge and technologies to understand disease pathogenesis. *Mol Metab* **6**, 943–957 (2017).

763. Cnop, M. *et al.* Mechanisms of Pancreatic β-Cell Death in Type 1 and Type 2 Diabetes: Many Differences, Few Similarities. *Diabetes* **54**, S97–S107 (2005).

764. Halban, P. A. *et al.* β-Cell Failure in Type 2 Diabetes: Postulated Mechanisms and Prospects for Prevention and Treatment. *Diabetes Care* **37**, 1751–1758 (2014).

765. Unger, R. H. & Cherrington, A. D. Glucagonocentric restructuring of diabetes: a pathophysiologic and therapeutic makeover. *J Clin Invest* **122**, 4–12 (2012).

766. Pan, F. C. & Wright, C. Pancreas organogenesis: From bud to plexus to gland. *Dev Dynam* **240**, 530–565 (2011).

767. Jennings, R. E., Berry, A. A., Strutt, J. P., Gerrard, D. T. & Hanley, N. A. Human pancreas development. *Development* **142**, 3126–3137 (2015).

768. Zhu, Z. *et al.* Genome Editing of Lineage Determinants in Human Pluripotent Stem Cells Reveals Mechanisms of Pancreatic Development and Diabetes. *Cell Stem Cell* **18**, 755–68 (2016).

769. Thompson, P. & Bhushan, A. β Cells led astray by transcription factors and the company they keep. *J Clin Invest* **127**, 94–97 (2017).

770. Arda, H. E. *et al.* Age-Dependent Pancreatic Gene Regulation Reveals Mechanisms Governing Human β Cell Function. *Cell Metab* **23**, 909–920 (2016).

771. Dai, C. *et al.* Islet-enriched gene expression and glucose-induced insulin secretion in human and mouse islets. *Diabetologia* **55**, 707–718 (2012).

772. Cyphert, H. A. *et al.* Examining How the MAFB Transcription Factor Affects Islet β Cell Function Postnatally. *Diabetes* **68**, db180903 (2018).

773. Hang, Y. *et al.* The MafA Transcription Factor Becomes Essential to Islet β-Cells Soon After Birth. *Diabetes* **63**, 1994–2005 (2014).

774. Guo, S. *et al.* Inactivation of specific β cell transcription factors in type 2 diabetes. *J Clin Invest* **123**, 3305–3316 (2013).

775. Dai, C. *et al.* Stress-impaired transcription factor expression and insulin secretion in transplanted human islets. *J Clin Invest* **126**, 1857–1870 (2016).

776. Talchai, C., Xuan, S., Lin, H. V., Sussel, L. & Accili, D. Pancreatic β cell dedifferentiation as a mechanism of diabetic β cell failure. *Cell* **150**, 1223–1234 (2012).

777. Brissova, M. *et al.* α Cell Function and Gene Expression Are Compromised in Type 1 Diabetes. *Cell Reports* **22**, 2667–2676 (2018).

778. Dorrell, C. *et al.* Human islets contain four distinct subtypes of β cells. *Nat Commun* **7**, 11756 (2016).

779. Wang, Y. J. *et al.* Single-Cell Mass Cytometry Analysis of the Human Endocrine Pancreas. *Cell Metab* **24**, 616–626 (2016).

780. Thompson, P. J. *et al.* Targeted Elimination of Senescent Beta Cells Prevents Type 1 Diabetes. *Cell Metab* **29**, 1045-1060.e10 (2019).

781. Meulen, T. van der & Huising, M. O. Maturation of Stem Cell-Derived Beta-cells Guided by the Expression of Urocortin 3. *Rev Diabet Stud* **11**, 115–132 (2014).

782. Blodgett, D. M. *et al.* Novel Observations From Next-Generation RNA Sequencing of Highly Purified Human Adult and Fetal Islet Cell Subsets. *Diabetes* **64**, 3172–3181 (2015).

783. Saunders, D. C. *et al.* Ectonucleoside Triphosphate Diphosphohydrolase-3 Antibody Targets Adult Human Pancreatic β Cells for In Vitro and In Vivo Analysis. *Cell Metab* **29**, 745-754.e4 (2019).

784. Itoh, M. *et al.* Partial loss of pancreas endocrine and exocrine cells of human ARX-null mutation: Consideration of pancreas differentiation. *Differentiation* **80**, 118–122 (2010).

785. Gosmain, Y., Cheyssac, C., Masson, M. H., Dibner, C. & Philippe, J. Glucagon gene expression in the endocrine pancreas: the role of the transcription factor Pax6 in α-cell differentiation, glucagon biosynthesis and secretion. *Diabetes Obes Metabolism* **13**, 31–38 (2011).

786. Courtney, M. *et al.* The Inactivation of Arx in Pancreatic α-Cells Triggers Their Neogenesis and Conversion into Functional β-Like Cells. *PLoS Genet* **9**, e1003934 (2013).

787. Wang, H., Brun, T., Kataoka, K., Sharma, A. J. & Wollheim, C. B. MAFA controls genes implicated in insulin biosynthesis and secretion. *Diabetologia* **50**, 348–358 (2007).

788. Bonnavion, R. *et al.* Both PAX4 and MAFA Are Expressed in a Substantial Proportion of Normal Human Pancreatic Alpha Cells and Deregulated in Patients with Type 2 Diabetes. *PLoS ONE* **8**, e72194 (2013).

789. Matsuoka, T. *et al.* The MafA transcription factor appears to be responsible for tissue-specific expression of insulin. *P Natl Acad Sci* **101**, 2930–2933 (2004).

790. Matsuoka, T. *et al.* MafA Regulates Expression of Genes Important to Islet β-Cell Function. *Mol Endocrinol* **21**, 2764–2774 (2007).

791. Artner, I. *et al.* MafA and MafB regulate genes critical to beta-cells in a unique temporal manner. *Diabetes* **59**, 2530–2539 (2010).

792. Otonkoski, T., Andersson, S., Knip, M. & Simell, O. Maturation of Insulin Response to Glucose During Human Fetal and Neonatal Development: Studies with Perifusion of Pancreatic Isletlike Cell Clusters. *Diabetes* **37**, 286–291 (1988).

793. Henquin, J.-C. & Nenquin, M. Dynamics and Regulation of Insulin Secretion in Pancreatic Islets from Normal Young Children. *PLoS ONE* **11**, e0165961 (2016).

794. Helman, A. *et al.* A Nutrient-Sensing Transition at Birth Triggers Glucose-Responsive Insulin Secretion. *Cell Metab* **31**, 1004-1016.e5 (2020).

795. Matsuoka, T. *et al.* Members of the Large Maf Transcription Family Regulate Insulin Gene Transcription in Islet β Cells. *Mol Cell Biol* **23**, 6049–6062 (2003).

796. Fang, Z. *et al.* Single-Cell Heterogeneity Analysis and CRISPR Screen Identify Key β-Cell-Specific Disease Genes. *Cell Reports* **26**, 3132-3144.e7 (2019).

797. Wortham, M. *et al.* Integrated In Vivo Quantitative Proteomics and Nutrient Tracing Reveals Age-Related Metabolic Rewiring of Pancreatic β Cell Function. *Cell Reports* **25**, 2904-2918.e8 (2018).

798. Russell, R. *et al.* Loss of the transcription factor MAFB limits β-cell derivation from human PSCs. *Nat Commun* **11**, 2742 (2020).

799. Kharchenko, P. V., Silberstein, L. & Scadden, D. T. Bayesian approach to single-cell differential expression analysis. *Nat Methods* **11**, 740–742 (2014).

800. Nasteska, D. *et al.* PDX1LOW MAFALOW β-cells contribute to islet function and insulin release. *Nat Commun* **12**, 674 (2021).

801. Kolic, J. *et al.* Differential effects of voclosporin and tacrolimus on insulin secretion from human islets. *Endocrinology* **161**, bqaa162- (2020).

802. Meier, J. J. & Nauck, M. A. SGLT-2 Inhibition and the Endocrine Pancreatic Alpha Cell: Direct or Indirect Mechanisms of Inhibition? *Endocrinology* **161**, (2020).

803. Tellez, K. *et al.* In vivo studies of glucagon secretion by human islets transplanted in mice. *Nat Metabolism* **2**, 547–557 (2020).

804. Ali, Y. *et al.* The anterior chamber of the eye is a transplantation site that supports and enables visualisation of beta cell development in mice. *Diabetologia* **59**, 1007 1011 (2016).

805. Speier, S. *et al.* Noninvasive in vivo imaging of pancreatic islet cell biology. *Nat Med* **14**, 574 578 (2008).

806. Guo, S. *et al.* Inactivation of specific β cell transcription factors in type 2 diabetes. *J Clin Invest* **123**, 3305 3316 (2013).

807. Redondo, M. J. *et al.* The clinical consequences of heterogeneity within and between different diabetes types. *Diabetologia* **63**, 2040–2048 (2020).

808. Sande, B. V. de *et al.* A scalable SCENIC workflow for single-cell gene regulatory network analysis. *Nat Protoc* **15**, 2247–2276 (2020).

809. Aibar, S. *et al.* SCENIC: single-cell regulatory network inference and clustering. *Nat Methods* **14**, 1083–1086 (2017).

810. Rai, V. *et al.* Single-cell ATAC-Seq in human pancreatic islets and deep learning upscaling of rare cells reveals cell-specific type 2 diabetes regulatory signatures. *Mol Metab* **32**, 109–121 (2019).